December 2018

Renalase as an Intracellular Metabolite Repair Enzyme

Matthew Robert Hoag
University of Wisconsin-Milwaukee

RENALASE AS AN INTRACELLULAR METABOLITE REPAIR ENZYME

by

Matt Hoag

A Dissertation Submitted in

Partial Fulfillment of the

Requirements for the Degree of

Doctor of Philosophy

in Chemistry

at

The University of Wisconsin - Milwaukee

December 2018

ABSTRACT

RENALASE AS AN INTRACELLULAR METABOLITE REPAIR ENZYME

by

Matt Hoag

University of Wisconsin Milwaukee, 2018
Under the Supervision of Professor Graham R. Moran

The human enzyme renalase was discovered in 2005 by nephrologist Gary Desir, who claimed the enzyme is secreted by the kidney into the blood where it was said to catabolize catecholamines in order to modulate blood pressure and heart rate. It has since been shown that the enzyme is expressed in all tissues and does not react with catecholamines. The research detailed in this dissertation led to the discovery that renalase oxidizes two highly toxic isomers of NAD(P)H to form innocuous NAD(P)+. We surmised that such an important cellular function would be pervasive in nature, and our lab was the first to identify an example of a prokaryotic renalase from *Pseudomonas syringae* pv. *phaseolicola*, the first renalase identified outside of the Animalia. Crystal structures of the bacterial enzyme including that of the product-bound complex and also with NADPH (serving here as a substrate analog) bound in the active site have been solved, and its mechanism has been studied in detail using transient state kinetic methods. We contrast the specificity profile of the bacterial enzyme with that of the human enzyme, report structural features, and review the history of renalase discovery and the current state of knowledge in the literature, defining the enzyme's recently proposed role in intracellular metabolite repair.

TABLE OF CONTENTS

LIST OF FIGURES v

LIST OF TABLES vii

LIST OF SCHEMES viii

LIST OF ABBREVIATIONS ix

ACKNOWLEDGEMENTS xi

CHAPTER

I. Recent Discoveries in Small-Molecule Metabolite Damage Control
- Abstract 1
- Introduction 2
- Rid A 3
- Nit 1 10
- Renalase 14
- Glutamate Formiminotransferase 21

II. The Enzyme: Renalase
- Abstract 26
- Introduction 27
- Structure 28
- Renalase Substrate and Mechanism 37
- Concluding Discussion 46

III. Renalase is an α-NAD(P)H Oxidase/Anomerase
- Abstract 51
- Introduction 52
- Materials and Methods 54
- Results 60
- Discussion 71

IV. Kinetics and Equilibria of the Reductive and Oxidative Half-Reactions of Human Renalase with α-NADPH
- Abstract 76
- Materials and Methods 79
- Results 84
- Discussion 92

V. A Metabolic Function for Human Renalase: Oxidation of Isomeric Forms of β-NAD(P)H that are Inhibitory to Primary Metabolism.
- Abstract 98
- Introduction 99
- Materials and Methods 101
- Results 111
- Discussion 123

VI. Renalase Does Not Catalyze the Oxidation of Catecholamines.
Abstract 128
Introduction 129
Materials and Methods 131
Results 134
Discussion 140
VII. Bacterial Renalase: Structure and Kinetics of an Enzyme with 2- and 6-Dihydro-β-NAD(P) Oxidase Activity from *Pseudomonas phaseolicola.*
Abstract 142
Materials and Methods 145
Results 154
Discussion 168
VIII. Ligand Binding Phenomena that Pertain to the Metabolic Function of Renalase
Abstract 174
Introduction 175
Materials and Methods 179
Results 189
Discussion 200
IX. Comparative Metabolomics in the Search for Endogenous Oxidative Substrates of OYE
Abstract 204
Introduction 205
Materials and Methods 208
Results 216
Discussion 224

References 226

Curriculum Vitae 238

LIST OF FIGURES

Figure 1.1. Renalase active site as determined by X-ray crystallography.
Figure 2.1. Human and Bacterial Renalase Primary Structures.
Figure 2.2. The 3-dimensional structure of renalase.
Figure 2.3. The Substrate Binding Site of Renalase.
Figure 2.4. The β-NADH Nicotinamide Binding Pose Observed in the $Ppren_{ox}$•β-NADH Complex Structure (PDB ID4ZCC).
Figure 2.5. An Approximation of the PpRen Catalytic Cycle Based on Available X-ray Crystal Structures.
Figure 2.6. Representative Structures of 6DHNAD•Dehydrogenase Inhibition Complexes.
Figure 2.7. A Timeline of the Primary Physiological and Biochemical Discoveries for Renalase.
Figure 3.1. Flavin Spectra of Native and Refolded Renalase.
Figure 3.2. Evaluation of the Renalase Active Fraction in NAD(P)H Stock Solutions.
Figure 3.3. HPLC Identification of α-NAD(P)H as the Substrate for Renalase Occuring as a Contaminant of β-NAD(P)H Solutions.
Figure 3.4. Identification of β-NAD(P)H as the Nicotinamide Product of the Renalase Reaction.
Figure 3.5. Evaluation of Epinephrine as a Substrate for Renalase.
Figure 4.1. Redox States of Renalase.
Figure 4.2. Reductive Half Reaction of Renalase.
Figure 4.3. Single Turnover of Renalase with Limiting α-NADPH.
Figure 4.4. Extent of Anomerization by Renalase in the Oxidized and Reduced States.
Figure 4.5. Conservation Within the Renalase Active Site.
Figure 5.1. Generation of Renalase Substrates by Reduction of β-NAD^+.
Figure 5.2. NMR Identification of the Purified Products of Sodium Borohydride reduction of β-NAD^+.
Figure 5.3. The Reductive Half-Reactions of Renalase with 2 & 6DHNAD.
Figure 5.4. Measurement of the Dissociation Constants for the Ren_{ox}•β-NADH and Ren_{ox}•β-NAD+ Complexes.
Figure 5.5. Inhibition of Dehydrogenases from Primary Metabolism by 2 & 6DHNAD.
Figure 6.1. HPLC analysis of oxidation of epinephrine to adrenochrome by renalase.
Figure 6.2. Catalytic turnover of renalase in the presence of neurotransmitters.
Figure 6.3. The Effect of Catecholamine and Plasma Preincubation.
Figure 7.1. Analytical HPLC of Renalase Turnover Reactions of Borohydride Reduced Mixtures of β-NAD(P)H Isomers.
Figure 7.2. Kinetics of the Reductive Half-Reactions of PpRen with Nicotinamide Dinucletide Substrates.
Figure 7.3. Kinetics of the Oxidative Half-Reaction of PpRen.
Figure 7.4. Measurement of the Dissociation Constants for the $PpRen_{ox}$•β-NADH, $PpRen_{ox}$•β-NADPH and PpRen•SO_3 Complexes.
Figure 7.5. Superposition of the PpRen•β-NADH and HsRen Tertiary Structures.
Figure 7.6. The Active Site of the PpRen β-NADH and β-NAD^+ complexes.
Figure 7.7. The Reductive Pose of Nicotinamide Dinucleotide Substrates.
Figure 8.1: Two-Dimensional Representation of Active Site Interactions of NAD(P)H Molecules with Bacterial and Human Renalase.

Figure 8.2. Oxidation of Dihydronicotinamide Nucleosides (NR) and Mononucleotide (NMN) Substrates by Renalase.
Figure 8.3. Reductive Half Reactions with 2- and 6Dihydro- NMN and NR with and without complementary ligands.
Figure 8.4. Estimates of Binding constants for substrate fragments and substrate analogs with HsRen.
Figure 8.5. β-NADH vs β-NADPH Binding to PpRen.
Figure 9.1. Overall fold of OYE1 and active site in complex with a ligand derived from R-carvone.
Figure 9.2. Proposed concerted mechanism for the reduction of activated alkenes by OYE.
Figure 9.3. Reductive half-reaction of OYE2 studied by anaerobic stopped-flow spectrophotometry.
Figure 9.4. Reductive half-reaction of OYE3 studied by anaerobic stopped-flow spectrophotometry.
Figure 9.5. Example EICs identified by XCMS as changing significantly between the two samples.

LIST OF TABLES

Table 1.1. Summary of the Measured Kinetic and Equilibrium Constants for Renalase.
Table 2.2. Binding Constants for NAD(P)H Isomers to Various Dehydrogenases.
Table 5.1. Chemical shift and H^1 coupling assignments for 2-, 4-, and 6DHNAD.
Table 7.1. Crystallographic data collection and model refinement statistics.
Table 7.2. Summary of Kinetic and Equilibrium Constants for PpRen
Table 8.1. Structural Statistics for the MDH•6DHNAD, LDH•6DHNAD and PpRen•NADPH complexes
Table 9.1. *S. cerevisiae* strains
Table 9.2. Oligonucleotide primers.
Table 9.3. Artificial hydride acceptors for OYE1 tested with OYE2 and OYE3.

LIST OF SCHEMES

Scheme 1.1. PurF (above) and TrpD (below) are involved in separate biosynthetic pathways.
Scheme 1.2. Proposed role of YjgF in the repair of reactive enamine and imine products of the IlvA reaction.
Scheme 1.3. Proposed RidA mechanism. Nucleophilic attack of a water molecule on the imino carbon of the substrate results in hydrolysis of the amino group and release of ammonia.
Scheme 1.4. Proposed mechanism of IlvE inactivation by 2-aminoacrylate.
Scheme 1.5. Proposed mechanism of alanine racemase inactivation by 2-aminoacrylate and its preemption by RidA.
Scheme 1.6. Similar reactions catalyzed by Nit1 and Nit2 nitrilase family members.
Scheme 1.7. Overall reactions catalyzed by renalase.
Scheme 1.8. Proposed chemical mechanism of renalase including relevant rate constants and equilibria.
Scheme 1.9. Histidine catabolism pathways.
Scheme 1.10. Overall formiminotransferase reaction (above) and observed formyltransferase side-reaction (below).
Scheme 2.1. The chemistry catalyzed by renalase.
Scheme 2.2. Proposed catecholamine oxidase activity.
Scheme 2.3. The chemical and kinetic mechanisms of renalase.
Scheme 3.1. Proposed overall oxidation/anomerization reaction.
Scheme 3.2. Initial proposed role of anomer recycling.
Scheme 3.3. Proposed oxidation/anomerization mechanism.
Scheme 4.1. Proposed overall oxidation/anomerization reaction.
Scheme 4.2. Thermodynamic box linking renalase reduction and β-NADP+ complexation.
Scheme 4.3. Proposed oxidation/anomerization mechanism.
Scheme 5.1. Oxidation of NAD(P)H isomers.
Scheme 5.2. Renalase reductive half-reaction as modeled for fitting.
Scheme 5.3. Proposed metabolic role of isomer oxidation.
Scheme 5.4. Proposed chemical mechanism of HsRen.
Scheme 6.1. Non-enzymatic redox reations in renalase catecholamine oxidase assays.
Scheme 6.2. Proposed native catalytic chemistry of renalase.
Scheme 7.1. Observed activites of renalase.
Scheme 7.2. Reductive half-reaction as modeled for fitting.
Scheme 7.3. Catalytic Cycle of PpRen with 2DHNAD as a Substrate.
Scheme 8.1. The chemistry catalyzed by renalase.

LIST OF ABBREVIATIONS

ADP	adenosine diphosphate
ADP-ribose	adenosine diphosphate ribose
AMP	adenosine monophosphate
DLD	lipoamide dehydrogenase
L-DOPA	L-3,4-Dihydroxyphenylalanine
Dopamine	4-(2-Aminoethyl)benzene-1,2-diol
Epinephrine	(*R*)-4-(1-Hydroxy-2-(methylamino)ethyl)benzene-1,2-diol
FAD	flavin adenine dinucleotide
HEPES	4-(2-hydroxyethyl)-1-piperazineethanesulfonic acid
HPLC	high-pressure liquid chromatography
IC50	50% inhibitory concentration
IPTG	isopropyl-β-thiogalactopyranoside
ITC	isothermal titration calorimetry
LB	Luria Bertani media
LDH	lactate dehydrogenase
MAO	monoamine oxidase
MDH	malate dehydrogenase
β-ME	beta-mercaptoethanol
NADP	nicotinamide adenine dinucleotide phosphate
NAD	nicotinamide adenine dinucleotide
β-NADPH	reduced nicotinamide adenine dinucleotide phosphate
β-NADH (4DHNAD)	reduced nicotinamide adenine dinucleotide

β-NAD^+	oxidized nicotinamide adenine dinucleotide
2DHNAD	2-dihydronicotinamide[a] adenine dinucleotide
6DHNAD	6-dihydronicotinamide adenine dinucleotide[a]
NESGC	North East Structural Genomics Consortium
NMN	nicotinamide mononucleotide
4DHNMN	4-dihydronicotinamide mononucleotide
6DHNMN	6-dihyronicotinamide mononucleotide
2DHNMN	2-dihydronicotinamide mononucleotide
NR	nicotinamide riboside
4DHNR	4-dihydronicotinamide riboside
6DHNR	6-dihydornicotinamide riboside
NMR	nuclear magnetic resonance
OYE	old yellow enzyme
PpRen	renalase from *Pseudomonas Syringae* (pv *phaseolicola* strain 1448A)
HsRen	renalase from *Homo sapiens*
PDB	Protein Data Bank
PCR	polymerase chain reaction
Renalase	human renalase variant 1

a – The naming convention used throughout this article is based on common usage for reduced nicotinamide bases. Early naming of reduced NAD(P) molecules used 1,2-, 1,4-, or 1,6-dihydroNAD. However, reduced nicotinamides gain only a single hydrogen at the position of reduction and are therefore formally 2, 4, or 6-monohydronicotinamides. We have chosen instead the descriptive hybrid name of n-dihydronicotinamide (n-DHNAD) based on the current convention of describing the reduced pyridyl ring of NAD as a dihydropyridyl moiety.

ACKNOWLEDGEMENTS

Above all I would like to thank my advisor, Dr. Graham Moran, for providing me the opportunity to work in your lab studying fascinating enzymes using exciting techniques. Your enthusiasm sparked my own interest in the field, and you have an innate talent for motivating students; I could never have come this far without it. Your continued guidance has proven invaluable to me in my studies and also with important decisions about my future.

I must also thank my fellow labmates and other collaborators whose valuable insight and hard work have proven essential and have yielded many papers I've had the privilege of contributing to, and a first author paper as well. Thanks to Dr. Brett Beaupre, Joe Roman, Brenton Carmichael, Dr. Dhara Shah, Dr. Nicholas Silvaggi, Dr. Audrey Lamb, Dr. Sergei Kuchin, Kathy Meneely, and Aishwarya Shevade. This project, and my own studies, couldn't have progressed without you.

Last but not least, I thank my graduate committee, Dr. Andy Pacheco, Dr. Nicholas Silvaggi, Dr. David Frick, and Dr. Alan Schwabacher; your creative ideas have inspired many experiments, and your astute guidance and insights have lent me fresh perspective and critical rigor. They have been greatly appreciated.

Chapter I
Recent Discoveries in Small-Molecule Metabolite Damage Control

Matthew R. Hoag and Graham R. Moran

Abstract

Metabolite damage repair and preemption encompasses an important but often overlooked class of cellular functions that are essential for cell viability, proliferation, and a host of other cellular and physiological faculties. Often problematic to study by normal means, many such mechanisms have only recently been elucidated, and as gene products of unknown function continue to be characterized, new metabolite damage repair and preemption mechanisms are being uncovered at an increasing rate. In this article we focus on the discoveries of four such damage control enzymes and their proposed mechanisms, each selected for their importance and novelty. The first enzyme we present is RidA (reactive intermediate deaminase A), which has been shown to detoxify reactive products of certain PLP-dependent reactions both in vitro and in vivo, thus preventing the covalent inactivation of various other PLP-dependent enzymes. The second enzyme we present is Nit1, a member of the nitrilase family of enzymes that has been shown to hydrolyze deaminated glutathione to α-ketoglutarate and cysteinylglycine. The third is renalase, an enzyme whose function was first misidentified but recently has been shown to oxidize toxic isomers of NAD(P)H back to NAD+. Finally, the discovery of a formyltransfer side-reaction of the glutamate formaminotransferase enzymes of certain organisms and its proposed role in the repair of damaged folates will be detailed.

Introduction

The “perfectionist paradigm” as described by Hanson [1] is the view that metabolism is “a set of precise, purpose-driven pathways”. This has been the prevailing view of metabolism in the literature over the past few decades. This confined perception of metabolism has likely arisen from the fact that side-reactions that damage intermediates and products are typically slow, and the damaged products are often present in low concentrations in the cell. As a result, the development of assays to investigate the production of these damaged metabolites is often impractical, and such molecules may go undetected and unidentified. Another reason for the prevalence of this view of metabolism is the need to map out mainline biochemical pathways first; the study of such pathways provides the foundation upon which others, like metabolite repair pathways, can be built. Additionally, repair mechanisms may be misidentified ([1], [2]). In recent years, it has become increasingly clear that metabolite damage in the cell is a considerable problem that much of the cell’s resources are devoted to mitigating. Such damage happens by a variety of means, including adventitious side-reactions either of sufficiently reactive products in solution or of enzyme intermediates. In addition, contrary to the “perfectionist paradigm,“ enzymes often make errors. Salient examples are DNA- and RNA polymerases; for decades they have been known as particularly error-prone enzymes, and considerable effort has been put into studying the corresponding nucleic acid proofreading and repair mechanisms [3-8]. Small-molecule metabolites also may be damaged, and control systems within the cell exist for these as well. With much of mainline metabolism mapped and studied in detail, and as new examples of small molecule metabolite damage and repair mechanisms are identified, a great deal of focus has shifted here recently. The following chapter will provide an overview of several more recent discoveries in the category of small-molecule metabolite

damage and control, and outline the study and current state of knowledge of each repair mechanism. It will be seen from the following examples, chosen both for their importance and novelty, that the study of metabolite damage and repair mechanisms and of moonlighting enzyme activities has begun to reveal a much deeper complexity in metabolism than what was once understood.

RidA

The cofactor thiamine pyrophosphate is essential for cell growth, and the study of its biosynthetic pathway has led to many interesting discoveries, including the annotation of several genes of unknown function. One such gene, yjgF, has recently been shown to code for an important enzyme involved in the pre-emption of metabolite damage. While studying the thiamine biosynthetic pathway of Salmonella enterica in 2006 [9], Browne et al., discovered that genetic knockouts of the enzyme glutamine phosphoribosyl pyrophosphate amidotransferase (PurF; EC 2.4.2.14), which produces phosphoribosyl amine (PRA) and serves as the first step in thiamine biosynthesis, were unable to grow in thiamine-deficient media but that a null mutation in the gene ygjF curiously restored the organism's ability to grow under thiamine-free conditions [9]. At this time, the function of the YjgF gene prduct was unknown; no biochemical evidence of its activity had been demonstrated, and neither its sequence nor structure [10-14] nor those of its family members bore significant homology to proteins of known function.

In a separate but related thread of inquiry, while the function of the enzyme anthranilate phosphoribosyltransferase (trpD of the trp operon) of tryptophan biosynthesis is to condense anthranilate and phosphoribosyl pyrophosphate to form phosphoribosyl anthranilate and inorganic phosphate (Scheme 1.1), it was shown [15] that TrpD is able to produce PRA *in vitro* if the enzyme threonine dehydratase (IlvA, EC 4.3.1.19) is included in the reaction.

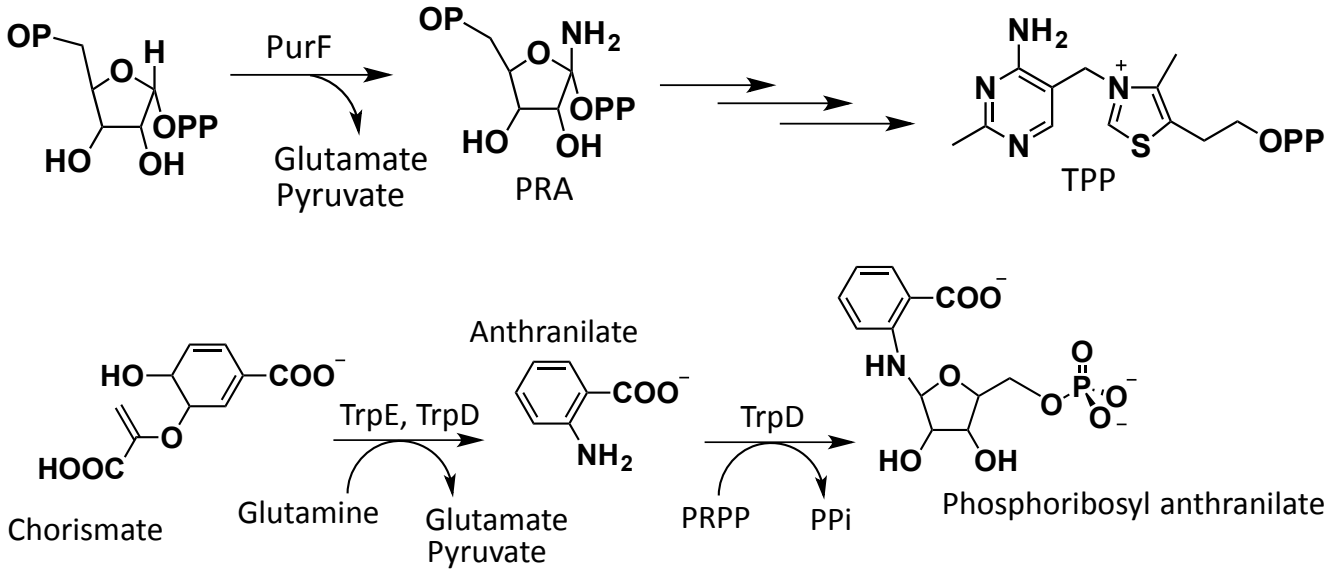

Scheme 1.1. PurF (above) and TrpD (below) are involved in separate biosynthetic pathways.

This suggested that TrpD could use a product of the threonine dehydratase reaction as the amino donor to produce PRA. Including YjgF in the reaction abolished the production of PRA however, suggesting that YjgF may act on the product of the IlvA reaction and prevent it from being used by TrpD. Thus, the PurF and YjgF null mutant would have this PurF-independent pathway of producing PRA, bypassing the defective PurF with a moonlighting TrpD and allowing the mutant to grow in thiamine-free media.

This working model by the Downs group served as the kernel of knowledge that lead to more detailed understanding of the function of the enigmatic YjgF and of the interplay of biochemical pathways it affects. The PLP-dependent enzyme threonine dehydratase may react with serine to produce 2-aminoacrylate (2AA), a reactive enamine, which tautomerizes to an imine and is finally hydrolyzed non-enzymatically to form pyruvate and ammonia.

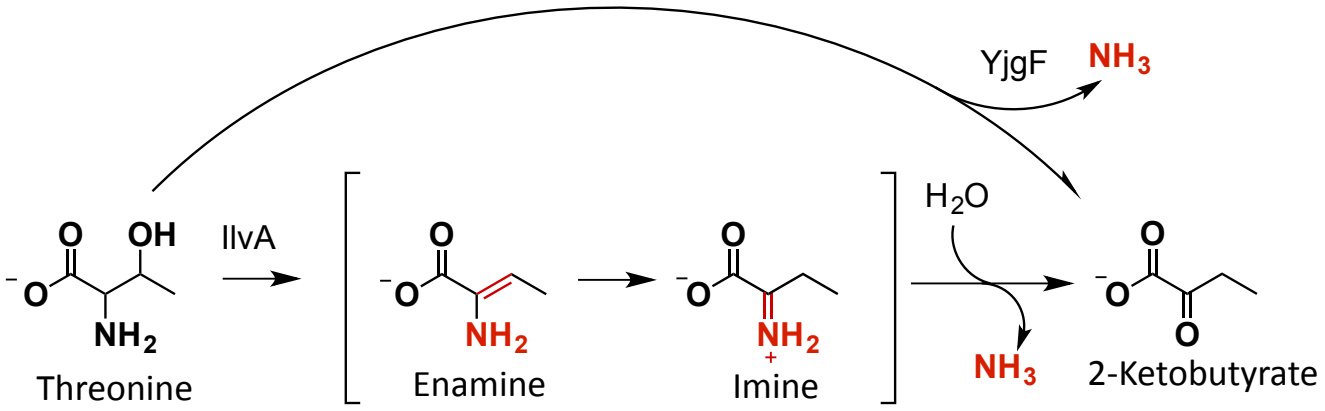

Scheme 1.2. Proposed role of YjgF in the repair of reactive enamine and imine products of the IlvA reaction. The amino group is hydrolyzed into solution as ammonia.

Evidence for the proposed mechanism of the 2AA hydrolysis activity of YjgF was obtained by the Downs group [16] from continuous *in vitro* assays of the IlvA reaction with and without added YjgF and in the presence of ferricyanide (ferricyanide was intended to decarboxylate available enamine/imine products in the reaction, and its reduction was followed by UV absorption spectrophotometry). 2-ketobutyrate concentrations were also measured by DNPH derivatization. Results showed that YjgF decreased the availability of enamine/imine products formed in the reaction to ferricyanide and increased the rate of α-ketobutyrate production. Coupled assays monitoring α-ketobutyrate production with and without added YjgF homologs from various organisms produced similar results, with each homolog significantly increasing the initial rate of α-ketobutyrate formation.

This suggested that the enamine/imine hydrolysis activity of YjgF is conserved across all domains of life. Upon demonstration of this activity, the hitherto uncharacterized YjgF was named RidA, for "reactive intermediate deaminase A".

Similar continuous *in vitro* assays were conducted with various active site RidA mutants, and together with CLUSTALW sequence alignments of RidA homologs, suggested active site residues critical for the demonstrated enamine/imine hydrolysis activity. Notably, the conserved residue Arg105 forms a salt bridge with the acrylate moiety of the substrate, and the hydroxyl group from conserved Tyr17 hydrogen bonds with the imine nitrogen. An ordered water molecule observed in the apo structure of the enzyme [14] hydrogen bonds to the backbone of Cys107 and the sidechain of conserved residue Glu120. This water molecule may effect nucleophilic attack on the substrate, forming a tetrahedral intermediate, and a subsequent rearrangement yields the α-ketoacid product, a mechanism similar to that of other deaminase enzymes (Scheme 1.3).

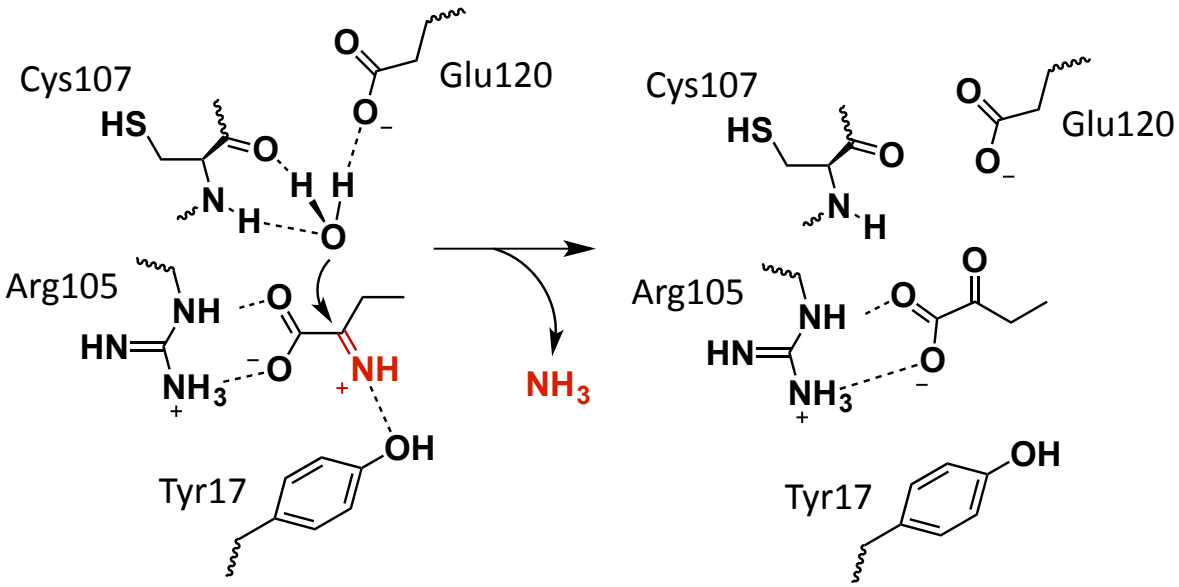

Scheme 1.3. Proposed RidA mechanism. Nucleophilic attack of a water molecule on the imino carbon of the substrate results in hydrolysis of the amino group and release of ammonia.

The metabolic importance of an enamine/imine scavenger such as RidA had yet to be demonstrated, however. It was noted that the enamine/imine products of the threonine dehydratase reaction may react with other enzymes or metabolites, damaging them. For example, *in vivo* studies suggested that a product of the IlvA reaction may inhibit branched-chain amino acid aminotransferase (IlvE, EC 2.6.1.42), and this was more recently confirmed *in vitro* by the Downs group [17]. In this paper, Lambrecht et al., conclude that the aminoacrylate produced by IlvA acts as a suicide inhibitor for the PLP-dependent IlvE, and possibly other PLP-dependent dehydratases as well.

The principal evidence for this was proffered from three experiments; in the first, mutant strains of *S. enterica* derived from SB300A1 and with a null mutation in ridA (*ridA*) were studied alongside the same strain lacking the mutation (*ridA*$^+$), and each were compared to *ridA* and *ridA*$^+$ variants that also harbored plasmids for the expression (under normal growth conditions) of another serine/threonine dehydratase native to *S. enterica*, TdcB. IlvE activity in each strain was measured by permeabilizing the cells and initiating the IlvE reaction in the presence of α-ketoglutarate by the addition of the substrate L-isoleucine. The reactions were incubated, and formation of the product 2-keto-3-methylvalerate (2KMV) was measured by DNPH derivatization and organic extraction, and 2KMV formation was normalized to total cellular protein. The results showed a significant decrease (25% activity, or 4-fold decrease) in IlvE activity in the *ridA* strains compared to the *ridA*$^+$ strains, both lacking the *tdcB*$^+$ plasmid. For reactions containing strains harboring the *tdcB*$^+$ plasmid, a similar trend was observed, though IlvE activity was decreased further, to 3% (30-fold). To differentiate the activities of the two serine/threonine dehydratases, the reactions were repeated with strains grown on isoleucine-enriched medium in order to allosterically inhibit the function of IlvA. The expected trend was observed, as IlvE activity was mostly restored in the *ridA* strain and no effect was observed in the *ridA*$^+$ strains. In the *ridA/tdcB*$^+$ strain, growth in isoleucine-rich media showed a small but

insignificant uptick in IlvE activity, suggesting that while IlvA may have been inhibited, TdcB (which is not inhibited by isoleucine) produced sufficient 2AA to inactivate IlvE in these cells. Together, these results suggest that in *S. enterica*, RidA serves to pre-empt IlvE deactivation *in vivo* by hydrolyzing the product of two at least two serine/threonine dehydratases, IlvA and TdcB.

In a second experiment, these effects were reproduced *in vitro*. Radioactive assays were performed with recombinant RidA, IlvA, and IlvE in solution with IlvA and IlvE substrates L-serine and α-ketoglutarate and the mixture was incubated to allow for IlvE inactivation. L-[U-^{14}C]isoleucine was then added to initiate the IlvE reaction, which was subsequently quenched by TLC, separating [^{14}C]isoleucine from [^{14}C]2KMV and IlvE specific activities were quantified. Various components were left out of the reaction, and results showed that IlvE activity was inhibited to 20% (a 5-fold decrease), but only when IlvA and serine were included in the reaction. It was also noted that including either of four RidA homologs from various organisms restored observed IlvE activity to nearly 100% for all homologs tested, suggesting that the damage pre-emption function of RidA is conserved among all domains of life.

Finally, mass spectrometry was used on IlvE isolated from *ridA* and *ridA*$^{+}$ strains, confirming the presence of a +317 Da adduct in only the *ridA* derived IlvE, consistent with a covalent PLP adduct with propionate linker. These results were verified by incubating recombinant IlvE with the serine analog and known IlvE suicide inhibitor 3-chloro-L-alanine (3CA). This inhibitor is known to produce an external aldimine with PLP active site, releasing chlorine to form PLP•2AA, and finally reacting with a nucleophilic residue in the active site, inactivating the enzyme. Mass spec results using this suicide inhibitor paralleled those using the native substrates, with incubated samples showing a peak corresponding to a +317 Da adduct with respect to the unincubated enzyme.

From these results, Lambrecht et al., concluded that the 2-aminoacrylate produced by IlvA and TdcB acts as a suicide inhibitor for the PLP-dependent IlvE, and possibly other PLP-dependent dehydratases as well. In their proposed mechanism of deactivation, 2-aminoacrylate enters the active site of IlvE and attacks the PLP internal aldimine, forming the external aldimine between the PLP cofactor and 2AA. The acrylate moiety of this aldimine intermediate is subsequently attacked by a nucleophilic residue in the IlvE active site, forming the suicide complex in which the PLP cofactor is covalently attached to the enzyme via a propionate linker. This irreversibly inactivates the enzyme, and a similar fate presumably awaits other PLP-dependent enzymes in the cell as well.

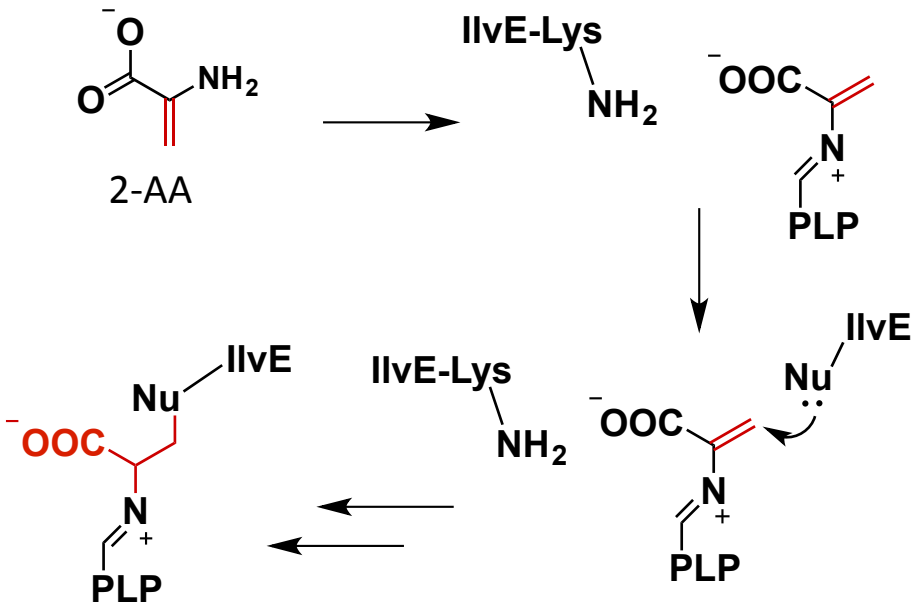

Scheme 1.4. Proposed mechanism of IlvE inactivation by 2-aminoacrylate.

In a related study of alanine racemase for example [18], similar results were observed both in vivo and in vitro, though the mechanism of deactivation and resulting suicide complex were distinct. In this case, the proposed mechanism features 2-aminoacrylate entering the active site and attacking the internal aldimine, forming a covalent adduct with the PLP itself and inactivating the enzyme. The

identity of complex was verified by base hydrolysis followed by ESI mass spectrometry and NMR confirming the expected product.

RidA, then, serves to accelerate the hydrolysis of 2AA and other enamine/imine products of the serine/threonine dehydratase reaction to their respective keto-acid products and ammonia, thus pre-empting the inactivation of other PLP-dependent enzymes.

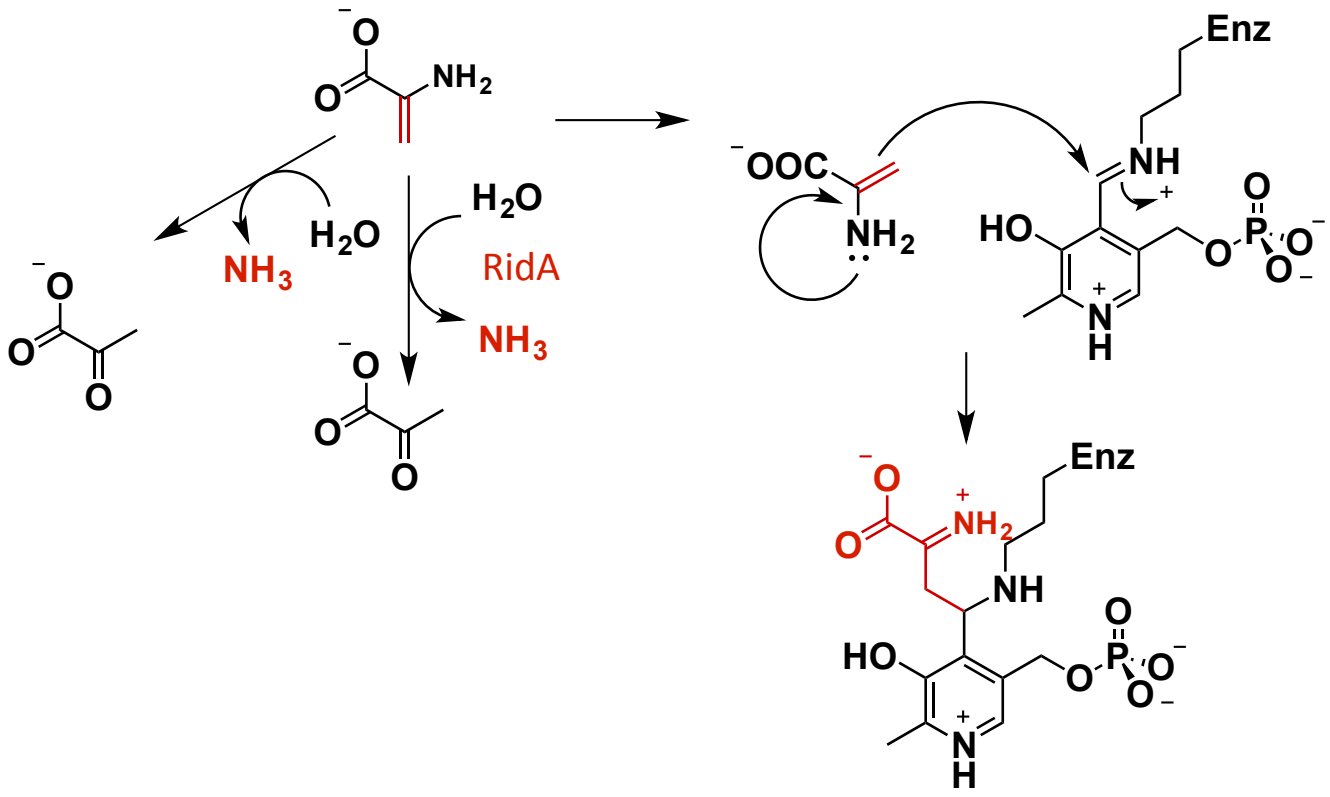

Scheme 1.5. Proposed mechanism of alanine racemase inactivation by 2-aminoacrylate and its preemption by RidA

Nit1

The nitrilase (EC 3.5.5.1) family of enzymes play diverse roles in nature, from biosynthesis to detoxification and nitrogen metabolism [19]. The defining characteristic of this family of enzymes is their ability to hydrolyze nitriles to carboxylic acids and ammonia, and the first example of this family was discovered in 1964 [20]. Many members of this family have been shown to take substrates to

products via a tetrahedral intermediate with a primary amino group [21-23], and several have been shown to include primary amines in their markedly promiscuous substrate profiles. One important member of this family is omega-amidase, or Nit2. This enzyme exists in humans and is widely distributed in nature and serves as the second step in the glutaminase II pathway, the net reaction of which converts glutamine, an α-keto acid, and a water molecule to α-ketoglutarate, an L-amino acid, and ammonia. Nit2 also hydrolyzes transaminated glutamate (α-ketoglutaramate or KGM) to produce α-ketoglutarate and ammonia. A more mysterious member of this family is Nit1, which is present in nearly all eukaryotes and which does not hydrolyze KGM, though it bears 35% sequence identity to Nit2. Crystal structures [24, 25] revealed that the active site of Nit1 contains many of the same residues as Nit2 but lacks steric crowding around the KGM amido group in the binding site; this area of the binding site is much more open in Nit1, suggesting a bulkier substrate.

It was speculated [26] that likely substrates of Nit1 might be produced by transamination reactions deaminating glutathione to produce dGSH (deaminated glutathione), or by the attachment of a CoA group to α-ketoglutarate, producing α-ketoglutaryl–CoA. Both proposals were tested, and it was found that dGSH reacts rapidly with Nit1 (k_{cat}: ~$3s^{-1}$) and with a K_m of ~100μM. The CrispR/Cas9 system was used to produce Nit1 knockouts in a human cell line (and Nit2 knockouts as a control), and these strains were then tested for intracellular dGSH accumulation by subjecting cell extracts to LC/MS analysis. Nit1 knockouts showed a 10-fold increase in intracellular dGSH concentrations (~180μM) with respect to WT, and dGSH concentrations in the Nit2 knockout strains were within error of those of the WT strains. Similar results were observed using *S. cerevisiae* mutants. Mouse Nit1 knockout models were also studied, measuring dGSH concentrations in the urine of these mutants by LC/MS and comparing them to those of WT animals, and was found to be 15-fold higher in the knockout models with respect to WT. The urinary concentrations of dGSH were so high from the knockout mice

that they were also measured using a coupled spectrophotometric assay which included only a few microliters of urine diluted with buffer; such a great accumulation and excretion of dGDH in Nit1 deficient mice suggests that Nit1 is the major contributor to dGSH metabolism in mice. Glutamate dehydrogenase (GDH) was included in the coupled reaction, and α-ketoglutarate production by Nit1 was measured by monitoring NADH consumption by GDH (defined?). dGSH concentrations measured by this method were in close agreement with those measured by LC/MS. Controls were included by spiking WT mouse urine with pure dGSH, matching both retention times and MS/MS fragmentation patterns of the control peak with that observed in urine from the knockout mice. Finally, these results were verified using GC/MS detection of derivatized dGSH from knockout mouse urine, and by high-resolution MS, which found that the exact mass agreed with the theoretical mass of a cyclic derivative of dGSH. Interestingly, such a derivative would be analogous to the cyclic anomer of KGM, the Nit2 substrate, which forms at a favorable equilibrium from the linear molecule in solution.

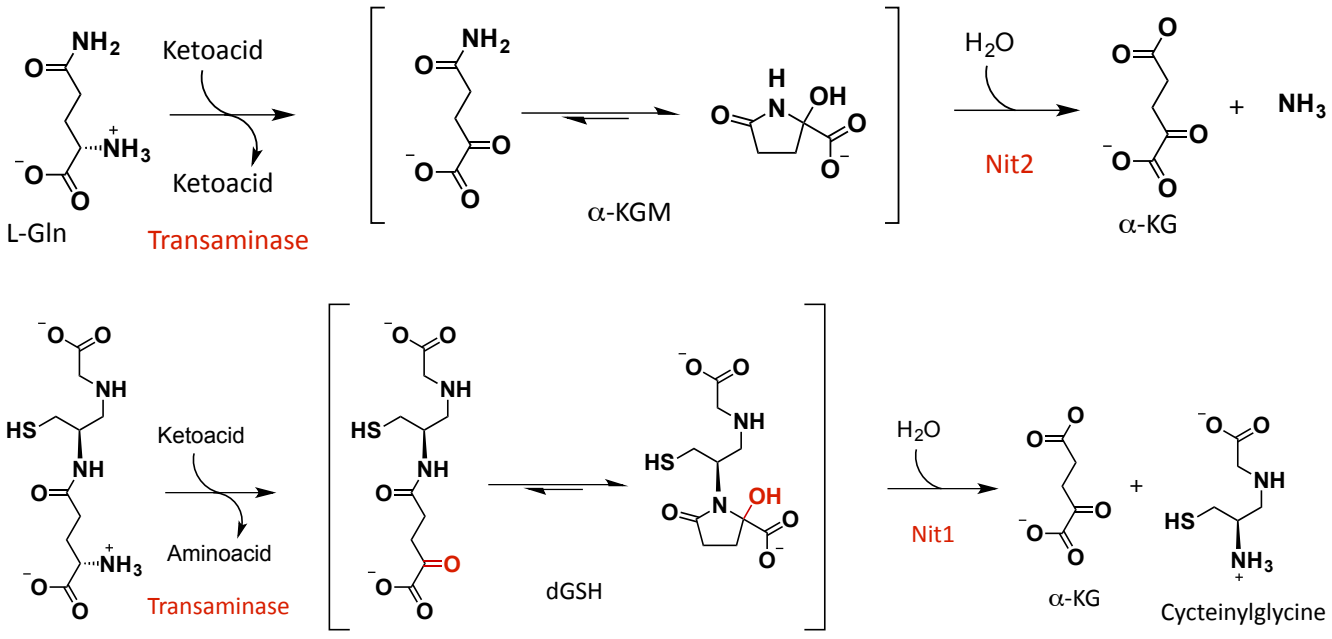

Scheme 1.6. Similar reactions catalyzed by Nit1 and Nit2 nitrilase family members.

With the dGSH substrate of Nit1 identified and its consumption observed *in vivo*, its origin in the cell remained a mystery. It was hypothesized that dGSH could be produced as a side-reaction by various transaminase enzymes. One likely candidate chosen was the promiscuous glutamine transaminase K. This enzyme was reacted with both glutathione and oxaloacetate, monitoring the PLP absorbance in each case. Over ~30 minutes, the PLP spectrum changed for both substrates, with decreasing absorbance at the 430nm peak and an increasing at 320nm, indicating conversion of the PLP cofactor to the pyridoxamine form PMP (no change took place in the absence of GSH or OA). Reaction mixtures of overnight incubations and controls lacking enzyme were separated by HPLC, and additional peaks were observed in the reaction mixtures for both GSH and OA. These peaks were identified using MS/MS as the deaminated species of either substrate, demonstrating *in vitro* that the promiscuous enzyme glutamate transaminase K reacts slowly with GSH and OA to produce the deaminated products, serving as the first demonstration of the origin of the damaged glutathione derivative dGSH. Additional transaminases were reacted with GSH and OA in coupled assays with Nit1 and GDH, monitoring NADH consumption, and suprisingly, all transaminases tested showed at least some low level of GSH deaminase activity. This suggests the activity producing these damaged metabolites, while slow, is ubiquitous among transaminase enzymes.

Finally, it was shown using fluorescence microscopy that transfecting with a GFP-conjugated form of Nit1 *in vivo* resulted in its localization to both the cytosol and mitochondria. Since transaminase enzymes are also localized in both the cytosol and mitochondria, this lends further credence to the proposed role of Nit1 in scavenging the damaged metabolite dGSH produced in adventitious side-reactions of various transaminase enzymes and recycling it back into usable α-ketoglutarate.

From database searches, sequence alignments, and *in vitro* assays verifying activity, it was noted that Nit1 homologs are found in nearly every organism that synthesizes glutathione; such a broad conservation of this enzyme would suggest the importance of its activity, though curiously, the knockout of Nit1 in mice produced no noticable deleterious effects.

Renalase

In 2005, a search of the Mammalian Gene Collection [27] by Gary Desir using an algorithm designed to identify genes coding for proteins with kidney secretory signals lead to the identification of the gene coding for a yet uncharacterized protein. Upon expression and purification, the gene product was determined to be a flavoenzyme of unknown function which Desir dubbed “Renalase”. After an extensive search for the native substrate using a high-throughput approach yielded scant results [28], Desir claimed that the enzyme oxidizes various catecholamines in a curious reaction involving NAD(P)H. In Desir’s proposed reaction, NAD(P)H is oxidized to NAD(P)+, mobilizing two electrons, and another two electrons are mobilized by oxidizing a catecholamine to its adenochrome derivative. The fate of these four mobilized electrons in Desir’s proposed reaction was not intimated.

The initial claim that renalase oxidized NAD(P)H molecules was based on dubious evidence of very slow turnover rates of NAD(P)H to NAD(P)+ measured using an Amplex® Red Hydrogen Peroxide/Peroxidase Assay Kit (ThermoFisher Scientific) in the presence of catecholamines. Dopamine, epinepherine, and norepinepherine were tested, and the rates observed were on the order of 0.1 – 66 min^{-1} [28]. Turnover rates this slow are on the order of free flavin reacting with nicotinamide dinucleotides in solution, and so Desir’s claim that this was evidence of enzymatic turnover was hotly debated [29-32]. Several groups were unable to replicate Desir’s results [31-33], and so the true function of renalase remained elusive.

In 2013, Beaupre *et al.* identified an impurity in aged NAD(P)H stocks that was shown to rapidly reduce the renalase FAD cofactor [33]. The reductive half-reaction of renalase with this contaminant molecule was explored using stopped-flow spectrophotometry with varying pseudo-first order concentrations of the aged NADPH stock, traces fit to single exponentials, and the observed rate constants for flavin reduction plotted against stock concentration to yield a hyperbolic curve characteristic of an irreversible chemical step preceded by a prequilibrium substrate binding. The measured K_d for the substrate molecule was 20 μM, and the rate constant for reduction of the flavin was measured to be 40 s^{-1}, both well within a range one might assume for physiological relevance. From the concentration of enzyme in the reactions and the proportion of the flavin reduced, it was determined that the substrate molecule accumulated in aged NADH stocks up to 4%, and was a 1% contaminant in aged NADPH stocks.

Assays using a clark-type oxygen electrode were also instrumental in identifying molecular oxygen as a substrate, reoxidizing the reduced FAD cofactor and producing hydrogen peroxide. This was confirmed by the subsequent addition of catalase in the reaction, which restored half the original concentration of oxygen in the reaction as expected. Oxidative half reactions were studied by stopped-flow spectrophotometry [34], reducing the enzyme with a fixed concentration of substrate but varying concentrations of oxygen. The oxidative rate constant was sufficiently slower than the reductive rate constant to allow for temporal separation of the two phases and accurate fitting to yield the second-order rate constant of 2900 $M^{-1}s^{-1}$ for the oxidation of the flavin by molecular oxygen.

With a substrate molecule found but not identified, the grand task of production, purification, and identification of this unstable substrate molecule commenced. HPLC studies clearly showed this contaminant molecule being consumed in the reaction, while the usual NAD(P)H remained mostly unreacted. [33]. It was found by Beaupre [35] that these substrate molecules could be produced

simply by making an aqueous stock of NAD(P)H and aging it at room temperature, or even at -20°C, and that the most rapid accumulation was found by adding a small amount of water to high-purity NAD(P)H powder; It has since been determined that this renalase substrate molecule had been very commonly produced by accident simply by leaving NAD(P)H powder exposed to moisture for any significant period of time. This lead the author to several papers from 1977 detailing contaminant molecules found in NAD(P)H stocks that inhibit lactate dehydrogenase [36, 37]. At this time, a method was developed to collect larger quantities of the substrate molecule after separation by HPLC and for lyophilization and stabilization of the renalase substrate molecules. This allowed stocks to be prepared at sufficiently high concentrations for two-dimensional NMR studies to be performed with the aim of determining the molecular structure of the substrate [35].

NMR and mass spectrometry identified the structures of the substrate molecules as identical to their NAD(P)H isomers save for the nicotinamide 4’ hydride being positioned at a different carbon on the pyridyl ring; in these molecules, the hydride resides at the 6’ and 2’ carbons (6DH- and 2-DHNAD(P), respectively). With this information, it was hypothesized that large quantities of these substrate molecules could more easily be produced by reacting NAD+ nonenzymatically with a hydride donor such as sodium borohydride, and that this would produce a mixture of the three NADH isomers, including NADH itself. The mixture could then be separated by preparative HPLC, collected, and desalted for use in assays and other experiments requiring concentrated stocks of either isomer. With concentrated stocks in hand, various static thermodynamic and pre-steady state kinetic studies were performed, enabling the detailed characterization of the renalase mechanism without the background of NADH in the reaction mixtures.

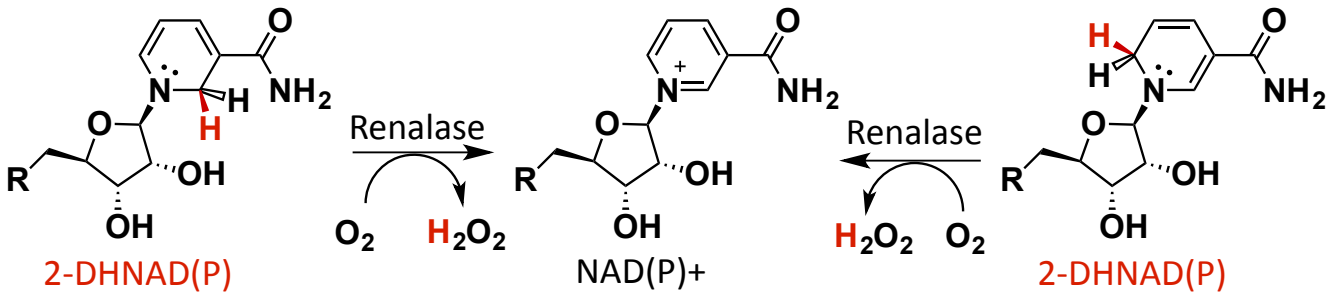

Scheme 1.7. Overall reactions catalyzed by renalase.

With the chemical mechanism now characterized, the metabolic role for renalase remained unsolved. It was hypothesized that the 2- and 6-DH isomers may inhibit other dehydrogenase enzymes owing to the pronounced similarity with NADH. Inhibition studies were conducted, measuring the activity of primary metabolic dehydrogenases in the presence of varied concentrations of either 6- or 2-DHNAD(P), and inhibition constants were measured [35]. K_i values ranged down to 16 nm for 6DHNAD for the critical enzyme malate dehydrogenase, suggesting that even low concentrations of this isomer in the cell could be toxic by shutting down the TCA cycle. Various other dehydrogenase enzymes were assayed, and all but lipoamide dehydrogenase were inhibited to a significant degree; lactate dehydrogenase, isocitrate dehydrogenase, and glyceraldehyde-3-phosphate dehydrogenase were inhibited to the nanomolar or low micromolar range. Together with the earlier kinetic studies, these findings suggest that 2- and 6DHNAD(P) and that renalase may serve to alleviate this inhibition of primary metabolism by oxidation of these isomers to the innocuous NAD+.

Soon after the enzyme was discovered, searches through genetic databases identified possible renalase homologs in the Animalia, but none outside of this kingdom. It was hypothesized at the time that renalase existed only in higher organisms. If the cellular role of renalase is to catabolize toxic NAD(P)H isomers, one would expect to find an enzyme with such a critical role in all kingdoms of life,

not only the Animalia; there was therefore a push to find examples of this enzyme in other kingdoms of life. It was noted by Hoag et al., that the Human renalase structure was solved using molecular replacement with a protein of unknown function from *Pseudomonas syringae* pv. *Phaseolicola*. This prior structure had been solved by the Northeast Structural Genomics Consortium and deposited in the PDB. Sequence identity based on alignments to the human enzyme was 14%, below the threshold of identity used in common sequence search algorithms to distinguish homology from random chance, explaining why initial sequence searches using the BLAST algorithm returned no possible homologs outside the Animalia.

This protein, like renalase containing a covalently-bound FAD cofactor, was subsequently expressed and purified [38], and early assays determined that it too had 2- and 6DHNAD(P) oxidase activity, identifying it as a renalase homolog. This was the first example of a prokaryotic renalase, and the first example identified outside of the Animalia. This lent credence to the proposed role of detoxification of NAD(P)H isomers, since the originally proposed role of modulation of blood pressure and heart rate by the oxidation of chatecholamines would not be applicable to prokaryotes. Pre-steady state kinetic assays and other biochemical studies on this bacterial enzyme served to characterize its chemical mechanism, which shows some distinction from that of its human counterpart. A marked difference in specificity between the four substrate molecules is observed; the bacterial enzyme reacts more rapidly with the 2DH isomers than with the 6DH isomers, and bind the NAD-derived isomers more tightly that the NADP-derived isomers. This is in contrast to the specificity profile of the human enzyme, which shows no significant preference among the isomers. The structural basis for this difference in specificity profiles was not known at the time, but would later be elucidated.

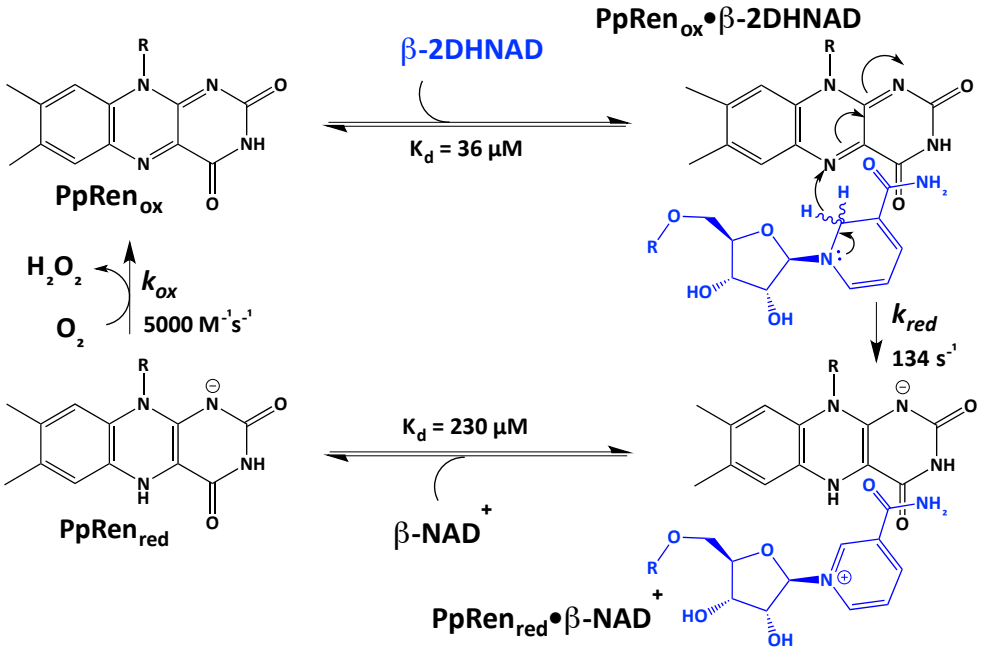

Scheme 1.8. Proposed chemical mechanism of renalase including relevant rate constants and equilibria.

Unlike the human enzyme, *phaseolicola* renalase crystallized readily. Structural complexes of the free enzyme, the product-bound enzyme, and of the enzyme bound to the substrate analog NADH were solved to high resolution, affording mechanistic insights that could not be gleaned by kinetic methods alone. It was observed that in the active site, a positionally conserved arginine residue (Arg280 of the bacterial enzyme) that rests over the nicotinamide moiety in the NADH-bound complex, while its guanidino group is flipped out of the active site in the NAD+ complex, suggested electrostatic repulsion between the positively charged nicotinamide and guanidino group. This repulsion may serve as a kind of ejection mechanism, increasing the K_d for the product, NAD+. This residue was mutated to various amino acids in order to test the effect on product K_d, but all mutants

regardless of conservativity proved highly unstable in solution and thus intractable by most analytical methods considered. Another curiosity was observed in the structures; the 2’ phosphate moiety in the NADPH bound complex appeared to be pointing into solution and not bound to the enzyme. It was hypothesized that the reason for the K_d values observed with the NADPH isomer substrates were increased relative to the NADH substrates was that the highly charged phosphate moiety partitions it off the enzyme and into the aqueous solvent. In the complex structures, it was also observed that the nicotinamide is positioned over the flavin with the 2’ carbon directly above and proximal to the N5 of the flavin, positioning it perfectly for hydride transfer at this carbon. The amide portion of the nicotinamide was seen in this structure to hydrogen bond with active site threonine 185, locking it in this position. It could be thought that if the nicotinamide were flipped 180° around the glycosidic bond, that the 6’ carbon would lie over the N5 of the flavin for hydride transfer; however, there exists no amino acid residues toward the other side of the flavin site that could hydrogen bond the amide moiety in this position but neither is there steric hindrance from any residue. It was hypothesized that it is this structural detail that gives rise to the markedly increased rate of flavin reduction observed using the 2DH substrates over the 6DH isomers.

BLAST Searches using the bacterial renalase sequence identified possible renalase homologs in other kingdoms, including Archaea, Fungi, and Plantae. Several of these homologs were expressed and purified, and characterization is underway.

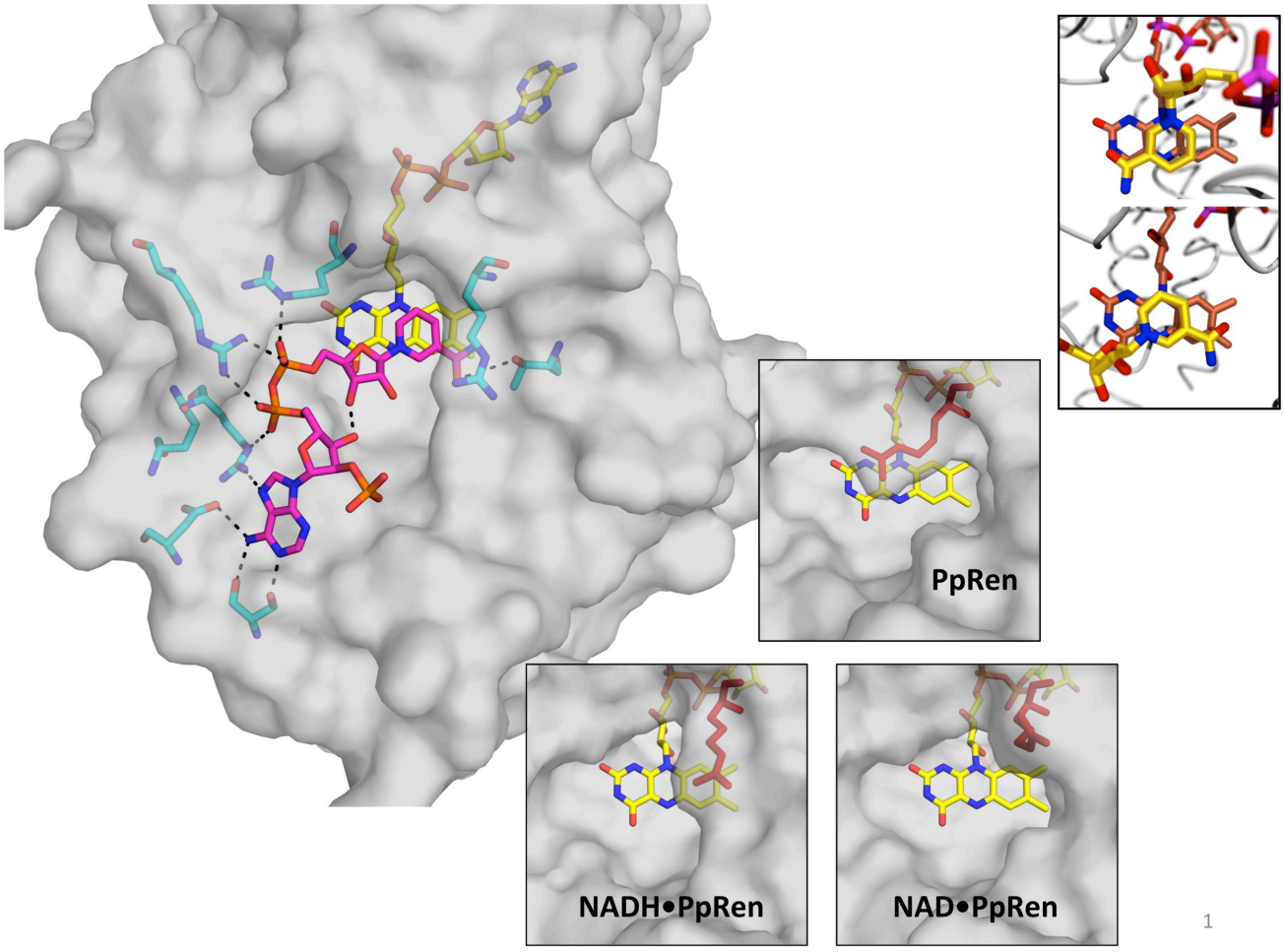

Figure 1.1 Renalase active site as determined by X-ray crystallography. Detailed views of relevant complexes included in insets (ligands omitted for clarity). Inset above, right: top image shows binding pose of nicotinamide in glutathione reductase complex; bottom image shows that of renalase.

Glutamate Formiminotransferase

5-formyltetrahydrofolate (5-FTHF), also known as leucovorin, is an endogenous metabolite that has also been used for decades in cancer chemotherapy, as a rescue agent for methotrexate toxicity and in combination with 5-fluorouracil [39]. Once thought to be of no physiological significance, recent findings suggest that it may play an important metabolic role. Comprising 3-10% of the cellular folate pool in mammals [40], 5-FTHF is not used as a one-carbon donor like other folate derivatives but inhibits other folate-dependent enzymes, including serine hydroxymethyltransferase (SHMT).

Notably, enzymes involved in *de novo* purine biosynthesis are inhibited by 5-FTHF with high potency [41]. For these reasons, it has been proposed that 5-FTHF may serve as a regulator molecule, especially in purine biosynthesis; however, owing to its chemical stability and the observation that it accumulates in seeds and spores, another possible role ascribed to this metabolite is that it serves as a storage form of folate, supported both by *in vitro* studies and in human neuroblastoma models [41]. Other evidence *in vivo* suggests it may be involved in the regulation of homocysteine methylation and serine metabolism by feedback inhibition of SHMT [42].

In 1990, Stover and Schirch [43] discovered that 5-FTHF may be produced in a side-reaction of the PLP-dependent enzyme serine hydroxymethyltransferase (SHMT) using 5,10-methenyltetrahydrofolate (MTHF) as its substrate, and it was shown in 2000 [44] that methenyltetrahydrofolate hydrolyzes nonenzymatically to 5-FTHF in aqeous solutions at low pH. Because of its inhibitory properties, the accumulation of 5-FTHF must be strictly regulated; in eukarytoes, this task is performed by the ATP-denpendent enzyme 5-formyltetrahydrofolate cycloligase (5-FCL), which converts 5-FTHF back to MTHF in a single step (Scheme 1.10). Most prokaryotes share this activity, and 5-FCL is the major enzyme responsible for 5-FTHF metabolism across all domains of life. Concurrent with a six-fold increase in 5-FTHF accumulation in E. coli 5-FCL knockouts [45], a severe cell growth defect was observed, underscoring the metabolic importance of this enzyme.

Curiously however, bionformatic approaches revealed a number of prokaryotes lacking a gene for 5-FCL [45]. 621 bacterial genomes and 19 archaeal genomes were analyzed using the SEED database, yielding 555 genomes containing a known SHMT gene along with 5-FCL, and 63 with SHMT alone and containing no known 5-FCL gene. It was unclear at the time what enzyme or pathway in these organisms is responsible for regulating the accumulation of 5-FTHF. Early evidence in identifying

such an enzyme was given by comparative genomics. In most organisms found to lack these genes, a pair of other genes were found, coding for the enzyme complex glutamate formiminotransferase-cyclodeaminase, a folate-dependent enzyme involved in histidine catabolism. This differs from the pathway usually found (especially in organisms harboring 5-FCL) in which N-formidoyl-L-glutamate is converted to L-glutamate by two separate enzymes, a deiminase followed by a deformylase, both folate-independent.

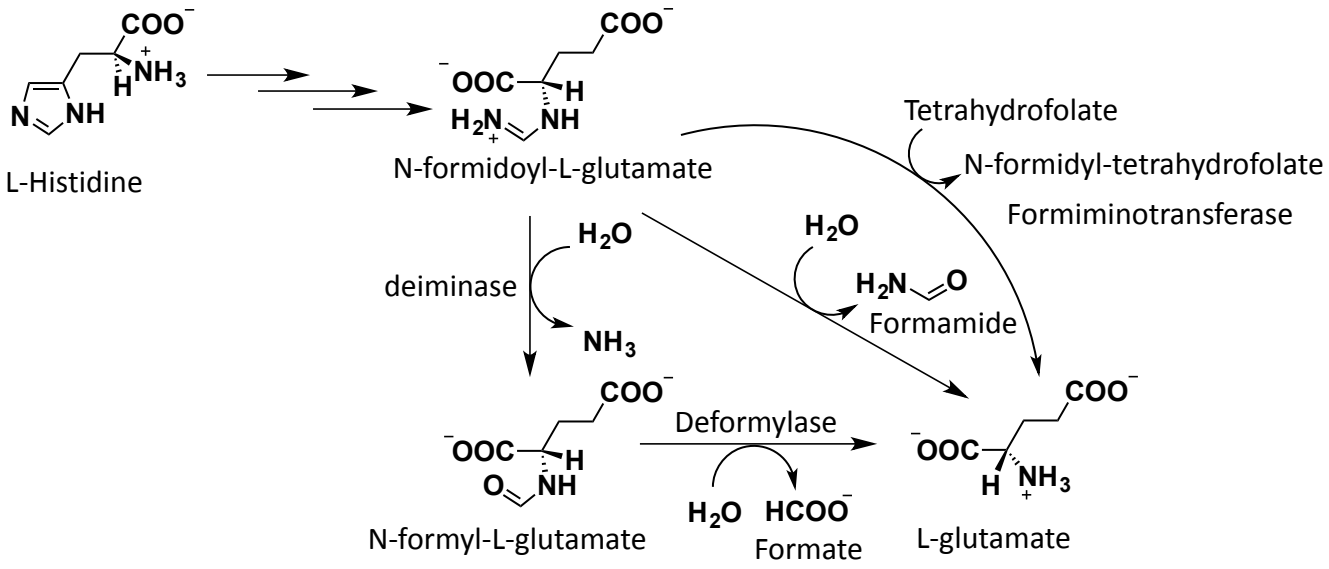

Scheme 1.9. Histidine catabolism pathways. Note that in certain organisms lacking the 5-FCL gene, the usual pathway is often supplanted by the activity of a formiminotransferase.

In some oragnisms lacking the 5-FCL gene, the formiminotransferase (FT) and cyclodeaminase (CD) genes are fused, and in several others, only a gene for the glutamate formiminotransferase domain is found; but most carry at least this FT gene. From this information, it was hypothesized that the isosteric nature of 5-formylTHF and 5-formiminoTHF might allow the former to be used as an alternative substrate for the formyltransferase enzyme, thus converting 5-FTHF and glutamate into tetrahydrofolate and *N*-formylglutamate.

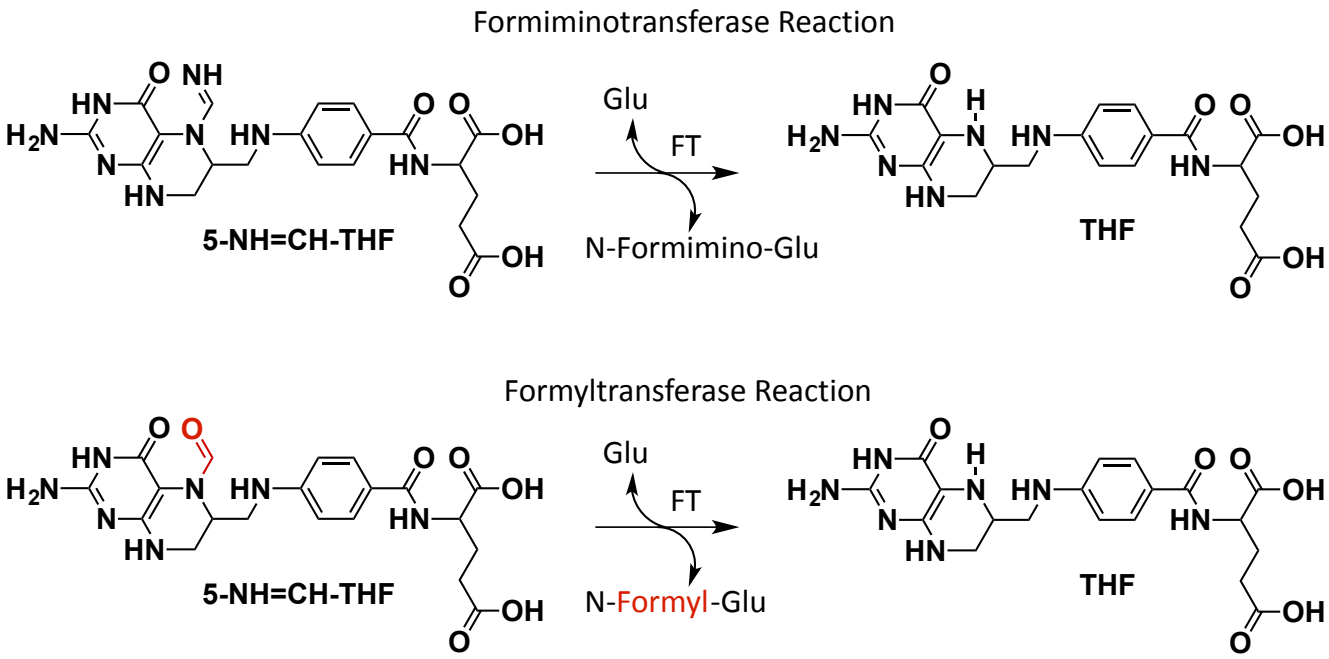

Scheme 1.10. Overall formiminotransferase reaction (above) and observed formyltransferase side-reaction (below).

Jeanguenin *et al.* devised a complementation assay in E. coli using 5-FCL deletion mutants. Cultures of the knockout strain showed a six-fold increase in intracellular 5-FTHF, and also displayed a severe growth defect when cultured using glycine as a nitrogen source. In deletion mutants each transformed with a plasmid harboring a gene encoding a FT from one of five different bacteria and two archaea (each lacking a native 5-FCL gene) was observed a partial or complete reversal of the growth defect. This evidence suggests the activities of the seven FT enzymes tested were able to functionally replace that of the deleted 5-FCL *in vivo*. In order to verify that the activities of the FT enzymes tested were directly responsible for the rescue of normal growth, recombinant enzymes were tested in vitro, detecting products of the formiminotransferase and reverse formyltransferase reactions using spectrophotometry, and of the forward formyltransferase reaction using HPLC for

folate separation and fluorescence for detection. Steady state parameters were measured, yielding k_{cat} vaules in the range of 0.1-1.2 min^{-1}, and K_m values for 5-FTHF and glutamate in the range of 0.4 - 5 µM and 30 µM – 1 mM, respectively. While each enzyme was shown to have lower specificity for the formyltransferase reaction than for its usual formiminotransferase activity, specificity of the former was still sufficient in most cases to suggest significant metabolic flux through this pathway, thus validating the results *in vivo*. It is also interesting to note that mammalian FT enzymes and those found in other organisms also containing 5-FCL have much lower specificites for the formyltransferase reaction than those measured here. Together, these results suggest that in these prokaryotes, the moonlighting formyltransferase activity of the enzyme glutamate formiminotransferase of histidine catabolism is able to functionally replace the activity of 5-FTHF cycloligase in regulating the pool of 5-FTHF, which is so vital to metabolism.

While MTHF may hydrolyze nonenzymatically to form 5-FTHF thus adding to the pool of this metabolite, there is a question as to whether the serine hydroxymethyltransferase side-reaction forming this molecule is adventitious or purposeful. Recent evidence suggests that 5-FTHF may play a role in folate storage or in regulating certain pathways including homocysteine methylation and serine biosynthesis. If purposeful, this side-reaction might not be classified as “metabolite damage”. That the distinction is unclear in this case is interesting because it highlights the fact that new functions may be discovered for endogenous molecules once thought to be adventitious damage products. Further, such a molecule without function in one organism may have one in another, and, a metabolic role for such a molecule once without function may even evolve over many generations.

Chapter II
The Enzyme: Renalase

Graham R. Moran and Matthew R. Hoag

Abstract

Within the last two years catalytic substrates for renalase have been identified, some 10 years after its initial discovery. 2- and 6-dihydronicotinamide (2- and 6-DHNAD) isomers of β-NAD(P)H (4-dihydroNAD(P)) are rapidly oxidized by renalase to form β-NAD(P)$^+$. The two electrons liberated are then passed to molecular oxygen by the renalase FAD cofactor forming hydrogen peroxide. This activity would appear to serve an intracellular detoxification/metabolite repair function that alleviates inhibition of primary metabolism dehydrogenases by 2- and 6-DHNAD molecules. This activity is supported by the complete structural assignment of the substrates, comprehensive kinetic analyses, defined species specific substrate specificity profiles and X-ray crystal structures that reveal ligand complexation consistent with this activity. This apparently intracellular function for the renalase enzyme is not allied with the majority of the renalase research that holds renalase to be a secreted mammalian protein that functions in blood to elicit a broad array of profound physiological changes. In this review a description of renalase as an enzyme is presented and an argument is offered that its enzymatic function can now reasonably be assumed to be uncoupled from whole organism physiological influences.

Introduction

Renalase is a flavoprotein oxidase whose name reflects the context of its discovery. First identified in 2005 by a nephrology group at Yale School of Medicine, renalase emerged from specific search criteria applied to the Mammalian Gene Collection Project. The search requirements included: low sequence similarity to known proteins, a lack of membrane association motifs, and sequence elements indicative of secretion. From 114 candidate proteins, renalase was selected as a result of a prominent expression profile in the kidney[46]. The kernel of the discovery article, that renalase is secreted into blood, has fueled a proliferation of ideas as to its actual role in mammalian physiology [47-70].

Since its discovery a sustained and corroborated research thread for a physiological function for renalase has remained elusive. In general, and despite some exceedingly profound therapeutic implications, a significant number of physiological claims made for renalase have remained thematically isolated as terminal assertions, unverified by subsequent supporting evidence or therapeutic use[47, 53, 57, 68, 69]. Amid the claims of both systemic and localized physiological functions, no role has emerged as the consensus understanding of renalase's physiological influence. Moreover, the preponderance of the renalase literature has been and continues to be studies based on correlation or association that is offered without associated causal links in the form of cellular mechanism (for reviews see [71, 72]). Other than the very initial claims of activity, the biochemistry of renalase specifically with regard to its catalytic function has developed along a path that is largely independent of physiological observations. Furthermore, relatively recent advances regarding the catalytic chemistry of renalase do seem to have identified a single catalytic function and defined

intracellular metabolic role for the enzyme. Rather than attempt to summarize the evidence for each physiological association made for renalase, this review will focus primarily on those observations that describe renalase as an enzyme and place it in the context of an apparent intracellular metabolic role that may yet prove to be common to many forms of life.

Structure

The transcript identified in the progenitor article for renalase described Northern blot analysis for various tissues. Detected were a dominant 1.5 kb mRNA prominent in the heart, skeletal muscle, kidney and liver, a less abundant mRNA of 1.2 kb in the kidney and liver and a 2.4 kb transcript observed primarily in skeletal muscle, indicating the potential for mRNA splice variants. The dominant mRNA proved to be 1,474 nucleotides in length and coded for a protein of 342 amino acids with a predicted mass of 37.8 KDa. The human renalase gene was mapped to chromosome 10 and spanned ~300,000 bp. In all there have been five conflicting reports of exon/intron arrangements and splice variants for renalase [46, 49, 60, 72, 73]. In the most recent, Baroni et al., define the renalase gene as having eleven exons from which the two dominant transcripts are formed from seven (Figure 2.1).

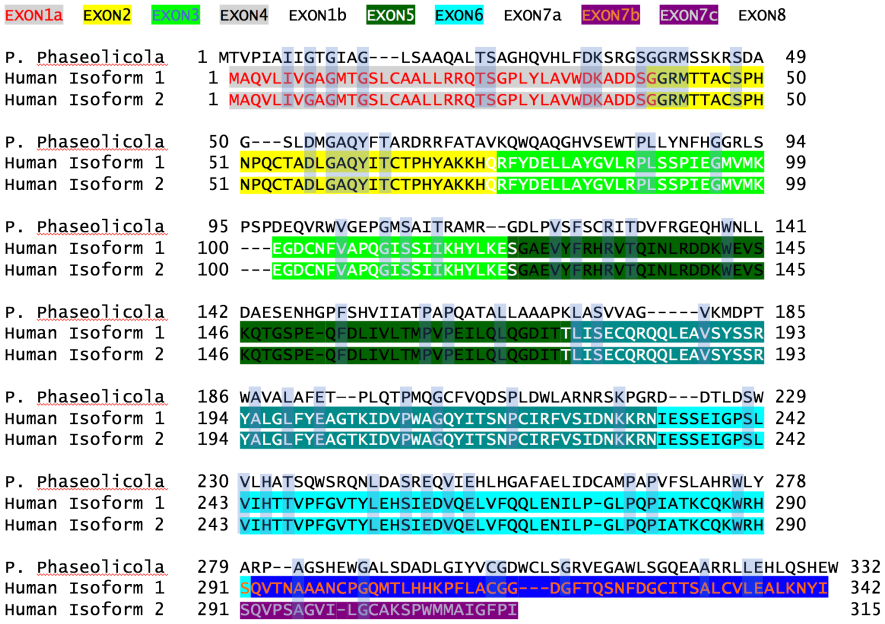

Figure 2.1 Human and Bacterial Renalase Primary Structures. The *Pseudomonas phaseolicola* and human renalase sequences are shown aligned by the ClustalW algorithm. Conserved residues are indicated by transparent blue rectangles. Coloration of the human renalase sequences indicate exon boundaries. Exons designated with a numeral 1 code for N-terminal protein sequences, whilst those with a numeral 7 code for C-terminal protein sequences according to the assignment of Baroni et al.[72]. The splicing arrangement for the two predominant isoforms is depicted but only isoform 1 has been shown to be catalytically active.

It is not currently possible to perform reliable cross-kingdom identification of a renalase from primary structure alignment. The annotation of genome sequences has assigned numerous predicted renalases [74], but at the time of this review only three renalases have been verified from a common catalytic activity. The primary structure of human renalase isoform 1 is relatively highly conserved among vertebrates (~52% identity), but this level of conservation can drop below 10% when a wider swath of putative renalase sequences from the *Animalia* are incorporated. The human sequence does not retrieve sequences from any Kingdom other than the *Animalia* when used as a reference sequence in BLAST (NCBI). This arises from the fact that a renalase sequence does not appear to have signature motifs that can be used to identify candidate renalase sequences with surety. The three

forms of renalase that have been identified by verification of a specific catalytic activity are Human[35], *Pseudomonas phaseolicola*[38] and *P. aeruginosa* (unpublished data, Moran laboratory). Conservation between the human and these bacterial renalases is less than 18%, well below the generally accepted threshold for significant similarity (~30 % [75]) (Figure 2.1).

Despite the lack of sequence conservation, known renalases have the same tertiary structure (Figure 2.2). Preceding the identification of substrates for renalase, the Aliverti group developed heterologous expression methods that provided soluble renalase in good quantity [76] and soon after determined the three-dimensional structure of the protein to a resolution of 2.5 Å (PDB ID 3QJ4)[77] using a molecular replacement routine based on another deposited structure of a putative oxidoreductase of unknown function from *P. phaseolicola* (PDB ID 3KKJ – deposited by the North East Structural Genomics Consortium and identified in the deposition as from *P. syringae* as a result of strain contamination). This reference oxidoreductase was shown to be a renalase four years later [38]. The tertiary structure of renalase is comprised of approximately equal proportions of α and β secondary structure, that together account for half the primary structure. The enzyme carries a flavin adenine dinucleotide (FAD) cofactor, the majority of which is buried within the protein in an extended conformation. The adenylate moiety interacts with a Rossman-fold that is formed from residues near to the N-terminus (see GXGXXG motif in Figure 2.1, position 8). The isoalloxazine ring emerges at one end of an extended cleft on the surface of the protein that is rimmed by four arginine residues (Figure 2.2).

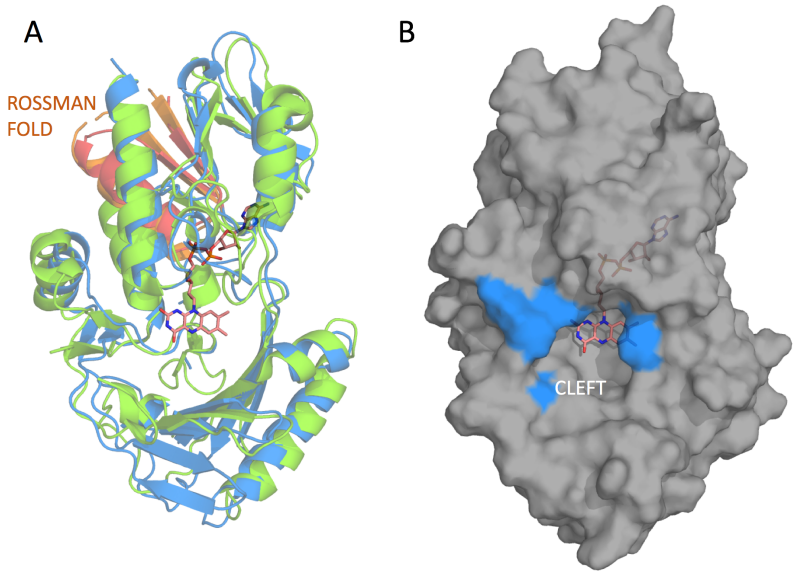

Figure 2.2. The 3-dimensional structure of renalase. A: Cartoon representation of Human (green) and *P. phaseolicola* (blue) protein folds. The Rossman fold for each is formed from the first ~30 residues and is highlighted in orange and red respectively. B: Solvent accessible surface of the open form of *P. phaseolicola* renalase indicating the exposed isoalloxazine of the FAD at one end of a cleft in the structure. The surface of arginine residues (61, 102, 280, and 308) that border the cleft, are colored in blue.

The renalase topology is a known fold that is common to a variety of redox active flavoproteins [77]. Milani et al., cataloged the more closely related members of this family in terms of root mean square deviation (RMSD) for 280-290 peptide Cα carbons. These were, 2.7 Å RMSD for protoporphyrinogen oxidase (PDB ID 3LOV), 2.5 Å RMSD for L-amino acid oxidase (PDB ID 2JB2), and 3.0 Å RMSD for monoamine oxidase (PDB ID 2BXR). An interesting aspect of the Human (HsRen) structure noted by Milani et al. is disorder in the K99-E100 loop that is also the relative structural position of inserted additional domains in the structurally related proteins that provide membrane association, oligomerization, or substrate access portal functionalities. While the broad reaction class to which the related enzymes belong is consistent with the activity that renalase was ultimately observed to possess, none of these proteins have active site residues that coincide with those observed in renalase.

β-NADH and β-NADPH were claimed as renalase co-substrates [55], but this was later disproven. Milani et al., showed that β-NADPH and β-NADH are slowly oxidized by renalase, but at limiting rates more consistent with flavin mediated autoxidation than enzyme catalysis (0.002-0.004 s^{-1})[77]. However, the Km values obtained in these experiments suggested a specific binding interaction was occurring (Km^{NADH} = 18 μM, Km^{NADPH}= 175 μM). In addition, low mMolar binding constants for β-NAD^+ and β-$NADP^+$ could be measured from isotherms based on perturbation of the flavin spectrum. It transpired that β-NADH and β-NADPH were isomeric substrate analogs and β-NAD^+ and β-$NADP^+$ were both products of renalase catalysis. Complexes of renalase from *P. phaseolicola* (PpRen) in complex with such ligands were solved in 2015 and 2016 [38, 78]. Crystals of this form of renalase were soaked with either β-NAD^+, β-NADH or β-NADPH and the structure of each complex determined (respective PDB IDs 4ZCD (1.66 Å), 4ZCC (2.0 Å), and 5KRQ (2.09 Å)). The $PpRen_{ox}$•β-NADH structure revealed a mode of association that was consistent with substrate reactivity (Figure 2.3). In each of these structures the conformation and relative position of the ligands is largely unchanging. Nicotinamide dinucleotides associate into the cleft in the surface of renalase and adopt a novel conformation in which the ribose of each mononucleotide moiety is within sufficient proximity to hydrogen bond to the other. Unexpectedly, the protein makes no hydrogen bonding interactions with either ribose and instead makes numerous apparent charge pair and hydrogen bond interactions with the pyrophosphate moiety (R308, R61, T59, Y57, Q100, and R102).

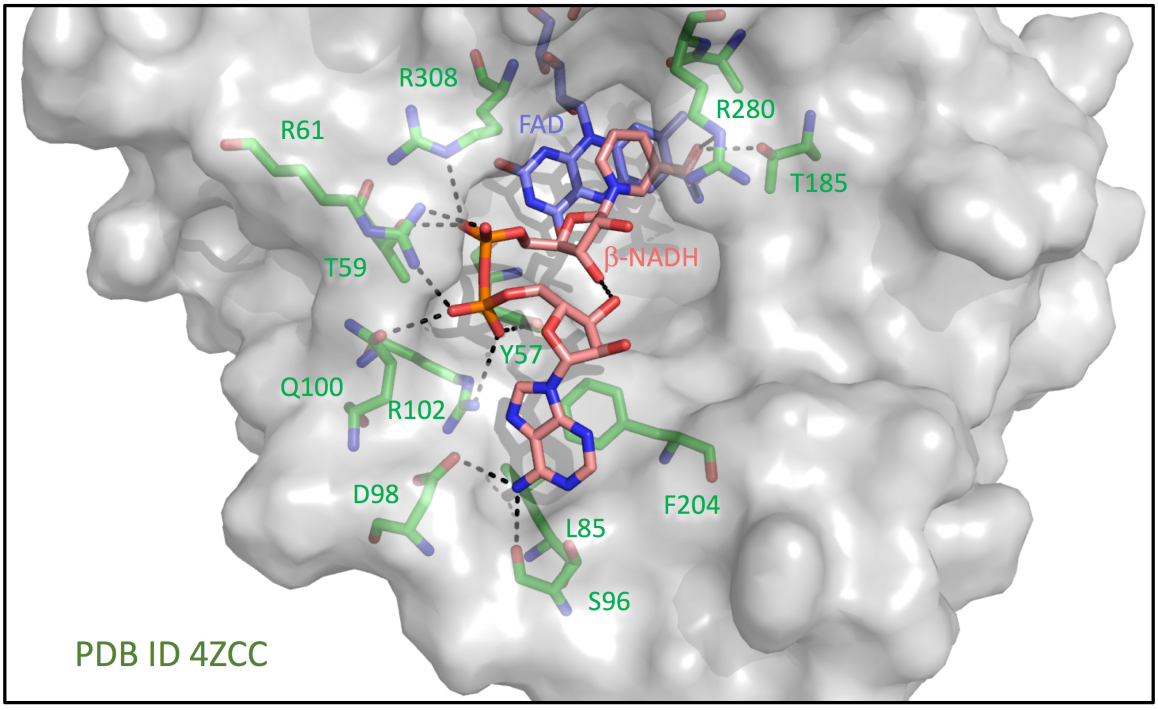

Figure 2.3. The Substrate Binding Site of Renalase. The figure depicts residues observed to come into contact with the substrate analog, β-NADH in the PpRen•NADH complex. Dashes indicate either apparent hydrogen bonds or charge pair interactions.

The apparent catalytic function of renalase is to oxidize isomeric forms of β-NAD(P)H molecules that are reduced at the 2 or 6 position of the nicotinamide ring instead of the metabolically active 4-position (Scheme 2.1)[35].

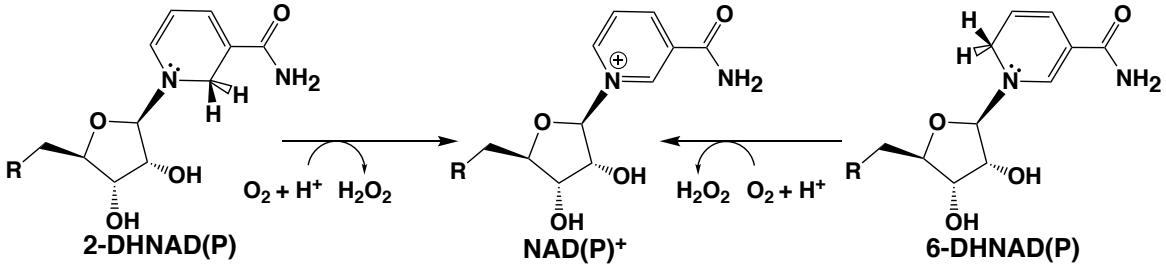

Scheme 2.1. The chemistry catalyzed by renalase.

In the $PpRen_{ox}$•β-NADH complex structure, the nicotinamide ring stacks in a central parallel position relative to the flavin isoalloxazine ring such that the 2-position is 3.6 Å from the flavin N5, a well-established proximity for hydride transfer in flavoproteins [79-81]. This pose of the β-NADH substrate analog accounts for the activity with 2-dihydroNAD(P) (2-DHNAD(P)) substrates but does not account for the oxidation of 6-dihydroNAD(P) (6-DHNAD(P)) substrates by renalase. It was noted that 180-degree rotation about the nicotinamide glycosidic bond would place the 6-position of the nicotinamide ring in an equivalent position with respect to the flavin (Figure 2.4) and two binding modes for the nicotinamide ring would account for the substrate specificity of renalase toward 2- and 6-DHNAD(P) molecules. Hoag et al., modelled the 6-position hydride transfer binding mode into the structure of the $Ppren_{ox}$•β-NADH structure [38]. This exercise indicated that no steric impediment occurs if the substrate were to bind in this conformation. That only the 2-position hydride transfer pose was observed is possibly a result of an apparent hydrogen bonding interaction of the nicotinamide amide with T185 (Figure 2.3), a residue that is unique to the bacterial form(s) of renalase and an interaction that likely accounts for the substrate isomer specificity of the *Pseudomonas* enzyme (see below).

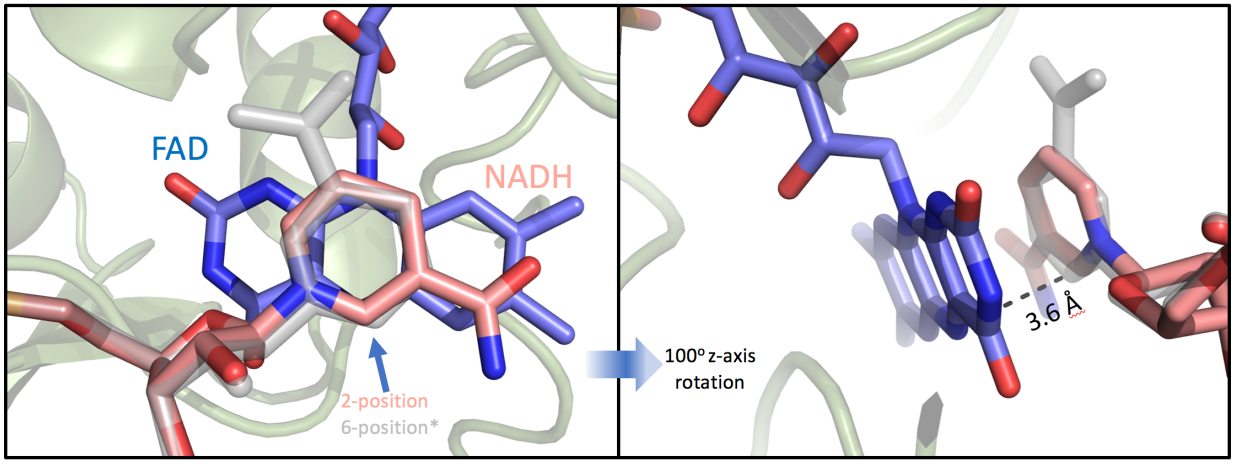

Figure 2.4. The β-NADH Nicotinamide Binding Pose Observed in the $Ppren_{ox}$•β-NADH Complex Structure (PDB ID4ZCC). Left: Superposition of the observed β-NADH binding conformation that is indicative of hydride transfer from the nicotinamide 2-position and the *hypothetical binding mode (transparent gray) for hydride transfer from the 6-position. Right: Approximately 100-degree rotation from what is depicted to the left; to illustrate the distance between the redox pair.

Together with the unliganded structure (PDB ID 3KKJ) that was deposited prior to the PpRen functional assignment, a relatively complete structural depiction of a single catalytic cycle of renalase can be assembled (Figure 2.5). In the resting state structure, R280 (N292 in HsRen) lies over the re-face of the flavin isoalloxazine. Based on the $PpRen_{ox}$•β-NADH structure, it was assumed that this residue must pivot about its side chain rotomers to expose the isoalloxazine in order for the substrate dihydronicotinamide ring to stack with the flavin and that the enzyme is in rapid equilibrium between these two forms. The open form permits association of the substrate that is catalytically transformed to the $PpRen_{red}$•β-NAD^+ complex. The representative structure obtained for this stage of catalysis was of the $PpRen_{ox}$•β-NAD^+ complex, a redox state that formally does not occur during catalysis of the bacterial enzyme as the $PpRen_{red}$•β-NAD^+ complex was shown to be unreactive with molecular oxygen [38]. However, the $HsRen_{red}$•β-NAD^+ complex is reactive with dioxygen and so the $PpRen_{ox}$•β-NAD^+ has associated mechanistic relevance[34]. Release of the β-NAD^+ product would then return to the free enzyme open/closed equilibrium. In the $PpRen_{ox}$•β-NAD^+ complex structure, R280 adopts a third

position more distant from the now positively charged pyridyl nicotinamide ring of the β-NAD^+ product, suggesting that this residue encourages egress of the product by electrostatic repulsion. The HsRen structure indicates that an arginine guanidino group (R193) is offered to approximately the same position by substituting an arginine in place of T185 (that ligands the substrate amide in the bacterial enzyme) (Figure 2.1).

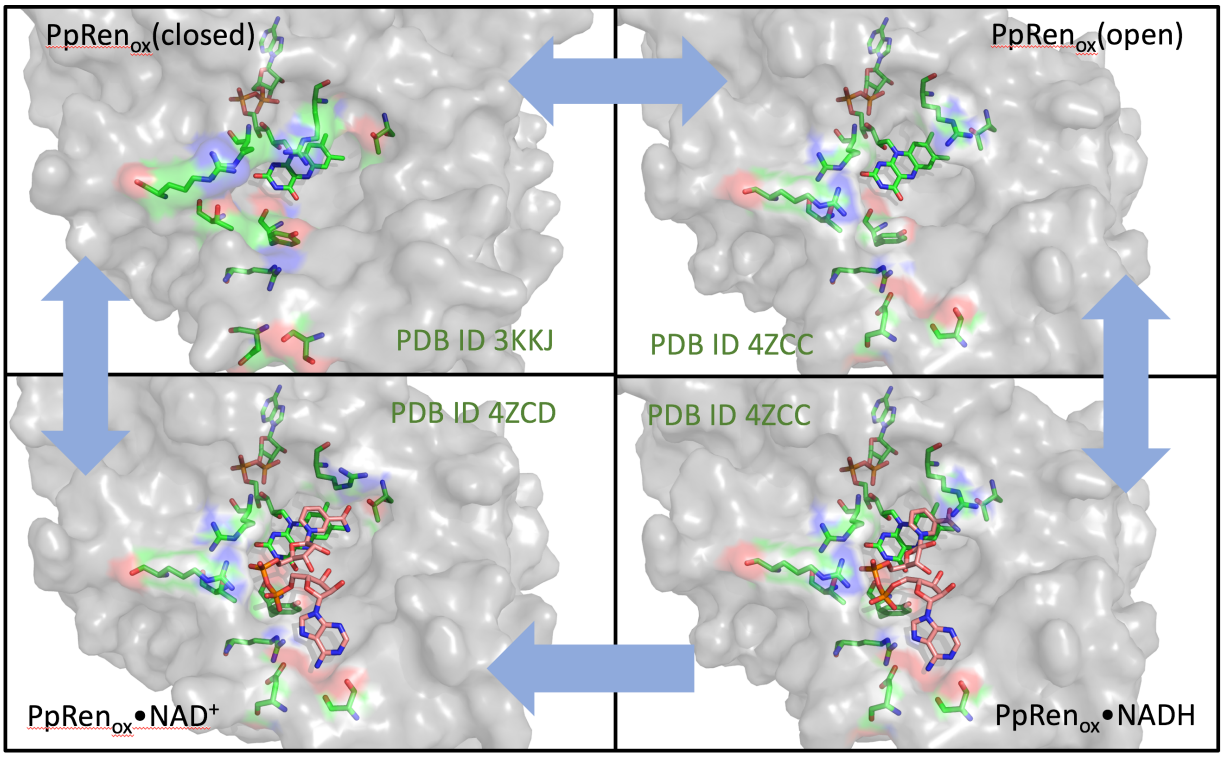

Figure 2.5. An Approximation of the PpRen Catalytic Cycle Based on Available X-ray Crystal Structures. The Figure is assembled from the three available structures for renalase from *P. phaseolicola*. Access of the dihydronicotinamide moiety to the flavin appears gated by the conformation of R280, as such it is proposed that the unliganded enzyme oscillates between open and closed conformation (top structures). Binding of the substrate is represented by the β-NADH complex (bottom right) and the oxidized enzyme product complex (bottom left) which, while descriptive for the binding of this ligand, does not occur in this oxidation state during normal turnover in the *P. phaseolicola* enzyme.

Renalase Substrate and Mechanism

The earliest account of renalase activity was largely based on questionable scientific conclusions. The context and chronology for the activity claims indicate that assignment of function for an enzyme without a functionally relevant operonic relationship to other enzymes or strong homology scores is a formidable undertaking. Sequence alignments, while valuable for the formulation of hypotheses, are not a reliable indicator of catalytic function. Alteration of a single key active site residue can change the reaction class to which an enzyme belongs [82, 83] Alternatively, two enzymes without significant sequence identity can adopt the same structural topology and catalyze the same chemistry, such as is the case for renalase. Or lastly, two enzymes with unrelated structures can possess the same active site residues and function [84]. Nonetheless, it was the very distant sequence similarity to monoamine oxidase enzymes, coupled with sub-borderline evidence for an N-terminal secretory sequence that brought the Desir group to hypothesize that renalase was involved in the oxidative degradation of circulating catecholamines [46]. This hypothesis was bolstered by the observation that a 4 mg/Kg injection of renalase could transiently lower the blood pressure of rats by as much as 40%. It was this latter physiological observation that became the principal driver for broad interest in the function of renalase. However, despite the profound implications of this early observation, this claim has been, from an experimental point of view, abandoned by its primary proponents. Rather than being adopted to a clinical role, ever more prescient mammalian physiological functions for renalase are continuing to be proposed [66-70]. The litany of physiological claims and correlations made for human renalase have been summarized in other recent reviews and are diagrammatically summarized in the last section of this review[72, 85].

The method initially chosen to test for catecholamine oxidase activity was the generic oxidase assay that is peroxidase-based modification of Amplex Red in the presence of hydrogen peroxide. While H_2O_2 was detected, it amounted to an exceedingly low rate of evolution equating to one catalytic cycle each ~42 minutes[46]. What was not accounted for was the known slow background autoxidation of catecholamines in the presence of trace metal ions that independently yields hydrogen peroxide [86, 87]. Together the foundational observations have to be regarded as exceedingly tenuous evidence for what are otherwise compelling ideas. It was Boomsma & Tipton who first questioned these initial renalase claims, noting that the catalytic rate was unlikely to be enzymatic conversion [88]. In the ensuing years, a number of researchers questioned the validity of the catechoalmine oxidase activity claim and other collateral claims [76, 85, 89, 90]. As a counter measure to this criticism the Desir group offered two articles in 2012 that amended the prior activity with catecholamines to include reduced nicotinamide adenine dinucleotides as co-substrates[55, 91], indicating both a much higher rate of H_2O_2 production and aminochrome(s) as the catecholamine oxidation product (Scheme 2.2).

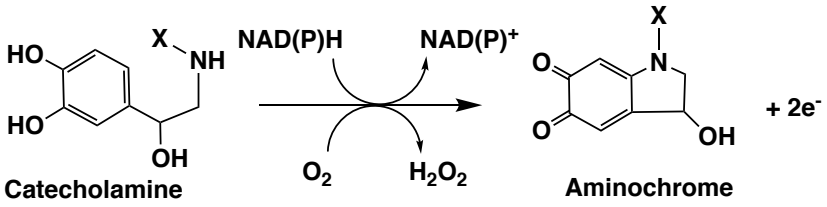

Scheme 2.2. Proposed catecholamine oxidase activity.

Unfortunately, these assertions compounded the errors made with the prior activity claims by neglecting to account for the four electrons liberated in such a reaction and by not gleaning in the interim that aminochromes are the autoxidation product of catecholamines[87]. Moreover, the renalase used in these experiments was heterologously expressed and refolded from inclusion body by a method that has been subsequently shown to yield misfolded inactive renalase peptide [92].

In addition to skepticism, a number of definitive refutations of the catecholamine oxidase activity have been published. Along with exhaustive renalase heterologous expression trials, Pandini et al. tested what proved to be natively folded renalase for activity with catecholamine and observed no evidence of chemistry even after 48 hrs of co-incubation[76]. In 2015, Beaupre et al. observed a complete lack of catecholamine oxidation with renalase that was validated to be highly active [93]. In this study, much like the work of Pandini, co-incubation with epinephrine, L-DOPA, dopamine yielded no indication of consumption or modulation of renalase kinetic behavior (noting that catalytic substrates had been identified prior to this publication – see below).

Ironically, the experimental process that ultimately revealed substrates for renalase was a fortuitous blend of less than ideal procedure, fleeting molecules and what proved to be incorrect assertions. During a series of experiments designed as tests of the validity of prior activity claims for renalase, our group was mixing renalase with β-NADPH under anaerobic conditions. As a consequence of using a β-NADPH solution that had been stored at -20 ^{o}C, fractional rapid reduction of the renalase flavin was observed[94]. A 100-fold excess of this "aged" β-NADPH solution brought about complete reduction of the renalase cofactor with a rate constant of ~40 s^{-1}. This indicated that the β-NADPH solution used contained a contaminant molecule that was a substrate for the enzyme. Plotting the fraction of reduction concentration for renalase versus the bulk β-NADPH concentration revealed the substrate to be a 1.5% impurity. Similar experiments with β-NADH revealed 4% accumulation of

substrate molecules. In both cases the reduced renalase formed reacted with molecular oxygen to form hydrogen peroxide and regenerate the resting enzyme. Analytical HPLC separated the contaminant substrates from the bulk of the sample to reveal unstable molecules (β-NAD or β-NADP derived) with spectrophotometric characteristics that differed from the parent β-NAD(P)H molecule(s). The addition of renalase oxidized the substrates to form β-NAD^+ and β-$NADP^+$ respectively, indicating that the substrates were β-NAD(P)H isomers. On the basis of the spectrophotometric characteristics (λmax 260, 345 nm) [94] and the proportion of each molecule accumulating in solution [95], an initial erroneous assignment of the substrates as α-NAD(P)H molecules was ventured. While this assignment proved to be incorrect, the proposed oxidase/epimerase activity did offer an explanation for the fact that α-$NAD(P)^+$ molecules do not accumulate in the cell despite the α-NAD(P)H/α-$NAD(P)^+$ redox pair having a 20 mV lower potential than the β-NAD(P)H/β-$NAD(P)^+$ redox pair[96, 97].

The actual identity of the fleeting substrate molecules was revealed by examination of a series of research articles that spanned the early-1960s through the late-1970s. Godtfredsen and Ottesen described the accumulation of a molecule that was inhibitory to lactate dehydrogenase when β-NADH was incubated with sparing amounts of water. A tentative assignment of the inhibitor as 6-DHNAD was offered [98]. Possibly as a consequence of their instability, isomer dihydropyridyl NAD(P) molecules, while proposed, had not been structurally assigned [99-101]. Chayken et al., had suggested that 6- and 2-DHNAD molecules could be formed by borohydride reduction of β-NAD^+[102-104]. In 2015 Beaupre et al., reacted the mixture of species formed from borohydride reduction of β-NAD^+ with renalase and observed that of the three products formed, two were oxidized to β-NAD^+ by the enzyme [35]. This suggested that renalase was capable of oxidizing two distinct isomer substrates. In the same study methods were published for the stabilization and preparation of the borohydride

reduction products. These methods allowed near complete structural assignment using NMR and mass spectrometry to definitively show that 6- and 2-dihydroNAD(P) isomers are both catalytically oxidized by renalase (Scheme 2.1). That renalase existed to oxidize these aberrant isomers suggested a metabolite repair or detoxification function that was required as a result of non-enzymatic redox chemistry producing some amount of these molecules intracellularly.

The ability to prepare substrates for renalase facilitated characterization of the enzyme's catalytic cycle. As mentioned above, to date two forms of renalase have been identified, Human (HsRen) and bacterial (PpRen). Both enzymes exhibit highly similar kinetic mechanisms to accomplish relatively simple classical diaphorase/oxidase chemistry and both have been studied using transient state kinetic methods applied to the reductive and oxidative half reactions. Scheme 2.3 depicts a catalytic cycle for renalase that is generic to the four known substrates and the two known forms of the enzyme. In all cases substrates bind rapidly and achieve equilibrium concentrations of the ES complex within one millisecond followed by reduction of the flavin. The $PpRen_{ox}$•β-NADH structure suggests that the substrate is positioned for hydride transfer (Figure 2.4) from the 2-position of the nicotinamide. If we assume that 6-position hydride transfer is permitted by the substrate associating with the enzyme with its nicotinamide base flipped about the glycosidic bond (the conformation that was not observed in the PpRen•β-NADH structure), the pro-S hydrogen would be transferred for both substrates.

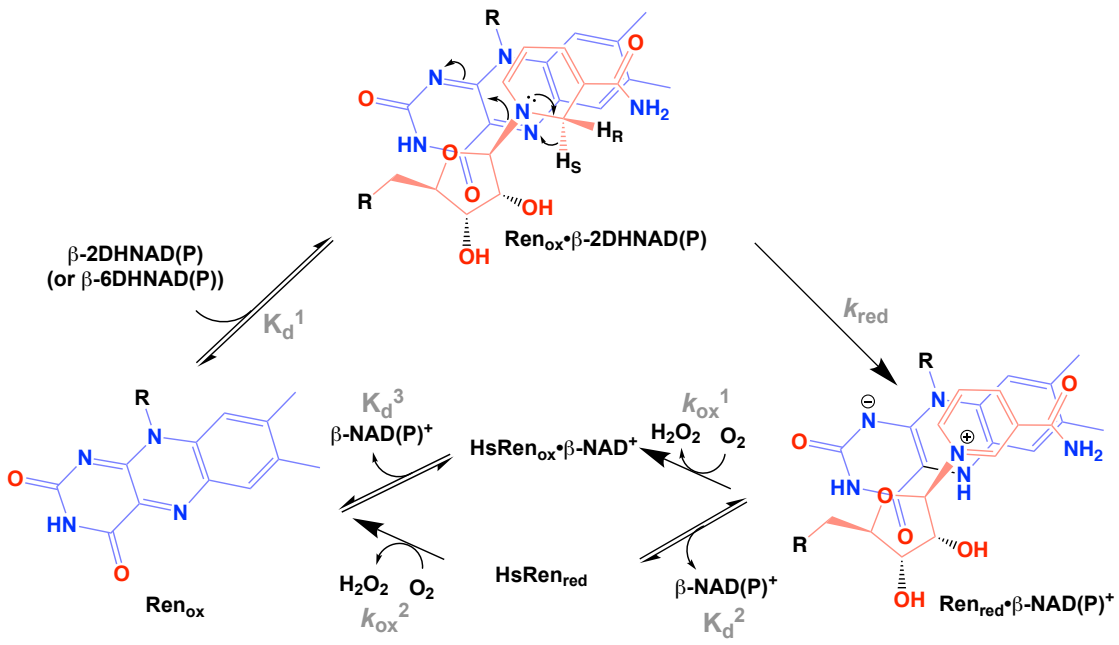

Scheme 2.3. The chemical and kinetic mechanisms of renalase.

The rate for hydride transfer (k_{red}) was observed to titrate to a limit in both the HsRen and PpRen enzymes. The dependence of the observed rate of reduction provided a means of determining the dissociation constant for the substrate in each case. These data indicate defined substrate isomer preferences (in terms of reduction rate constant) in the bacterial enzyme and suggest relatively little discrimination in the human (these data are summarized in Table 2.1). Overall the data available are more complete for the bacterial form of the enzyme. PpRen is observed to reduce rapidly with 2-DHNAD(P) substrates (~80-130 s^{-1}) but quite slowly with 6-DHNAD(P) substrates (0.4-0.5 s^{-1})[38]. HsRen however, reduces only ~4-fold more rapidly with the 2-DHNAD compared to 6DHNAD[35]. The bacterial from of the enzyme also displays dinucleotide specificity in terms of binding constant (K_d^1). In each case β-NAD^+ derived substrates bind 10-50-fold more tightly than do those derived from β-$NADP^+$, equating to a 7-10 kJ/mol difference in binding energy. The substrate specificity profile of the bacterial enzyme can be accounted for by examination of the structures of the $PpRen_{ox}$•β-NADH and

$PpRen_{ox}$•β-NADPH complexes. The relative fast rate constant for reduction observed with 2-DHNAD(P) substrates would appear to be a result of a hydrogen bond from the nicotinamide amide to T185 that pre-organizes the substrate for hydride transfer from the nicotinamide 2-position (Figure 2.2). The decrease in binding affinity for β-$NADP^+$ derived substrates is apparently a result of the 2'-phospho group being highly solvent exposed and having no apparent favorable interactions with the protein, indicating that substrates of that type are more partitioned into solvent[78].

Table 2.1. Summary of the Measured Kinetic and Equilibrium Constants for Renalase.

PpRen	Ligand	K_d^1 (μM)	k_{red} (s^{-1})	k_{red}/K_d ($\mu M^{-1}s^{-1}$)	K_d^2(μM)	K_d^3(μM)
	2DHNAD	36 ± 8	134 ± 2	3.7 ± 0.8		
	2DHNADP	468 ± 71	84 ± 3	0.18 ± 0.02		
	6DHNAD	28 ± 3	0.39 ± 0.01	0.014 ± 0.002		
	6DHNADP	1380 ± 210	0.50 ± 0.05	$3.6 \pm 0.7 \times 10^{-4}$		
	β-NADH	81 ± 7	~0.0008 ± 0.00001	$9.8 \pm 0.8 \times 10^{-6}$		
	β-NADPH	1540 ± 370	n.m.[a]	n.m.[a]		
	β-NAD^+				234±10	n.a.[b]
	β-$NADP^+$				n.m.[a]	n.a.[b]
HsRen						
	2DHNAD	166±6	860±190	5.1±1.2		
	6DHNAD	173±14	234±7	1.4±0.1		
	β-NADH	580±90	n.m.[a]			
	β-NADPH	1500±400	n.m.[a]			
	β-NAD^+				5,950±800	5,950±800
	β-$NADP^+$				3,200	2,200±100

a- not measured, *b*- not applicable

With hydride transfer the Ren_{red}•β-$NAD(P)^+$ complex is formed. Compared to other flavoproteins that use dioxygen as a substrate[105], reduced renalase enzymes react relatively slowly with molecular oxygen (forming hydrogen peroxide). The reactivity of this complex toward molecular oxygen defines another difference between the human and bacterial enzymes. The $HsRen_{red}$•β-$NAD(P)^+$ complex is reactive with dioxygen with a bimolecular rate constant of ~3,000 $M^{-1}s^{-1}$. Titration of product (β-$NAD(P)^+$) does not modulate the observed rate of reoxidation, indicating that the

$HsRen_{red}$•β-NAD(P)$^+$ and $HsRen_{red}$ states are equally reactive. This dictates that the process of product release is formally random in the human enzyme (Scheme 2.3). However, the release of products is in all likelihood kinetically-ordered as there is no evidence that the release of the β-NAD(P)$^+$ products contributes to the turnover number, indicating that the dissociation of the β-NAD(P)$^+$ greatly outpaces the reoxidation reaction (even at the solubility limit of dioxygen). The bacterial form of the enzyme reoxidizes with a rate constant of ~5,000 $M^{-1}s^{-1}$, but the observed rate can be suppressed to zero by titrating β-NAD(P)$^+$, dictating that the $PpRen_{red}$•β-NAD(P)$^+$ complex is unreactive with dioxygen and that the evolution of products is strictly ordered (via K_d^2 to k_{ox}^2 in Scheme 2.3). As such, the differing product release mechanisms arising from changes to the dioxygen reactivity do not distinctly alter the kinetic mechanism of one enzyme relative to the other. Within the cell, however, β-NAD(P)$^+$ will suppress the rate of turnover for the bacterial enzyme by hindering reoxidation.

The question of intrinsic inhibition of renalase under cellular conditions is a particularly curious one. Human renalase displays a 3-fold isomer selectivity, binding 4-DHNAD (β-NADH) with slightly less affinity than 2-DHNAD and 6-DHNAD[35]. Bacterial renalase however, has ostensibly no isomer binding selectivity[38](K_d^1, Table 2.1, Scheme 2.3). Moreover, the reduced form of the bacterial enzyme exhibits relatively high affinity for β-NAD$^+$, whereas the reduced human enzyme has considerably less affinity for product (K_d^2, Table 2.1, Scheme 2.3). Given that β-NAD(P) molecules abound intracellularly, renalases must perform their specific metabolic function whilst partially inhibited by either of the non-catalytic isomer(s) (β-NAD(P)H) or product(s) (β-NAD(P)$^+$). The former is likely a function of the fact that the dihydronicotinamide ring, when reduced at the 2, 6 or 4-position is as electron replete and largely geometrically unchanged, undermining the ability of renalase to discriminate between the isomers. Added to this phenomenon is the fact that any binding constant for a β-NAD(P) derived ligand will be composite for both binding modes (Figure 2.4), modified by one or

both of the proposed binding modes. As such, it is reasonable to conclude that renalases function in a partially inhibitory environment.

The inability of renalase to discriminate between β-NAD(P)H isomers led Beaupre et al., to propose a metabolic function for renalase[35, 98]. It was presumed that other β-NAD(P)H-dependent enzymes may experience inhibition by 2- and 6-DHNAD molecules. As such a variety of β-NAD(P)H-dependent enzymes were tested for inhibition by 2- and 6-DHNAD(P) (Table 2.2). These data convincingly indicate that the non-cononical β-NAD(P)H isomers are potentially highly toxic to the cell, impeding the function of multiple primary metabolism dehydrogenase enzymes with μM to low nM Ki values.

Table 2.2. Binding Constants for NAD(P)H Isomers to Various Dehydrogenases.

Enzyme	6DHNAD K_i (μM)[a]	2DHNAD K_i (μM)[b]
P. phaseolicola **GAPDH**[d]	176±33.5	1.63±0.195
P. phaseolicola **IDH**[d]	0.445±0.043	1.39±0.130
P. phaseolicola **ME**[d]	2.33±0.130	4.51±0.185
P. phaseolicola **DLD**[d]	n.i.[c]	n.i.[c]
Rabbit LDH	0.512±0.065	0.585±0.037
E. coli **MDH**	0.034±0.003	3.1±0.3
Pig DLD	n.i.[c]	n.i.[c]

a-determined by global fits of nested Michaelis curves to a competitive inhibition model, *b*-determined by IC_{50} analysis at a β-NAD(P)H substrate concentration equivalent to the Km value. *c*-no inhibition observed. *d*-unpublished data, Moran group. GAPDH-glyceraldehyde-3-phosphate dehydrogenase, IDH-isocitrate dehydrogenase, ME-malic enzyme, DLD – lipoamide dehydrogenase, LDH-lactate dehydrogenase, MDH-malate dehydrogenase.

To demonstrate the mode of inhibition, the structure of two dehydrogenases were solved in complex with 6DHNAD [78]. The structures of *E. coli* malate dehydrogenase and rabbit lactate dehydrogenase confirmed that in each enzyme the inhibitor binds in the site normally occupied by β-NADH (Figure 2.6). For the protein crystals used to determine both structures, occupancy of the ligand

was verified by single crystal spectrophotometry where the dihydronicotinamide chromophore was confirmed. An interesting observation associated with this study is that the otherwise unstable 6DNADH added to form these crystal complexes persisted throughout the period required to form crystals (3-14 days)[78], indicating that inhibitory complexes may, at least in some cases, sequester and stabilize the renalase substrate β-NAD(P)H isomers from solution where they tend to decompose.

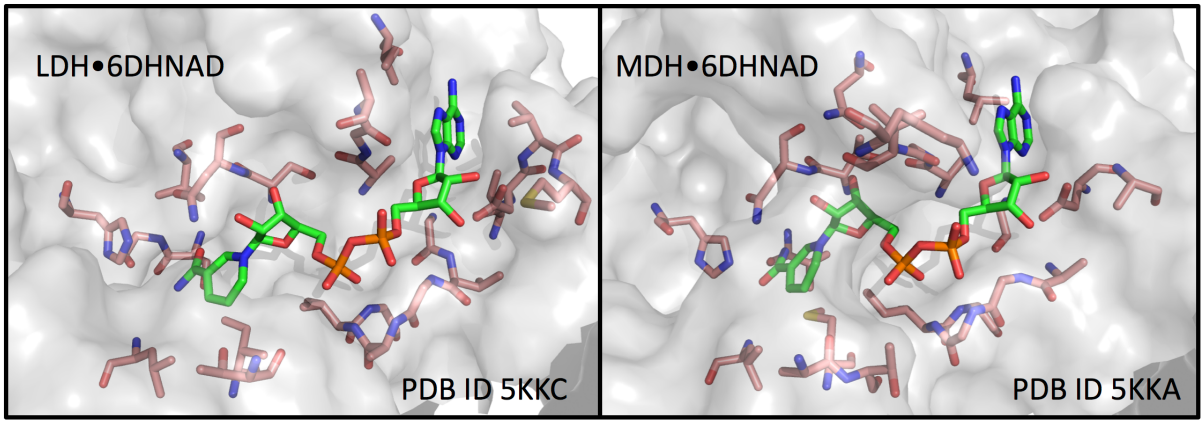

Figure 2.6. Representative Structures of 6DHNAD•Dehydrogenase Inhibition Complexes. Left: lactate dehydrogenase in complex with 6DHNAD. Right: malate dehydrogenase in complex with 6DHNAD. In both cases the residues that contact the inhibitor (within 4 Å) are shown.

Concluding Discussion

Within the last five years it has become evident that the catalytic function of renalase is most likely uncoupled from systemic influence of mammalian physiology. Since its discovery, the breadth of inquiry has grown to encompass additional physiological influences that do not rely on renalase catalysis. In Figure 2.7 a timeline of the primary physiological and biochemical discoveries for renalase is depicted. From this diagram, it is possible to quickly visualize the diverse themes within the chronology of research pertaining to renalase. In this review, we have primarily described the data that supports an intracellular catalytic function for renalase that accomplishes detoxification/metabolite repair of relatively unstable isomeric forms of β-NAD(P)H molecules (depicted in violet in Figure 2.7). A deficiency in this argument is that this somewhat obscure set of

molecules has not yet been observed within cells. The rather convenient rationalization for this is that they form in rare non-enzymatic redox events and decay relatively rapidly and/or are maintained near zero concentration by the activity of renalase [34]. Evidence for their potential occurrence is that, 2- and 6DHNAD molecules are observed to accumulate in solutions of β-NAD(P)H molecules [98, 101] and both can be formed by *in vitro* reduction of β-NAD(P)$^+$ molecules[102]. However, it is correct to acknowledge that whether β-NAD(P)H dihydronicotinamide isomers are endogenous to cells remains to be supported by experiment. What is clear is that they are inhibitory to a variety of enzymes that have β-NAD(P) molecules as substrates.

The initial proposed function of renalase as a globular mammalian protein that is secreted from the kidney into the circulatory system to influence blood pressure and heart rate by the oxidation of catecholamines is arguably debunked [76, 88, 89, 93] (indicated in black in Figure 2.7). Moreover, the unlikely validity of these linked notions has been conceded by its initial proponents, to their credit [60]. It is therefore unfortunate that these ideas persist in current literature and that the arguments and experiments that refute them have not been fully accepted [59, 65, 106-108]. It is reasonable to conclude that the claim of catecholamine oxidase activity was a legacy of the failure to account for slow catecholamine autoxidation phenomena, as was originally proposed by Boomsma and Tiption in 2007 [88]. Furthermore, if renalase was able to lower blood pressure to the extent claimed (15-40%) [47, 49, 51, 55, 91, 109], it might be expected that it would currently be moving toward clinical use for hypertension indications, but there is no evidence that this is the case (clinicaltrials.gov) nor is there indication that any research group is currently investigating the renalase/hypertension mechanism as publications in support of this theme ceased in ~2012 (Figure 2.7).

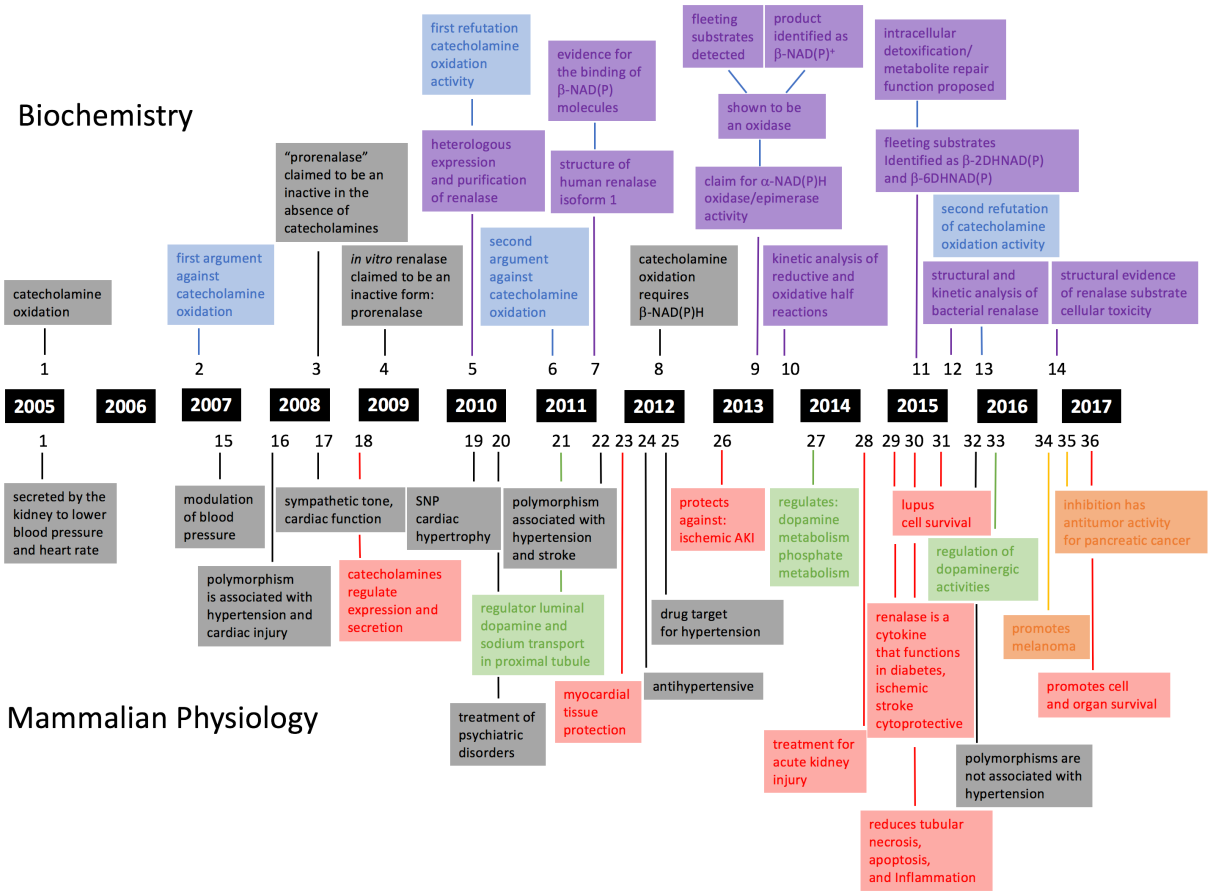

Figure 2.7. A Timeline of the Primary Physiological and Biochemical Discoveries for Renalase. The figure illustrates the chronology of ideas presented since the discovery of the enzyme in 2005 divided into biochemical (above) and physiological (below). Each blue vertical line represents a single research article as follows: 1-[46], 2-[88], 3-[110], 4-[49], 5-[76], 6-[89], 7-[77], 8-[55], 9-[94], 10-[34], 11-[35], 12-[38], 13-[93], 14-[78], 15-[47] 16-[111], 17-[48], 18-[110], 19-[111], 20-[73], 21-[112], 22-[51], 23-[53], 24-[55], 25-[109], 26-[57], 27-[58], 28-[113], 29-[60], 30-[64], 31-[114], 32-[115], 33-[65], 34-[69], 35-[68], 36-[67]. This list excludes some duplicative observations, review articles, and research based solely on association. The discoveries are colored by theme: black is for catecholamine oxidase/hypertension, red is for cellular damage, green is for catecholamine regulation, orange is for cancer, blue is for argument or evidence against catecholamine oxidase activity, and violet is for biochemical observations.

The perceived catalytic function of renalase has passed through a number of phases. First believed to oxidize catecholamines and form hydrogen peroxide [46], then thought to conduct single electron chemistry to make superoxide as an oxidant for catecholamines [55, 59], then said to utilize β-NAD(P)H as a co-substrate with catecholamines to bring about an oxidation and cyclization to form

aminochrome molecules [55] and soon after claimed to oxidize and epimerize α-NAD(P)H molecules [34, 94]. Lastly, and more definitively, renalase has been shown to oxidize 2 and 6-DHNAD(P), an activity presumed to alleviate toxicity resulting from inhibition of dehydrogenase enzymes [35]. This activity would appear to benefit the cell from within and have no clear link to a systemic effect in mammalian physiology. Though initially misidentified, 2- and 6DHNAD(P) molecules are clearly substrates for renalase. These molecules are oxidized with rate constants up to ~1000 s^{-1}; many orders of magnitude more rapid than observations made with catecholamines with or without added β-NAD(P)H[55, 77, 91]. Moreover, renalase enzymes have been identified in *Pseudomonas* species, a form of life that does not require catecholamines or experience hypertension[38].

It would appear that the considerable research investment applied to document the physiological role renalase plays in mammals has diverged from what is now understood of its function as an enzyme. Twelve years on, the net account of the function of renalase in the scientific literature remains quite incongruent. If we remove modulation of vascular tone by the oxidation of catecholamines as a valid thread of scientific inquiry from the renalase record, is it possible to then reconcile the remaining physiological discoveries with what is known of the enzyme's catalysis? Such an endeavor has been made moot by recent findings. Circulating renalase is (or is additionally) a cytoprotective cytokine (indicated in red in Figure 2.7). In this role, renalase is proposed to be the delivery vessel for its N-terminal peptide (CIRFVSIDNKKRNIESSEIG) that binds to PMCA4b calcium-transporting ATPase, stimulating mitogen-activated protein kinases to elicit cellular survival mechanisms [60, 66]. Using only the short peptide it was shown that this role is "independent of its intrinsic enzymatic activities". Another more recent and also potentially highly significant physiological role for renalase, apparently allied with the cytoprotective theme, is as an exacerbatory factor for proliferation of cancers (colored orange in Figure 2.7). Renalase was observed to be upregulated in

certain cancers (amongst many other proteins) [116] and cancer cells with this property are favored for survival and correlated with higher mortality [68, 69]. In addition, anti-renalase antibodies were reported to slow proliferative activity, tying the observation to intercellular signaling via PMCA4b calcium ATPase mediation [60, 66].

Of the ~160 research articles pertaining to renalase, 12 describe experiments that have advanced the biochemical and/or catalytic understanding of the enzyme. Excluding the disproportionate number of review articles (33) and also letters (5), the remainder (107) are focused on the role renalase plays in mammalian physiology. All such articles are predicated on the notion that renalase is secreted into and functions in blood. However, this very fundamental factor has not been independently corroborated [46], despite the fact that renalase has no clear secretion signal (SignalP score of 0.41). There is no disputing that renalase is found in blood [51, 52, 108, 110, 117-123], but it has not been established if the enzyme was purposefully secreted by a specific cell type or simply liberated by cell death, as might be expected for basal cell turnover and additively for numerous pathologies, thereby serving as the basis (and inherent limitation) of correlation[61, 62, 70, 113, 124-132]. What is apparent is that the most current evidence for the physiological function of renalase, as a delivery vessel for a cyto-active peptide, has severed the link to the observations that initially generated and subsequently sustained research interest in this enzyme, i.e. catecholamine oxidation and blood pressure modulation. No doubt, further inquiry and eventual consensus will settle the matter, but at this point in time the continued absence of clinical use or sustained research themes remain juxtaposed to the many profound claims offered for the function of the enzyme (Figure 2.7).

Chapter III
Renalase is an α-NAD(P)H Oxidase/Anomerase

Brett A. Beaupre, Brenton R. Carmichael, Matthew R. Hoag, Dhara D. Shah, and Graham R. Moran

Abstract

Renalase is a protein hormone secreted into blood by the kidney that is reported to lower blood pressure and slow heart rate. Since its discovery in 2005, renalase has been the subject of conjecture pertaining to its catalytic function. While it has been widely reported that renalase is the third monoamine oxidase (monoamine oxidase C) that oxidizes circulating catecholamines such as epinephrine, there has been no convincing demonstration of this catalysis *in vitro*. Renalase is a flavoprotein whose structural topology is similar to known oxidases, lysine demethylases and monooxygenases, but whose active site bears no resemblance to that of any known flavoprotein. We have identified the catalytic activity of renalase as an α-NAD(P)H oxidase/anomerase, whereby low equilibrium concentrations of the α-anomer of NADPH and NADH initiate rapid reduction of the renalase flavin cofactor. The reduced cofactor then reacts with dioxygen to form hydrogen peroxide and releases nicotinamide dinucleotide product in the β-form. These processes yield an apparent turnover number (0.5 s^{-1} in atmospheric dioxygen) that is at least two-orders of magnitude more rapid than any reported activity with catechol neurotransmitters. This highly novel activity is the first demonstration of a role for naturally occurring α-NAD(P)H anomers in mammalian physiology and the first report of a flavoprotein catalyzing an epimerization reaction.

Introduction

Human renalase was first discovered in 2005 by Xu et al. [46, 117] and its discovery spurred considerable interest as the protein was reported to be secreted into blood by the kidney as a hormone to down-modulate blood pressure and cardiac output. [76] These observations have since been associated with the high incidence of cardiovascular disease in patients with end-stage renal disease [53], emphasizing that diminishment of the endocrine function of the kidney is wholly detrimental to cardiac function. [46, 108, 133] In addition, mice deficient in renalase have been reported to exhibit elevated blood pressure [53] and human renalase polymorphisms have been linked with an increased incidence of diabetes and stroke. [124, 134] Since its discovery a definitive demonstration of the catalytic function of renalase has remained elusive. While it has been widely reported that renalase lowers blood pressure and modifies heartbeat by catabolizing circulating catecholamines [49-52, 55, 91, 109], neither the specific substrate(s) and product(s) nor the overall stoichiometry for the reaction has been convincingly established. *In vivo* studies in rodents show that the concentration of circulating catecholic neurotransmitters is lowered by intravenous injection of renalase. [46, 53, 55] However, *in vitro* studies have failed to demonstrate significantly catalytic consumption of catecholic neurotransmitters (or their precursors). [55, 72] It has been claimed that renalase mobilizes four electrons by acquiring two electrons from NAD(P)H in order to catalyze a net two-electron oxidation and cyclization of epinephrine to form adrenochrome. [91] Such a transformation for epinephrine is, however, facile in the absence of an enzyme catalyst and readily observed in oxygenated solutions under a variety of conditions. [135, 136] Similarly, the observation of apparent slow oxidation of reduced pyridine nucleotide cofactors in the presence of renalase is complicated by the inherent instability of these molecules at pH values near or below neutral pH.

[137] As a consequence, claims of renalase directly catalyzing the breakdown of catecholamines has been challenged in both letters and research articles. [72, 73, 88]

The discord in regard to the activity of renalase has developed both from its reported physiological function and from its structural similarity to known redox enzymes. The primary structure of the protein has at least 4 forms that result from RNA splicing patterns for seven exons. Only the two longest sequences that include protein derived from at least six exons show direct similarity to known flavoproteins. [49, 73] The three-dimensional structure of renalase isoform 1 (342 amino acids) was published by Milani et al. 2011. [77] This structure indicated a fold consistent with a large structural family of flavoproteins that include oxidases, lysine demethylases, and monooxygenases. [138-142] The apparent active site of renalase was observed to be a clearly delineated pocket in the surface of the protein that provides access to the *si*-face of a non-covalently bound flavin adenine dinucleotide (FAD) cofactor. Within this cavity, the constellation of residues that are conserved in renalase primary structures gave no clear indication for any known activity of a flavoprotein. However, renalase was observed to readily form an adduct with sulfite ions at the FAD isoalloxazine N5 position, a curious characteristic that is most commonly associated with oxidase activity. [77, 143, 144]

In this article we identify renalase as an α-NAD(P)H oxidase/anomerase whereby the substrate α-dihydropyridyl ring is oxidized by transferring two electrons to the flavin cofactor and the configuration of the ribose C1 is converted from α to β. The reduced FAD cofactor then reoxidizes by reacting with dioxygen to yield hydrogen peroxide (Scheme 3.1). This highly novel transformation is both unprecedented catalytic chemistry and the first physiological link to α-pyridine nucleotides in higher organisms.

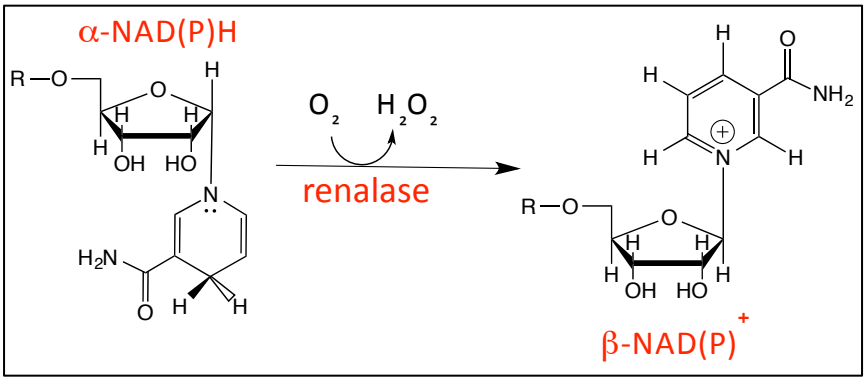

Scheme 3.1. Proposed overall oxidation/anomerization reaction.

Materials and Methods

Materials: Plasmids were purified using the Qiagen Midi-Prep plasmid preparation kit. Oligonucleotides were synthesized by Operon. Vector pET28a(+) was obtained from Novagen. Restriction enzymes, DNA modification enzymes and competent (DH5α and BL21 (DE3)) *E. coli* were obtained from New England Biolabs. FAD, (4-(2-hydroxyethyl)-1-piperazineethanesulfonic acid (HEPES), potassium phosphate, isopropyl-β-thiogalactopyranoside (IPTG) and sodium chloride were from ACROS. Electrophoretic grade agarose was obtained from ICN Biomedicals. Luria Bertani broth (Lennox) powder was from Fisher Scientific. Kanamycin and β-NADPH were purchased from Alexis. β-$NADP^+$ was purchased from Calbiochem. β-NADH, β-NAD^+ and epinephrine were from Sigma-Aldrich.

Cloning and expression of Human Renalase: The gene encoding full length WT Human renalase (isoform 1) optimized for expression in *E. coli* and incorporating Nde I and Xho I sites at the 5' and 3' ends was purchased from Enzymax. The gene was supplied in plasmid pUC57 and subcloned into the Nde I and Xho I restriction sites of pET-28a(+) expression vector (Novagen). The Nde I insertion of pET-28a(+) plasmid incorporates an N-terminal His-Tag fusion. This plasmid (pHSRENHT) was transformed into chemically competent *E. coli* BL21 (DE3) cells (Novagen). All media used with transformed cells

included 100 μg/mL kanamycin. Transformants were plated onto LB agar and a single isolated *E. coli* colony was cultured in LB broth. Individual 1 mL cell stocks were made by adding sterile glycerol to a final concentration of 20% to cells grown to early log phase and these were then stored at -80°C.

Renalase Expression and Purification: For expression, 1 mL cell stocks were thawed, plated onto LB agar, 100 μg/mL kanamycin, and grown overnight at 37°C (50 μL/plate). The lawn of cells obtained were then transferred to LB broth (two plates/L of broth) and grown at 37°C in a shaking incubator (220 rpm) to mid-log phase (OD_{600nm}=0.5) and the temperature lowered to 22°C. The culture was then grown to ~ OD_{600nm}=1.0 (~1 hr) and induced with 0.1 mM IPTG and left to express renalase for 20 hrs before the cells were harvested by centrifugation (4,000 g for 30 min). Unless otherwise stated, all subsequent purification steps were performed at 4°C. Cell pellets were resuspended in 20 mM HEPES buffer pH 7.5 (approximately 10 mL/L culture) and lysed by sonication using a Branson 450 sonicator (3 x 240 seconds at 50 W). The temperature of the cell suspension was maintained below 10°C by immersing the sample vessel in a slurry of ice and water. Lysed cells were centrifuged at 32,800 x g for 30 min, the pellet was discarded and the supernatant loaded onto a 12.5 x 150 mm Co^{2+} Talon column (BD Biosciences) equilibrated with 20 mM HEPES buffer pH 7.5. Protein was eluted with a 1 mL/min two-step protocol. Initially contaminating proteins were eluted with 150 mL of 10 mM imidazole, 50 mM HEPES buffer pH 7.5, then a gradient from 10 mM to 150 mM imidazole in the same buffer was used to elute renalase. Distinctly yellow fractions were pooled. Imidazole was removed and the buffer exchanged to PBS (10 mM Na_2HPO_4, 2 mM KH_2PO_4, 2.7 mM KCl, 137 mM NaCl, pH 7.4) by repeated concentration and dilution using 10 kDa nominal molecular weight cut-off centrifugal concentrator (Millipore, Amicon) to achieve a net ≥1000-fold exchange. Aliquots of purified concentrated renalase were then stored at -80°C.

Quantitation: The concentration of NADPH and NADH solutions were determined using the published 340 nm extinction coefficient of 6200 $M^{-1}cm^{-1}$ [95]. The extinction coefficient for Renalase was determined by liberating the FAD cofactor from the protein. Initially, the absorption spectrum of 9 μM renalase was recorded using a Hewlett Packard 8453 spectrophotometer. SDS to 1% final concentration was then added to denature the protein and release the flavin and the spectrum was again recorded. The spectrum of the unbound flavin was then corrected for dilution and the known extinction coefficient for this molecule at 450 nm (ε_{450nm} = 11,300 $M^{-1}cm^{-1}$) was used to calculate the extinction coefficient of renalase (ε_{458nm} = 11,330 $M^{-1}cm^{-1}$). Epinephrine was quantified by weight.

Substrate/Product Analysis: The apparent substrate for renalase was detected as a contaminant of β-NAD(P)H stocks that caused rapid reduction of the renalase flavin cofactor. The proportion of the substrate in NAD(P)H solutions was determined by two methods. First, relatively high concentrations of β-NADPH were mixed with renalase using a Hi-Tech (now TgK) stopped-flow spectrophotometer under anaerobic conditions. Prior to the experiment, the instrument was scrubbed of residual dioxygen for ~16 hrs using a solution of 50 mM glucose and 15.5 U/mL glucose oxidase. Renalase in PBS buffer was prepared in a tonometer by adding 8 μM enzyme with 1 mM glucose in the body of the vessel and 16 U of glucose oxidase in a side arm (U is defined as 1 unit of enzymatic activity or 1 μmole/min). The tonometer was then subject to 45 cycles of low vacuum followed by argon gas with mild agitation to exchange all dissolved dioxygen. Once anaerobic, the renalase/glucose solution was mixed with the glucose oxidase from the tonometer side arm and the vessel was mounted onto the stopped-flow instrument. NADPH solutions were prepared with 1 mM glucose and made anaerobic by sparging with argon for 5 minutes and then adding in 8 U of glucose oxidase immediately prior to

mounting onto the instrument. Renalase and NADPH were then mixed and the extent of flavin cofactor reduction was recorded at 458 nm. The second method used to determine the proportion of substrate in NAD(P)H solutions was to observe the change in molecular oxygen concentration when high concentrations of NAD(P)H were added to low μMolar concentrations of renalase in PBS buffer using a Hansetech dioxgen electrode. Assuming 1:1 substrate to dioxygen reaction stoichiometry (*vide infra*), the concentration of substrate could be determined from the amplitude of the observed change in molecular oxygen concentration.

Evidence for the identity of the substrate was obtained from HPLC analysis. NAD(P)H solutions (10 mM) were diluted by a factor of 50 and filtered using a Millipore 0.5 mL 10 kDa nominal molecular weight centrifugal filter device. 50 μL of this solution was then injected onto a Waters Xterra C18 cartridge column (4.6 x 150 mm) run isocratically at 0.5 mL/min with 10 mM NaPi pH 7.5 coupled to a waters 600E pump and Waters 2487 detector. The elution of components was observed at both 260 and 340 nm. The dominant components having absorbance at 340 nm were collected and their spectra recorded. A second sample was then prepared in an equivalent manner but with the addition of renalase to 5 μM. After incubation for 2 min this sample was filtered to remove the enzyme and subject to HPLC analysis.

HPLC identification of the product of the renalase reaction was based on co-elution. Chromatography conditions were as described above. Initially, a 50 μL control sample from a solution of 340 μM NADH in PBS buffer was separated into its α and β-NADH components. A second 50 μL sample was then reacted with 5 μM renalase for 2 minutes and filtered using a Millipore 0.5 mL 10 kDa nominal molecular weight centrifugal filter device before being chromatographed in an equivalent manner. A third 340 μM sample was then prepared with the addition of 15 μM β-NAD^+ and

chromatographed. The retention time of the product of the renalase reaction was compared to that of the sample spiked with β-NAD^+ to identify the product.

The nicotinamide product of a renalase/NADPH reaction was identified as β-$NAD(P)^+$ by nuclear magnetic resonance (NMR). A 40 mM solution of NADPH was prepared in 10 mM NaPi buffer pH 7.4 in deuterium oxide solvent. The ^1H NMR spectrum was then recorded by collecting and transforming 256 FIDs soon after preparing the sample on a Bruker 300 MHz NMR instrument. Renalase (10 μM – 0.3 U) and catalase (0.2 U) were then added to the NMR tube and mixed by repeated pipetting with a Pasteur pipette. Further spectra were then recorded at specific times over the next 100 minutes. A control NADPH sample was then prepared at the same concentration in the same buffer and monitored similarly. Prior to each spectrum (sample and control) the contents of the NMR tube were re-equilibrated with atmospheric molecular oxygen by repeatedly drawing the solution into a Pasteur pipette. The concentration of the product was approximated from the relative integrations of known resonances for β-NADPH and the singlet resonance for proton N2 (2 position of the nicotinamide) of the species observed to accumulate in the reaction. These spectra were compared to the proton spectra of 1 mM β-$NADP^+$ alone and 1 mM β-$NADP^+$ in the presence of 40 mM β-NADPH.

Evaluation of Epinephrine as a Substrate for Renalase: Epinephrine was tested as a substrate for renalase using four approaches. In the first, the reported accumulation of adrenochrome in the presence of renalase was evaluated. The concentration dependence of the formation of adrenochrome was observed by adding varied concentrations of epinephrine (0-400 μM) (prepared in 10 mM HCl) to a solution of PBS buffer and then observing the increase in absorbance at 480 nm at 25^oC. The initial rate at each epinephrine concentration was measured by fitting the first 200 seconds

to a straight line and dividing the slope by the extinction coefficient for adrenochrome (4020 $M^{-1}cm^{-1}$). [136] To determine if renalase and/or NADPH accelerates this process, 10 μM renalase and then 10 μM renalase with freshly prepared β-NADPH to 400 μM was added to 400 μM epinephrine (final) and the initial rate recorded.

In the second approach the effect of epinephrine on the observed single-turnover kinetics was assessed by stopped-flow spectrophotometry. Non-pseudo first order single-turnover reactions were initiated by mixing a limiting concentration of the α-NADPH (~6 μM in 400 μM β-NADPH) in PBS buffer equilibrated with atmospheric dioxygen (~250 μM) with 11.4 μM aerobic renalase in the same buffer. The reaction was monitored by observing the reduction and reoxidation of enzymes' flavin cofactor at 458 nm. Epinephrine (400 μM) was then added to the α-NADPH solution and the observation repeated. In order to evaluate if some soluble component of blood modulated or reacted with renalase, this observation was repeated with the α-NADPH/epinephrine solution prepared in fresh cell free blood plasma. Solely for comparison the data were fit to Equation 3.1 that describes three successive first order events. In this equation k_1 is the rate apparent constant for reduction, k_2 is an additional unassigned phase and k_3 is the apparent rate constant for reoxidation, ΔA_{1-3} are the respective absorbance amplitudes for the phases observed, and C is the endpoint absorbance.

Equation 3.1. $A_{458nm} = \Delta A_1 e^{-k1t} + \Delta A_2 e^{-k2t} + \Delta A_3 e^{-k3t} + C$

Isothermal titration calorimetry was used to assess if epinephrine associates with renalase. Renalase (350 μL of 339 μM in PBS buffer at 25°C) was injected into a TA instruments Nano ITC Model 5303 microcalorimeter. This sample then had 21, 2 μL additions of 1.84 mM epinephrine injected over 2 h. The pattern of heat liberated was then fit to a single independent site model correcting for

constant cell volume and injection dilution using NanoAnalyze Data Analysis software (TA instruments) to obtain a measure of the binding constant for the renalase•epinephrine complex. [145]

Perturbation of the renalase flavin absorption and fluorescence emission spectra in the presence of epinephrine was used as a qualitative measure to evaluate if the ligand formed a complex with the enzyme that had close association with the FAD isoalloxazine. Absorption spectra of renalase (30 μM) were measured at 25^{o}C in PBS buffer in the presence and absence of epinephrine (100 μM) using a Cary 3 dual beam spectrophotometer. The free enzyme spectrum was then subtracted from the spectrum obtained in the presence of the ligand to obtain the difference spectrum and accentuate changes. Similarly, fluorescence emission spectra were obtained under the same conditions with excitation at 450 nm. The emission spectrum (475-650 nm) of 4 μM renalase in PBS buffer was recorded in the absence and presence of 40 μM epinephrine using an Hitachi F-4500 spectrofluorometer at 25^{o}C.

Results

Expression and purification: Human N-terminally His-tagged renalase isoform 1 was expressed in BL21 DE3 *E. coli* to highest yield at 22 ^{o}C. Typically the yield of purified enzyme was 6 mg/L of culture. The enzyme was purified to homogeneity using a cobalt affinity column from which it eluted at approximately 30 mM imidazole and was assessed to be greater than 95% pure by SDS polyacrylamide gel electrophoresis. Consistent with prior reports, the renalase flavin spectrum was red-shifted compared to that of free flavin (Figure 3.1) . [76, 77] The two visible maxima of the enzyme bound flavin spectrum occur at 387 and 458 nm with extinction coefficients of ε_{387nm} = 10,750 $M^{-1}cm^{-1}$ and ε_{458nm} = 11,330 $M^{-1}cm^{-1}$. The purified enzyme was stable in PBS buffer, could be stored indefinitely at -80^{o}C and did not exhibit diminished activity with thawing. Heterologous expression of renalase in *E.*

coli resulted in significant inclusion body accumulation at all temperatures tested. Attempts were made to refold this peptide to form active renalase following the methods of Desir et al. 2012. [55] The refolded peptide acquired FAD and was soluble to high concentration, but had a cofactor spectrum ostensibly unchanged from free FAD (Figure 3.1). Moreover, the refolded material did not have the activity described hereafter and was deemed to be misfolded inactive protein.

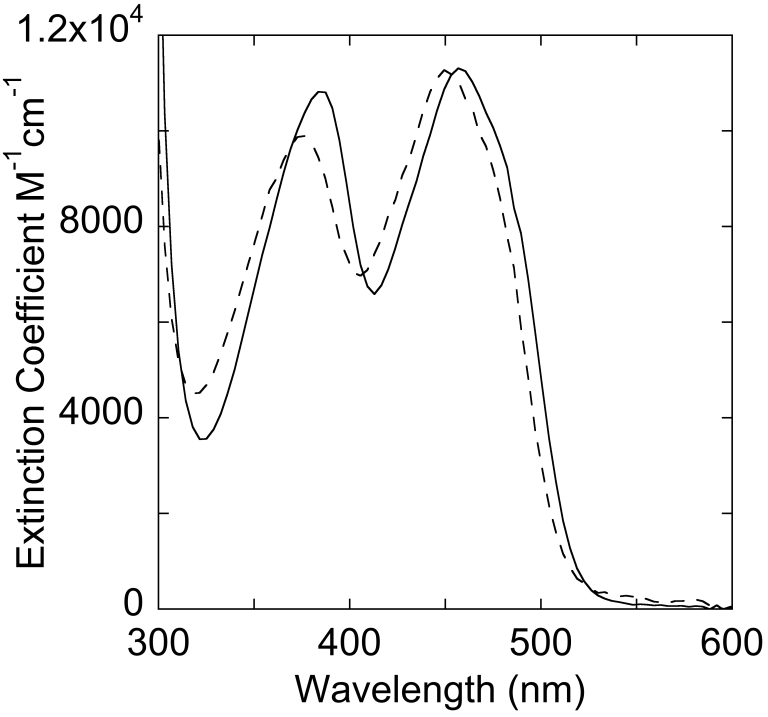

Figure 3.1. Flavin Spectra of Native and Refolded Renalase. Spectra shown are for heterologously expressed renalase from the soluble (solid line) and refolded from the insoluble or inclusion body (dashed line) fractions. The insoluble fraction was refolded using the methods of Desir et al. 2012. [14] The extinction coefficients of both forms were determined as described in the methods section.

Identification of a Renalase Substrate in NAD(P)H Stock Solutions: A substrate for renalase was detected whilst validating prior claims that β-NAD(P)H can serve as a renalase reductant in the production of adrenochrome from epinephrine. [91] Figure 3.2 depicts quantitative evidence for a renalase substrate occurring as a 1-4% impurity in β-NAD(P)H solutions. Figure 3.2A shows that rapid fractional reduction of renalase occurs when the enzyme is mixed with relative high concentrations of NADPH under strict anaerobic conditions. The measured ε_{458nm} value (7945 $M^{-1}cm^{-1}$) for reduction, obtained when the substrate contaminant was added in apparent excess (449 μM NADPH reduction trace), permitted the concentration of the actual substrate at all limiting values to be calculated. When the concentration of fractionally reduced renalase was plotted against the NADPH stock concentrations a slope of 1.3% was determined (Figure 3.2B). In a separate experiment, high concentrations of NADPH were added to 5 μM renalase in a dioxygen electrode and the concentration of oxygen consumed was measured (Figure 3.2C). The amplitude measured in this experiment indicated that the substrate contaminant was present to 1.5% of the total NADPH concentration. Higher apparent substrate fractions (4-5%) were observed with NADH stock solutions (Figure 3.2D). When catalase was included in these assays close to one half of the dioxygen consumed by renalase was regained from the catalase disproportionation reaction indicating that hydrogen peroxide is a product of renalase activity. Collectively these data establish multiple characteristics of the renalase reaction. In regard to the contaminant substrate, the proportion in NAD(P)H solutions is small and can vary with the parent molecule suggesting degradation and/or equilibrium processes result in the substrate accumulation. The complete and monophasic reduction of the flavin cofactor in excess substrate under anaerobic conditions (Figure 3.2A – 449 μM NADPH trace) suggests that one substrate molecule transfers two electrons to the flavin. The dioxygen electrode assays define that dioxygen is also a substrate for renalase with an observed rate of dioxygen consumption in solutions equilibrated

with atmospheric dioxygen (~250 μM) of ~0.5 s^{-1}. The total dioxygen consumption also indicated that multiple (Figure 3.2 C&D) turnovers occurred in the presence of the substrate component of both NADPH and NADH solutions. That the reduction (Figure 3.2A) and dioxygen uptake (Figure 3.2C) experiments indicate a similar proportion of substrate in the NADPH stocks suggests that the stoichiometry of the reaction is 1:1 for dioxygen and the NADPH contaminant. Moreover, that we regain 0.5 equivalents of O_2 in the presence of renalase and catalase suggests that the product stoichiometry is also 1:1; product:H_2O_2.

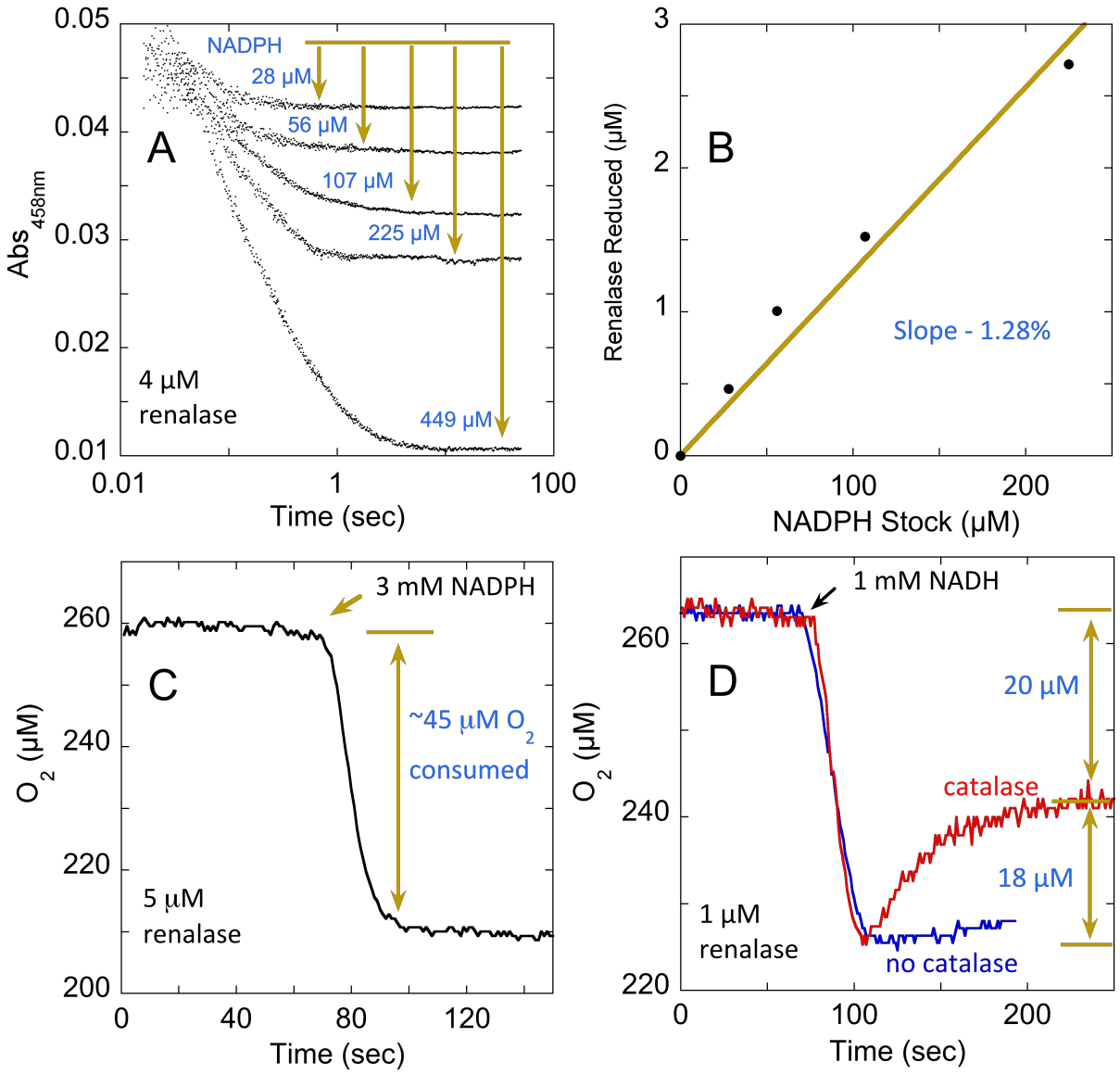

Figure 3.2. Evaluation of the Renalase Active Fraction in NAD(P)H Stock Solutions. **A**: Stopped-flow traces of fractional reduction of renalase as observed at 458 nm. Renalase (4.0 µM) was mixed under anaerobic conditions with varied concentrations of NADPH as shown. **B**: The fraction of NADPH consumed in the reduction in A based on the change in extinction coefficeint of the renalase flavin cofactor at 458 nm vs the stock concentration of NADPH. **C**: Demonstration of multiple turnovers with excess substrate. 5 µM renalase was added to PBS buffer in a dioxygen electrode and 3 mM of NADPH was added at the arrow. **D**: Stoichiometry of the renalase reaction with respect to dioxygen. Renalase (1 µM) was mixed with 1 mM NADH with and without 1 U of catalase. The traces shown in C and D are representative traces of typically 3-5 replicates for each observation.

HPLC product analysis was used to separate the components present in NADPH solutions and identify the substrate component (Figure 3.3). HPLC chromatograms were collected at known maxima for NADPH and NADH (340, 260 nm). Chromatograms collected at 340 nm indicated respective ~1.5% and 4% contaminants (by area) for NADPH and NADH solutions (Figure 3.3A & B). This component was largely consumed when the sample was incubated with renalase for two minutes (Figure 3.3A and B – red chromatograms) while the area of the major components (β-NADPH and β-NADH) remained unchanged. This indicated that the reactive component absorbed light at 340 nm and that this absorption was lost when reacted with renalase. An increase in absorption at 260 nm coinciding with a component already present in the NADH solution was observed in the sample to which renalase was added (Figure 3.3A lower). Coinjection of 15 μM of β-NAD^+ in the control sample identified the product of the renalase reaction as β-NAD^+ and indicated that the substrate concentration in the unreacted sample was ~13 μM (4.0%). For NADPH and NADH samples, the spectra of the substrate components (Figure 3.3C) exhibited maxima at 260 and 346 nm suggesting that the nicotinamide and adenine bases are intact in the substrate molecule. The loss of the 346 nm absorption of the substrate component when reacted with renalase is consistent with the dihydropyridyl base transferring a hydride equivalent to enzyme cofactor.

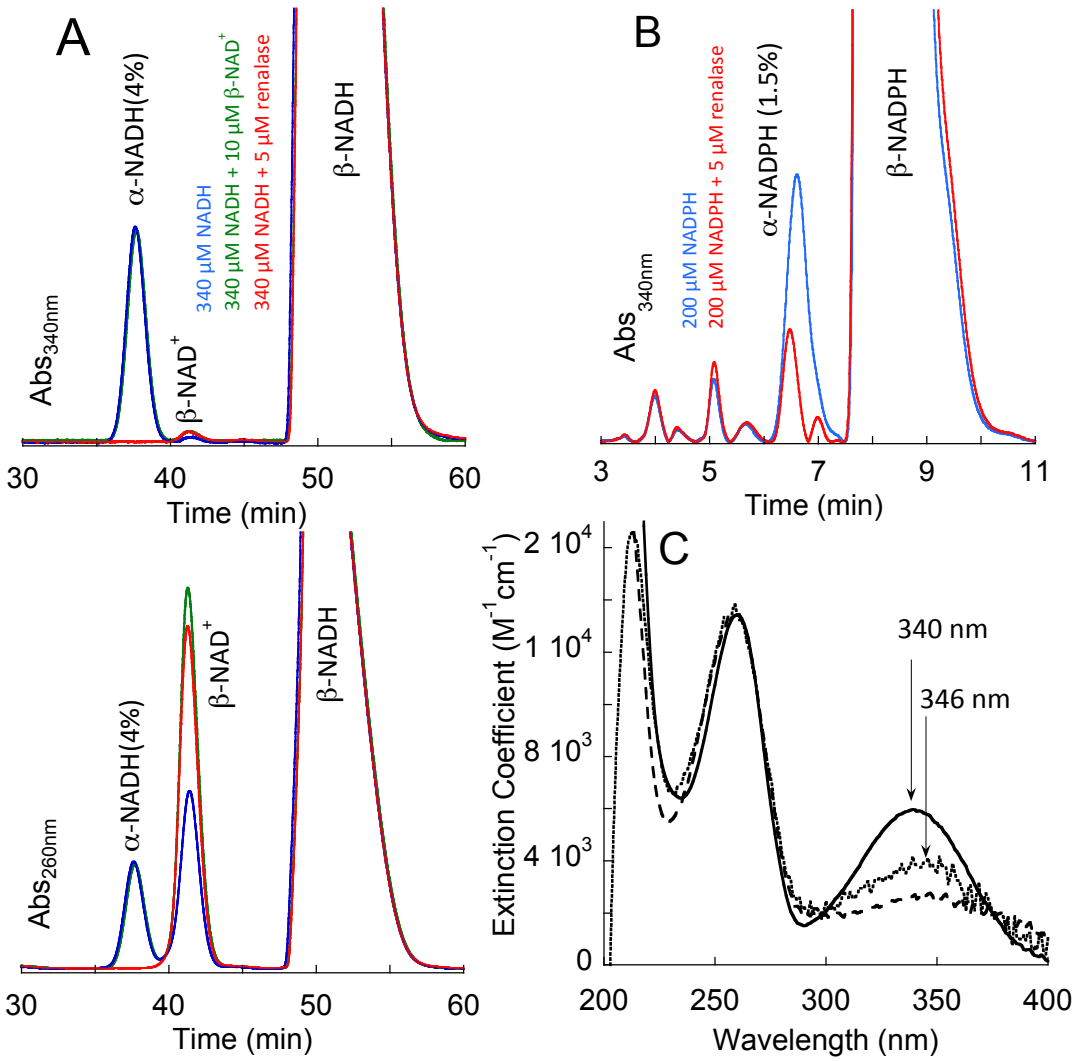

Figure 3.3. HPLC Identification of α-NAD(P)H as the Substrate for Renalase Occuring as a Contaminant of β-NAD(P)H Solutions. **A**&**B**: Species were separated using a Xterra reverse phase C18 column running isocratically in 10 mM sodium phosphate buffer, pH 7.5. In each the blue line is the control β-NAD(P)H stock while the chromatograms depicted as a red line were prepared identically to the control sample but were reacted with 5 µM renalase and then filtered to remove the enzyme. The chromatogram depicted with a green line in **A** is the same as the control sample but with 15 µM β-NAD+ added. **A**: Chromatographic separation of NADH solutions detected at 340 nm (upper) and 260 nm (lower-7-fold smaller scale) **B**: Chromatographic separation of NADPH solutions detected at 340 nm. C: Spectra of the renalase substrate species resolved in A&B. The spectrum represented with an unbroken line is β-NADPH and was included for reference. The dotted line spectrum was of the substrate peak in A. The dashed line spectrum was of the substrate peak in B. Spectra were normalized at 260 nm for clarity.

Red-shifted nicotinamide spectra of the active components of NADPH and NADH solutions is characteristic of α-NAD(P)H molecules. [95, 146] In amongst the numerous decay paths possible for pyridine nucleotides are anomerization equilibria that bring about the accumulation of a small fraction of the α-dihydronicotinamides in dissolved β-NAD(P)H solutions [147] (Scheme 3.1). Anomerization is only possible for the reduced form as the ribose ring-open Schiff base intermediate can form only when electrons are delocalized from the electron-replete dihydropyridyl ring; the oxidized forms are thus configurationally stable. Reduced nicotinamide nucleotides are one of the two naturally occuring nucleotides that exhibit anomerization in solution, the other being pseudouridine nucleotide.[148] The α/β equilibrium constants for NADPH and NADH are reported as 0.015 and 0.11 respectively [95], largely consistent with the ~1.5% and ~5% fractions observed for the experiments described above.

NMR was used to confirm the product of the renalase reaction. The oxidized nicotinamide proton resonances of the α and β forms of NAD(P) are readily discerned by NMR. [137] With respect to β-NAD(P), the resonances of protons of the α-nicotinamide moiety move to higher field while the discriminating proton attached to the anomeric carbon of the nicotinamide ribose moves downfield. Figure 3.4A depicts proton NMR spectra for the accumulation of β-$NADP^+$ from a stock solution (40 mM) of β-NADPH in the presence of renalase (blue spectra). In such a reaction α-NADPH is expected to be consumed by renalase as a burst of product formation before the reaction becomes limited by both available dioxygen and/or the rate of anomerization. What is observed is an ~200 μM burst in product accumulation that did not occur in the absence of renalase (Figure 3.4B). That the observed product nicotinamide resonances are shifted upfield relative to those of β-$NADP^+$ alone (Figure 3.4A green and blue spectra) indicates only the influence of the high concentration of β-NADPH in these samples. When the proton resonances and coupling constants are compared to those of a control

sample having the same ratio of β-NADP$^+$ to β-NADPH, the product and control spectra coincide (Figure 3.4A orange and blue spectra), indicating that the product of the reaction is β-NADP$^+$.

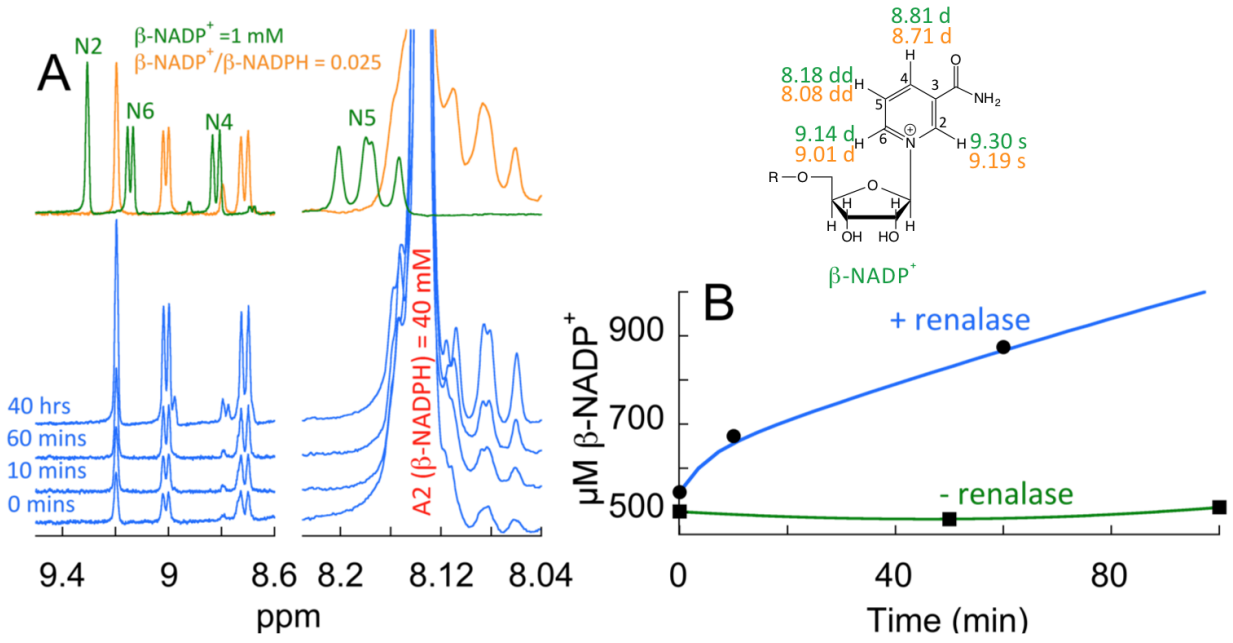

Figure 3.4. Identification of β-NAD(P)H as the Nicotinamide Product of the Renalase Reaction. **A**: 300 MHz ^{1}H NMR spectra. Blue spectra show the accumulation of resonances when 10 μM renalase was added to a freshly prepared solution of 40 mM β-NADPH in 10 mM sodium phosphate buffered deuterium oxide, pH 7.4. The upper spectra are control samples. For positional assignments the N designation refers to the nicotinamide base, while A references the adenine base. The green spectrum is that of 1 mM β-NADP$^+$ and the orange spectrum is that of 1 mM β-NADP$^+$ in the presence of 40 mM β-NADPH (both control samples prepared in 10 mM sodium phosphate buffered deuterium oxide, pH 7.4). Assignments of the shifts of the nicotinamide are shown to the right of the control spectra. **B**: Relative accumulation of β-NADP$^+$ in the presence and absence of renalase based on the integration of the N2 proton and the known concentration of the β-NADPH in the sample.

Evaluation of Epinephrine as a Substrate for Renalase: The substrate for renalase has been the subject of some dispute since the discovery of the enzyme in 2005. [72, 88, 89] Figure 3.5 summarizes the data obtained for three approaches used to assess the response of renalase to the presence of epinephrine. In Figure 3.5A, non-pseudo-first order single turnover reactions of renalase with limiting

α-NADPH and atmospheric dioxygen (observed at 458 nm) indicated reduction and reoxidation of the flavin cofactor. Under the conditions used these data could be fit to three exponential phases without significant systematic error in the residuals (11.6 s^{-1}, 1.63 s^{-1}, 0.54 s^{-1}). However, the number of phases, the values for rate constants and absorbance amplitudes are only apparent measures of the single turnover kinetics that provide a means to compare the data in the presence of and absence of epinephrine. It has been suggested that renalase obtains reducing equivalents from β-NADPH and then catalyzes a net two-electron oxidation of epinephrine to form adrenochrome, a process that would mobilize four electrons. [91] The addition of 200 μM epinephrine to single turnover reactions with α-NADPH and dioxygen did not change the observed kinetics (11.0 s^{-1}, 1.82 s^{-1}, 0.66 s^{-1}) indicating that no rate constant is significantly altered and no new intermediates accumulate in response to the catechol. It has been suggested that renalase is only activated in blood and is isolated as a relatively inactive pro-renalase. [49] In order to assess if some additional soluble component of blood is required to activate renalase to consume epinephrine the experiment was repeated in 50% fresh cell-free human blood plasma. This condition also did not significantly alter the observed single turnover kinetics (12.1 s^{-1}, 1.90 s^{-1}, 0.64 s^{-1}). The conclusion is that epinephrine is not catalytically consumed by renalase as isolated and that no soluble ligand in blood activates the enzyme to display this activity.

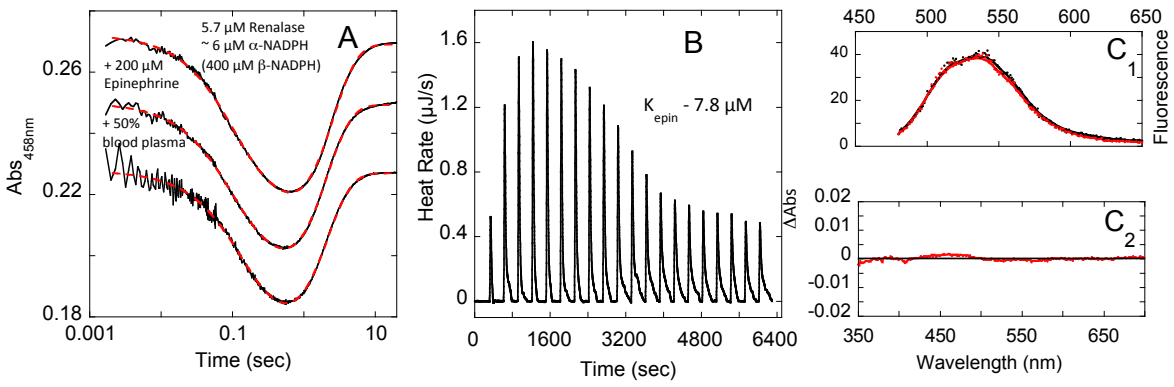

Figure 3.5. Evaluation of Epinephrine as a Substrate for Renalase. **A**: Single Turnover of renalase with limiting α-NADPH. Traces were observed at 458 nm when 5.7 µM renalase was reacted with with ~6 µM α-NADPH at atmospheric concentrations of molecular oxygen (~250 µM). Dashed red lines indicate fits to Equation 3.1. **B**: Isothermal titration calorimetry of 339 µM renalase with 21, 2 µL injections of 1.84 mM Epinephrine. **C**: The extent of spectrophometric perturbation of the flavin spectrum by epinephrine. C_1: Black line - flouresence emission spectrum of 4 µM renalase when excited at 450 nm. Red line - flouresence emission spectrum of 4 µM renalase plus 40 µM Epinephrine when excited at 450 nm. C_2: Absorption difference spectra. Black line – zero perturbation difference spectrum of 20 µM renalase. Red line – difference spectrum (sample-control) for 20 µM renalase plus 200 µM epinephrine.

To evaluate if renalase binds epinephrine, the enzyme was titrated with epinephrine in an isothermal titration calorimeter (Figure 3.5B). The data obtained suggest an exothermic binding event with a dissociation constant for the renalase•epinephrine complex of ~8 µM. This complexation is either adventitious (and coincidental) or is a binding event whose link to physiology is yet to be established. The lack of influence of epinephrine on the observed kinetics of reduction and reoxidation of renalase by α-NADPH implies that the binding of epinephrine does not occur in the active site of the enzyme. To test this hypothesis, spectrophotometric observations using the flavin absorption and emission spectra as sensitive measures of ligand proximity were undertaken (Figure 3.5C). These experiments show no appreciable perturbation of the flavin environment in the presence

of epinephrine concentrations at least 4-fold higher than the measured binding constant, suggesting that the binding site for epinephrine is distant from the active site.

The accumulation of adrenochrome from epinephrine can be observed at 480 nm. [136] Our experiments indicated that the initial rate of oxidation of epinephrine to form adenochrome in atmospheric oxygen at 25 ^{o}C oxygen in PBS buffer was ostensibly zero for all concentrations tested. The addition of freshly dissolved β-NADPH did not bring about adrenochrome formation nor did the addition of 10 μM renalase (data not shown). As such it was concluded that renalase does not utilize β-NAD(P)H (or α-NAD(P)H) to catalyze a reaction that forms adrenochrome.

Discussion

Eight years after its initial discovery, we have identified an activity for human renalase as an α-NAD(P)H oxidase/anomerase. This activity is the first demonstration of a potential physiological role for α-NAD(P)H in mammals and the first example of a flavoprotein catalyzing an anomerization reaction. This discovery runs contrary to the persistent assertion that renalase catabolizes adrenergic catecholamines. Renalase has often been described as “MAO C”; the third monoamine oxidase [55, 91, 110] that oxidizes the catechol ring rather than the distal amine. We suggest that epinephrine and other catechols have most often been reported as the substrate for renalase as they exhibit instability at or above neutral pH values and form chromophoric products (aminochromes) that may be easily taken for slow catalytic activity. [91] Our data suggest that epinephrine has no influence on the activity of the enzyme.

It may be possible to reconcile our observations with the majority of earlier reports of adrenochrome formation by renalase. *In vitro* catalytic adrenochrome production by renalase are solely for the refolded renalase peptide. [55] In our hands, this form of the protein exhibits none of

the α-NADPH oxidase/anomerase activity described herein. It is thus tentatively proposed that the refolded form may have a solvent exposed flavin isoalloxazine ring (Figure 3.1) that due to the difference in reduction potentials (-320 vs -207mV) will be reduced by NADPH in a slow steady-state reaction that forms H_2O_2 autocatalytically. This molecule will readily oxidize epinephrine to initially form a quinone species prior to nucleophilic attack by the distal amine of the side chain to yield the adenochrome product. The natively folded renalase enzyme does not promote this chemistry to any significant extent as it selects against binding of the β-form from the NAD(P)H reductant pool (Figures 3.1, 3.2 and 3.3). Moreover, it may be possible to observe the accumulation of aminochromes with natively folded renalase in the presence of reduced nicotinamide dinucleotides when long incubations are employed as non-enzymatic anomerization will form α-NAD(P)H as a minor component resulting in the formation of product H_2O_2 and hence promote the ensuing non-enzymatic oxidation and cyclization of the catechol.

From an experimental perspective α-NAD(P)H molecules are highly elusive. The apparent rate constants to attain equilibrium from the α-NAD(P)H anomer is on the order of 10^{-5}-10^{-6} s^{-1}. [95] As such the concentration of pure α-NADPH is altered within hours of a solution being prepared, to some extent undermining the systematic use of the pure substrate in activity assays. The use of the β-anomer to obtain the α-form requires prolonged incubation to reach anomer equilibrium and verification of the α-fraction before use as a stock solution but has the advantage of supplying a constant α/β ratio throughout the period of observation. While α-NAD(P)H will invariably be the minor component it must be assumed that renalase is highly discriminatory for the α-anomer given that it was destined to function in an environment in which the β-anomer is predominant.

More evidence is needed to define the means by which the activity of renalase transmits a signal to the circulatory system to induce the reported vasodilation. However, this oxidase/anomerase

activity may have a core physiological role that is separate and more pervasive than blood pressure modulation. The necessity for renalase to harbor two functionalities may arise from the fact that α-NAD(P)$^+$ molecules are metabolically isolated. In Scheme 3.2 the α/β equilibria are depicted with the redox pathways for both anomers of NAD(P)H molecules. The inherently lower reduction potential of α-NAD(P) molecules and the lack of participation in other metabolic pathways dictates that there would be an inexorable loss of nicotinamide dinucleotide cofactors as □-NAD(P)$^+$. Without considering other redox partners, the anomer equilibrium and redox potential difference would predict that ~50% of the β-NAD(P)H would ultimately accumulate as α-NAD(P)$^+$. [137] If renalase were not to catalyze oxidation in addition to anomerization these molecules would accumulate and deplete both the total concentration of NAD(P)H molecules and the normal NAD(P)H/NAD(P)$^+$ ratio. The α-NAD(P)H oxidation couples the reaction to dioxygen reduction providing a large driving force that in concert with the anomerization activity recycles α-NAD(P)H molecules back to the β-pool maintaining the α-NAD(P)H concentration near zero.

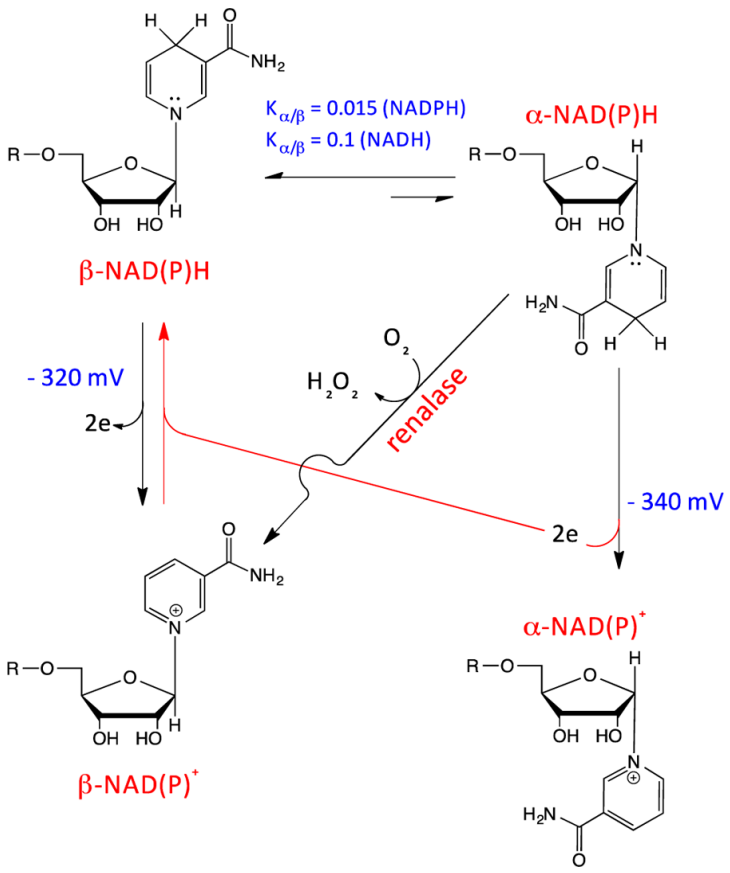

Scheme 3.2. Initial proposed role of anomer recycling.

This activity for renalase raises numerous chemical and physiological questions. From an enzyme chemistry perspective, hydride transfer to a flavin is not unusual, though the timing of this process with respect to the anomerization reaction is highly intriguing. While it may be reasonable to conclude that anomerization occurs after reduction of the FAD cofactor in order that the enzyme be selective for α-NAD(P)H, this raises the question as to what redox state of renalase catalyzes the anomerization. That is, is α-NAD(P)$^+$ (or β-NAD(P)$^+$) a substrate for the reduced or oxidized enzyme and if the reduced enzyme catalyzes anomerization of the oxidized nicotinamide dinucleotide how is the ribose ring cleaved if the otherwise requisite schiff base/ring open intermediate can no longer form? A hypothetical mechanism that circumvents these apparent conundrums is depicted in Scheme 3.3. In this mechanism the oxidized enzyme is selective for the α-NAD(P)H substrate and first

promotes the formation of a ring open ribose/Schiff base intermediate. It is then this intermediate that reduces the flavin, concomitantly forming the β-NAD(P)$^+$ product prior to reoxidation.

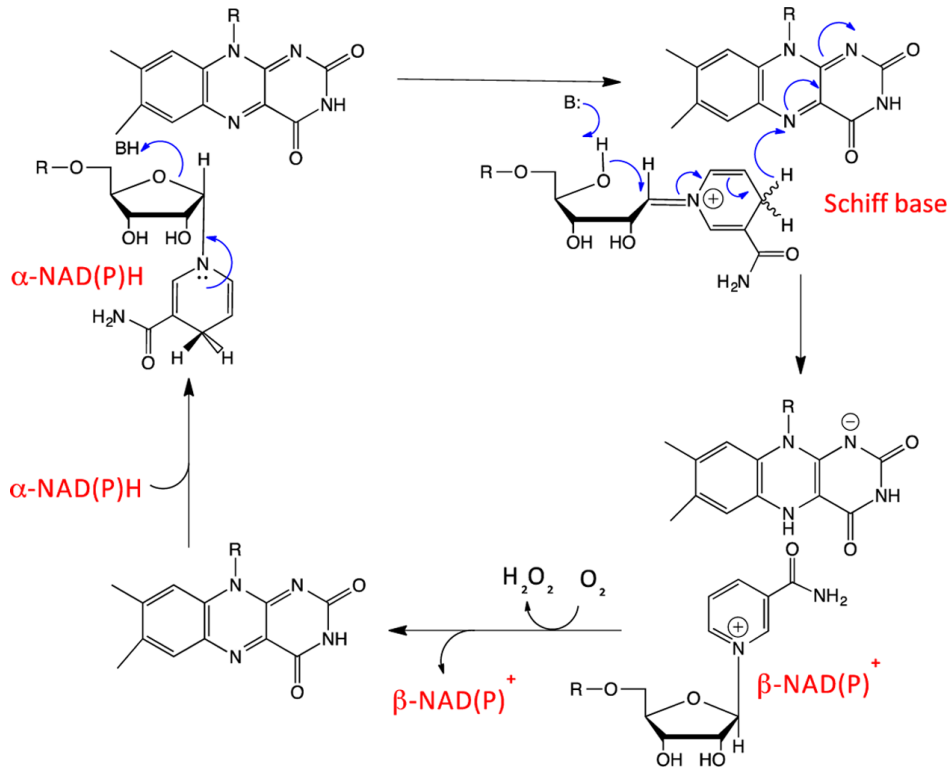

Scheme 3.3. Proposed oxidation/anomerization mechanism.

This research does not address the manner in which this newly identified activity of renalase is imparted *in vivo* in regard to vasodilation. It may be ventured that the observed decrease in blood pressure and slowing of the heart rate is not a result of diminishment of either of the substrates or the accumulation of the β-NAD(P)$^+$ product as each of these molecules are ubiquitous in mammalian circulation. It therefore seems reasonable to implicate H_2O_2 as the signal for vasodilation arising from renalase activity. [149-151]

Chapter IV
Kinetics and Equilibria of the Reductive and Oxidative Half-Reactions of Human Renalase with α-NADPH

Brett A. Beaupre, Matthew R. Hoag, Brenton R. Carmichael, and Graham R. Moran

Abstract

Renalase is a recently discovered flavoprotein that has been reported to be hormone produced by the kidney to down-modulate blood pressure and heart rate. The consensus belief has been that renalase oxidizes circulating catecholamine neurotransmitters thereby attenuating vascular tone. However, a convincing *in vitro* demonstration of this activity has not been made. We have recently discovered that renalase has α-NAD(P)H oxidase/anomerase activity. Unlike most naturally occurring nucleotides, NAD(P)H can accumulate small amounts of the α-anomers that once oxidized are configurationally stable and unable to participate in cellular activity. Thus anomerization of NAD(P)H would result in a continual loss of cellular redox currency. As such, it appears that the root purpose of renalase is to return α-anomers of nicotinamide dinucleotides to the β-anomer pool. In this article we measure the kinetics and equilibria of renalase in turnover with α-NADPH. Renalase is selective for the α-anomer that binds with a dissociation constant of ~20 ± 3 μM. This association precedes monophasic two-electron reduction of the FAD cofactor with a rate constant of 40.2 ± 1.3 s^{-1}. The reduced enzyme then delivers both electrons to dioxygen in a second order reaction with a rate constant of ~2900 $M^{-1}s^{-1}$. Renalase has modest affinity for its β-$NADP^+$ product (K_d = 2.2 mM), and the FAD cofactor has a reduction potential of -155 mV that is unaltered by saturating β-$NADP^+$. Together these data suggest that the products are formed and released in a kinetically ordered sequence (β-$NADP^+$ then H_2O_2), however, the reoxidation of renalase is not contingent on the dissociation of β-$NADP^+$. Neither the oxidized nor the reduced form of renalase is able to catalyze anomerization,

implying that the redox and anomerization chemistries are inextricably linked through a common intermediate.

Reported initially in 2005, renalase was said to be a new renal hormone that is secreted into blood by the kidney to induce lower blood pressures and slowed heart rate. [46, 152] In subsequent studies it has been reported that mice deficient in renalase have elevated blood pressures and that renalase polymorphisms result in a higher incidence of stroke and diabetes. [48, 124, 134] The consensus belief has been that renalase imparts its physiological response by catabolizing circulating catecholamine neurotransmitters (chiefly adrenaline) thereby attenuating vascular tone. [46, 53, 55] The expression of renalase has been reported in additional tissues [46, 49, 73] with at least four variants arising from altered splicing of seven exons. [49, 73] The X-ray structure of the longest variant, isoform 1, (342 amino acids) was published in 2011, revealing a protein whose structural topology was similar to known flavoprotein oxidases, monooxygenases and demethylases, but whose activity could not be readily discerned from conserved active site residues. [72, 77, 138-141] Given the similarity of the structural fold of renalase to monoamine oxidases A & B, catabolism of catecholamines would appear to be a reasonable, albeit contextual, function for renalase. However, there has been considerable difficulty establishing this activity *in vitro,* leading to the assertion that renalase as isolated is “prorenalase”; a form that must be activated in blood by catecholamines or other modifiers. [110] Slow accumulations of adrenochrome in the presence of renalase, epinephrine and NADPH have been offered as evidence that renalase catalyzes the oxidation of the catecholamines and promotes nucleophilic attack by the side-chain distal amine. [91] The difficulty is that this is a facile, well-established degradative reaction for catecholamines that exhibits measureable rates under mildly oxidizing conditions in the absence of an enzyme catalyst. [135, 136, 153] Moreover, the stoichiometry of such a reaction in regard to the fate of the mobilized electrons has not been

established. [91] As such, the claim that renalase catabolizes circulating catecholamines has been questioned by a number of researchers. [72, 88, 89]

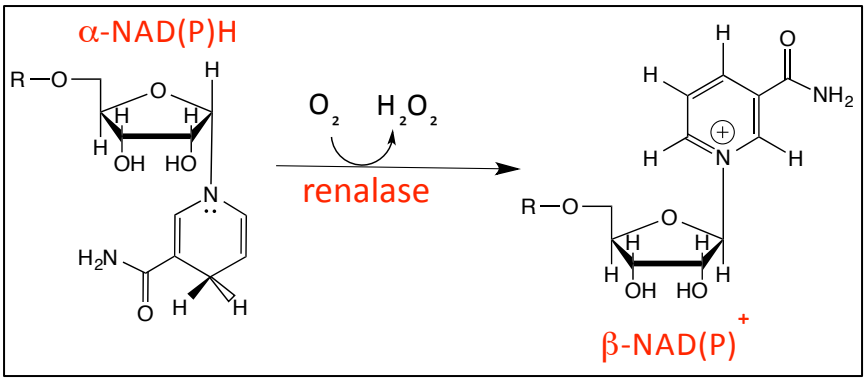

Scheme 4.1. Proposed overall oxidation/anomerization reaction.

We have recently discovered an activity for renalase as a bifunctional α-NAD(P)H oxidase/anomerase. [154] Renalase oxidizes the dihydropyridyl ring of α-pyridine nucleotides, that arise naturally as a small equilibrium component of NAD(P)H solutions, and manages to also epimerize the nicotinamide ribose to form β-NAD(P)+ products (Scheme 4.1). Importantly, renalase does this chemistry at least two orders of magnitude more rapidly than any reported turnover rate for catecholamine oxidation. The electrons acquired from the α-NAD(P)H substrate are initially transferred to the enzyme's FAD cofactor and then to dioxygen to yield hydrogen peroxide. How and if this activity is linked to the reported physiological response to renalase has not been addressed, but the only known vasoactive molecule to be consumed or arise from this activity is H_2O_2. [150, 151] Coupling NAD(P)H oxidation to α-β anomerization and dioxygen reduction provides a large driving force for this chemistry and suggests the more pervasive physiological function for renalase is to drive the α/β NAD(P) ratio to zero. In this article we offer evidence for the kinetics and equillibria of the reductive and oxidative half reactions of human renalase reacting with α-NADPH.

Materials and Methods

Materials: Potassium phosphate, isopropyl-β-thiogalactopyranoside (IPTG) and sodium chloride were obtained from ACROS. Luria Bertani broth (Lennox) powder was from Fisher Scientific. Kanamycin and β-NADPH were purchased from Alexis. β-$NADP^+$ was purchased from Calbiochem and Axxora. β-NADH, β-NAD^+, xanthine, methyl viologen and epinephrine were from Sigma-Aldrich. Indigo carmine was from ICN. Xanthine oxidase was acquired from Calzyme. Renalase was expressed and purified according to our previously published methods. [154] α-NADPH was from the α/β-NAD(P)H equilibrium mixture (reliably 1.5% (NADPH) and 4% (NADH) alpha anomers at equilibrium). Anomer equilibrium was achieved by dissolving β-NADPH in PBS or HEPES pH 7.5 and placing this solution in a sealed vessel at 4^{o}C for ~72 hours. [95] Prior to using stock solutions, the α-NAD(P)H concentration was determined by dioxygen electrode. Typically 1-2 μM renalase was added to 1-3 mM of the NAD(P)H solution in PBS buffer at 25 ^{o}C. The observed amplitude of dioxygen consumption was used to define the fraction of the α-NAD(P)H component.

Quantitation: The concentration of NADPH and NADH solutions were determined using the published 340 nm extinction coefficient of 6200 $M^{-1}cm^{-1}$. [95] An extinction coefficient for renalase was determined in prior work (ε_{458nm} =11,330 $M^{-1}cm^{-1}$). [154] NADP+ and NAD+ solutions were quantified using published 260 nm extinction coefficients. [146]

Reduction Potentials Measurements and β-$NADP^+$ Binding Affinity. Reduction potentials were measured for unliganded oxidized renalase and the Ren_{ox}•β-$NADP^+$ complex using the xanthine/ xanthine oxidase reduction system of Massey. [155] A Hewlett Packard 8453 diode-array spectrophotometer was used to monitor the reduction of the enzyme in the presence of indigo

carmine (E^o = -130 mV). The reaction mixture was placed in an anaerobic cuvette and consisted of 300 μM xanthine, 5 μM methyl viologen, 10 μM of indigo carmine, 10 μM renalase (with or without 30 mM β-$NADP^+$) in PBS buffer pH 7.5 at 25° C. Once the mixture was made anaerobic by 45 cycles of argon and vacuum (as above), xanthine oxidase (1-2 μM final) was added from a side arm to initiate the reduction of both the enzyme and dye. Spectra were recorded every two minutes until both species were fully reduced. The data were analyzed at wavelengths where the dye (610 nm) or the enzyme (470 nm) had absorption contributions that were spectrophotometrically independent of the other chromophore. At each of these wavelengths the ratio of oxidized and reduced species was determined. The log of the ratio of the oxidized and reduced forms of indigo carmine was then plotted against the log of the same ratio for renalase and the indigo carmine midpoint was substituted into the pH-corrected Nernst equation[156] to obtain the reduction potential for the renalase flavin cofactor.

The dissociation constant for the Ren_{ox}•β-$NADP^+$ complex was measured by monitoring the spectrophotometric perturbation of the flavin cofactor between 400 and 600 nm when β-$NADP^+$ was titrated to the oxidized enzyme. Renalase (20 μM) in PBS buffer at 25°C was titrated with β-$NADP^+$ (0-8 mM). With each addition of β-$NADP^+$ the flavin absorption spectrum was measured. All spectra were corrected for dilution and the fractional occupancy assessed by the fraction of the extrapolated total perturbation observed at each β-$NADP^+$ concentration. This value was then used to obtain the concentration of unbound ligand. Plotting fractional occupancy versus unbound ligand gave a hyperbola that was fit to Equation 4.1, where f is fractional occupancy, $K_{\beta\text{-}NADP+}$ is the dissociation constant for the Ren_{ox}•β-$NADP^+$ complex and [β-$NADP^+_f$] is the concentration of unbound β-$NADP^+$.

Equation 4.1. $f = [\beta\text{-NADP}^+_f]/(K_{\beta\text{-NADP+}} + [\beta\text{-NADP}^+_f])$

Reductive Half-Reaction: The reduction of the renalase flavin cofactor was observed by mixing the anaerobic enzyme with anaerobic NADPH solutions at anomer equilibrium on a stopped flow spectrophotometer. Prior to the experiment the instrument was made anaerobic by introducing a solution of glucose (20 mM) and glucose oxidase (15.5 U/mL) for approximately 16 hrs. Renalase (4 μM) in PBS buffer with 1 mM glucose was made anaerobic by placing it in a tonometer and exchanging the dissolved dioxygen for argon. Prior to sealing the vessel, ~16 U of glucose oxidase was added to the side arm of the tonometer. The tonometer was then sealed and connected to an anaerobic manifold where 45 cycles of argon and mild vacuum were applied. Between each three exchanges, the solution was gently agitated to promote exchange of gases in the headspace of the vessel. After this procedure the renalase/glucose solution was mixed with the glucose oxidase from the sidearm and then mounted onto a Hi-Tech (now TgK) DX-2 stopped-flow spectrophotometer. This solution was then reacted with varied concentrations of α-NADPH (~20-300 μM). Substrate solutions were prepared in PBS buffer with 1 mM glucose and sparged in an inverted glass syringe with purified Argon for 10 minutes before 8 U of glucose oxidase was added and the syringe was mounted to the stopped-flow instrument. The two solutions were then mixed and the bleaching of the flavin cofactor during reduction was observed at 458 nm. The data obtained was fit to a single exponential decay according to Equation 4.2, where k_{obs} is the observed rate constant for reduction of the FAD cofactor, ΔA is the amplitude for the absorbance change and C is the Abs_{458nm} endpoint.

Equation 4.2. $A_{458nm} = \Delta A_1 e^{-kobst} + C$

The dependence of the observed rate constant was then plotted against α-NADPH concentration and fit to Equation 4.3 to determine the limit of the rate constant of reduction (k_{red}) and the dissociation constant for α-NADPH ($K_{\alpha\text{-NADPH}}$).

Equation 4.3 $$k_{obs} = k_{red}[\alpha\text{-NADPH}]/(K_{\alpha\text{-NADPH}} + [\alpha\text{-NADPH}])$$

In order to observe potential NADP/FAD charge-transfer bands at longer wavelengths, the reductive process was also observed for 20 μM (final) renalase prepared in an equivalent manner and mixed with saturating α-NADPH (328 μM).

Oxidative Half-Reaction. The reoxidation of the renalase cofactor in the presence of dissolved dioxygen was observed in single turnover reactions by stopped-flow spectrophotometry. Renalase (14 μM) was prepared in tonometer in an equivalent manner to that described above. This solution was then mixed with α/β-NADPH mixture of known ratio to supply sufficient α-NADPH to achieve ~50% reduction. The dissolved oxygen concentration in this solution was defined by sparging an inverted syringe containing the α/β-NADPH mixture with blended nitrogen and oxygen gases of known partial pressures supplied by a Maxtec maxblend gas mixer. The concentration of dissolved oxygen was confirmed by first sparging the reaction chamber of a Hansatech dioxygen electrode filled with PBS buffer with the blended gases to define the equilibrium concentration of dissolved dioxygen. Once the molecular oxygen concentration was established, the gas blend was applied to the α/β-NADPH mixture and sparged for 10 minutes before mounting the solution on the stopped-flow instrument. The solutions were then mixed and the reduction and ensuing reoxidation were observed at 458 nm. The data were fit to Equation 4.4 in which k_{red} is the apparent rate constant for reduction and k_{ox} is the

rate constant for reoxidation, ΔA_1 and ΔA_2 are the amplitudes for the two phases, and C is the endpoint absorbance.

Equation 4.4. $A_{458nm} = \Delta A_1 e^{-kred t} + \Delta A_2 e^{-kox t} + C$

The influence of exogenous β-$NADP^+$ on the kinetics of the oxidative half reaction was observed by reacting renalase (10 μM) with excess α-NADPH (20 μM) in the presence of 250 μM dioxygen and varied β-$NADP^+$ concentration (100-1600 μM). The reductive and oxidative processes were observed at 458 nm.

T*he Extent of Anomerization of an α/β-$NADP^+$ Mixture by Renalase:* The capacity of renalase to catalyze anomerization independent of FAD cofactor reduction by α-NAD(P)H was assessed by incubation with an $NADP^+$ solution of known α/β ratio followed by high pressure liquid chromatography (HPLC). A 1/2.66 mixture of α/β-$NADP^+$ (275 μM total) was prepared by placing 40 mM β-NADPH in a solution of 10 mM sodium phosphate pH 7.4 and allowing it to age at room temperature for 14 days. The inherently lower reduction potential of α-NADP and the anomer bias for the β-form ensures that similar amounts of the α and β $NADP^+$ anomers accumulate. [137] The oxidized forms were separated from the reduced and other contaminants by loading the aged sample onto a 20 cm x 12.5 mm Q-sepharose column and eluting with a linear gradient of NaCl from 0-150 mM. The α/β-$NADP^+$ mixture was then diluted to 75 μM and 50 μL chromatographed using a 4.6 x 150 mm Xterra C18 reverse phase column coupled to a Waters 600 E HPLC pump and a Waters 2487 dual wavelength detector. The α and β-anomer mixture was then separated using an isocratic mobile phase of 10 mM sodium phosphate pH 7.5. Renalase (5.6 μM final) was then added to the α/β $NADP^+$

solution and 50 μL volumes were withdrawn periodically, filtered through a 0.5 mL Amicon 10 KDa centrifugal filter and chromatographed as above.

The propensity of the reduced enzyme to catalyze anomerization of $NAD(P)^+$ was assessed using similar methods but with prior reduction of renalase. The enzyme was reduced using an adaptation of the methods used to reduce the chromophores in the reduction potential measurements described above. The reaction mixture was placed in an anaerobic cuvette and consisted of 300 μM xanthine, 2 μM methyl viologen, 6.0 μM renalase in PBS buffer pH 7.5 at 25° C. The mixture was made anaerobic by 45 cycles of argon and vacuum (as above) and then xanthine oxidase (1-2 μM final) was added from a side arm to initiate the reduction of the enzyme. The extent of reduction was assessed spectrophotometrically using a Hewlett Packard 8453 spectrophotometer. 75 μM (final) of a 1/2.66 mixture of α/β-$NADP^+$ was then added from a second sidearm and the sample was allowed to incubate for 60 minutes before removing the protein components by filtering through a 10 KDa nominal molecular weight centrifugal filter. The chromatograms obtained were then compared to two controls, the first that included all reaction components minus the mixture of α/β-$NADP^+$ and the second that included only the α/β-$NADP^+$ mixture.

Results

Redox-Linked Measurement of β-$NADP^+$ Binding Affinities. The renalase reduction potential was determined using a spectrophotometric method that compares the extent of reduction of the enzyme relative to a dye of known potential when electrons are supplied from xanthine oxidase reacting with xanthine under anaerobic conditions. [155] In this experiment the dye serves a similar function to that of a reference electrode. Figure 4.1A includes spectra obtained as renalase and indigo carmine are reduced by the xanthine/xanthine oxidase system. Figure 4.1B shows the midpoint for the dye

compared to extent of reduction of renalase. This plot allowed a reduction potential for renalase of -155 mV to be calculated. The experiment was repeated with saturating β-NADP$^+$ (*vide infra*) to obtain a reduction potential for the Ren$_{ox}$•β-NADP$^+$ complex of -151 mV. No flavin semiquinone is observed to accumulate during reduction suggesting that the second one-electron potential is higher than the first. The reduction potential for α-NAD(P)H is -340 mV [137] indicating that the redox driving force (excluding the contribution of anomer equilibria) for the reduction of the flavin is -35.6 kJ/mole. Coupling this the reduction of dioxygen yields -122.5 kJ/mole driving force for the complete catalytic cycle.

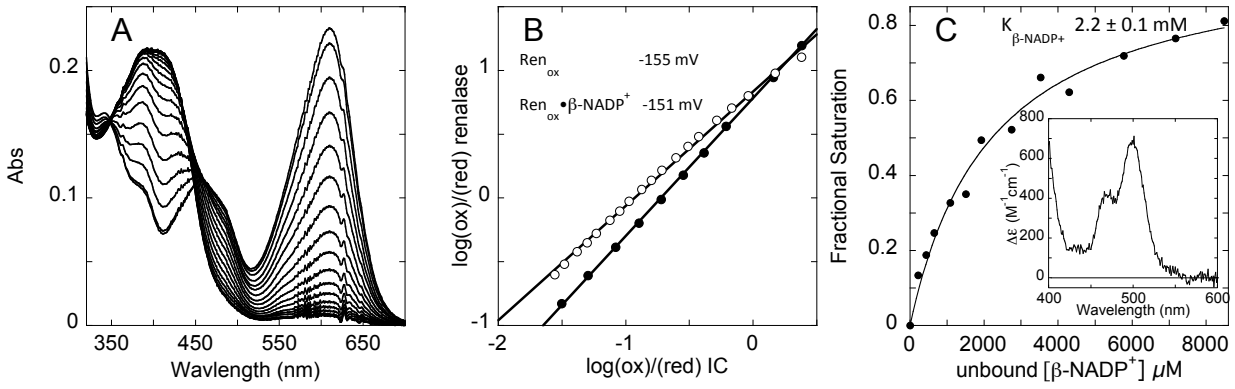

Figure 4.1. Redox States of Renalase. **A**: Simultaneous reduction of renalase (10 μM) and indigo carmine (10 μM) when reacted with 150 nM xanthine oxidase, 5 μM methyl viologen, 300 μM Xanthine in PBS buffer under anaerobic conditions. **B**: Analysis of the data in A. The extent reduced for the enzyme and the dye was assessed where neither had a changing contribution from the other; 470 nm for renalase and 610 nm for indigo carmine. The data for Ren$_{ox}$ are depicted in open circles and that for Renox•β-NADP$^+$ are shown as filled circles. **C**: Measurement of the dissociation constant for the Ren$_{ox}$•β-NADP$^+$ complex. Renalase (20 μM) was titrated with β-NADP$^+$ and the perturbation of the flavin spectrum observed. Inset depicts the ~80% saturation difference spectrum.

The dissociation constant for the renalase product complex (Ren_{ox}•β-$NADP^+$) was measured using perturbation of the flavin absorption spectrum in the presence of the ligand (Figure 4.1C). These data indicate a relatively weak complex with a dissociation constant of 2.2 mM and are consistent with the prior work of Milani et al. who measured a value of 1.6 mM under similar conditions. [77] The reduction potentials of Ren_{ox} and the Ren_{ox}•β-$NADP^+$ complex and the dissociation constant for the Ren_{ox}•β-$NADP^+$ complex complete three sides of a thermodynamic box linking enzyme reduction and β-$NADP^+$ complexation. The small difference in reduction potentials for Ren_{ox} and Ren_{ox}•β$NADP^+$ indicate that the dissociation constants of the oxidized or reduced renalase β-$NADP^+$ complexes are similar (Scheme 4.2). These data suggest that in the Ren_{ox}•β-$NADP^+$ complex the nicotinamide ring and the isoalloxazine ring of the renalase FAD cofactor are not in sufficient proximity to influence the cofactor's reduction potential.

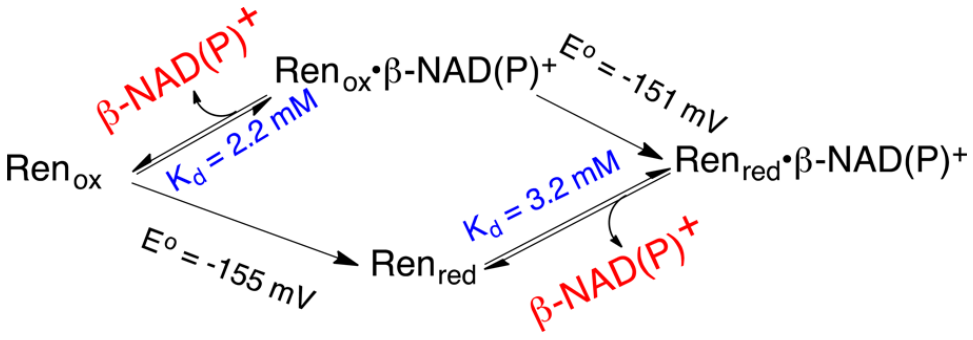

Scheme 4.2. Thermodynamic box linking renalase reduction and β-NADP+ complexation.

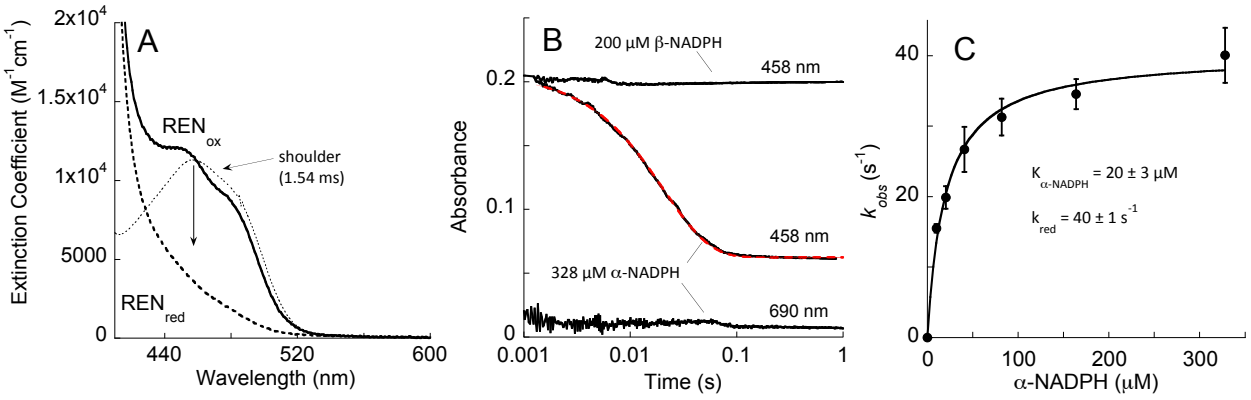

Figure 4.2. Reductive Half Reaction of Renalase. **A**: Initial (solid line) and final (dashed line) absorption spectra when 328 μM α-NADPH was reacted with 20 μM renalase under anaerobic conditions. The dotted line spectrum is the spectrum of resting oxidized renalase. **B**: Absorbance traces at 458 nm and 690 nm when 328 μM α-NADPH was reacted with 20 μM renalase under anaerobic conditions. The dashed line is the fit (red) to a single exponential phase (Equation 4.2) with a rate constant of 41 s^{-1}. Upper trace is for the reaction of 20 μM renalase with 200 μM solution freshly dissolved β-NADPH under anaerobic conditions. **C**: Dependence of the observed rate constant for reduction when when varied pseudo-first order concentrations of α-NADPH were reacted with 2 μM renalase under anaerobic conditions. The fit is to equation 4.3 and gave a limiting rate constant for reduction of 40±1 s^{-1} and a dissociation constant for α-NADPH of 19.8±2.6 μM.

Reductive Half-Reaction: The reductive half reaction of renalase was observed independent of oxidative chemistry by combining the enzyme with α-NADPH and excluding dioxygen (Figure 4.2). The α-NADPH substrate was supplied from a solution of NADPH at anomeric equilibrium (1.5% α-anomer). Under these conditions the α-NADPH substrate initiates reduction of the flavin observed as a decrease in the absorption transitions centered around 458 nm (Figure 4.2A & B). Freshly dissolved β-NADPH does not induce flavin reduction (Figure 4.2B). The dependence of the observed rate constant for reduction of the renalase flavin cofactor on the α-NADPH concentration could be fit to a rectangular hyperbola according to Equation 4.2 (Figure 4.2C). This equation assumes rapid equilibrium binding that diminishes the observed rate constant of reduction at subsaturating substrate

concentrations. [157] The asymptote is thus the limit of the rate constant for reduction (k_{red} = 40.2±1.3 s^{-1}) and the concentration at which the observed rate constant for reduction is half maximal is the dissociation constant for α-NADPH ($K_{\alpha\text{-NADPH}}$ = 19.9±2.6 μM). These experiments required the use of low renalase concentration (2 μM) in order to be pseudo-first order with a range of α-NADPH concentrations that reasonably span the α-NADPH binding isotherm according to the $K_{\alpha\text{-NADPH}}$ value. A second experiment was also undertaken with relative high renalase concentration (20 μM) and α-NADPH (328 μM) concentrations in order to observe potential charge-transfer absorption transitions at longer wavelengths that would indicate proximity of the nicotinamide and FAD isoalloxazine rings (Figure 3.2A & B). [158, 159] Figure 4.2B includes a long wavelength trace that indicates no significant accumulation of charge-transfer transitions before, during or after reduction. Figure 4.2A includes deconvoluted component spectra obtained from single exponential fits to photo-diode array data for the reductive half reaction. These spectra also show that no significant new absorbance transitions indicative of charge-transfer absorption transitions were observed. It is therefore conceivable that neither α-NAD(P)H nor β-$NAD(P)^+$ nicotinamide rings stack with the flavin isoalloxazine ring (*vide infra*). The first spectrum acquired at 1.54 ms indicates that the flavin absorption transitions become resolved directly prior to reduction (Figure 4.2A – solid line). This perturbation may arise either in the Ren_{ox}•α-NADPH complex or potentially in a ribose ring-open iminium ion complex that forms rapidly prior to flavin reduction such as proposed in the hypothetical catalytic cycle depicted in Scheme 4.3.

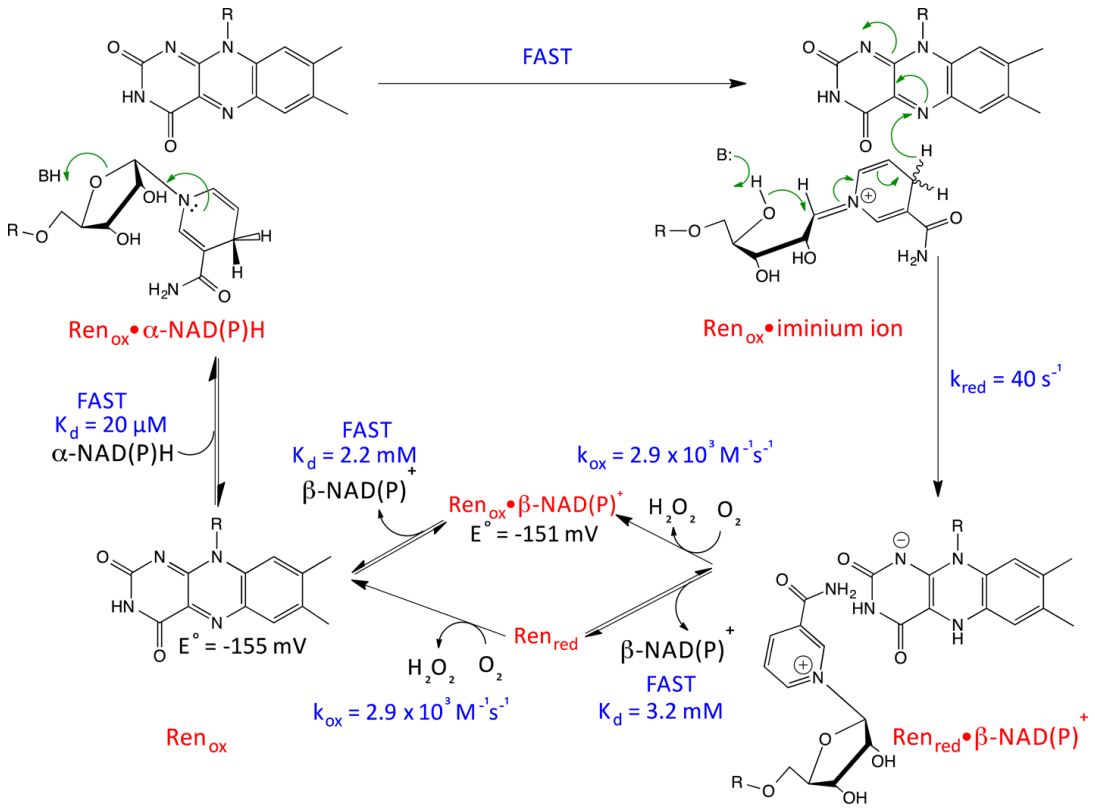

Scheme 4.3. Proposed oxidation/anomerization mechanism.

Oxidative Half-Reaction. The oxidative half reaction of renalase is observed as a monophasic return to the oxidized state of the flavin cofactor. Figure 4.3A summarizes the data obtained when renalase was reduced by limiting concentrations of α-NADPH in the absence or presence of pseudo-first order concentrations of dioxygen. The reductive and oxidative processes differ sufficiently to allow both phases to be observed. When dioxygen concentration was titrated in successive reactions the observed rate constant for reoxidation had a linear dependence on the molecular oxygen concentration that passed through the origin (Figure 4.3B). This indicates that the reaction of reduced renalase with dioxygen is reliant on collision without prior complexation. The slope of the dependence indicated a rate constant of 2.95 x10^3 ± 70 $M^{-1}s^{-1}$, a value similar to that of autooxidation of FAD in solution [160] suggesting that renalase does not promote the reaction of its cofactor with dioxygen

and dictating that reoxidation will generally be the rate-limiting process *in vitro* under conditions of atmospheric dioxygen (~250 μM).

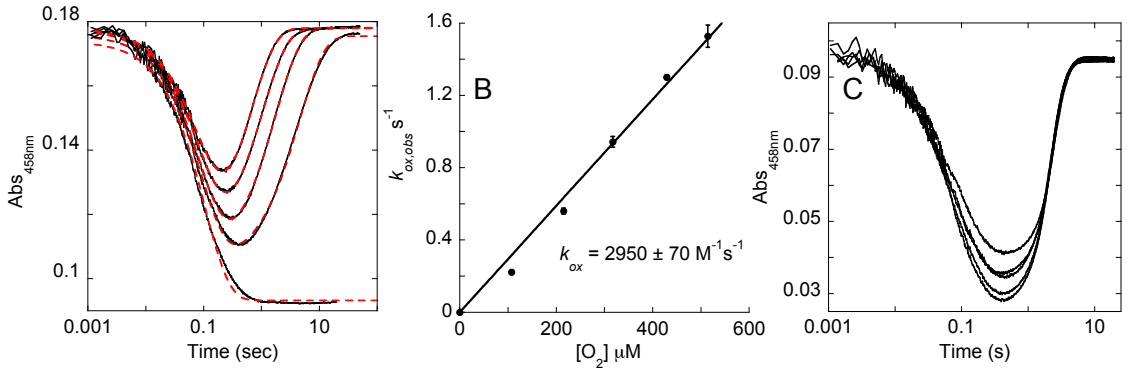

Figure 4.3. Single Turnover of Renalase with Limiting α-NADPH. **A**: Traces observed at 458 nm when 14 μM renalase was reacted with 5.7 μM α-NADPH in varied pseudo-first order concentrations of molecular oxygen. The traces shown in ascending order are for 0, 107, 215, 317, 514 μM dioxygen. Data obtained without dioxygen were fit to a single exponetial decay (Equation 4.2) and data obatined with dioxygen were fit to two exponential phases (Equation 4.4) (fits shown as dashed red lines). **B**: The dependence of the observed rate constant for reoxidation (k_2) on the concentration of molecular oxygen fit to a straight line that passes through the origin. The slope of the line indicates a second order rate constant for the addition of dioxygen of 2.9 x 10^3 $M^{-1}s^{-1}$. **C**: Influence of β-$NADP^+$ on Single Turnover Kinetics. Renalase (10 μM) was mixed with α-NADPH (20 μM) and varied β-$NADP^+$ (0-1600 μM) in the presence of 250 μM dioxygen. The traces in ascending order are for 100, 200, 400, 800, 1600 μM β-$NADP^+$.

In order to evaluate the timing of the release of the β-$NAD(P)^+$ product with respect to reoxidation of the flavin cofactor, exogenous β-$NAD(P)^+$ was titrated in single turnover reactions (Figure 4.3C). These data indicated that increasing concentrations of the β-nicotinamide product had no influence on the observed rate constant for reoxidation suggesting that reoxidation is not contingent on the release of β-$NAD(P)^+$. Consistent with the observed complexation of β-$NADP^+$ with the oxidized enzyme, our data show that this molecule is weakly competitive with α-NADPH as the observed rate of reduction slows with increasing β-$NADP^+$ concentration (observed as a decrease in the amplitude for the reductive phase). Therefore we conclude that dioxygen and the nicotinamide

ring of β-NAD(P)$^+$ do not compete for access to the reduced flavin cofactor during reoxidation. Overall the data are consistent with a kinetically ordered release of products with β-NAD(P)$^+$ dissociating prior the reoxidation of the enzyme. Exogenous β-NAD(P)$^+$ can populate the Ren_{ox}•β-NAD(P)$^+$ complex and hinder α-NADPH association to the oxidized enzyme, however, the physiological relevance of this observation is negligible as the concentration of β-NAD(P)$^+$ in the blood is low relative to its dissociation constant. [161]

Extent of Anomerization of α/β-NADP$^+$ by Oxidized Renalase: The ability of oxidized and reduced renalase to catalyze non-redox coupled anomerization was assessed by incubating oxidized or reduced renalase with an α/β-NADP$^+$ mixture of known anomer ratio. The ratio of both anomers was remeasured after incubations with oxidized or reduced renalase for defined times over an hour. Figure 4.4 illustrates that for renalase in either oxidation state the ratio of α- to β-NADP$^+$ is unchanged. This establishes that anomerization does not occur before FAD cofactor reduction, while it is reduced or after its reoxidation and suggests that the oxidative and epimerization activities of renalase are mechanistically linked via a common intermediate.

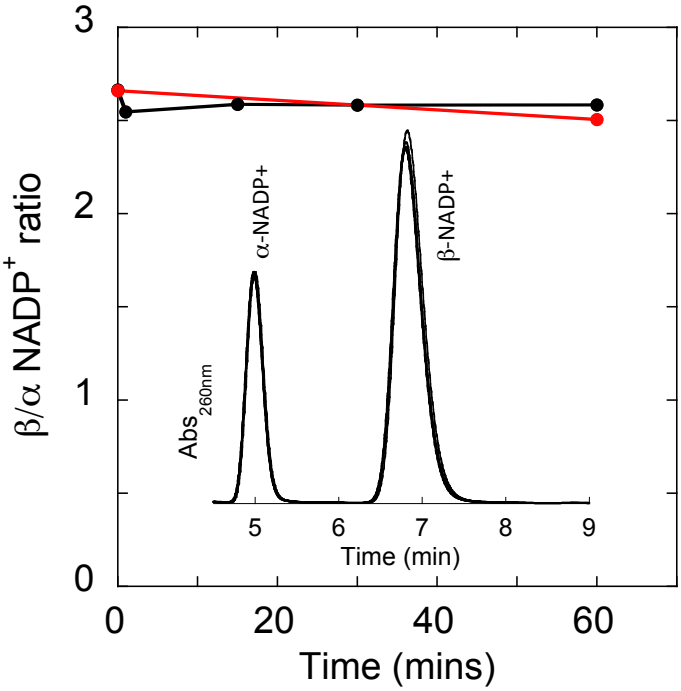

Figure 4.4. Extent of Anomerization by Renalase in the Oxidized and Reduced States. Data depict the extent of anomerization of a 75 μM mixture of 1/2.66 α/β-$NADP^+$ in the presence of 5.6 μM oxidized (black line) and 6.0 μM reduced (red line) renalase. The observed α/β $NADP^+$ ratio was based on HPLC peak area integration. The inset shows HPLC data for the oxidized enzyme experiment (four overlaid chromatograms are shown). Species were separated using a Xterra reverse phase C18 column running isocratically in 10 mM sodium phosphate buffer, pH 7.5.

Discussion

Renalase is a recently discovered flavoprotein that has been widely reported to be a kidney hormone whose endocrine function is to lower circulating concentrations of catecholamine neurotransmitters, such as epinephrine, thereby lowering blood pressure and heart rate. [46] Reported slow rates of turnover with catecholamine substrates *in vitro* do not address catalytic enhancements, nor do they offer a definitive demonstration of the products formed or the reaction stoichiometry[91, 110][91, 110][91, 110][91, 110].[16,17] As such the claimed “monoamine oxidase C”

activity of renalase continues to be challenged in the literature[85, 88, 89, 162][85, 88, 89, 162][85, 88, 89, 162][85, 88, 89, 162].[21,22,37,38] The identification of α-NAD(P)H oxidase/anomerase activity for renalase calls for re-evaluation of many of the reported physiological observations as the only known vasoactive molecule to be consumed or liberated by this activity is H_2O_2. [149-151] However, the concentration of this product is contingent on the low equilibrium concentration of α-NADPH that would be maintained near zero by renalase activity, meaning that the rate of H_2O_2 production by renalase would be dependent on the *in vivo* β to α NAD(P)H anomerization rate constant (ca 10^{-6} s^{-1}). [95]

Reconciling each of the observations and conclusions made for renalase is complicated by the use of different preparations of the enzyme. Renalase was initially expressed as a recombinant glutathione synthase fusion and isolated using glutathione sepharose. [2] Later preparations were isolated from urine using an anti-renalase affinity column.[46, 110] More recent preparations have used heterologous expression in *E. coli* from a synthetic codon-optimized renalase gene. Heterologous expression from the optimized gene yields a modest fraction of folded enzyme and a large fraction of inclusion body peptide. [55] The smaller, as expressed, soluble fraction can be purified by conventional methods [76, 77, 154] and was the form used to obtain the available X-ray crystal structure [77]. It is likely that this is the native form of renalase as it is this form that exhibits the α-NAD(P)H oxidase/anomerase activity described herein. [154] The second reported preparation method involves solubilizing inclusion body peptide and refolding by dilution and pH titration. [55] This form of renalase does not have the spectrophotometric properties of the soluble fraction and does not exhibit the α-NAD(P)H oxidase/anomerase activity [154] but has been used in a number of physiological studies of renalase that report vasoactivity[55, 91].

We have completed a preliminary examination of the catalytic cycle of the, as expressed, soluble renalase reacting with α-NADPH. We define substrate affinities, the rate constants for those steps that contribute to the turnover number and propose a hypothetical mechanism for the observed activity. Scheme 4.3 depicts an annotated chemical mechanism that accounts for each of the observations made in this study. The data suggest the redox and anomerization activities of renalase are coupled via a shared intermediate as neither the oxidized nor the reduced enzyme can catalyze anomerization of $NADP^+$ (Figure 4.4). Catalysis commences with the association of α-NAD(P)H to renalase to form the Ren_{ox}•α-NAD(P)H complex (K_d ~ 20 μM). The lack of charge-transfer absorbance transitions for this complex suggests that the nicotinamide base does not stack with the flavin isoalloxazine (Figure 4.2). [79] It is proposed instead that rapid delocalization of the dihydropyridine lone pair and protonation of the bridging oxygen atom of the ribose ring forms a iminium ion intermediate. The iminium ion then recyclizes at the ribose, simultaneously causing the formation the β-$NAD(P)^+$ product with concerted reduction of the flavin cofactor (k_{red} ~40 s^{-1}). Much like the Ren_{ox}•α-NAD(P)H complex, the nicotinamide ring of the Ren_{red}•β-$NAD(P)^+$ complex is oriented with respect to the flavin isoalloxazine ring system such that it does not promote charge-transfer transitions (Figure 4.1C & Figure 4.2B). In this position, the β-nicotinamide of the product complex does not impede the reaction of the reduced flavin with dioxygen (k_{ox} ~2.9x10^3 $M^{-1}s^{-1}$) so that the β-$NAD(P)^+$ release and reoxidation steps occur independently (Figure 4.3C). Further evidence for this is that the reduction potentials of the unliganded oxidized enzyme and the Ren_{ox}•β-$NAD(P)^+$ complex are ostensibly the same. This also indicates that the dissociation constant of the Ren_{ox}•β-$NAD(P)^+$ complex (K_d ~2.2 mM) is similar to the Ren_{red}•β-$NAD(P)^+$ complex (Figure 4.1, Scheme 4.2, Scheme 4.3). In addition, the lack of influence of β-$NAD(P)^+$ on the observed rate constant for reoxidation indicates that the rate constant for reoxidation (k_{ox} ~ 2.9 x 10^3 $M^{-1}s^{-1}$) is the same for the unliganded

reduced enzyme and the Ren_{red}•β-NAD(P)$^+$ complex (Figure 4.3C). A weak reassociation propensity of β-NADP$^+$ with oxidized renalase forms a dead-end complex that can retard binding of α-NAD(P)H (Figure 4.3C) suggesting that the nicotinamide substrate and product occupy the same or overlapping binding pockets.

Renalase turnover has two rate contributing chemistries, two-electron reduction of the flavin (~40 s^{-1}) and its subsequent re-oxidation (2.9 x 10^3 $M^{-1}s^{-1}$). The latter of these will typically have the greatest contribution to the turnover number *in vitro* under conditions of atmospheric oxygen (~250 μM O_2). However, in blood the concentration of available α-NAD(P)H will be negligible as a consequence of the large driving force for the renalase reaction (ΔG~120 kJ/mol) [95], while dissolved dioxygen will be approximately constant at ~140 μM. Under these conditions renalase activity will be primarily responsive to the α-NAD(P)H concentration, consistent with a role for renalase of minimizing the α/β-NAD(P) ratio.

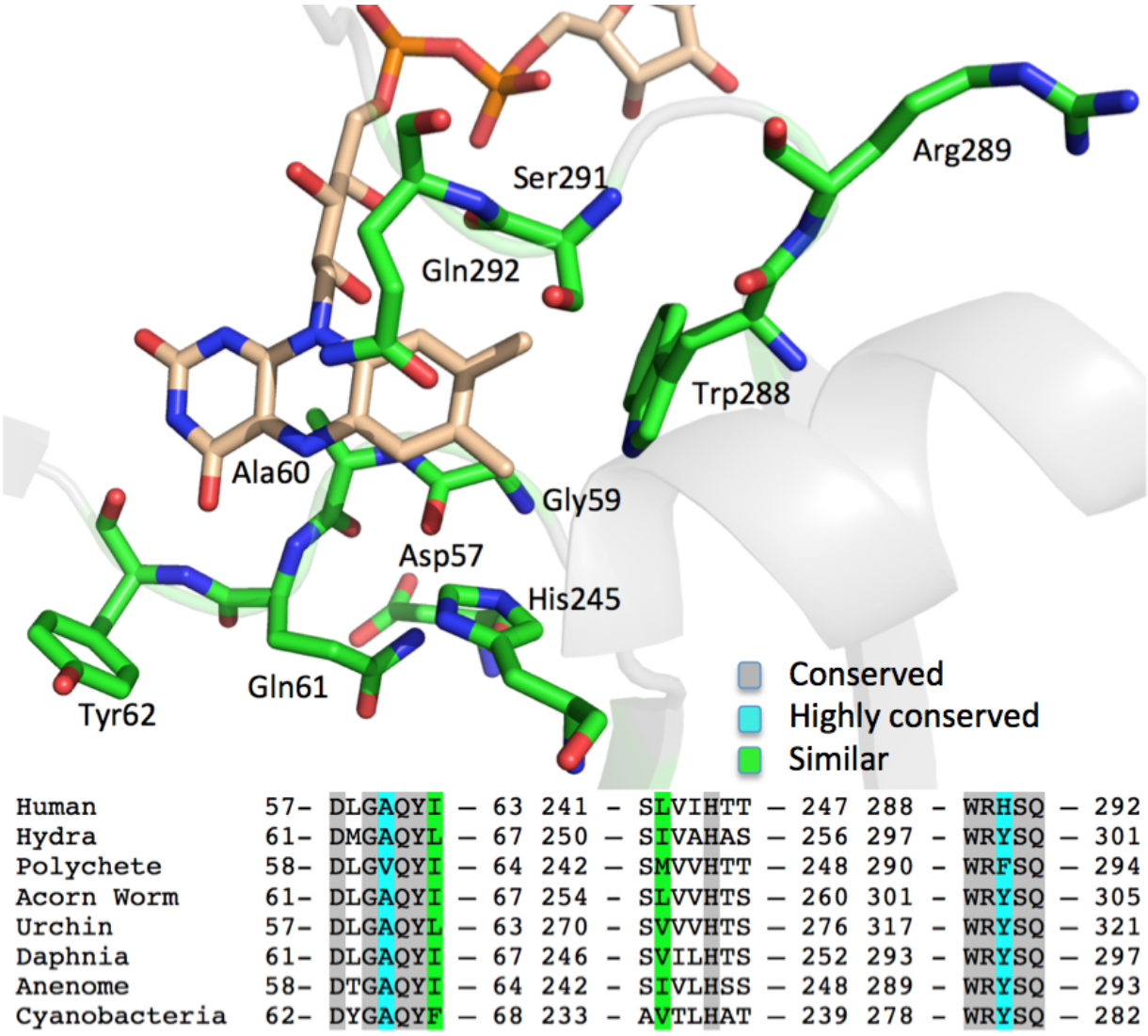

Figure 4.5. Conservation Within the Renalase Active Site. Structure shown is for human renalase (PDB ID 3QJ4). Sequence data are for the primary structures of renalase and unconfirmed renalase-like proteins from a number of divergent phyla.

Renalase is reported to be expressed in numerous tissues [46, 73] and the conserved active site residue motif can be identified in homologous proteins from animals such as anemones, polycheates, daphnia and even single-celled organisms such as cyanobacteria (Figure 4.5). This implies that the root physiological role of renalase is more pervasive than vasodilation. The α-NAD(P)H oxidase/anomerase activity of renalase is significantly exothermic which implies that the purpose of

this activity is to use the considerable oxidative power of dioxygen to deplete the α-NAD(P)H concentration. In the absence of renalase, the inherently lower reduction potential of α-NAD(P)H molecules (-340 mV) dictates that they will tend to oxidize by reducing β-NAD(P)$^+$ or other singlet molecules of higher potential and become isolated, unable to be reincorporated into metabolism. This would result in a steady but inexorable loss of function for a major fraction of available NAD(P) molecules. It is therefore reasonable to conclude that the renalase α-NAD(P)H oxidase/anomerase activity is important to all metabolism in order to maintain the α/β-NAD(P)H ratio at ostensibly zero such that the preponderance of nicotinamide dinucleotides remain available for redox cycling.

Chapter V
A Metabolic Function for Human Renalase: Oxidation of Isomeric Forms of β-NAD(P)H that are Inhibitory to Primary Metabolism.

Brett A. Beaupre, Matt R. Hoag, Joseph Roman, F. Holger Försterling, Graham R. Moran

Abstract

Renalase is a recently identified flavoprotein that has been associated with numerous physiological maladies. There remains a prevailing belief that renalase functions as a hormone, imparting an influence on vascular tone and heart rate by oxidizing circulating catecholamines, chiefly epinephrine. This activity however, has not been convincingly demonstrated *in vitro*, nor has the stoichiometry of this transformation been shown. In prior work we demonstrated that renalase induced rapid oxidation of low-level contaminants of β-NAD(P)H solutions (Beaupre, B. A., Hoag, M. R., Carmichael, B. R., and Moran, G. R. (2013), *Biochemistry 52*, 8929-8937, Beaupre, B. A., Carmichael, B. R., Hoag, M. R., Shah, D. D., and Moran, G. R. (2013), *J Am Chem Soc 135*, 13980-13987). Slow aqueous speciation of β-NAD(P)H resulted in the production of renalase substrate molecules whose spectrophotometric characteristics and equilibrium fractional accumulation closely matched those reported for α-anomers of NAD(P)H. The fleeting nature of these substrates precluded structural assignment. Here we structurally assign and identify two substrates for renalase. These molecules are 2-, and 6-dihydroNAD(P), isomeric forms of β-NAD(P)H that arise either by non-specific reduction of β-$NAD(P)^+$ or by tautomerization of β-NAD(P)H (4-dihydroNAD(P)). The pure preparations of these molecules induce rapid reduction of the renalase flavin cofactor (230 s^{-1} for 6-dihydroNAD, 850 s^{-1} for 2-dihydroNAD) but bind only a few fold tighter than β-NADH. We also show that 2-, and 6-dihydroNAD(P) are potent inhibitors of primary metabolism dehydrogenases and therefore conclude that the metabolic function of renalase is to oxidize these isomeric NAD(P)H molecules to β-$NAD(P)^+$, eliminating the threat they pose to normal respiratory activity.

Introduction

Renalase is a flavoprotein that has been proposed to be an enzyme/hormone produced by the human kidney to attenuate blood pressure and slow the heart [46]. It has been asserted that this physiological response is achieved by catabolizing circulating catecholamines [110]. However, this claimed activity has never been convincingly demonstrated and a number of factors portend a more prevalent metabolic role for renalase. The first is that renalase transcripts have been detected in numerous mammalian tissues [73, 163, 164]. The second is that the X-ray crystal structure of renalase has revealed a unique constellation of conserved residues about an active site flavin isoalloxazine ring that form a structural motif that is identifiable in homologs as far removed as the cyanobacteria [34, 77]. Despite numerous reports of physiological relevance, a definitive catalytic reaction for renalase has remained elusive [57, 58, 60, 72, 108, 165-168]. The most persistent claim is that renalase acts as the third monoamine oxidase (MAO C), oxidizing and cyclizing epinephrine and requiring NADH as a reductant to form the aminochrome molecule, adrenochrome [57, 91]. The reported rates for this conversion, however, are exceedingly slow and the apparent odd stoichiometry of this reaction, in which four electrons are mobilized, has not been established.

In prior work, we identified fleeting minor contaminants of β-NAD(P)H solutions as substrates for renalase. These molecules induced rapid reduction of the active site flavin that then reoxidized by reduction of dioxygen. Product analysis indicated β-NAD(P)$^+$ and hydrogen peroxide as products in 1:1:1:1 stoichiometry leading to the conclusion that renalase is an oxidase. On the basis of both spectrophotometric characteristics and aqueous equilibrium proportions we erroneously proposed that the substrates for renalase were the α-anomers of NAD(P)H [34, 94-96] and that the function of renalase was therefore to oxidize and epimerize α-NAD(P)H anomers to avoid an inexorable loss of

cellular redox currency as α-NAD(P)$^+$ (molecules that have no known metabolic role in mammalian metabolism). This proposed activity seemed to satisfy a long standing conundrum whereby despite reported lower reduction potentials for α-anomers, α-NAD(P)$^+$ molecules are not observed to accumulate to any significant level in normal metabolism [137].

The purpose of this article is to correct the renalase literature, provide direct evidence for the structure of the renalase substrate(s) molecules described in our prior reports and link these molecules to an apparent important metabolic role for the activity observed. In this study we show that the substrate(s) for renalase are 2-dihyhdroNAD (2DHNAD(P)) and 6-dihydroNAD (6DHNAD(P)), both of which are isomeric forms of β-NAD(P)H where the hydride equivalent resides on either the 2 or the 6 position of the nicotinamide instead of the native 4 position. These molecules arise from non-specific (non-enzymatic) reduction of β-NAD(P)$^+$ or tautomerization of β-NAD(P)H and can inhibit multiple dehydrogenase enzymes of primary metabolic pathways. Renalase would therefore appear to alleviate this inhibition by oxidizing 2DHNAD(P) and 6DHNAD(P) to form β-NAD(P)$^+$ (Scheme 5.1).

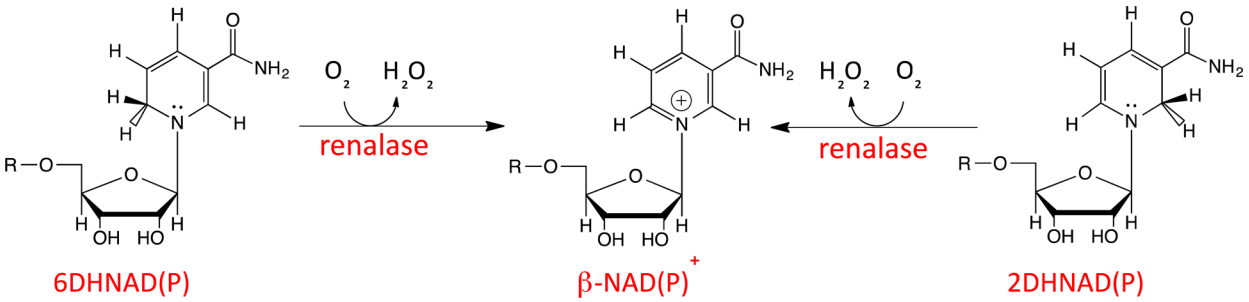

Scheme 5.1. Oxidation of NAD(P)H isomers.

Materials and Methods

Materials. β-NADH (disodium salt, trihydrate) was obtained from Amresco. β-NAD^+, oxaloacetate, (±)-α-lipoamide and lactate dehydrogenase (LDH) (rabbit muscle) were each sourced from Sigma-Aldrich. Sodium borohydride, potassium phosphate (mono and dibasic), β-mercaptoethanol and pyruvate were from Acros. Deuterium oxide was from Cambridge Isotopes. Sep-Pak cartridges were purchased from Waters. Competent NEB5 and BL21 DE3 *Escherichia coli* cells were obtained from New England Biolabs. Q-sepharose was from Bio Rad. Lipoamide dehydrogenase (DLD) (porcine heart) was from Calzyme.

Malate dehydrogenase (MDH) was cloned from *E. coli*. Genomic DNA was isolated from 100 mL of log-phase cells (OD_{600nm} ~0.5) using a Qiagen Genomic DNA preparation kit and protocol. The MDH gene was amplified using oligonucleotides complementary to the 3' and 5' ends of the gene that incorporated respective Nde I and Xho I restriction sites (5' ATTATTATTATTCAT**ATG**AAAGTCGCAGTCCTCGCGT 3', 5' TTTTTTTTTTTTTTCTGGAG**TTATTA**CTTATTAACGAACTTCGCC 3'; start and stop codons are depicted bolded and restriction sites underlined). The amplified gene was then digested with the above two restriction enzymes and ligated with pET17b plasmid that had been digested in the same way. The ligation was then transformed into competent NEB5 *E. coli* cells and plated onto Luria Bertani (LB) agar, 100 μg/mL ampicillin. Transformant cultures prepared from individual colonies were grown in LB broth, 100 μg/mL ampicillin and were screened for the correct plasmid insert by agarose gel electrophoresis. Plasmid DNA from each transformant was prepapred using the Qiagen Mini-prep kit and protocol followed by digestion with Nde I and Xho I restriction enzymes. The plasmid from verified cell lines were then prepared in sufficient quantity for DNA sequencing using the Qiagen Midi-prep kit and protocol. After sequence confirmation the plasmid, pECMDH, was then transformed into

competent BL21(DE3) *E. coli*. A single colony was selected and grown in LB broth medium containing 100 μg/mL ampicillin. Cells from this culture were harvested in early log phase and mixed with 0.22 μm filter sterilized glycerol to a final concentration of 20% v/v and stored as 1 mL aliquots at -80 ^{o}C.

MDH was expressed and purified by thawing cell stocks and plating 100 μL per plate onto LB agar plates (100 μg/mL ampicillin) and grown at 37 ^{o}C for 16 hrs. The lawn of cells from two plates was then resuspended into 10 mL of LB broth and used as an inoculum for 1 L LB broth culture (100 μg/mL ampicillin) pre-warmed to 37 ^{o}C. The cell culture was then shaken at 220 rpm and the temperature maintained at 37 ^{o}C. When the density of the culture reached OD_{600nm}~1.0, 0.1 mM isopropyl-β-thiogalactopyranoside (IPTG) was added to induce over-expression of the MDH protein. After two hours the culture was harvested by centrifugation at 4000 g in an RC-3C Sorvall centrifuge and the cell pellet resuspended in 20 mL of ice-cold 20 mM HEPES buffer, 2 mM β-mercaptoethanol (βME), pH 7.0. All subsequent methods maintained the temperature of the sample at 4 ^{o}C, unless otherwise noted. The cell slurry was then sonicated for a total of 5 minutes at 20 Watts using a Branson sonicator fit with a blunt tungsten tip. The resulting sonicate was then centrifuged at 15,600 g for 30 minutes using an Eppendorf 5804R centrifuge. The supernatant was then brought to 1.5% streptomycin over a period of 20 minutes and centrifuged at 12,850 g for 10 minutes. The supernatant obtained was decanted and brought to 45% ammonium sulfate saturation over 25 minutes and centrifuged again at 12,850 g for 10 minutes. The supernatant was retained and brought to 75% ammonium sulfate saturation over a period of 25 minutes and centrifuged at 12,850 g for 10 minutes. The pelleted protein was then redissolved in 20 mM HEPES, 2 mM βME, pH 7.0 (100 mL per liter of culture) and loaded onto a 2.5 x ~25 cm Q-sepharose column at a flow rate of 2 mL/min. Pure MDH protein was then eluted using a linear gradient to 200 mM NaCl spanning a volume of 400 mL supplied from a Biorad Biologic LC chromatographic system. The MDH obtained was then concentrated using 15 mL

Amicon, 10 kDa nominal molecular weight cutoff centrifugal concentrator and stored at -80 ^{o}C. The pure enzyme was quantified using the calculated extinction coefficient for 280 nm of 6085 $M^{-1}cm^{-1}$ [169].

The gene for *Saccharomyces cerevisiae* old yellow enzyme (OYE, isoform 1) cloned into the Nde I and Xho I restriction sites of pET28a was obtained from Enzymax as an *E. coli* XL-1 blue transformant culture. Cloning into the Nde I restriction site fuses the OYE1 gene to an N-terminal His-Tag. A 50 µL aliquot of these cells was used to make cell stocks by culturing in 20 mL of LB broth (25 µg/mL kanamycin) incubated at 37 ^{o}C with shaking at 220 rpm for 6 hrs. Cells from this culture were stored in sterile 20% glycerol at -80 ^{o}C. Plasmid (pSCOYE) was prepared from 5 mL cultures of these cells using the Qiagen mini-prep kit and protocol and transformed into *E. coli* BL21(DE3) and prepared as cell stocks from a single colony as described above for pECMDH plasmid. OYE was expressed and purified by spread plating onto LB agar (25 µg/mL kanamycin, 100 µL of cells per plate) and incubating at 37 ^{o}C for 20 hrs. The lawn of cells from two plates was resuspended in ~20 mL of LB broth and used as an inoculum for a 1 L culture of LB both (25 µg/mL kanamycin). Expression of the OYE protein and harvesting of the cells proceeded in an identical manner to that described above for *E. coli* MDH.

To prepare pure OYE the harvested cells were resuspended 20 mL/L of culture, 20 mM HEPES pH 7.5 and sonicated for ~10 min at 20 Watts. The lysed cell slurry was then centrifuged at 15,600 g for 30 minutes and the supernatant (~25 mL/L of culture) was then loaded onto a Talon cobalt affinity column at a flow rate of 1 mL/min and the column was washed with 200 mL 50 mM HEPES, 10 mM imidazole, pH 7.5. OYE was then eluted with a 400 mL linear gradient to 50 mM HEPES, 300 mM imidazole, pH 7.5 using a Biorad Biologic liquid chromatography device. Fractions containing OYE activity were then pooled and the buffer exchanged to 10 mM potassium phosphate buffer, pH 7.5

using an Amicon 15 mL, 10,000 nominal molecular weight cutoff filter/concentrator. The pure OYE obtained was then aliquoted and stored at -80 ^{o}C. OYE was quantified using the 461 nm extinction coefficient of the flavin cofactor (10,400 $m^{-1}cm^{-1}$) that was determined using an SDS denaturation method based on the extinction coefficient of free flavin [94].

Preparation, Separation and Analysis of 2 & 6DHNAD. 2- & 6DHNAD were prepared by reduction of β-NAD^{+}. The ratio of reactants used was developed empirically such that the fractional accumulation of 2DHNAD (the less stable of the products) was comparable to that of 6DHNAD and β-NADH (4DHNAD). Initially, a 37 mM sodium borohydride solution was prepared in 20 mM potassium phosphate titrated to pH 11. A 200 µL aliquot of this solution was then added to a freshly prepared 15.5 mM solution of β-NAD^{+} in 100 mM potassium phosphate pH 7.5. Analytical high-pressure liquid chromatography (HPLC) separation of the products of β-NAD^{+} reduction was achieved using an Xterra C18 reverse phase column (4.6 x 150 mm, 3.5 µM particle size) run isocratically at 0.5 mL/min in 10 mM potassium phosphate buffer pH 7.5. Purification of 2 & 6DHNAD was achieved by preparative HPLC. The partially reduced β-NAD^{+} solution was injected (50-500 µL) onto a Phenomenex reverse-phase phenyl HPLC column (21.2 x 250 mm) run isocratically at 5 mL/min with a mobile phase of 10 mM potassium phosphate, pH 7.5. Both the analytical and preparative columns were coupled to a Waters 600E pump and Waters 2487 dual wavelength detector and the elution of component species was observed simultaneously at 260 and 340 (or 394) nm. To prepare samples for nuclear magnetic resonance (NMR) and mass spectrometry, reduced products were collected individually into 400 mL glass vessels immersed in liquid nitrogen. The pure dilute solutions were then thawed and desalted at 4 ^{o}C by loading onto a 35 cc C18 Sep-Pak cartridge (Waters) and eluted with a 200 mL gradient from 10 mM to 0 mM potassium phosphate pH 7.0 using a Biorad Biologic liquid chromatography device. The desalted

samples were then dried by lyophilization (in order to minimize ambient temperature decomposition, the lyophilization vessels were embedded in ice throughout). Each of the desalted, dry and pure reduction products was then dissolved in cooled deuterium oxide (D_2O) and used immediately for NMR or dissolved in cooled water for mass spectrometry. For kinetic studies, the product identified as 6DHNAD was collected, desalted and concentrated and redissolved in D_2O as described above and stored at -80 ^oC. The product identified as 2DHNAD could not be stored due to pronounced instability and was instead collected from the HPLC and used immediately (within 1-5 mins).

Spectrophotometric Quantification of NAD Molecules. The concentration β-NADH was determined using published 340 nm extinction coefficient of 6220 M^{-1} cm^{-1} *[95].* Dihydronicotinamide chromophore extinction coefficients for 2 & 6DHNAD (and the 260 nm extinction coefficient for β-NAD^+) were obtained using renalase to oxidize both molecules to β-NAD^+. Initially, the spectrum of each of the HPLC purified molecule (70-90 μM) was acquired using a Hewlett Packard 8453 spectrophotometer. The 2 & 6DHNAD were then oxidized to β-NAD^+ by adding 30 nM renalase. 4DHNAD (β-NADH) prepared in the same manner was oxidized to β-NAD^+ by the addition of 30 nM OYE. Under these conditions complete oxidation was achieved in 2-3 minutes. The pairs of fully reduced and fully oxidized spectra obtained from each reaction were then multiplied by the factor required to normalize the β-NAD^+ spectra and then all spectra were multiplied by the factor required to convert the β-NADH spectrum to equal its known extinction coefficient at 340 nm. This method gave extinction coefficient of ε_{394nm} = 5360 $M^{-1}cm^{-1}$ for 2DHNAD, ε_{345nm} = 6580 $M^{-1}cm^{-1}$ for 6DHNAD (*cf.* α-NADH ε_{345nm} = 6170 $M^{-1}cm^{-1}$) and ε_{260nm} = 18800 $M^{-1}cm^{-1}$ for β-NAD^+.

Mass Spectrometry. For both 2 & 6DHNAD, an HPLC purified and C^{18} Sep-Pak desalted sample (~50-100 μM, prepared as described above) was collected. This sample was injected via a Shimadzu LC-2010C liquid chromatography system onto a Shimadzu 2020 mass spectrometer. In each case, 10 μL of sample was delivered in a 1:1 mixture of water and methanol. Data were collected in negative ion mode in the mass range 100-800. This procedure was also followed for β-NADH, β-NAD^+ as controls.

Nuclear Magnetic Resonance. NMR experiments were carried out at 280 K in D_2O solvent using a Bruker DRX-500 NMR spectrometer equipped with a triple axis gradient inverse (BBI) probe operating at a frequency of 499.832389 MHz for proton and 125.6936644 MHz for ^{13}C. Chemical shifts are reported relative to the methyl signal of the sodium salt of 3-(trimethylsilyl) propanesulfonic acid using the residual HDO signal as indirect reference. One-dimensional experiments were performed by accumulating 128 scans using a spectral width of 10330 Hz (^1H) and 20161 Hz (^{31}P) and using relaxation delays of 1s and 3s, respectively. For a typical gradient selected DQF -COSY experiment 960 t_1 increments with 32 transients of 2048 points covering a spectral width of 5000 Hz were acquired. $^1H\{^{13}C\}$-HSQC spectra were acquired with gradient selection and multiplicity editing, using 730 t_1 increments with 64 transients of 1600 points each, covering a spectral width of 5000 Hz and 22624 Hz in f2 and f1, respectively. A mixing time of 3.4 ms was used. $^1H\{^{13}C\}$-HMBC spectra utilized gradient selection acquiring 820 t_1 increments with 160 transients of 4096 data points each with a spectral widths in f2 and f1 of 5000 Hz and 25140 Hz, respectively, and a mixing time of 50 ms. A low-pass filter was employed to suppress one bond J_{CH} couplings. All spectra were analyzed and assigned using Topspin 3.2 software (Bruker BioSpin).

Reductive Half-Reaction of Renalase with 2 & 6DHNAD. The reductive half-reaction of renalase could be observed independent of subsequent oxidative processes by exclusion of dioxygen. Renalase (5 mL, 20 μM) in 2 x PBS buffer containing 1 mM dextrose was added to the main chamber of a glass tonometer and glucose oxidase (25 μL, 25 units) was added to a detachable side arm. The tonometer was then assembled and embedded in ice and the renalase and glucose oxidase solutions were made anaerobic by exchanging argon for dissolved dioxygen. This was achieved by 45 alternating cycles of low-level vacuum followed by the introduction high-purity argon gas (at 5 psi). The argon was passed through an Alltech oxygen-reactive cartridge and sparged through anaerobic water. Throughout this procedure the sample was equilibrated with the argon atmosphere by gentle agitation after each set of three exchange cycles. Once anaerobic, the glucose oxidase was combined with the renalase/dextrose solution and mounted onto a Hitech (now TgK) DX2 stopped flow instrument. 6DHNAD samples were thawed (see above) and diluted to target concentrations in water containing 1 mM glucose. Each 6DHNAD sample was then placed in a glass syringe, inverted and sparged with argon gas for 5 minutes. Before capturing and mounting the substrate solution to the stopped flow instrument, 10 μL of glucose oxidase (10 units) was injected via the luer tip. 2DHNAD substrate solutions were prepared in an equivalent manner but were collected directly from preparative HPLC purification (50-90 μM) and used immediately (see above).

Renalase and substrate solutions were mixed and reduction of the renalase cofactor was observed at 458 nm. The stability of 6DHNAD substrate allowed it to be prepared in sufficient concentrations to achieve pseudo-first order reaction conditions. As such the data for this substrate was fit to a linear combination of two exponentials according to Equation 5.1 using Kinetic Studio software (TgK Ltd). In this equation A_1 and A_2 are the amplitudes associated with the first and second rate constants, k_{1obs} and k_2, and C is the absorbance at end of the reaction. The dependence of the

k_{1obs} values determined was then fit to the hyperbolic form of the single-site binding equation (Equation 5.2) according to Strickland, where k_{red} is the limiting rate constant for reduction and K_{6DHNAD} is the dissociation constant for 6DHNAD [157].

Equation 5.1 $$A_{458} = A_1(e^{-k_{1obs}t}) + A_2(e^{-k_2 t}) + C$$

Equation 5.2 $$k_{obs} = \frac{k_{red}[6DHNAD]}{(K_{6DHNAD}+[6DHNAD])}$$

For 2DHNAD, 100 µM was the approximate maximum concentration obtained from preparative HPLC; as such, the reductive half-reaction with this substrate was conducted under second-order reactant conditions and the data obtained were fit globally using Kintec Explorer to the model shown in Scheme 5.2. In this model the Ren_{ox}•2DHNAD complex k_{on} rate constant was arbitrarily assigned to ~10^8 $M^{-1}s^{-1}$, and the ratio of the k_3 and k_{-3} for the Ren_{red}•β-NAD^+ complex was confined to equal the measured dissociation constant for the Ren_{ox}•β-NAD^+ complex (for justification, see below).

$$Ren_{ox} + 2DHNAD \underset{k_{-1}}{\overset{k_1}{\rightleftharpoons}} Ren_{ox}\ 2DHNAD \xrightarrow{k_2} Ren_{red}\bullet\beta\text{-}NAD^+ \underset{k_{-3}}{\overset{k_3}{\rightleftharpoons}} Ren_{red} + \beta\text{-}NAD^+$$

Scheme 5.2. Renalase reductive half-reaction as modeled for fitting.

The Dissociation Constants for the Ren_{ox}•β-NADH and Ren_{ox}•β-NAD^+ Complexes. The dissociation constants for the Ren_{ox}•β-NADH and Ren_{ox}•β-NAD^+ complexes were measured by perturbation of the renalase flavin spectrum in the presence of each ligand. In order to avoid slow non-specific reduction of the renalase flavin by β-NADH during the experiment, a ~10 mL stock of renalase (15 μM) was prepared in PBS buffer at 25 ^oC. From this stock a 0.9 mL aliquot was added to a 1.5 mL quartz cuvette and 0.1 mL of β-NADH was added to this sample from a set of eight 2-fold serially diluted stocks. As such the spectrophotometric data are compiled from eight separate renalase samples observed shortly after the addition of β-NADH for concentrations that spanned the range 0 - 3.51 mM. The dissociation constant for the Ren_{ox}•β-NAD^+ complex was measured by preparing a single 20 μM solution of renalase in PBS buffer at 25 ^oC. To this solution β-NAD^+ was titrated such that a range of concentrations from 0-~6mM was achieved (higher concentrations induced marked precipitation of the enzyme).

For both β-NADH and β-NAD^+ titrations, spectra (250-900 nm) were acquired for each ligand concentration using a Shimadzu 1800 spectrophotometer. After correction for dilution, the change in absorption at 550 nm and 500 nm was used to determine the dissociation constant for the Ren_{ox}•β-NADH and the Ren_{ox}•β-NAD^+ complexes respectively. The changes in absorbance were fit to the hyperbolic form of the single site binding equation (Equation 5.3) in which f is fractional saturation and K_{ligand} is the dissociation constant for either β-NADH or β-NAD^+ for the respective Ren_{ox} complex.

Equation 5.3. $$f = \frac{[ligand]}{(K_{ligand}+[ligand])}$$

2 & 6DHNAD Dehydrogenase Inhibition. Inhibition of dehydrogenases from primary metabolism by 2 & 6DHNAD was assessed using two approaches. The relative stability of 6DHNAD allowed the collection of a series of nested Michaelis-Menten curves each acquired in the presence of a different concentration of the candidate inhibitor. The relative instability of 2DHNAD dictated that the 50% inhibitory concentration (IC50) method of Cheng and Prusoff was used for determination of Ki [170, 171]. Via this approach, 2DHNAD need only be separated from 6DHNAD and β-NADH using preparative HPLC, quantified and diluted to the target concentration before adding to the assay; as such the pure 2DHNAD is used within five minutes of purification.

6DHNAD and 2DHNAD Ki values were measured for three dehydrogenase enzymes of primary metabolism; malate dehydrogenase (MDH), lactate dehydrogenase (LDH), and lipoamide dehydrogenase (DLD). To limit the influence of enzyme instability encountered with the MDH and LDH enzymes, a solution of 0.3 U/mL was prepared in 10 mM potassium phosphate pH 7.5 and then frozen at -80 ^{o}C as 2 mL aliquots. These samples were then thawed and used as required. By contrast, DLD (0.3 U/mL) maintained activity when incubated at 4 ^{o}C and so was prepared in 100 mM potassium phosphate pH 7.5 and placed on ice until used in assays. For assessment of 6DHNAD inhibition of MDH and LDH a series of five Michaelis-Menten analyses were completed using β-NADH concentrations from 0-80 μM in the presence of saturating respective oxaloacetate (0.4 mM) and pyruvate (0.5 mM). For MDH and DLD, 6DHNAD were varied from 0-2 μM, while for LDH the range of 6DHNAD used was 0-20 μM. The data obtained for MDH and LDH were fit globally to the competitive inhibition model using the non-linear least squares analysis provided by Prism 6 software (Graphpad Software Inc.).

Ki values for 2DHNAD with MDH, LDH, and DLD were assessed using the IC50 method. In this method the extent of inhibition for a range of 2DHNAD concentrations was measured at a concentration of β-NADH equivalent to the measured Michaelis constant for this substrate. This value was determined in the absence of inhibitor and at near saturating concentrations of the oxidized substrate (0.4 mM oxaloacetate, 0.5 mM pyruvate, 1 mM lipoamide acid for MDH, LDH and DLD respectively). All data were fit using non-linear least squares analysis available from Kalieidagraph software (Synergy Software Inc). The data obtained in the absence of the inhibitor was fit to equation 5.4, the Michaelis-Menten equation, where v is the observed rate, V_{max} is the maximal rate of reaction and $K_{\beta\text{-NADH}}$ is the Michaelis constant for β-NADH. The extent of inhibition was then measured for a range of 2DHNAD concentrations and the data obtained was fit to the Hill equation (equation 5.5) to derive the IC50 mid-point as a measure of the Ki value for 2DHNAD.

Equation 5.4 $$v = \frac{V_{max}[\beta-NADH]}{(K_{\beta-NADH}+[\beta-NADH])}$$

Equation 5.5 $$v = V_{min} + \frac{V_{max}-V_{min}}{(1+(\frac{[2DHNAD]}{K_i})}$$

Results

Renalase Substrates are Generated by Non-Specific Reduction of β-NAD$^+$. In prior work we identified small equilibrium proportions of molecules in β-NAD(P)H solutions that were oxidized by renalase. The absorption maxima, extinction coefficients and apparent equilibrium proportions correlated well with those reported for α-anomers of NAD(P)H molecules, but the fleeting behavior of these molecules precluded rigorous structural assignment. We have since devised methods to both form

larger fractional accumulations of these molecules by reduction of β-NAD^+ and prolong the decay half-life such that structural assignments can be made. Figure 5.1A illustrates the chromatographic separation of the reduced products obtained when β-NAD^+ is reduced by both hydrosulfite and borohydride. While hydrosulfite (E^o=-0.62 V) yields only β-NADH (4DHNAD), reduction by borohydride (E^o=-1.24 V) yields three products, two of which are substrates for renalase (Figure 5.1B). The third component, that was not a substrate for renalase, had a retention time identical to that of β-NADH. When reacted with renalase, the product from both substrate molecules was identified here (and in prior work) as β-NAD^+ and this product was made in near equimolar concentration to the amount of dioxygen consumed (Figure 5.1B inset)[94]. The absorption spectra of the reduction products indicate distinct UV/Vis maxima at 345, 394, and 340 nm for the dihydro-nicotinamide moiety in each case (Figure 5.1C).

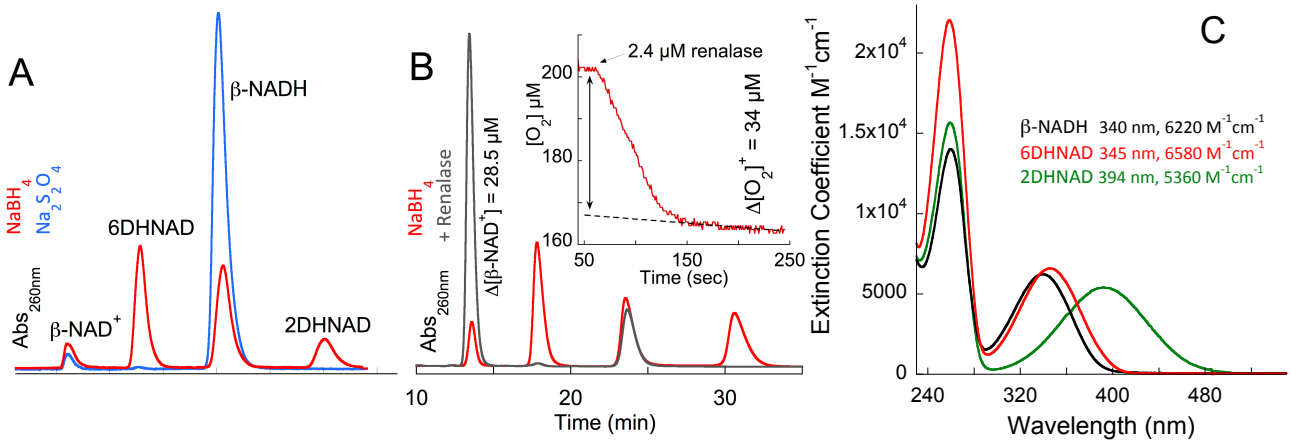

Figure 5.1. Generation of Renalase Substrates by Reduction of β-NAD^+. **A** – Analytical HPLC chromatograms recorded after the reduction of 50 μM β-NAD^+ with 50 μM sodium hydrosulfite (blue line) or 50 μM sodium borohydride (red line). **B** - Analytical HPLC chromatograph demonstrating the consumption of two of the three products of sodium borohydride reduction by the addition of 2.4 μM renalase. The inset is taken from observation of the reaction shown in **B** using a Clark-type dioxygen electrode. After cessation of dioxygen consumption (~100 s) the sample was filtered using an Amicon 0.5 mL 10 kDa centrifugal filtration device and re-chromatographed as described (gray vs red chromatogram). **C** – Molar absorptivity absorption spectra of the purified reduction products.

Structural Assignment of Renalase Substrates. The unique absorption maxima of each borohydride reduction product were used to aid isolation of sufficient quantities by preparative HPLC for structural characterization. The mass of all reduction products was found to be 664.40±0.05, equal to the mass of the β-NADH control. The mass of the product formed from renalase activity was 662.40±0.00, equivalent to that of the β-NAD^+ control. NMR spectra were recorded at 280 K in D_2O solvent. For each product, one-dimensional H^1 (1D), H^1 homonuclear correlation (COSY), H^1-C^{13} heteronuclear single quantum coherence (HSQC) and H^1-C^{13} heteronuclear multiple bond correlation (HMBC) spectra were obtained. Chemical shift and H^1 coupling assignments are included in Table 5.S1 in the supplementary materials section. Figure 5.2 depicts the proton resonances assigned to the dihydronicotinamide rings of three products obtained from borohydride reduction. In terms of homonuclear H^1 geminal and vicinal coupling, nicotinamide dinucleotides have four isolated sets of protons; those for the adenine and nicotinamide bases and two for the ribose moieties. Structural assignment of the nicotinamide bases therefore relies heavily on HMBC spectra to link the proton residing on the ribose anomeric carbon to the proximal N2 and N6 carbons and/or the protons residing on N2 and N6 to the anomeric carbon. These multi-bond heteronuclear couplings both orient the nicotinamide nuclear spin-system with respect to the ribose and also permit deconvolution of the individual ribose resonances that are then identified by sequential geminal homonuclear coupling. The pivotal geminal, vicinal homonuclear couplings and heteronuclear multiple bond couplings are indicated in Figure 5.2 by respective blue and red arrows. Correlations of this type were readily made for the 340 nm and 345 nm absorption maxima species, and these were assigned as 4- (β-NADH), and 6DHNAD respectively (Figure 5.2A & 5.2B). Note that the multiplet for the nicotinamide N5' proton of 6DHNAD is obscured by the residual water resonance and is instead depicted inset as the

homonuclear coupling crosspeak to the N6’ protons. The relative instability of the reduction product that exhibited the 394 nm absorption maximum precluded obtaining assignments by this approach. Control H^1 1D NMR spectra taken before and after two-dimensional heteronuclear spectra acquisition repeatedly indicated substantial degradation of the 394 nm species. As such the structural assignment of the 394 nm species as 2DHNAD is principally based on H^1 homonuclear couplings. For this species we observe a ~6-7 Hz geminal coupling for the N4’ (d), N5’(m) and N6’(d) protons and a absence of geminal couplings in the resonances assigned to N2’ protons that each exhibit only a vicinally coupled ~12 Hz doublet (Table 5.1, Figure 5.2).

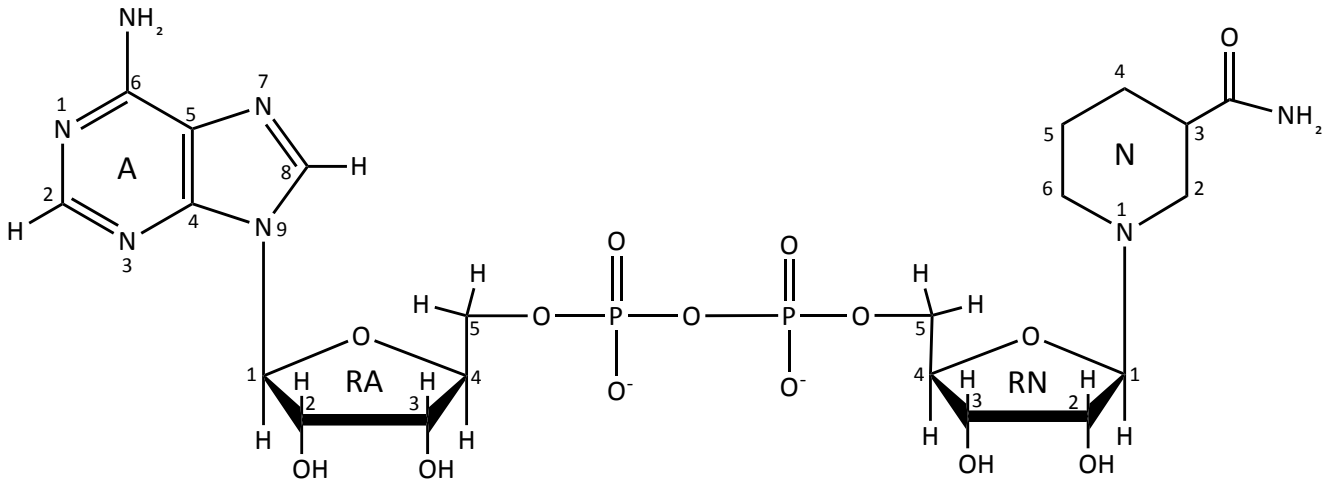

	β-NADH			6DHNAD			2DHNAD		
Position	^{1}H Shift (ppm)	multip.,J(Hz)	^{13}C Shift (ppm)	^{1}H Shift (ppm)	multip.,J(Hz)	^{13}C Shift (ppm)	^{1}HShift (ppm)	multip.,J (Hz)	^{13}C Shift (ppm)
	6.57	s	138.3	6.74	s	145.1	3.25	d, 12.4	
N2							3.68	d, 12.9	
	2.38	dt,17.8, 2.2	21.7	5.42	d	119.0	6.31	d, 6.1	
N4	2.22	dd, 18.4, 3.1							
N5	4.39	dd,	74.4	4.67	m*	112.6	4.45	t, 6.7	
	5.61	d, 8.14	122.9	3.60	dd, 15.1, 2.9	42.1	6.10	d, 7.1	
N6				3.40	dt, 15.1, 2.9				
R1 1	4.44	d, 7.48	94.7	4.51	d, 7.21	97.1	4.48	d, 7.48	
	3.85	dd, 7.48, 6.73		3.98	dd, 7.26,	67.9	4.02	m, nm	
R1 2					5.46				
R1 3	3.94	m	64.8	3.88	m	70.5	3.89	m, nm	
R1 4	3.90	m	n/a	3.79	m	82.1	3.84	m	
R1 5	3.766	m	65.8	3.74	m	65.6	3.62	m	
R2 1	5.79	d, 5.4	86.6	5.78	d, 5.8	86.5	5.75	d, 5.7	
	4.37	dd, 5.42, 5.16	74.4	4.41	dd,	74.2	4.38	t, 5.4	
R2 2					5.39,5.99				
	4.17	dd, 5.16, 4.13	70.0	4.18	dd, 5.14,	70.0	4.17	m	
R2 3					3.58				
R2 4	4.050	m, n/a	83.5	4.04	m	83.5	4.07	m	
R2 5	3.90	dd,dd,	65.0	3.89	m	64.9	4.00	m	
A2	7.87	s	152.3	7.88	s	152.3	7.89	s	
A8	8.15	s	139.5	8.18	s	139.1	8.17	s	

Table 5.1. Chemical shift and H^1 coupling assignments for 2-, 4-, and 6DHNAD.

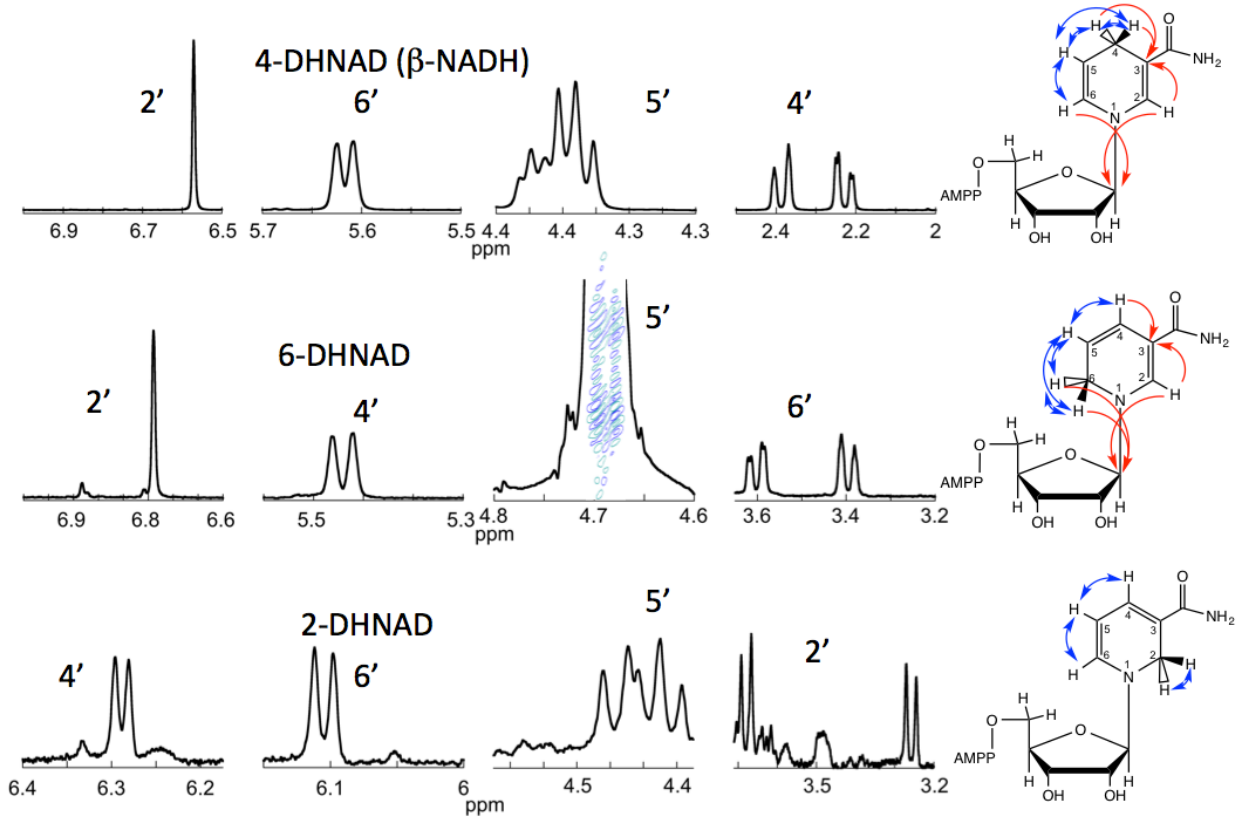

Figure 5.2. NMR Identification of the Purified Products of Sodium Borohydride reduction of β-NAD^+. Spectra were recorded at 280 K in deuterium oxide. Structures to the right depict the primary couplings used for identification of the β-NADH isomers. Blue arrows indicate homonuclear coupling, while red arrows indicate heteronuclear multi-bond coupling.

Renalase Reductive Half-Reaction. In prior work we published data for the reductive half-reaction of renalase [34]. In these experiments the substrate was supplied to the enzyme in an apparent equilibrium mixture arising from aqueous speciation of β-NADPH (Scheme 5.S1). As such the data obtained were not for a pure substrate molecule and included potential competitive inhibition effects from the β-NADPH background (see below). Here we show the reductive half-reactions for renalase with pure 2- and 6DHNAD. While 6DHNAD has sufficient stability to be purified and stored for use in such experiments, 2DHNAD does not and typically decomposes with a half-life of approximately 30

minutes. For this reason 2DHNAD was used immediately after preparative HPLC isolation and was limited to ~100 μM concentration by the capacity to resolve 2DHNAD from other reduction products with the preparative reverse-phase phenyl HPLC column used for purification. To observe reduction of the renalase flavin cofactor by 2- and 6DHNAD, anaerobic renalase (10 μM final) was mixed with varied concentrations of the anaerobic substrates. For 6DHNAD the range of substrate concentration used spanned approximate pseudo-first order reactant ratios (50-800 μM). The data obtained were thus fit to exponential decay(s) (Equation 5.1). Two phases were observed in the reduction traces. The first phase accounted for ~90% of the amplitude change and was indicative of flavin reduction. The rate constants for this phase (k_{1obs}) derived from fitting displayed a hyperbolic dependence that was fit to Equation 5.2 to derive the limiting rate constant for reduction from the asymptote (234 s^{-1}) and the dissociation constant for the Ren_{ox}•6DHNAD complex (173 μM). The rate constant for the second phase did not exhibit a 6DHNAD dependence, and was fit to ~20 s^{-1} in all traces. We propose that flavin reduction forms the Ren_{red}•β-NAD^+ complex whose flavin spectrum is altered by the proximity of the flavin and nicotinamide rings. This phase is thus tentatively assigned as the decay of the Ren_{red}•β-NAD^+ complex with the egress of β-NAD^+ from the active site. A complete mechanistic assignment of the reductive half-reaction is beyond the scope of this study.

Our limited capacity to isolate and stabilize 2DHNAD dictated that the reductive half-reaction for renalase oxidizing this substrate was observed within a range of substrate concentrations that were second-order with respect to the enzyme concentration. As such the data obtained could only be analyzed by fitting the integrated rate expression for a more complete kinetic model as shown in Scheme 5.2. In this model the ratio of the β-NAD^+ dissociation and association rate constants (k_3:k_{-3}) was fixed to that defined by the dissociation constant for the Ren_{ox}•β-NAD^+ complex. This fitting restriction was based on our prior observation that the β-NAD^+ product does not modulate the

reduction potential of the flavin cofactor and therefore has equal affinity for the Ren_{ox} and Ren_{red} forms (see below) [34]. In addition the reductive step (k_2) in which the hydride equivalent is transferred from 2DHNAD to the flavin was defined as irreversible in accord with the assumption that the difference in reduction potential of these two species is greater than 100 mV (ΔG>-20 kJ/mole). Lastly, the association rate constant for 2DHNAD (k_1) was confined as ~10^8 $M^{-1}s^{-1}$, close to the limit of diffusion. The fit obtained indicated a k_{red} for 2DHNAD of 860 s^{-1}, 3.6-fold faster than that measured for 6DHNAD but with a similar a dissociation constant of 166 µM.

Dissociation Constants for the Ren_{ox}•β-NADH and Ren_{ox}•β-NAD^+ Complexes. We propose that the metabolic function of renalase is to alleviate inhibition of primary metabolism by oxidizing isomers of β-NAD(P)H molecules that arise through tautomerization and/or non-specific reduction of β-NAD^+ (Scheme 5.3). As such renalase operates in an environment of near-isosteric non-substrate molecules

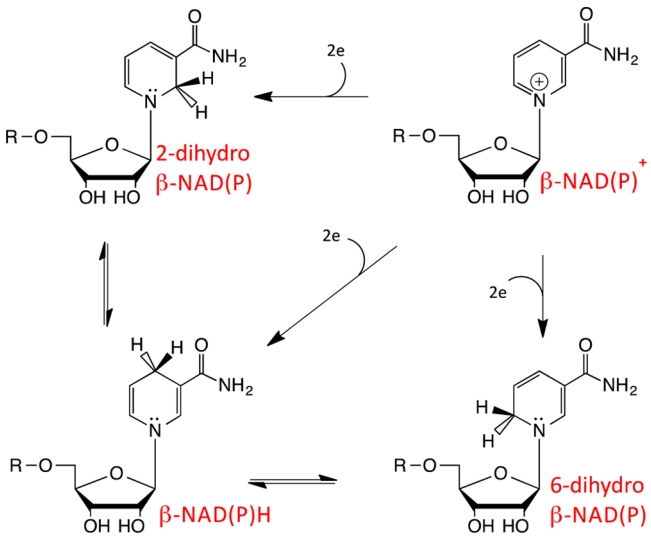

Scheme 5.3. Proposed metabolic role of isomer oxidation.

such as β-NAD(P)H and β-NAD(P)$^+$ that are present in considerably higher concentration and presumably inhibitory. In order to gauge selectivity for 2- and 6DHNAD the dissociation constants for the Ren$_{ox}$•β-NADH and Ren$_{ox}$•β-NAD$^+$ complexes were measured using perturbation of the renalase flavin spectrum as physical evidence of association. These data fit well to a single site binding equation (Equation 5.3) and indicated that renalase is only three-fold selective against β-NADH ($K_{β\text{-NADH}}$ = 570±90 μM) (Figure 5.4A), but is 34-fold selective against β-NAD$^+$ ($K_{β\text{-NAD+}}$ = 5960±800 μM) (Figure 5.4B). Association of β-NADH induced new absorption transitions at long wavelength indicative of charge-transfer presumably made possible by proximity of the dihydronicotinamide and flavin rings [158] (Figure 5.4A inset).

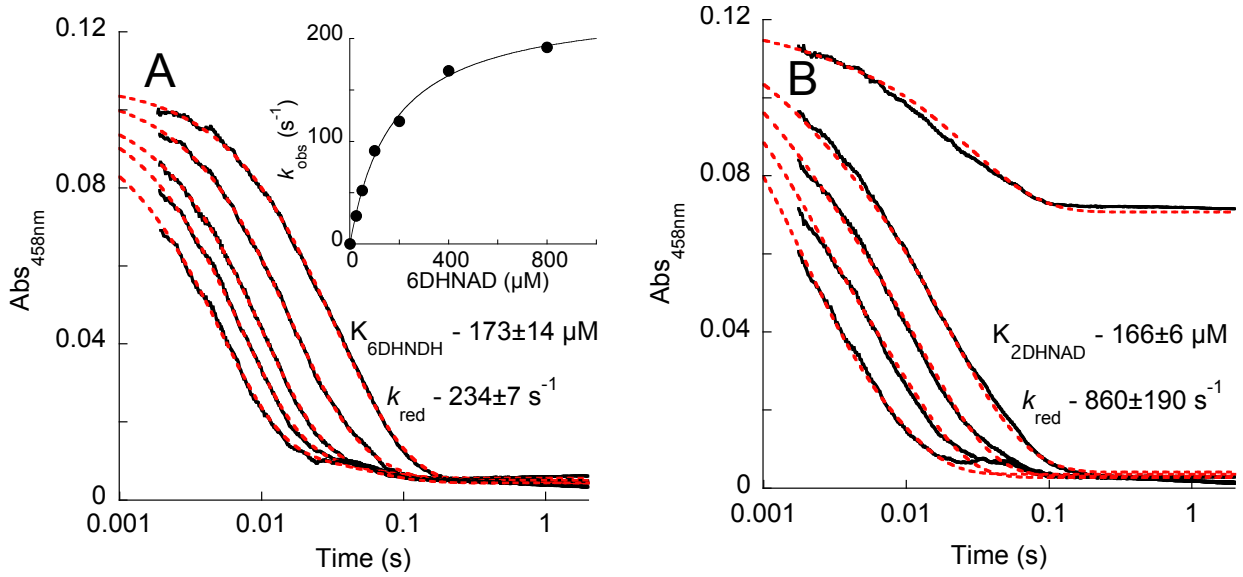

Figure 5.3. The Reductive Half-Reactions of Renalase with 2 & 6DHNAD. A – Reduction of the renalase cofactor (10 μM) in the presence of 6DHNAD. Traces shown are for 25, 50, 100, 200, 400, and 800 μM 6DHNAD. The data were fit (red dashed lines) to a linear combination of two exponential decays according to Equation 5.1. Inset shows the dependence of the observed rate constants on the concentration of 6DHNAD fit to Equation 5.2. **B** – Reduction of the renalase cofactor (10 μM) in the presence of 2DHNAD. Traces shown are for 3.7, 14.5, 21.3, 30.0, 43.5 μM 2DHNAD. These data were fit globally to the kinetic model depicted in Scheme 5.2.

Dehydrogenase Inhibition. Lowry et al. and Dalziel reported that β-NADH preparations contained contaminants that were inhibitory to LDH [172, 173], and this observation has since been confirmed by numerous other authors [98, 99, 174, 175]. In this study we measure K_i values for 2- and 6DHNAD to three dehydrogenase enzymes from primary metabolism. These data are summarized in Figure 5.5. Predictably, 6DHNAD inhibition was best fit to a competitive pattern with respect to β-NADH. The instability of 2DHNAD precluded categorization the inhibition pattern, though it can be reasonably assumed that 2DHNAD competes with β-NADH similarly. The data indicate that both 2- and 6DHNAD have high affinity for dehydrogenases and therefore pose a threat to primary metabolism. For *E. coli* MDH, 6DHNAD has exceedingly high affinity (K_i = 34 ± 3 nM) while 2DHNAD has only modest inhibitory affinity for this enzyme (K_i = 3.05 ± 0.33 μM). LDH from rabbit muscle shows similar high affinity for both 2- and 6DHNAD (K_i ~ 500-600 nM). DLD is a β-NADH-dependent dehydrogenase component of both the pyruvate decarboxylase complex and the α-ketoglutarate decarboxylase complex. Curiously, this dehydrogenase does not appear to bind either 2- or 6DHNAD with significant affinity. Collectively these data establish a credible metabolic function for renalase; oxidation of NAD(P)H isomers that arise from tautomerization or non-specific reduction of β-$NAD(P)^+$ in order to alleviate stringent inhibition of essential dehydrogenase enzymes.

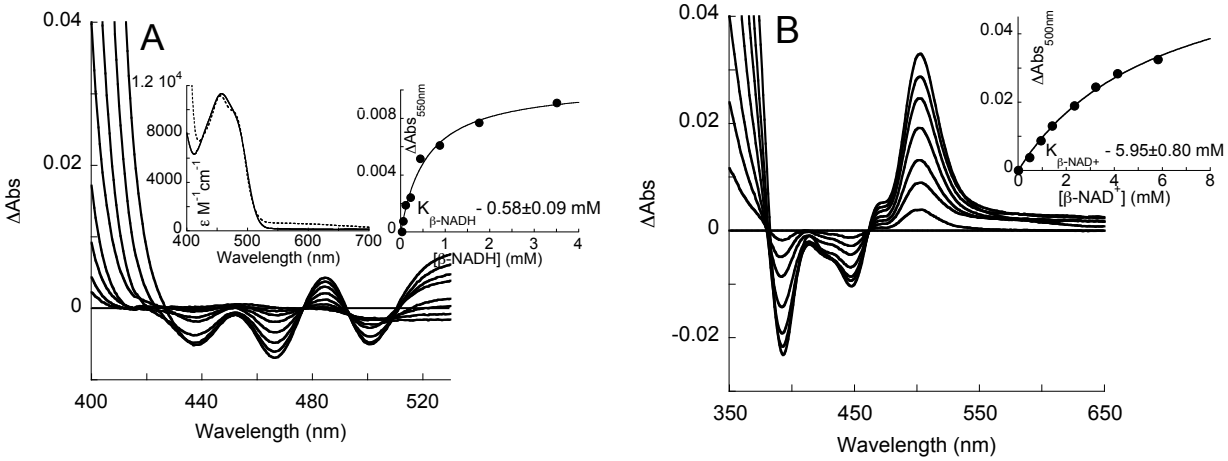

Figure 5.4. Measurement of the Dissociation Constants for the Ren_{ox}•β-NADH and Ren_{ox}•β-NAD+ Complexes. **A -** Difference absorption spectra for the renalase flavin at various concentrations of β-NADH. Inset(left) shows the charge transfer absorption band observed when 3.51 mM β-NADH was added (dashed line) to renalase. Inset(right) depicts the perturbation of the flavin spectrum at 550 nm as a function of β-NADH concentration fit to Equation 5.3. **B -** Difference absorption spectra for the renalase flavin at various concentrations of β-NAD^+. Inset depicts the perturbation of the flavin spectrum at 550 nm as a function of β-NADH concentration fit to Equation 5.3.

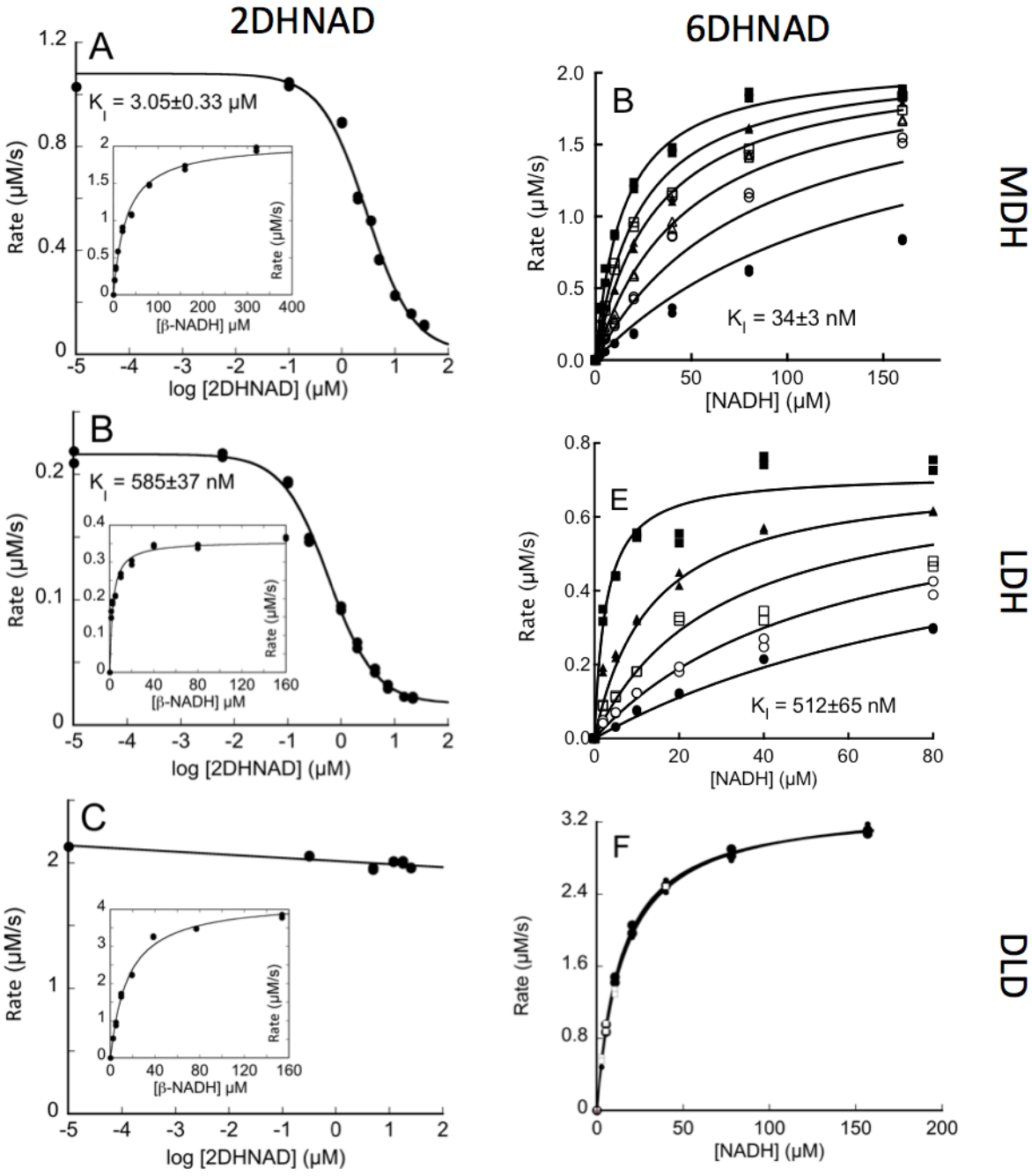

Figure 5.5. Inhibition of Dehydrogenases from Primary Metabolism by 2 & 6DHNAD. **A** & **D** depict evidence for the inhibition of *E. coli* malate dehydrogenase by 2DHNAD and 6DHNAD respectively. In **D** the 6DHNAD concentrations used were 0, 20, 40, 80, 160, 320 nM. **B** & **E** depict evidence for the inhibition of porcine heart lactate dehydrogenase by 2DHNAD and 6DHNAD. In **E** the 6DHNAD concentrations used were 0, 2, 5, 10, 20 μM. **E** & **F** depict evidence for the absence of inhibition of *rabbit muscle* lipoamide dehydrogenase by 2DHNAD and 6DHNAD respectively.

Discussion

In this report we provide a credible thesis for the metabolic function of renalase. We assert that renalase oxidizes inhibitory isomers of β-NADH, forming β-NAD^+ and delivers the electrons harvested to dioxygen. We offer evidence for the structures of two substrate molecules that arise from non-specific reduction of β-NAD^+ and present an initial characterization of the kinetics of the reductive half-reaction observed with these substrates. This study also serves to correct our earlier erroneous claim that renalase oxidizes α-NADH molecules [34, 94]. The data presented here indicate that the substrate molecule identified in prior work was not α-NAD(P)H but instead 6DHNAD(P), a species that has the same λmax (345 nm), ostensibly the same extinction coefficient and similar reported aqueous fractional accumulation at equilibrium [95].

In 1953 Mathews and Conn noted that the β-NADH prepared by borohydride reduction was only partially oxidized by LDH and proposed that in addition to β-NADH (4-DHNAD), 2-DHNAD and 6DHNAD were produced and that these forms were not able to react with enzymes [176]. Later Chaykin and Meissner reported absorption spectra of the partially purified products of borohydride reduction and used tritium label elimination methods to establish the positions of reduction on the nicotinamide ring [102]. A number of other studies have examined the properties of these non-specific reduction products (including a variety of misidentifications) [99, 100, 102-104], but it was Lowry et al. and Dalziel who first reported that β-NADH preparations contained contaminants that were inhibitory to LDH. Soon after, Godtfredsen and Ottesen described 6DHNAD as a humidity-induced lactate dehydrogenase inhibitor that arises in NADH powder [98, 101]. Together, these and numerous other studies establish that lactate dehydrogenase inhibitors arise by non-specific reduction of β-NAD^+ and/or via tautomerization of β-NADH (Scheme 5.3). The activity we have

observed for renalase suggests that non-enzymatic redox and/or proton-movement mediated intercoversion of NAD(P)+/NAD(P)H isomers is also an *in vivo* phenomenon that suppresses primary metabolism.

We also show that renalase catalytically oxidizes both known isomeric forms of the β-NAD(P)H nicotinamide ring. Positionally, the 2 and 6 carbons of the nicotinamide ring are equivalent if the base is allowed to pivot about the glycosidic bond. This suggests that the nicotinamide amide substituent can be accommodated in two locations within the renalase active site and in these two binding modes the substrates are otherwise conformationally equivalent. Two orientations for the nicotinamide base implies there are also two binding modes for β-NAD(P)H and for β-NAD(P)$^+$ and that the dissociation constant measured for these molecules is an average of both binding modes. Moreover, it also follows that up to half of the binding events for 2- and 6DHNAD result in inhibitory complexes that cannot transfer the hydride equivalent to the renalase flavin; that we do not observe any inhibitory delay in the reductive half reaction suggests that binding and release of 2- and 6DHNAD from Ren_{ox} is rapid.

In prior studies we observed the reductive half-reaction of renalase by mixing the enzyme with an apparent equilibrium mixture of β-NADH and 6DHNAD [34]. Here we use pure preparations of 2DHNAD and 6DHNAD to show that the rate constant for reduction is dramatically more rapid than previously reported. We observe rate constants for flavin reduction of 230 s^{-1} for 6DHNAD and 860 s^{-1} for 2DHNAD as opposed to ~40 s^{-1} observed with the equilibrium mixture. We also show that renalase has only a modest ability to distinguish between the 2-, 4- and 6DHNAD molecules (Figure 5.3 & 5.4) as β-NADH (4DHNAD) binds to renalase forming a complex with a dissociation constant of ~600 μM, only ~3.5-fold weaker than that observed for 2- and 6DHNAD. However, renalase has a considerably greater capacity to distinguish between its substrates and β-NAD(P)$^+$ molecules, the renalase complex(es) of which has an order of magnitude higher dissociation constant (Figure 5.4B)[34]. As

such the relative high background of β-NAD(P)H and β-NAD(P)$^+$ in the cellular environment will populate and inhibit renalase to some extent. Given the ostensibly isosteric form of all three reduced isomers it is not unexpected that β-NAD(P)H would compete for access to the renalase active site. The apparent lack of β-NAD(P)H isomer binding stringency is only a limitation to the extent that 2- and 6DHNAD accumulate *in vivo*. The considerable driving force for the renalase reaction derived from the reduction of dioxygen provides a rather unrelenting capacity to scavenge these substrates. Provided renalase activity can scavenge both isomers at a rate that meets or exceeds their formation, its metabolic contribution is sufficient.

We have assessed the interaction of 2- and 6DHNAD with three dehydrogenases from primary metabolic pathways. 2- and 6DHNAD presumably act as inhibitors of these enzymes as they are highly similar in shape and electrostatic character to β-NADH, yet cannot associate in a manner that permits hydride transfer. These data indicate that both MDH and LDH are subject to inhibition by both 2- and 6DHNAD while DLD is not. Given the structural similarity of 2-, 4- and 6DHNAD it is interesting that DLD can select only the 4-dihydro isomer while renalase, the enzyme apparently destined to rid the cell of 2- and 6DHNAD, cannot. The inhibition of MDH by 6DHNAD is an order of magnitude more potent suggesting that this interaction is the principal threat to primary metabolism from β-NAD(P)H isomers. While the *in vivo* concentrations of 2- and 6DHNAD are not known, such high affinity would suggest that, in the absence of renalase, even minute accumulations of 6DHNAD would undermine primary energy pathways. While, 2-DHNAD is much less stable than 6DHNAD, on a molecular timescale its half-life is more than sufficient to expect that it will also exert an influence over key dehydrogenase enzymes. The extent of the threat these molecules pose is likely to be organism specific and it cannot yet be stated that dehydrogenase inhibition of this type is a universal phenomenon. That porcine DLD is not inhibited by either 2- or 6DHNAD indicates that binding

selectivity for these three forms of reduced β-NADH is possible. However, renalase is found throughout the *animalia* implying that key dehydrogenases found within all organisms of this kingdom, such as rabbit LDH shown here, are subject to inhibition by β-NADH isomers.

As stated, in prior work we mistakenly proposed that α-NAD(P)H anomers were substrates for renalase. It now seems appropriate to graft our earlier mechanistic observations with the data obtained in this study using pure 2- and 6DHNAD. Scheme 5.4 depicts the proposed mechanism for renalase based on prior and current observations. For simplicity this scheme depicts only the catalytic cycle for the 6DHNAD substrate though it is assumed that catalysis in the presence of 2DHNAD differs only in the position of the nicotinamide amide substituent (meta with respect to the position depicted). In this catalytic cycle 6DHNAD associates rapidly with a dissociation constant for the Ren_{ox}•β-6DHNAD(P) complex of 170 μM. The nicotinamide locates in the active site such that the ortho positions with respect to the dihydropyridyl nitrogen are adjacent to the flavin N5 and oriented for conventional hydride transfer. Reduction of the flavin forms the Ren_{red}• β-$NAD(P)^+$ complex. Our prior studies indicated that the reoxidation of this complex occurs by a bimolecular reaction with dioxygen with a rate constant of $2.9x10^3$ $M^{-1}s^{-1}$ that forms hydrogen peroxide and is fully rate determining under conditions of normal mammalian physiological oxygen concentration (~ 140 μM) [34]. The rate constant for reoxidation was not influenced by the addition of exogenous β-$NAD(P)^+$ indicating that the reaction with dioxygen is neither contingent on nor influenced by the release of β-$NAD(P)^+$. Consistent with this observation was that the reduction potential of the renalase flavin is the same within error for the unliganded oxidized enzyme and the Ren_{red}•β-$NAD(P)^+$ complex[34]. As such the reoxidation/product release phase of catalysis is represented as random, but is kinetically ordered by the fact that β-$NAD(P)^+$ is released somewhat more rapidly (20 s^{-1}) than the reaction of the reduced enzyme with dioxygen under physiological conditions (0.4 s^{-1}).

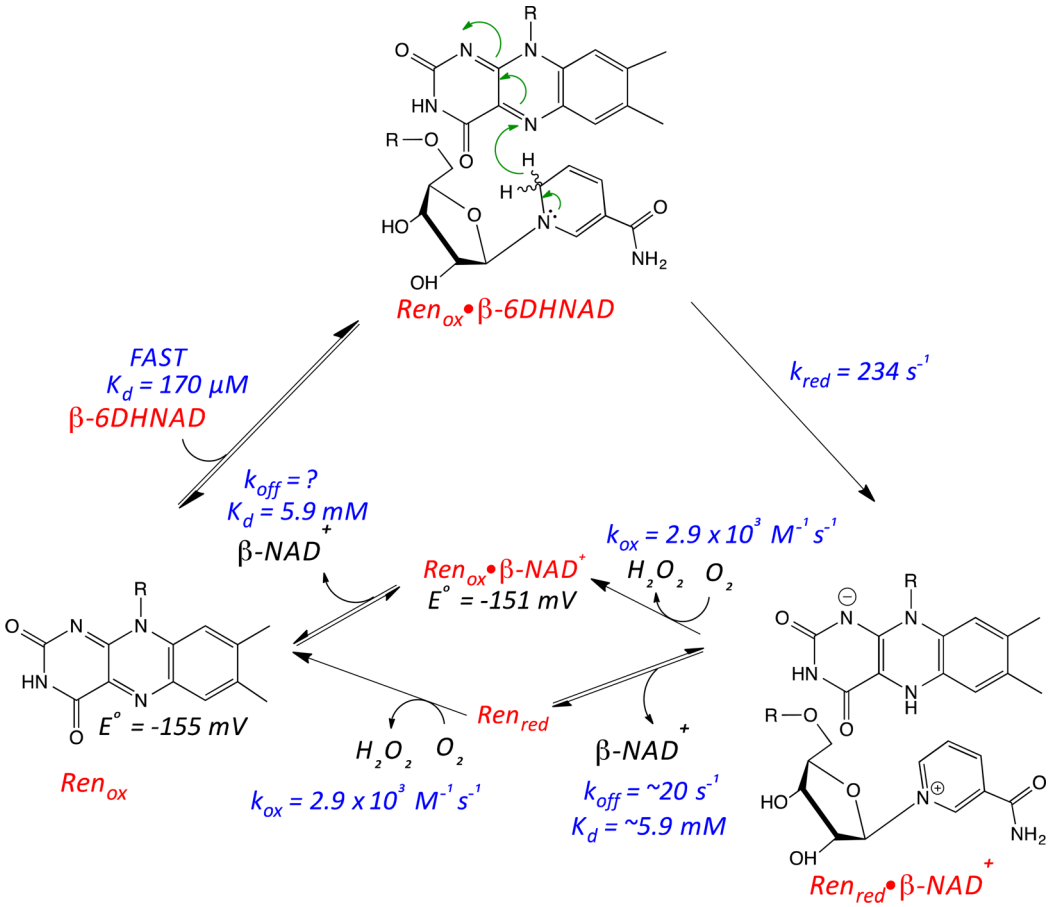

Scheme 5.5. Proposed chemical mechanism of HsRen.

The number and breadth of physiological observations associated with renalase is expanding in an exponential manner. In addition to being linked to the control of blood pressure and heart rate[46, 47], renalase has also been associated with renal dopamine and phosphate metabolism [58, 108], diabetes [56, 60, 112], and amelioration of myocardial damage [53]. Our earlier conclusions were based on recycling of α-anomers of NAD(P)H molecules and could not be linked to any known endocrine or other physiological role for renalase. While we make no attempt here to connect our current data to specific physiological responses, it does seem that the threat to normal primary

metabolism posed by β-NAD(P)H isomers does allow for renalase deficiencies to manifest as physiological abnormalities, in particular those associated with local ischemia.

Chapter VI
Renalase Does Not Catalyze the Oxidation of Catecholamines.

Brett A. Beaupre, Matthew R. Hoag and Graham R. Moran

Abstract

It is widely accepted that the function of human renalase is to oxidize catecholamines in blood. However, this belief is based on experiments that did not account for slow, facile catecholamine autoxidation reactions. Recent evidence has shown that renalase has substrates with which it reacts rapidly. The reaction catalyzed defines renalase is an oxidase, one that harvests two electrons from either 2-dihydroNAD(P) or 6-dihydroNAD(P) to form β-NAD(P)$^+$ and hydrogen peroxide. The apparent metabolic purpose of such a reaction is to avoid inhibition of primary dehydrogenase enzymes by these β-NAD(P)H isomers. This article demonstrates that renalase does not catalyze the oxidation of neurotransmitter catecholamines. Using high-performance liquid chromatography we show that there is no evidence of consumption of epinephrine by renalase. Using time-dependent spectrophotometry we show that the renalase FAD cofactor spectrum is unresponsive to added catecholamines, that adrenochromes are not observed to accumulate in the presence of renalase and that the kinetics of single turnover reactions with 6-dihydroNAD are unaltered by the addition of catecholamines. Lastly we show using an oxygen electrode assay that plasma renalase activity is below the level of detection and only when exogenous renalase and 6-dihydroNAD are added can dioxygen be observed to be consumed.

Introduction.

Renalase is widely defined to be a kidney-derived flavoprotein enzyme/hormone whose function is to oxidize circulating catecholamines in order to lower blood pressure and slow the rate of contraction of the heart [46-49, 51, 110, 177]. The initial basis of this claim for renalase activity was an exceedingly small accumulation of hydrogen peroxide in the presence of common neurotransmitter catecholamines when assayed using a generic Amplex Red-based oxidase assay. However, in these initial experiments no account, in the form of a control reaction, was made for background autoxidation [46, 51, 55, 91, 110]. Catecholamines are prone to oxidation in the presence of dioxygen due to their capacity to form semiquinones [87]. The superoxide ion that results rapidly disproportionates to dioxygen and hydrogen peroxide providing a steady non-enzymatic background signal for an Amplex Red assay (Scheme 6.1). The very low level of H_2O_2 production was subsequently rationalized by proposing that renalase is isolated in a quiescent state that can only be activated in blood in the presence of specific catecholamine neurotransmitters [55, 110]. The chemical transformation ultimately claimed for renalase was that oxidized and cyclized aminochrome molecules were the native products and that the reaction was somewhat faster in the presence of NAD(P)H [55]. However, even in these latter studies, no control was made for the addition of the catecholamine or the reductant, despite that NAD(P)H that would greatly increase the complexity of the assay by increasing the number of non-enzymatic redox reactions that yield H_2O_2 (Scheme 6.1). That no control reactions were used to support any of the early catalytic claims emphasizes the overall tenuous foundation on which renalase catecholamine oxidase activity is based.

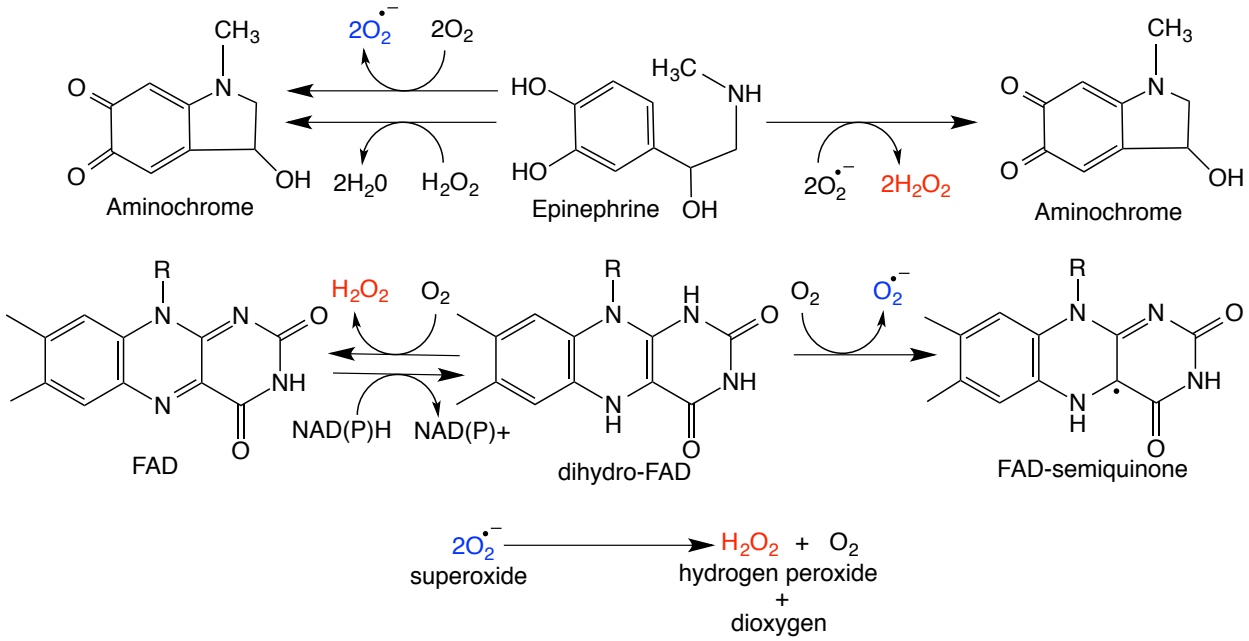

Scheme 6.1. Non-enzymatic redox reations in renalase catecholamine oxidase assays.

Boomsma and Tipton were first to register well-reasoned skepticism concerning a catecholamine oxidase role for renalase [88] and were joined by others expressing similar dissent and eventually direct experimental refutation was presented by Pandini et al. [72, 89, 90]. However, the flawed initial *in vitro* evidence and counter evidence have been insufficient to quell the passive consensus that the function of renalase is to oxidatively consume catecholamine neurotransmitters from blood. Consequently, the early claims for catecholamine oxidase activity continue to be adduced and correlated with a wide variety of physiological measurements [47-54, 57-59, 62, 91, 107-112, 118, 121, 122, 128-130, 166, 177-183].

We recently demonstrated that 2-dihydroNAD (2DHNAD(P)) and 6-dihydroNAD(P) (6DHNAD(P)), both isomers of β-NAD(P)H (4DHNAD(P)), rapidly reduce the FAD coenzyme of renalase (230 s^{-1} for 6DHNAD, 850 s^{-1} for 2DHNAD) and in doing so become oxidized to β-$NAD(P)^+$. The reduced enzyme then reoxidizes by reducing molecular oxygen to form H_2O_2 (2.9 x 10^3 $M^{-1}s^{-1}$) (Scheme 6.2).

Moreover, this genuinely catalytic reaction has an apparent metabolic purpose, as both 2DHNAD and 6DHNAD are inhibitory to primary metabolism dehydrogenases [35, 98]. The fundamental purpose of this study is corrective; using a verifiably active form of renalase, we demonstrate that no catalytic link exits between renalase and catecholamine oxidation. We show also that renalase it is not activated by blood plasma nor is, what we surmise to be, the native activity influenced by the presence catecholamines.

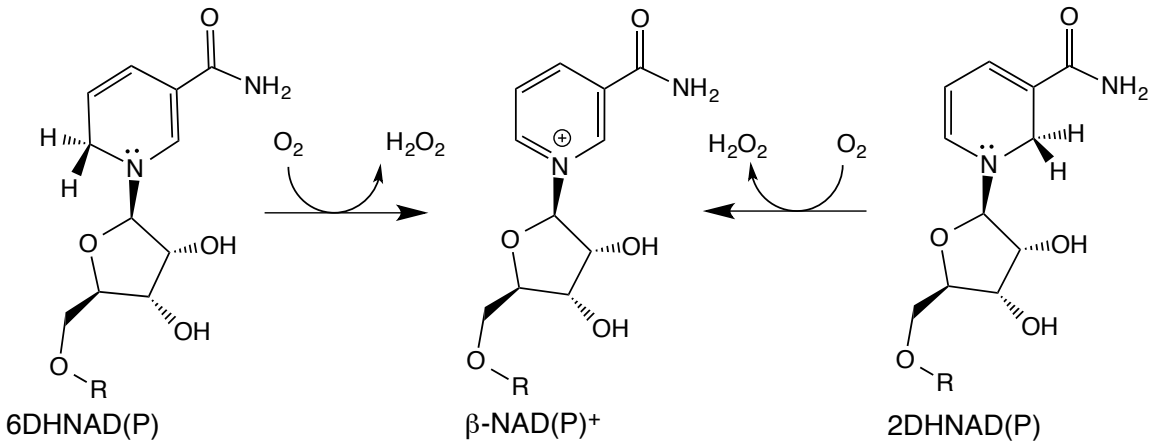

Scheme 6.2. Proposed native catalytic chemistry of renalase.

Materials and Methods.

Materials. Potassium phosphate, L-DOPA, epinephrine hydrochloride, and sodium chloride were obtained from ACROS. Dopamine hydrochloride was purchased from Alfa Aesar. Renalase was expressed and purified according to our previously published methods[94]. β-NADH (disodium salt, trihydrate) was obtained from Amresco; β-NAD^+ was purchased from Sigma. 6DHNAD was prepared by reduction of β-NAD^+ as previously described [35]. Human blood plasma was a gift from Dr. Julie A. Oliver (Biological Sciences Department-University of Wisconsin-Milwaukee). Freshly drawn blood was treated with 10 U/mL heparin (Sagent Pharmaceuticals) to inhibit clotting. The sample was centrifuged at 2,200 rpm until blood cell pellet was formed (~15 minutes). The plasma was separated

from the blood cell pellet and hematocrit and stored on ice until needed. Plasma samples were collected, purified, diluted (50% PBS), and used in experiments within 3 hours.

HPLC Product Analysis: In order to demonstrate the extent to which epinephrine, the catecholamine most often claimed or accepted as a substrate for renalase [46-48, 109, 110], is consumed by renalase, a mixture of β-NADH (50 μM) and epinephrine (150 μM) was prepared in PBS buffer at 25 ^{o}C. The sample was then divided into two and renalase (9 μM final) was added to one while the other served the role of a sample age control. A second set of mixtures were prepared in an identical manner, but FAD (9 μM final) was added in place of renalase. All samples were incubated for 10 minutes prior to ultrafiltration using a 0.5 mL Amicon 10 KDa centrifugal filter (removing renalase from the mixture). 50 μL of each filtrate was then chromatographed by HPLC using a Xterra C18 reversed phase column (4.6 x 150 mm, 3.5 μM particle size) run isocratically at 0.4 ml/min in 10 mM potassium phosphate pH 7.5 coupled to a 600 E HPLC pump and Waters 2487 dual wavelength detector (260nm and 340nm). Components eluting from the HPLC column were identified by their characteristic retention time compared to authentic compounds. The chromatograms derived from the renalase and FAD samples were corrected for the minor dilution that occurred with the addition of these components.

Spectrophotometric Evidence of Neurotransmitter Oxidation: Reactions were performed to assess the rates of autoxidation of catecholamines in the presence of renalase (or FAD control) when incubated with a reductant (β-NADH or 6DHNAD). Renalase was prepared by dilution to 40 μ□□in 2x PBS buffer and mounted onto a onto a Hitech-DX2 (now TgK) stopped-flow spectrophotometer instrument. Reaction mixtures in which renalase (or FAD control) was combined with 100 μM catecholamine (epinephrine, dopamine or L-DOPA) and 15 μM β-NADH (or 6DHNAD control) in water were observed

at 458 nm which allows observation of both the FAD redox state and the formation of aminochrome species (λmax~480 nm). All solutions were equilibrated with atmosphere at 25 ^{o}C and contained ~250 μM dioxygen.

To assess if catecholamine neurotransmitters (epinephrine, dopamine and L-DOPA) modulate the catalytic behavior of renalase, single turnover reactions with 6DHNAD were performed in the presence and absence of catecholamines with atmospheric dioxygen (~250 μM). Under these conditions the reduction and subsequent reoxidation of the renalase flavin coenzyme can be clearly observed. A native substrate solution, 6DHNAD (30 μM), was prepared in H_2O. This solution was mounted onto the stopped-flow spectrophotometer and mixed with the renalase (40 μM) sample described above and the turnover was observed at 458 nm, the visible absorption maximum for the FAD coenzyme bound to the enzyme. To determine if catecholamine neurotransmitters modulate the turnover of renalase, 200 μM of epinephrine, dopamine or L-DOPA was added to the 6DHNAD solution before mixing.

Dioxygen Consumption to Assess Renalase Activity in Blood and the Affect of Preincubation: In order to establish the constitutive level of renalase activity in human blood and the effect of preincubation with plasma and/or epinephrine as compared to PBS buffer control, a variety of assays were monitored by dioxygen consumption. Reactions were observed using a Hansatech Oxygraph oxygen electrode and all reaction components were pre-equilibrated with atmospheric dioxygen (~250 μM) at 25^{o}C. Reactants were added to the following final concentrations: 50% human blood plasma (diluted in PBS buffer), 10 μM epinephrine, 500 nM renalase and 30 μM 6DHNAD. Each assay was initiated by the addition of 6DHNAD, following either a 5 minute or 20 minute preincubation and then observed for an additional 700 seconds.

Results.

HPLC Product Analysis: Renalase is claimed to consume neuroactive catecholamines, chiefly epinephrine, in order to lower blood pressure[55]. To demonstrate the extent to which verified active renalase can consume epinephrine in the presence of β-NADH, standardized HPLC chromatograms were collected and compared to controls that contained FAD in place of renalase (Figure 6.1). 150 μM Epinephrine was combined with 50 μM β-NADH (that has a β-NAD^+ impurity). The sample was divided into two and renalase added to one. Both samples were then incubated for 10 minutes (Figure 6.1A). Two similar mixtures were prepared as controls but with FAD substituted for renalase (Figure 6.1B). Analysis of the chromatograms showed that no significant consumption of epinephrine could be observed in the 10-minute window of the incubation. The renalase sample did show significant loss of β-NADH (11 μM) that was not entirely accounted for by a gain in the β-NAD^+ peak area (2 μM). This fraction of the β-NADH was accounted for by the modest dissociation constant for Ren_{ox}•β-NADH complex (K_d~600 μM) and the ~20-fold increase in the renalase concentration (180 μM) during filtration that together predict the 11 μM retention. [35]. The FAD control chromatograms indicate no non-enzymatic chemistry has occurred within the 10 minute incubation window. Together these data definitively show that the consumption of epinephrine cannot be detected in the presence of high concentrations (9 μM) of fully active renalase.

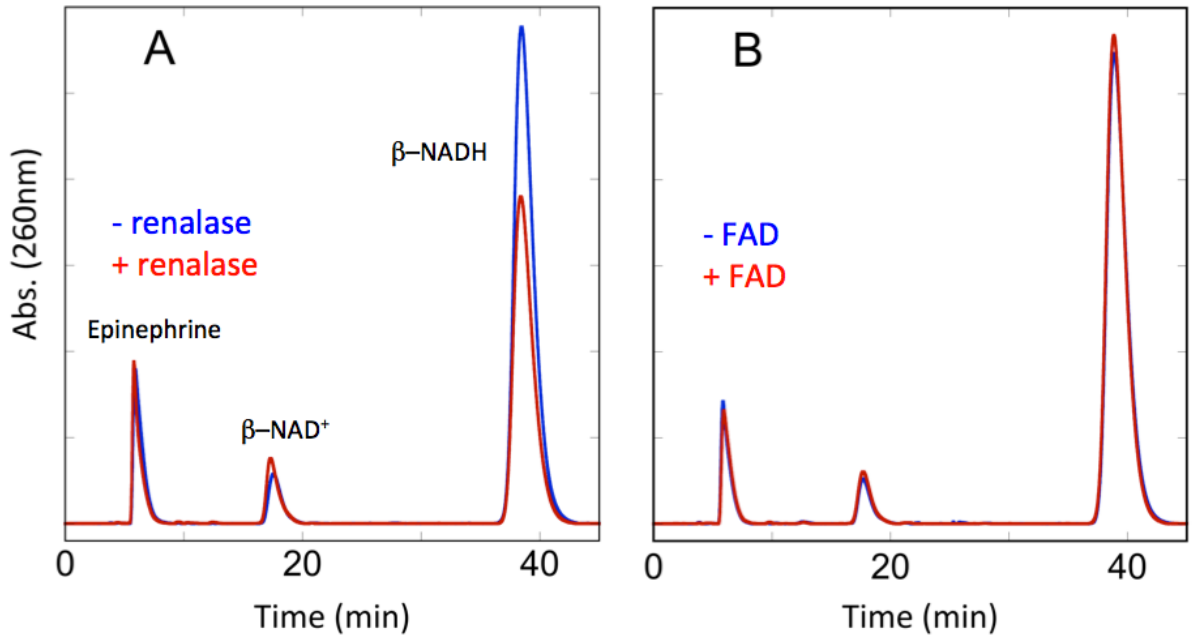

Figure 6.1. HPLC analysis of oxidation of epinephrine to adrenochrome by renalase. **A&B** were separated using a Xterra reverse phased C18 run isocratically in 10 mM Kpi, pH 7.5 and monitored at 260 nm. **A.** The blue line represents the mixture of 150 µM epinephrine and 50 µM β-NADH (4DHNAD) in PBS buffer at 25°C before the addition of 9 µM renalase and the red trace was taken after the addition of 9 µM renalase and incubation for 10 minutes at 25°C; renalase was removed from the sample by centrifugal (Amicon) ultra-filtration prior to injection. **B.** The reaction described in A was repeated except FAD was substituted for renalase.

Spectrophotometric Evidence of Neurotransmitter Oxidation: Renalase has been reported to oxidize catecholamines to aminochromes (Scheme 6.1)[91]. It has also been proposed that catecholamines modulate the redox activity of renalase to the extent that the enzyme is largely inactive in the absence of epinephrine [55]. In order to show the capacity of renalase to oxidize catecholamines to form aminochromes, two sets of reactions were performed one in the presence and one in the absence of renalase. Aminochromes are the oxidized and cyclized forms of catecholamines that have a puce color as a result of a broad absorption centered around 480 nm (ε_{480} ~4020 $M^{-1}cm^{-1}$) which provides a simple physical signal to observe their accumulation in solution. The absorption peak of aminochromes is sufficiently broad that at 458 nm, the wavelength of observation used, the extinction

coefficient is only 2% lower, permitting simultaneously assessment of the FAD coenzyme and the catecholamine oxidation/cyclization. Three common neuroactive catecholamines were mixed with reductant (β-NADH or 6DHNAD) and renalase (20 μM final) or FAD (20 μM final). In the first control β-NADH was combined with epinephrine, L-DOPA, or dopamine and subsequently mixed with renalase to determine if renalase could enhance the rate of oxidation of the catechols to their associated aminochromes in the presence of NADH. No change in absorbance was observed indicating that renalase does not promote the oxidation and cyclization catecholamines. As a control, FAD was substituted for renalase and the above experiment repeated. This data showed small accumulations of absorption (epinephrine, 0.0035; DOPA, 0.015; L-DOPA, 0.0025) equating to ~ 1-3 μM aminochrome after 300 seconds, indicating that a mixture of β-NADH and free FAD can enhance the rate of catecholamine autoxidation and that renalase actually provides some degree of protection from this chemistry presumably as a result of the active site flavin being inherently unreactive with β-NAD(P)H molecules in order to avoid wasteful diaphorase activity.

In our previous work we have demonstrated that renalase catalyzes rapid oxidation of 6DHNAD(P) and 2DHNAD(P) to β-NAD(P)$^+$ where a hydride equivalent is transfered from the nicotinamide base to the renalase flavin coenzyme that then reoxidizes by reducing dioxygen to form hydrogen peroxide (Scheme 6.2)[34, 35, 94]. In order to show the extent of the influence of catecholamines on the kinetics of this chemistry, reduction and reoxidaton of the renalase flavin coenzyme that occurs in single turnover with 6DHNAD was observed at 458 nm (Figure 6.2B). The data obtained indicate that neither epinephrine, L-DOPA, or dopamine have influence on the catalytic behavior of renalase. The FAD, 6DHNAD (± catecholamines) control for the single turnover reactions where ostensibly the same as those for FAD, β-NADH and catecholamine in Figure 6.1A (data not shown).

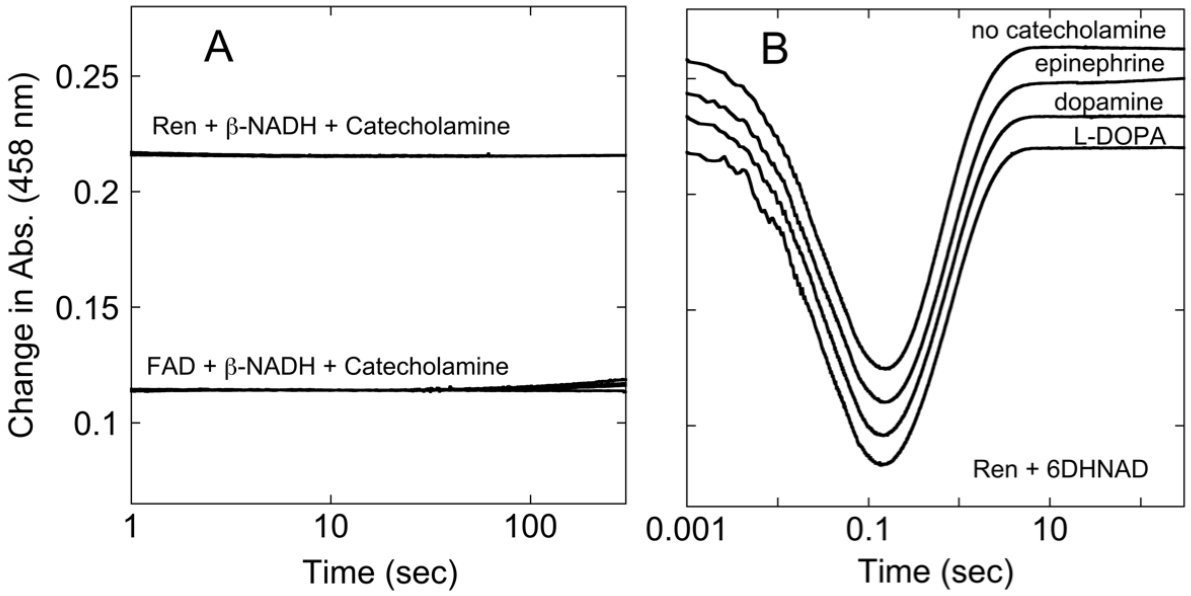

Figure 6.2. Catalytic turnover of renalase in the presence of neurotransmitters. **A&B.** Renalase single turnover(B) and control(A) stopped-flow spectrophotometer traces were observed at 458 nm for 200 sec. **A.** The extent of auto-oxidation of epinephrine was monitored; *top*, stopped-flow spectrophotometer trace of 20 µM renalase with 15 µM β-NADH(4DHNAD) in the absence and presence of 100 µM catecholamine of interest (epinephrine, DOPA, L-DOPA); *bottom;* stopped-flow spectrophotometer trace of 20 µM FAD with 15 µM β-NADH(4DHNAD) and 100 µM of catecholamine of interest (epinephrine, DOPA, L-DOPA). **B.** Single turnover of 20 µM renalase with 15 µM 6DHNAD in the absence and presence of 100 µM catecholamine of interest (epinephrine, DOPA, L-DOPA).

Dioxygen Consumption to Assess Renalase Activity in Blood and the Affect of Preincubation: There are three near constant elements in all scientific articles that pertain to renalase; all claims for activity involve the reduction of dissolved dioxygen, most report or cite that catecholamines are substrates and the majority pivot their investigations on the role of renalase in blood[72, 125]. Moroever, the low *in vitro* catecholamine oxidase activity has been claimed to be a consequence of a “prorenalase” form that is largely inactive when separated from some unidentified activator [91, 110]. Given that renalase oxidizes 2- and 6DHNAD(P)[35], does renalase exhibit modified catalytic behavior in blood? In order to demonstrate the effects of preincubation with catecholamine and/or blood plasma we conducted a

series of assays using a oxygen electrode (Figure 6.3). All assays had 6DHNAD added either after a short (5 min) or long (20 min) preincubation.

In Figure 6.3, assays 1 & 6, we see that epinephrine is slow to oxidize and does not promote significant consumption of dioxygen prior to or after the addition of 6DHNAD. In addition, assays 1 & 5 indicate that the basal level of renalase activity in blood is sufficiently low to be below the sensitivity of these methods. Using antibody detection, Zbroch et al. determined that the concentration of renalase in plasma was 4 μg/mL (100 nM) [108] approximately one fifth of the exogenous concentration added in assays 2, 3, 4, 7, 8 & 9. That each of these traces show marked dioxygen consumption with added renalase and those without show no dioxygen consumption (assays 1 & 5) suggests that there is very little renalase in blood or that the majority of it is inactive. Comparison of assays 2 & 4 to assays 7 & 9 indicates that preincubation of renalase in plasma does not alter its behavior. Both sets of assays indicate linear consumption of dioxygen that is equimolar to the amount of 6DHNAD added and then cessation of activity. Assays 2, 3 & 4 show recovery of approximately half the dioxygen consumed in the renalase catalytic phase presumably as a consequence of catalase activity in the plasma. Contrary to claims that epinephrine activates renalase [55], neither assay 1 or 6, those preincubated with epinephrine in plasma and PBS respectively, show any evidence of activity, strongly suggesting that the circulating catecholamine does not activate a quiescent form of renalase.

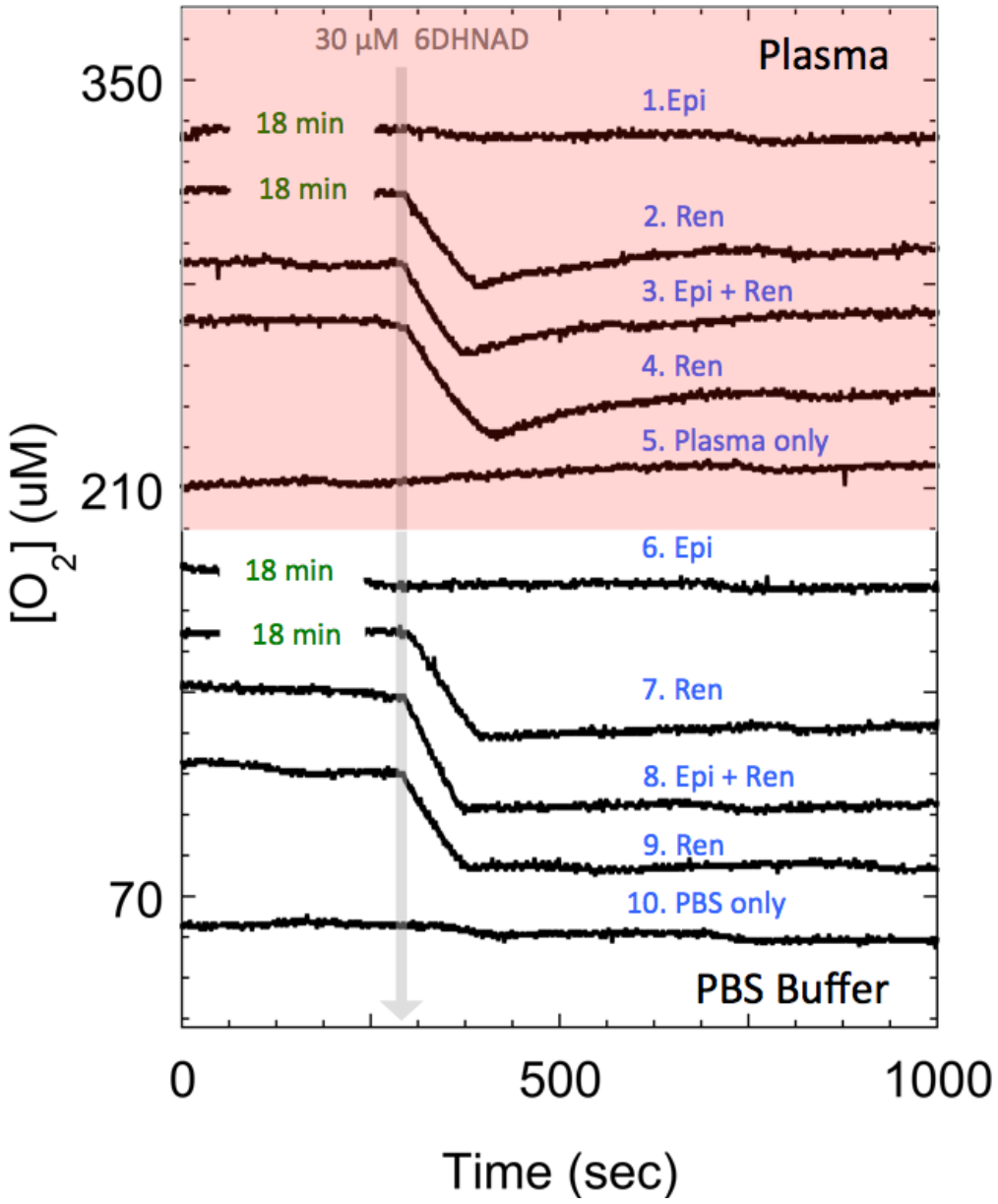

Figure 6.3. The Effect of Catecholamine and Plasma Preincubation. Renalase activity in 50% blood plasma and PBS buffer was determined by monitoring dioxygen consumption. Reactions were performed by reacting 30 µM 6DHNAD ion the absence or presence of 500 nM renalase and 10 µM epinephrine in either PBS buffer or 50 % blood plasma. Traces 1, 2, 6, and 7(from top) were incubated at 25°C for 20 minutes prior to the addition of 6DHNAD all other traces were incubated at 25°C for 5 minutes before 6DHNAD addition. Traces were aligned so the addition of 6DHNAD appears in the same time position in all reactions. Assays were separated by adding or substracting values for clarity. Only Assay 5 is not plotted on an actual molecular oxygen scale.

Discussion.

The chronology of reported activities for renalase elaborate the erroneous initial claim. In the progenitor article it was proposed that renalase is secreted by the kidney to oxidize circulating catecholamines and that the electrons mobilized are delivered to dioxygen [46]. However, this was surmised only from the data obtained from a generic oxidase assay method and without the use of appropriate controls. Nonetheless, the association of renalase with catecholamines continues to become ever more conflated. Catecholamines are said to regulate the activity, secretion and synthesis of renalase [110]. A variety of complex regulatory feedback pathways have been proposed [49-51, 109, 110]. Aminochromes are claimed as the native products [91] and the active oxidizing agent is said to be superoxide [55]. However, the extremely low levels of claimed *in vitro* catecholamine oxidase activity has been cited as a deficit by a number of researchers [72, 77, 88] and this was then rationalized by invoking "prorenalase" a claimed quiescent form of the enzyme that requires activation [49, 110] that occurs only in blood in the presence of a catecholamine [55, 110]. It can now be stated with some certainty that this successive affirmative set of claims describes a compounding of an initial scientific deficit; the failure to employ appropriate control reactions to assess catalysis.

The purpose of this study is to clearly demonstrate that renalase is not the third monoamine oxidase. The apparently indelible mark of the early and recent activity claims for renalase must be dispelled if the field is to advance in a purposeful manner. We recently reported two isomeric forms of β-NAD(P)H as substrates for renalase that are clearly catalytically consumed (Figure 6.2B) and have redefined renalase as having a house-keeping activity that is unrelated to blood pressure regulation. Renalase functions instead to oxidize reduced forms of nicotinamide adenine dinucleotides that harbor the hydride in non-metabolically accessible positions of the nicotinamide base (positions 2 &

6). We have proposed that this activity exists to relieve inhibition of primary metabolism by these molecules. A principal benefit of having identified native substrates for renalase is that we can now test the validity of previously proposed activities using a form of the enzyme that we have verified is fully active (Figure 6.2B) [35]. In sum our data show that renalase does not consume catecholamines (Figures 6.1 & 6.2A), is not kinetically regulated by catecholamines (Figure 6.2B), is not isolated in an inhibited form and as such cannot be activated by blood plasma or catecholamines (Figure 6.3). In addition, our data suggests that blood has very little if any active renalase (Figure 6.3) an observation that is consistent with its newly identified activity that we would suggest has an exclusively intracellular/metabolic role.

Catecholamines form hydrogen peroxide as they oxidize in oxygenated media. That the initial accounts of renalase activity did not employ appropriate control reactions and reported vanishingly low activity undermines the subsequent affirmative claims. The case has also been made that in the absence of genuine substrates, no sample integrity measures have been established and as such there has been no means to discriminate natively folded and active renalase from misfolded inactive but soluble renalase [72]. The vast majority of reports that describe direct use of the enzyme do not indicate the color of the protein (that is conspicuously yellow) or the unique absorption maxima of the flavin in the natively folded enzyme [76]. Nonetheless, in the ten years since its initial discovery, the terms renalase and monoamine oxidase C have become somewhat synonymous [50, 73, 184] and this has occurred despite sound argument and evidence to the contrary [72, 88, 89]. In this article we have presented evidence that verifiably active renalase does not catalyze the oxidization of catecholamines.

Chapter VII

Bacterial Renalase: Structure and Kinetics of an Enzyme with 2- and 6-Dihydro-β-NAD(P) Oxidase Activity from *Pseudomonas phaseolicola.*

Matt R. Hoag, Joseph Roman, Brett A. Beaupre, Nicholas R. Silvaggi, Graham R. Moran

Abstract

Despite a lack of convincing *in vitro* evidence and a number of sound refutations, it is widely accepted that renalase is an enzyme unique to animals that catalyzes the oxidative degradation of catecholamines in blood in order to lower vascular tone. Very recently, we identified isomers of β-NAD(P)H as substrates for renalase (Beaupre B.A., Hoag M.R., Roman J., Försterling F.H. and Moran G.R. (2015) Biochemistry 54, 795-806). These molecules carry the hydride equivalent on the two or six position of the nicotinamide base and presumably arise in non-specific redox reactions of nicotinamide dinucleotides. Renalase serves to rapidly oxidize these isomers to form β-NAD(P)$^+$ and then pass the electrons to dioxygen forming H_2O_2. We have also shown that these substrate molecules are highly inhibitory to dehydrogenase enzymes and thus have proposed an intracellular metabolic role for this enzyme. Here we identify a renalase from an organism without a circulatory system. This bacterial form of renalase has the same substrate specificity profile as human renalase but, in terms of binding constant (K_d), shows a marked preference for substrates derived from β-NAD$^+$. However, 2-dihydroNAD(P) substrates reduce the enzyme with rate constants (k_{red}) that greatly exceed those for 6-dihydroNAD(P) substrates. Taken together, k_{red}/Kd values indicate a minimum 20-fold preference for 2DHNAD. We also offer the first structures of a renalase in complex with the catalytically relevant ligands β-NAD$^+$ and β-NADH (the latter being an analog of the substrate(s)). These structures show potential electrostatic repulsion interactions with the product and a unique binding orientation for the substrate nicotinamide base that is consistent with the identified activity.

Renalase was discovered in 2005 and purported to be a flavoprotein hormone produced by the kidney that catalyzes the oxidation of catecholamines in order to lower blood pressure and slow the heart [46, 47]. However, the initial experiments used to identify the substrates focused on only a handful of molecules and did not include control reactions to account for the inexorable oxidation of catecholamines in oxygenated buffer. Despite claimed physiological verifications of this activity [47-49, 111, 177, 178] no convincing *in vitro* evidence of catecholamine oxidase activity has been offered. The deficiencies in the original methods were compounded in subsequent claims that suggested an, as isolated, quiescent renalase state and ever more unlikely chemistries for which catalysis and the stoichiometry were not established [55, 110]. A number of researchers have attempted to counter the expanding belief that renalase catalysis is associated with vascular tone, by either questioning the original methods used to establish activity [88, 89] or demonstrating that, relative to appropriate controls, there is no evidence of catecholamine consumption by the enzyme [76]. These refutations have gone largely unheeded and the preponderance of scientific studies pertaining to renalase continue to be predicated on passive acceptance of an unproven catalytic role [47-54, 57-59, 62, 91, 107-112, 118, 121, 122, 128-130, 166, 177-183].

We have recently shown that human renalase (HsRen) is indeed a flavoprotein oxidase, but one that catalyzes the oxidation of β-NAD(P)H isomers. These isomers carry the hydride on the nicotinamide base in the non-canonical 2 and 6 positions (2- and 6-dihydroNAD(P)) (Scheme 7.1). The oxidation of these isomers occurs as much as five orders of magnitude more rapidly than any prior claim for renalase activity and the turnover reaction with these molecules has a defined stoichiometry and substrate specificity profile. Moreover, we have proposed that the purpose of this activity is to avoid inhibition of primary metabolism by these NAD(P)H isomers that have low nano-Molar Ki values for specific dehydrogenases [35, 172, 173]. If 2- and 6-dihydroNAD(P) molecules are prone to form in

non-enzymatic reduction reactions of β-NAD(P)$^+$ and are truly a detriment to respiratory activity, it is reasonable to assume that this is an intracellular enzymatic activity that will exist in organisms that do not have a circulatory system.

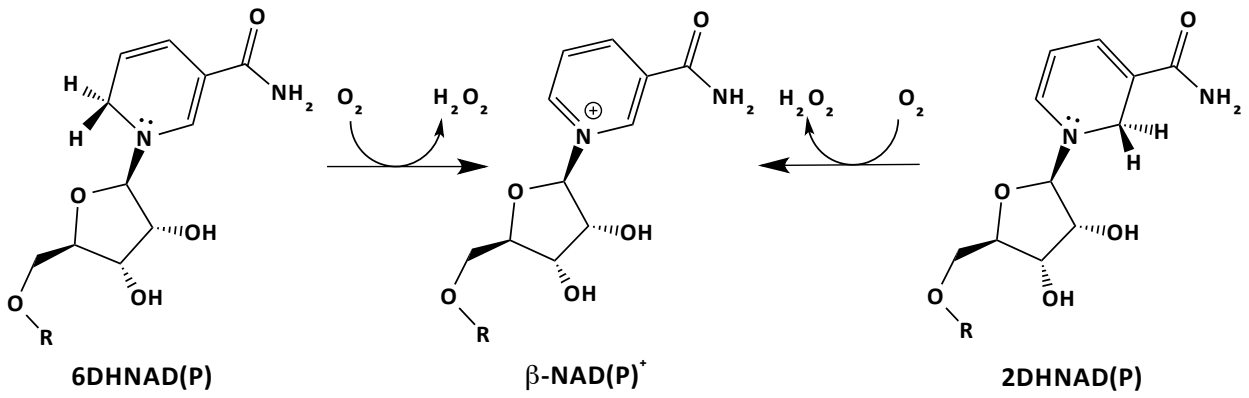

Scheme 7.1. Observed activites of renalase.

The structure of HsRen was determined by the Aliverti group in 2011[77] using the model of a generically assigned "amine oxidase" from *Pseudomonas syringae* (PDB ID 3KKJ) whose structure was solved and deposited in the Protein Data Bank (PDB) by the North East Structural Genomics Consortium (NESGC). While not highly homologous with the HsRen primary structure (19.5% identitical), this protein had the renalase fold (a topology that is common to numerous redox-active flavoproteins [139-142, 185, 186]) and a very similar constellation of active site residues proximal to the FAD isoalloxazine [77]. We surmised that this protein was likely a bacterial form of renalase. In this article we show that this "amine oxidase" from *Pseudomonas syringae* (van Hall pathovar *phaseolicola* strain 1448A) harbors the same catalytic activity observed for HsRen but with unique kinetic properties and stark substrate preferences. We also present the X-ray crystal structures of this enzyme

in complex with nicotinamide dinucleotides that show a reductive pose of the nicotinamide base with respect to the flavin cofactor that is consistent with the proposed activity.

Materials and Methods

Materials. β-NAD^+ was sourced from Sigma-Aldrich. Sodium borohydride, potassium phosphate (mono and dibasic), sodium formate and glycerol were from Acros. Sep-Pak C18 (35 cc) cartridges were purchased from Waters. Competent NEB5 and BL21 DE3 *Escherichia coli* cells were obtained from New England Biolabs. Talon© metal affinity resin was from Thermo-Fisher Scientific. Sodium acetate was purchased from Mallinckrodt. 2- and 6-DHNAD and 2- and 6-DHNADP were prepared using an adaptation of our previously published methods [35]. Both sets of substrates were formed by sodium borohydride reduction of β-NAD^+ or β-$NADP^+$. The products of reduction, β-NAD(P)H, 2-dihydroNAD(P) (2DHNAD(P)) and 6-dihydroNAD(P) (6DHNAD) (and residual β-NAD(P)+) were separated using a Waters X-Bridge 19 x 250 mm 5 μM C18 column. 6DHNAD(P) molecules were relatively stable and could be prepared as previously described and stored indefinitely at -80 ^oC, whereas 2DHNAD(P) molecules were unstable and used immediately after collection from preparative HPLC.

Spectrophotometric Quantification. Dihydronicotinamide chromophore extinction coefficients were as follows: β-NADH, β-NADPH - ε_{340nm} = 6220 M^{-1} cm^{-1} *[95]*, 2DHNAD(P) - ε_{394nm} = 5360 $M^{-1}cm^{-1}$, 6DHNAD(P) - ε_{345nm} = 6580 $M^{-1}cm^{-1}$ and β-NAD^+ - ε_{260nm} = 18800 $M^{-1}cm^{-1}$[35]. *Pseudomonas Syringae* renalase (PpRen) was quantified using the measured extinction coefficient for the enzyme-bound flavin (ε_{452nm} = 11,000 $M^{-1}cm^{-1}$), as determined using an SDS denaturation method as previously described [94].

Expression and Purification of PpRen: A plasmid derived from pET21a (pET21_NESG) containing the gene for PpRen was provided by the NESGC. This construct was prepared by PCR amplification of the PpRen gene from *Pseudomonas Syringae* (van Hall pathovar *phaseolicola* strain 1448A) followed by cloning into the Nde I and Xho I restriction sites, fusing the PpRen gene to a C-terminal 6His-tag. This construct has a single variant amino acid from what is reported for this *phaseolicola* strain; a serine is coded in place of glycine 145. The plasmid was transformed into competent BL21 DE3 cells and plated onto Luria Bertani (LB) agar (100 μg/mL Ampicillin) and grown overnight at 37 ^{o}C. Individual colonies were then selected and grown in LB broth with shaking (250 rpm) at 37 ^{o}C until growth reached early log phase. 1 mL cell stocks were made by adding filter sterilized glycerol to a final concentration of 20% and then storing at -80°C.

For expression, 1 mL cell stocks were thawed, plated onto LB agar, 100 μg/mL ampicillin, and grown overnight at 37°C (100 μL cells/plate). The lawn of cells obtained was resuspended in LB broth and transferred to LB broth cultures (two plates/L of broth) and grown at 37^{o}C in a shaking incubator (220 rpm) until mid-log phase (OD_{600nm}=0.8). The temperature was then lowered to 17 ^{o}C and the culture was grown to OD_{600nm}~1.0 (~1-2 hr) and induced with 0.1 mM IPTG. 30 hrs after induction the cells were harvested by centrifugation (4,000 g for 30 min) and subjected to one freeze/thaw cycle. All purification steps were performed at 4°C. Cell pellets were resuspended in 20 mM sodium HEPES buffer pH 7.5 (approximately 20 mL/L culture) and placed in a stainless steel beaker and lysed by sonication using a Branson 450 sonicator (3 x 240 seconds at 50 W). During this procedure the cell suspension vessel was seated in a slurry of ice and water. Lysed cells were centrifuged at 12,800 x g for 30 min, the pellet was discarded and the supernatant loaded onto a 12.5 x 150 mm Co^{2+} Talon© affinity column equilibrated with 20 mM sodium HEPES buffer pH 7.5. Initially contaminating proteins

were eluted with 150 mL of 10 mM imidazole, 50 mM sodium HEPES buffer adjusted to pH 7.5 with H_2SO_4, then a gradient from 10 mM to 300 mM imidazole in the same buffer was used to elute ostensibly pure PpRen as a single symmetrical peak. Distinctly yellow fractions were pooled. Imidazole was removed and the buffer exchanged to 10 mM potassium phosphate, pH 7.5 by dialysis using 10 kDa nominal molecular weight cut-off dialysis tubing to achieve a net ≥100,000-fold buffer exchange. Aliquots of purified concentrated renalase (<120 μM) were then stored at -80°C.

Analytical HPLC: Evidence of the substrate specificity profile was obtained by adding sodium borohydride (250 μM) to β-NAD(P)+ (250 μM). The sample was divided into two and PpRen (30 μM) was added to one and incubated for 3 minutes while the other was frozen in liquid nitrogen. PpRen was then removed from the first sample by centrifugal ultrafiltration using a 0.5 mL Amicon 10 kDa cutoff filter. Both samples were then chromatographed by analytical HPLC. Separation of the resulting mixtures was achieved using a Waters X-Bridge 4.6 x 150 mm, 3.5 μM C18 column coupled to a Waters 600E pump and Waters 2487 dual wavelength detector. Elution of components of the mixture was observed simultaneously at 260 and 340 (or 394) nm. The components were separated isocratically at 1.0 mL/min in either 10 mM (β-NAD^+ derived) or 50 mM (β-$NADP^+$ derived) potassium phosphate buffer pH 7.5.

Reductive Half-Reaction of PpRen with 6DHNAD(P): The reductive half-reaction of PpRen could be observed independent of subsequent oxidative processes by exclusion of dioxygen using previously published methods [34]. Anaerobic PpRen (5 mL, 14-16 μM) in 20 mM potassium phosphate buffer containing 1 mM dextrose and 5 U/mL glucose oxidase (25 μL, 25 units) was mounted onto a Hitech (now TgK) DX2 stopped-flow instrument that had been scrubbed of residual dioxygen by incubation

for 16 hr with a solution of 1 mM dextrose, 10 U/mL glucose oxidase. 6DHNAD(P) samples were thawed and diluted to target concentrations in water containing 1 mM glucose. 2DHNAD(P) was collected into a glass syringe (that had a small amount of concentrated dextrose added prior (≤1 mM final)) directly from preparative HPLC, diluted to approximate target concentration and used immediately. All substrate solutions were sparged with argon gas for 5 minutes. Before capturing and mounting the substrate solution to the stopped flow instrument, 10 μL of glucose oxidase (10 units) was injected via the luer tip.

Anaerobic PpRen and substrate solutions were mixed and reduction of the renalase cofactor was observed at the absorption maximum of the PpRen FAD, 452 nm. The stability of the 6DHNAD substrate allowed for it to be prepared in sufficient quantity to achieve a high range of concentrations ranging from second order to pseudo-first order reaction conditions. The pseudo-first order data were fit to a linear combination of two exponentials according to Equation 7.1 using Kinetic Studio software (TgK Ltd). In this equation A_1 and A_2 are the amplitudes associated with the first and second rate constants, k_{1obs} and k_2 and C is the absorbance at end of the reaction. The dependence of the observed rate constants (k_{1obs}) for the largest amplitude phase (~90%) was fit to the hyperbolic form of the single-site binding equation (Equation 7.2) according to Strickland, where k_{red} is the limiting rate constant for reduction and $K_{6DHNAD(P)}$ is the binding constant for 6DHNAD [157]. 2DHNAD(P) are prone to decompose within minutes. Reduction data for these substrates were obtained primarily from second order reactant ratios and as such could not be fit meaningfully to linear combinations of exponential terms. The data for 2DHNAD(P) substrates were fit to a the mechanism depicted in Scheme 7.2 using KinTek Explorer to obtain the dissociation constant for the substrate (k_{-1}/k_1) and the intrinsic rate constant for reduction (k_2). The concentration of these substrates was estimated by

recording a spectrum immediately prior and immediately after each kinetic observation and averaging.

Equation 7.1 $$A_{452nm} = A_1(e^{-k_{1obs}t}) + A_2(e^{-k_2t}) + C$$

Equation 7.2 $$k_{obs} = \frac{k_{red}[6DHNAD(P)]}{(K_{6DHNAD(P)} + [6DHNAD(P)])}$$

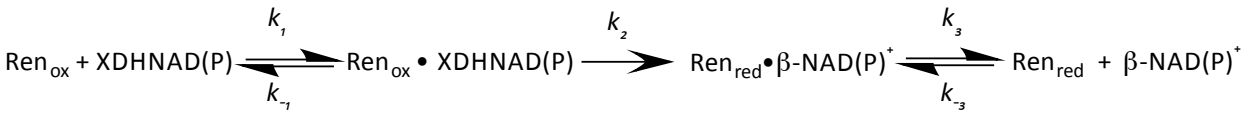

Scheme 7.2. Reductive half-reaction as modeled for fitting.

Oxidative Half-Reaction of PpRen: Reoxidation of the renalase cofactor in the presence of dissolved dioxygen was observed by double mixing stopped-flow spectrophotometry. PpRen (16 μM) was prepared in a tonometer in an equivalent manner to that of the reductive half reaction (though without dextrose or glucose oxidase). In the first mix, this solution was combined with 12 μM 6DHNAD. The reduction reaction was allowed to proceed for 150 seconds prior to the second mix that introduced dissolved dioxygen of defined concentration (Final concentrations after the second mix, 4 μM PpRen, 3 μM β-NAD$^+$, varied dioxygen). The dissolved oxygen concentration in this solution was defined by sparging an inverted syringe containing 10 mM phosphate buffer pH 7.5 with blended dinitrogen and dioxygen gases of known partial pressures supplied by a Maxtec Maxblend gas blender. The concentration of dissolved oxygen was confirmed by first sparging the reaction chamber of a Hansatech dioxygen electrode filled with the same buffer to define the equilibrium concentration of

dissolved dioxygen. The reduced anaerobic PpRen solution was then mixed and the ensuing reoxidation observed at 452 nm. The data were fit to Equation 7.3 in which k_{oxobs} is the observed rate constant for reoxidation, A_1 is the absorption amplitude for the phase observed, and C is the endpoint absorbance. The dependence of the observed rate constant was fit to a straight line that passed through the origin according to equation 7.4 where k_{ox} is the second order rate constant for reoxidation and $[O_2]$ is the concentration of dioxygen.

Equation 7.3 $$A_{452nm} = A_1(e^{-k_{oxobs}t}) + C$$

Equation 7.4 $$k_{oxobs} = k_{ox}[O_2]$$

The influence of β-NAD^+ on the rate constant for reoxidation was observed by similar methods to those described above using the double mixing facility of the stopped-flow instrument. PpRen (23.2 μM) was mixed with 6DHNAD (20 μM) and allowed to age for 150 seconds. This mixture was then mixed with 238 μM dioxygen and the reoxidation observed at 452 nm. β-NAD^+ (0-4 mM) was then added to the third solution and the experiment repeated. The dependence of the observed rate constant for reoxidation (k_{oxobs}) was then fit to Equation 7.5 to determine the extent of inhibition (Δk_{ox}) and the binding constant for β-NAD^+ to the reduced form of the enzyme (K_{NAD+}), where k^i_{ox} is the rate constant observed in the absence of exogenous β-NAD^+.

Equation 7.5 $$k_{oxobs} = k^i{}_{ox} - \left(\frac{\Delta k_{ox}[NAD+]}{(K_{NAD+}+[NAD+])}\right)$$

The Dissociation Constants for the $PpRen_{ox}$•β-NADH, $PpRen_{ox}$•β-NADPH and PpRen•SO_3 adduct Complexes: The dissociation constants for the $PpRen_{ox}$•β-NADH, $PpRen_{ox}$•β-NADPH and PpRen•SO_3 complexes were measured by perturbation of the renalase flavin spectrum when each ligand was titrated. For both the β-NADH and β-NADPH titrations, slow non-catalytic reduction of the PpRen flavin during the experiment (0.0008 s^{-1}) was avoided by preparing eleven 0.9 mL stocks (17 μM for β-NADH, 12 μM for β-NADPH) of the enzyme in 10 mM potassium phosphate buffer, pH 7.5 at 25 ^{o}C. To each 0.9 mL aliquot, 0.1 mL of a range of β-NADH or β-NADPH stocks were added and the spectrum recorded. As such, the spectrophotometric data are compiled from eleven PpRen renalase samples after the addition of β-NADH (0-1 mM) or β-NADPH (0-7 mM).

Titration of PpRen with sodium sulfite formed a labile sulfite adduct that is commonly observed with flavoprotein oxidases. In this experiment 7 μM PpRen in 10 mM potassium phosphate buffer pH 7.5 (25 ^{o}C) was titrated with sulfite by incremental additions spanning the range 0-310 mM. Spectra were recorded after each addition.

For β-NADH and sufite titrations, spectra were recorded using a Shimadzu 1800 UV-Vis spectrophotometer. For the β-NADPH titration, spectra were recorded using a Shimadzu 2600 UV-Vis spectrophotometer. After correction for dilution, the changes in absorption at 492 nm, 468 nm and 452 nm were used to determine the dissociation constants for the Ren_{ox}•β-NADH, Ren_{ox}•β-NADPH and the Ren_{ox}•β-NAD^+ complexes respectively. The changes in absorption were fit to the quadratic solution form of the single site binding equation (Equation 7.6) in which [E] is the PpRen concentration, [EL] is concentration of the PpRen•ligand complex and K_L is the dissociation constant of the PpRen•ligand complex. For both β-NADH, β-NADPH and sulfite, the raw data were fit. That is, change in absorbance at defined wavelengths was used as a measure of [EL] and the maximal change in absorbance as a representation of [E].

Equation 7.6. $$[\mathrm{EL}] = \frac{([\mathrm{L}]+[\mathrm{E}]+ \mathrm{K}_L)-\sqrt{([\mathrm{L}]+[\mathrm{E}]+ \mathrm{K}_\mathrm{L})^2-4([\mathrm{L}]+[\mathrm{E}])}}{2}$$

Crystallization, Structure Determination, and Model Refinement. Initial crystallization conditions were those identified by the NESGC and included 2 M sodium formate, 100 mM sodium acetate pH 4.6 at 20 °C. Diffraction-quality crystals were obtained by the hanging drop vapor diffusion method. The droplet was formed from three 1 µL additions; 1 µL of the well solution, 1 µL of PpRen (104 µM) and 1 µL of H_2O. Crystals appeared after 2−4 days and grew to maximal dimensions of ~200 µm x 50 µm x 10 µm. Crystals were harvested from the hanging drops, and soaked for 1-3 minutes in 2.5 M sodium formate, 120 mM sodium acetate pH 4.7 with 20% glycerol and 166 mM β-NAD^+ or 10 mM β-NADH. The mounted crystal was then flashed-cooled in liquid nitrogen. Crystals were initially screened for diffraction quality using the rotating anode X-ray source at Marquette University (Milwaukee, WI). X-ray diffraction data for PpRen•β-NAD+ were collected at beamline 21-ID-D of the Life Science Collaborative Access Team (LS-CAT) at the Advanced Photon Source (APS). Data for the PpRen·β-NADH complex were collected at LS-CAT beamline 21-ID-F. Data were processed with HKL2000 [187].

The structure of PpRen was determined by molecular replacement in PHASER [188] with a search model derived from chain A of the *P. syringae* Q888A4 renalase structure (PDB ID 3KKJ, Northeast Structural Genomics Consortium) with all non-protein atoms removed and all B-factors set to 20.0. After iterative cycles of manual model building in COOT [189] and maximum likelihood based refinement using the PHENIX package (phenix.refine) [190], ordered solvent molecules were added in phenix.refine automatically and culled manually in COOT. After adding solvent atoms, the FAD cofactor and β-NAD+ or β-NADH were added to the model in COOT. During the last rounds of refinement,

hydrogen atoms were added to the model using phenix.reduce [191] to improve the stereochemistry of the model. Positions of H atoms were refined using the riding model with a global B-factor. Regions of each model to be used in translation-libration-screw (TLS) refinement were identified using phenix.find_tls_groups and the TLS parameters were refined in phenix.refine. Once the refinement converged, the model was validated using the tools implemented in COOT and PHENIX [192], [193]. Side chains with poor or missing electron density were modeled in favored rotameric conformations. The B-factors were allowed to refine without additional restraints, and the occupancies were held to 1.0. Data collection and model refinement statistics are listed in Table 7.1. Coordinates and structure factors for the PpRen·β-NAD^+ and PpRen·β-NADH complexes have been deposited in the Protein Data Bank with accession codes 4ZCD and 4ZCC, respectively.

Table 7.1. Crystallographic data collection and model refinement statistics.

	PpRen·β-NAD$^+$	**PpRen·β-NADH**
Space group	C 2	P 2_1
Unit cell parameters	a=144.7, b=37.6, c=138.2 Å	a=63.5, b=71.5, c=143.8 Å
	α=γ=90, β=120 °	α=γ=90, β=97.5 °
Resolution (Å)	33.2-1.66	46.2-2.00
(last shell)a	(1.69-1.66)	(2.03-2.00)
Wavelength (Å)	0.97895	0.97872
No. of reflections		
Observed	286455 (12871)	328721 (15867)
Unique	76829 (3588)	86594 (4305)
Completeness (%)[a]	99.7 (94.0)	100.0 (100.0)
Rmerge (%)[a,b]	0.044 (0.336)	0.096 (0.628)
Multiplicity	3.7 (3.6)	3.8 (3.7)
$\langle I/\sigma(I)\rangle$[a]	26.3 (3.7)	13.7 (2.2)
Model Refinement Statistics		
Reflections in work set	73035	77722
Reflections in test set	2971	2892
R_{cryst} (R_{free})	0.151 (0.176)	0.170 (0.215)
No. of residues	651	1288
No. of solvent atoms	748	736
Number of TLS groups	4	28
Average B-factor (Å^2)[c]		
Protein atoms	16.0	33.1
Ligand atoms	15.5	32.5
Solvent	28.8	36.6
RMS deviations		
Bond lengths (Å)	0.012	0.014
Bond angles (°)	1.490	1.634
Coordinate error (Å)	0.15	0.19

[a] Values in parentheses apply to the high-resolution shell indicated in the resolution row.
[b] $R = \Sigma(||F_{obs}|-scale*|F_{calc}||) / \Sigma |F_{obs}|$.
[c] Isotropic equivalent B factors, including contribution from TLS refinement.

Results

Properties of PpRen and Substrate Identification: PpRen can be expressed by the above methods to yield ~17 mg of purified enzyme per liter of culture. The absorption spectrum of the purified enzyme indicates characteristic visible maxima indicative of bound flavin. The flavin maxima are observed at 380 nm (ε = 10.1 $mM^{-1}cm^{-1}$) and 452 nm (ε = 11 $mM^{-1}cm^{-1}$) distinct from those observed for HsRen

(385 nm (ε = 10.9 $mM^{-1}cm^{-1}$), 458 nm (ε = 11.3 $mM^{-1}cm^{-1}$)) and free flavin (375 nm (ε = 9.7 $mM^{-1}cm^{-1}$), 450 nm (ε = 11.3 $mM^{-1}cm^{-1}$)). The enzyme is stable at 25 ^{o}C and below in phosphate buffer at pH 7.5, but prone to precipitate at concentrations above 4.5 mg/mL (~120 μM).

Borohydride reduction of β-NAD^{+} or β-$NADP^{+}$ yields three reduced isomers of each: 2-dihydroNAD(P) (2DHNAD(P)), 4-dihydroNAD(P) (β-NAD(P)H) and 6-dihydroNAD(P) (6DHNAD(P)). We have shown that HsRen catalytically oxidizes both 2- and 6DHNAD(P) to form β-$NAD(P)^{+}$ [35]. HPLC analysis indicated that when PpRen was added to the mixture of reduction products only 2- and 6DHNAD(P) molecules were consumed (Figure 7.1) indicating that this *Pseudomonas* form of renalase has the same substrate profile as the human. When chromatographed at 260 nm, where the adenine chromophore has maximal absorption, the net concentration lost from the 2- and 6DHNADP peaks (based on standard curves for each) was gained by the β-$NAD(P)^{+}$ peak indicating that the product formed from both types of substrate is the oxidized form of the nicotinamide dinucleotide (Scheme 7.1).

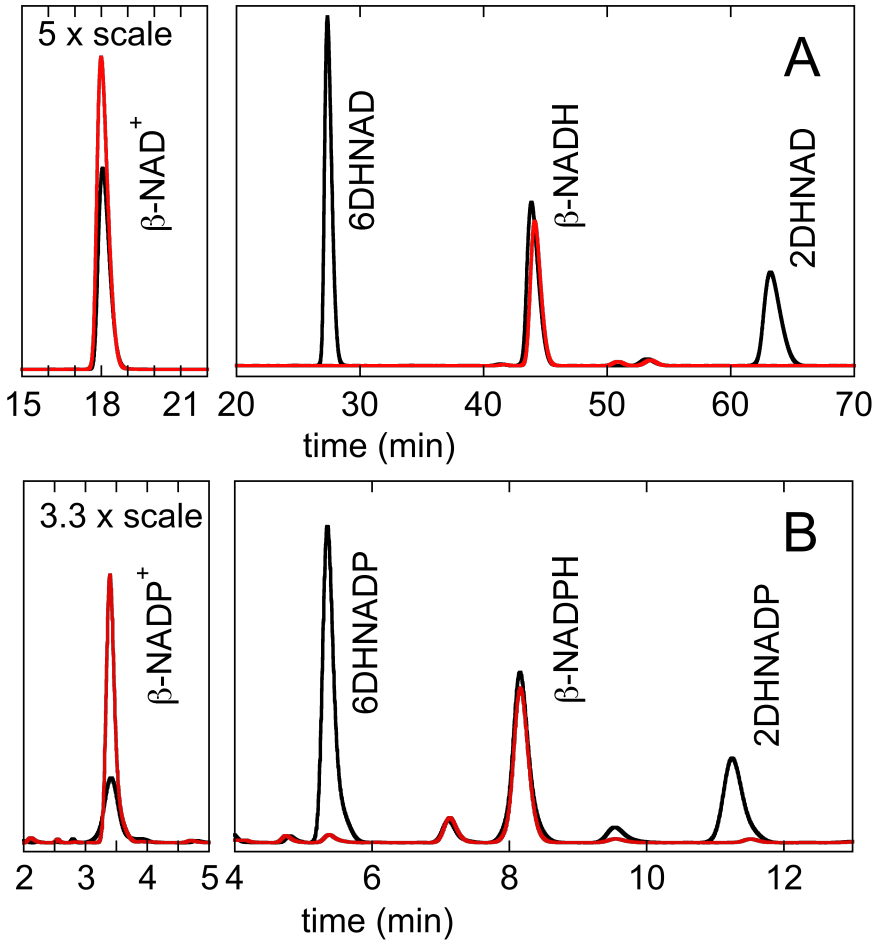

Figure 7.1. Analytical HPLC of Renalase Turnover Reactions of Borohydride Reduced Mixtures of β-NAD(P)H Isomers. HPLC separation was achieved using an analytical Waters X-bridge C18 column run isocratically in potassium phosphate buffer (10 mM for NAD derived mixtures, and 50 mM for NADP derived mixtures). All eluting species were detected at 260 nm, the absorption maximum for the NAD(P) adenine base. A. The black chromatogram is the separation of the components formed from borohydride reduction of β-NAD^+. The red chromatogram is three minutes after the addition of 30 µM PpRen. B. The black chromatogram is the separation of the components formed from borohydride reduction of β-$NADP^+$. The red chromatogram is three minutes after the addition of 30 µM PpRen.

Reductive Half-Reaction of PpRen with 6DHNAD(P): The reductive half-reaction was observed by mixing PpRen with varied concentrations of 6DHNAD, 6DHNADP, 2DHNAD and 2DHNADP, in the absence of molecular oxygen. The transfer of a hydride from the DHNAD(P) substrate to the PpRen flavin is observed as a large change in extinction coefficient of the flavin as it converts to the reduced state (Figure 7.2). The equilibrium and kinetic constants derived from these experiments are

summarized in Table 7.2. Both 6DHNAD and 6DNADP substrates were titrated and the largely monophasic reduction and hyperbolic dependence of the observed rate constant for reduction indicated that these substrates bind rapidly and reversibly to the enzyme prior to hydride transfer. The substrate dissociation constants obtained from the reductive-half reaction data indicated relative higher binding affinity for β-NAD^+-derived substrates (K_{2DHNAD}~36 μM, K_{6DHNAD}~28 μM) compared to the β-$NADP^+$-derived substrates ($K_{2DHNADP}$~500 μM, $K_{6DHNADP}$~1400 μM). This apparent preference for β-NAD^+-derived substrates is consistent with our proposed function for renalase; to protect primary metabolism dehydrogenases from inhibition by 2- and 6DHNAD [35]. However, both 6-dihydro substrates exhibited a relative slow reduction rate constant (k_{red}6DHNAD =0.4 s^{-1} and k_{red}6DHNAP =0.5 s^{-1}), approaching three orders of magnitude slower than those observed for the the 2-dihydro forms (k_{red}2DHNAD~180 s^{-1} and k_{red}2DHNAP~120 s^{-1}). When these data are viewed as a ratio they define a measure of substrate capture (k_{red}/Kd), it is apparent that PpRen has a twenty-fold preference for 2DHNAD over its next preferred substrate, 2DHNADP (Table 7.2). Both β-NAD^+- and β-$NADP^+$-derived substrates accelerate the reduction rate constant by 10^3-10^5 compared to that observed for β-NADH (~0.0008 s^{-1} at 2 mM β-NADH). A pronounced preference for the position of the nicotinamide hydride was not observed for HsRen that exhibited ostensibly the same dissociation constant for either β-NAD^+-derived substrate isomers ($K_{2DHNAD,}$ K_{6DHNAD}~170 μM) and only modest differences in the reduction rate constant (k_{red}6DHNAD ~230 s^{-1} and k_{red}2DHNAP ~850 s^{-1}) [35].

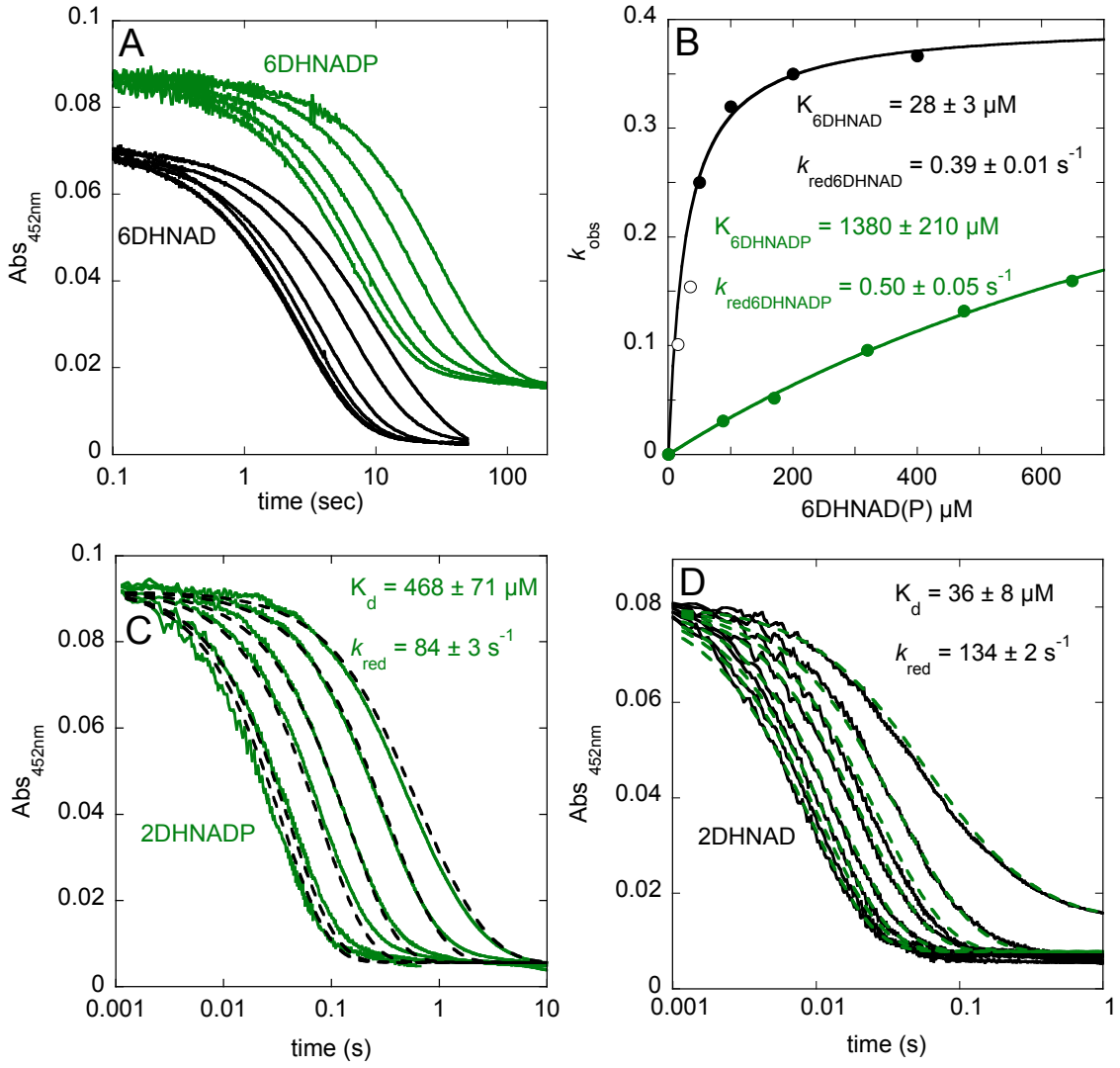

Figure 7.2. Kinetics of the Reductive Half-Reactions of PpRen with Nicotinamide Dinucletide Substrates. Oxidized anaerobic PpRen was mixed with varied concentrations of anaerobic substrates and the reduction of the enzyme's cofactor was observed at 452 nm. **A**. Reduction of the PpRen by 6DHNAD(P) substrates. Approximately 7 μM PpRen was reacted with either 6DHNAD (15, 35, 50, 100, 200, 400 μM) or 6DHNADP (88, 170, 320, 475, 613 μM). Traces for 6DHNAD are offset (down) for clarity. **B.** The dependence of the observed rate constant for reduction on the concentration of 6DHNAD and 6DHNADP fit to the hyperbolic form of the single site binding equation (equation 7.2). NB: observed rate constants obtained from exponential fits to non-pseudo first order reactant concentrations for 6DHNAD are shown as open circles. **C**. The reduction of PpRen (8 μM) by 2DHNADP (11.3, 21.5, 49.8, 93.0, 211.9, 263.8 μM) fit globally (dashed lines) to the model shown in Scheme 7.2. **D**. The reduction of PpRen (8 μM) by 2DHNAD (6.3, 13.0, 19.0, 26.4, 45.6, 72.1, 97.2, 163.2 μM) fit globally (dashed lines) to the model shown in Scheme 7.2. For **C.** and **D.** concentrations are based on the average of two spectra, one recorded immediately prior to and one immediately after collection of kinetic data.

Table 7.2. Summary of Kinetic and Equilibrium Constants for PpRen

Substrate/Ligand	K_d (μM)	k_{red} (s^{-1})	k_{red}/K_d ($\mu M^{-1}s^{-1}$)
2DHNAD	36 ± 8	134 ± 2	3.7 ± 0.8
2DHNADP	468 ± 71	84 ± 3	0.18 ± 0.02
6DHNAD	28 ± 3	0.39 ± 0.01	0.014 ± 0.002
6DHNADP	1380 ± 210	0.50 ± 0.05	$3.6 \pm 0.7 \times 10^{-4}$
β-NADH	81 ± 7	~0.0008 ± 0.00001	$9.8 \pm 0.8 \times 10^{-6}$
β-NADPH	1540 ± 370	n.m.[a]	

a- not measured

Oxidative Half-Reaction of PpRen: The reoxidation of PpRen was observed by double mixing stopped flow. The anaerobic oxidized enzyme was first mixed with anaerobic 6DHNAD at a concentration sufficient to reduce 75% of the enzyme. After a 150 second age-time that accounted for >6 half-lives for the predicted reduction rate constant at the reactant concentrations used, the partially reduced enzyme was mixed with defined pseudo-first order concentrations of dioxygen and observed to reoxidize at 452 nm (Figure 7.3A). The dependence of the observed reoxidation rate constant on the concentration of dioxygen was linear with a zero intercept indicating a collision-based reaction (Figure 7.3A inset). The second order reoxidation rate constant was obtained from the slope of the dependence according to Equation 7.4 and was found to be $5x10^3$ $M^{-1}s^{-1}$, similar to that observed for HsRen ($2.9x10^3$ $M^{-1}s^{-1}$) [34].

Exogenous β-NAD^+ impeded the rate constant for reoxidation (Figure 7.3B). The dependence of the inhibition yielded a dissociation constant for the PpRen(red)•β-NAD^+ complex of 230 μM (Figure 7.3B inset), 7-fold higher affinity than the same complex in HsRen. Suppression of the reoxidation rate constant extrapolated to ~0 s^{-1}, indicating an ordered product release mechanism in which β-NAD^+ (and presumably β-$NADP^+$) must dissociate before dioxygen can react with the reduced flavin cofactor. This differs from HsRen whose reoxidation rate constant was not influenced by exogenous nicotinamide product and as such displayed a formally random product release mechanism [34].

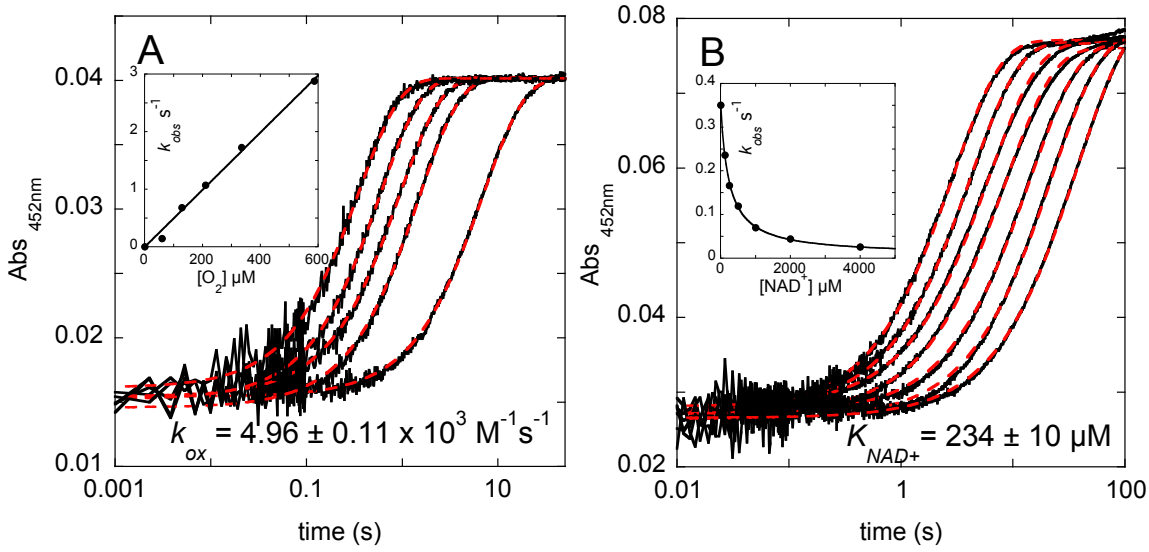

Figure 7.3. Kinetics of the Oxidative Half-Reaction of PpRen. **A.** Reoxidation of PpRen in the presence of varied concentrations of molecular oxygen observed at 452 nm. Reduced anaerobic PpRen (3 μM) was reacted with pseudo-first order concentrations (59, 128, 210, 335, 587 μM) of dioxygen. Traces were fit to Equation 7.3 (red dashes) Inset. The dependence of the observed rate constant for reoxidation fit to Equation 7.4. **B.** The dependence of the observed rate constant for reoxidation on the concentration of added β-NAD^+. Traces are shown for 5.8 μM PpRen reoxidizing in the presence of 119 μM dioxygen with 0, 125, 250, 500, 1000, 2000, 4000 μM added β-NAD^+ fit to Equation 7.3 (red dashes). Inset. The dependence of the observed rate constant for reoxidation on the concentration of exogenous β-NAD^+ fit to equation 7.5.

The Dissociation Constants for the $PpRen_{ox}$•β-NADH, $PpRen_{ox}$•β-NADPH and PpRen•SO_3 adduct Complexes: The dissociation constants for β-NADH and β-NADPH were measured by titration and observation of perturbation of the absorption spectrum of the PpRen FAD isoalloxazine moiety (Figure 7.4A). Consistent with the apparent preference for β-NAD^+-derived substrates, the dissociation constant for the PpRen•β-NADH complex was found to be ~80 μM, comparable to that for the 2DHNAD and 6DHNAD substrates (Figure 7.4). This low-level of β-NADH isomer selectivity was also observed in the human enzyme [35] and indicates that renalases are not able to discriminate between each of the reduced forms of β-NADH and therefore function in a partially inhibitory ligand environment. However, the PpRen•β-NADH dissociation constant is seven-fold lower than that

measured for the human enzyme, facilitating soaking strategies intended to form this complex in the crystal state (*vide infra*). Consistent with the dissociation constants measured in the reductive half reaction for 6DHNADP and 2DHNADP, the dissociation constant for β-NADPH was observed to be 19-fold larger than that for β-NADH.

Flavin-sulfite adduct formation is a peculiar characteristic of many oxidase enzymes. The Aliverti group showed that natively folded HsRen formed a dissociable sulfite adduct with the flavin cofactor [77]. In order to offer an additional reactivity correlation to HsRen, we titrated sulfite to PpRen (Figure 7.4B). Characteristic bleaching of the long wavelength transitions of the flavin spectrum were observed along with the appearance of a UV-transition at ~320 nm. When the data obtained at 452 nm were fit to the quadratic solution of the single-site binding equation, a dissociation constant for sulfite of 105 mM was obtained, substantially weaker than the sulfite affinity observed for HsRen (K_{SO3} = 1.8 mM).

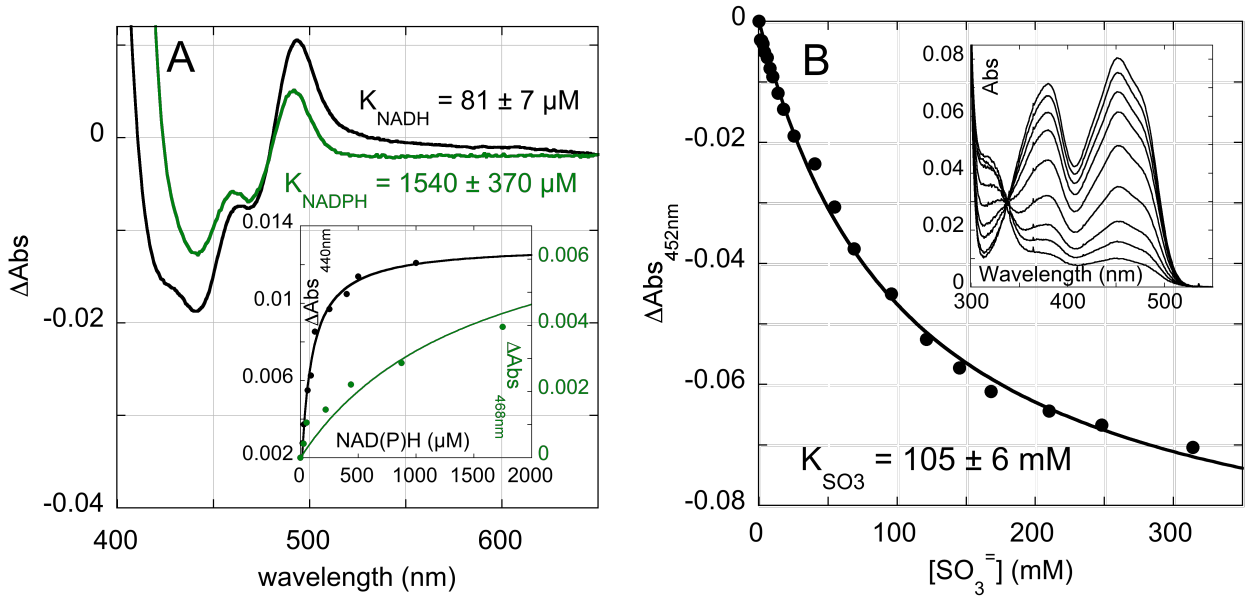

Figure 7.4. Measurement of the Dissociation Constants for the PpRen$_{ox}$•β-NADH, PpRen$_{ox}$•β-NADPH and PpRen•SO_3 Complexes. **A.** Flavin difference spectra and binding isotherms for the association of NADH and NADPH with PpRen. For the PpRen$_{ox}$•β-NADH titration (black), 17 µM PpRen was titrated with NADH (0-1 mM) and the spectrum at each ligand concentration recorded. The observed absorption changes in the spectrum at 494 nm were fit to Equation 7.5 (inset). For the PpRen$_{ox}$•β-NADPH titration (green), 12 µM PpRen was titrated with NADPH (0-7 mM) and the spectrum at each ligand concentration recorded. The observed absorption changes in the spectrum at 468 nm were fit to Equation 7.5 (inset). **B.** The titration of PpRen (10 µM) with sulfite (0-310 mM). The observed absorption changes in the spectrum at 452 nm were fit to Equation 7.5 (inset).

Structure of the PpRen•β-NAD$^+$ and PpRen•β-NADH complexes: PpRen proved highly apt to form crystals. Both rectangular rods and hexagonal plates were obtained using the conditions that were provided with the PDB ID 3KKJ structure deposited by the NESGC. Only the plate-like crystals displayed uniform high diffraction. By soaking, structures of the PpRen•β-NAD$^+$ (1.78 Å) and PpRen•β-NADH (2.0 Å) complexes were obtained (Table 7.1). Respectively, these structures are the PpRen$_{ox}$•product (EP) complex and a close representation of the PpRen•substrate (ES) complex. For both structures two protomers of PpRen are arranged together with a large primarily Van der Waals contact interface of ~1100 Å^2 in which no ionic pairs and only 8 hydrogen bonds contribute to association of the protomers.

Despite low sequence identity (19%), the fold of PpRen is highly similar to that of HsRen (PDB ID 3QJ4) with an RMSD of 2.1 Å for 298/326 Cα carbons (Figure 7.5). It is interesting to note that the initial structure of PpRen deposited in the PDB (ID 3KKJ) was the search model used to solve the structure of HsRen by molecular replacement. This study therefore serves as the functional assignment of the 3KKJ protein, annotated previously as an amine oxidase. The renalase fold is not characteristic to renalase and is observed with numerous redox-active flavoproteins [77]. However, the constellation of conserved active site residues is unique to renalase activity (Figure 7.6). Consistent with the observations of Milani et al, (that pertain to renalase sequences from *Animalia*) the active site opening is lined with three aromatic residues. In two of the three positions only the aromatic character of the side chain is conserved (PpRen W212, F204 corresponding to F223, Y214 in HsRen) whilst the third is a conserved tyrosine (PpRen Y57 corresponding to Y62 in HsRen). The inner surfaces of the active site pack closely to the *si* face of the flavin isoalloxazine and provide a substrate binding cavity adjacent to the *re* face. Conserved residues that line the substrate-binding cavity are H232 (HsRen H245) and W276 (HsRen W288). A guanidino group is supplied by R280 (HsRen Q292) and a similar placement of a guanidino group is accomplished in HsRen from R193 (PpRen T185) that is conserved in the *Animalia* and extends from a different element of secondary structure.

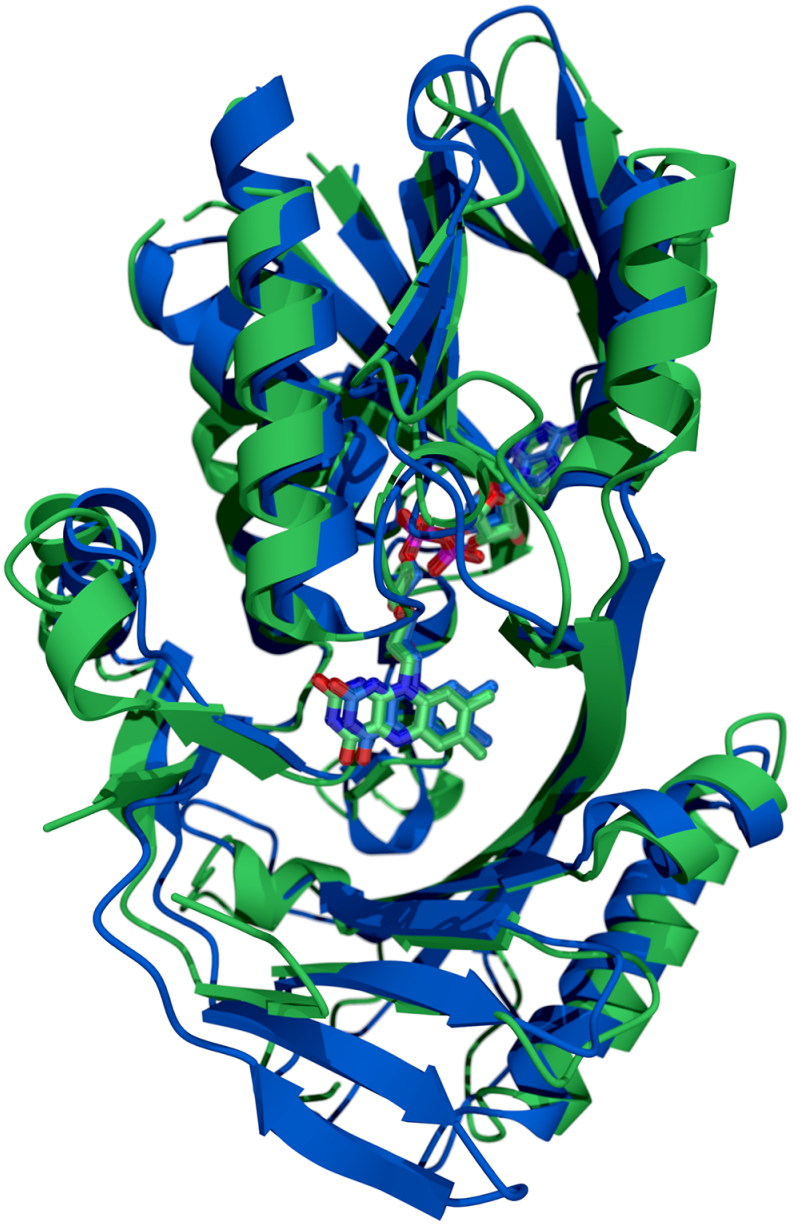

Figure 7.5. Superposition of the PpRen•β-NADH and HsRen Tertiary Structures. PpRen•β-NADH is depicted in blue and HsRen is depicted in green (PDB ID 3QJ4).

The primary advancement in understanding the chemistry of renalase was that the PpRen structures were solved with catalytically relevant ligands occupying the active site cavity. Stereo views of the active site with both ligands and representative ligand density are depicted in Figure 7.6. The PpRen•β-NADH complex structure provides a representation of the ES complex. The reduced nicotinamide base of β-NADH has an overall neutral charge and is ostensibly isosteric with the bases of 2DHNAD(P) or 6DHNAD(P) and presumably localizes in a position similar to that of the native substrates. Evidence of this is that the 2-position of the base is most proximal to the N5 of the isoalloxazine (3.6 Å), the assumed position of hydride delivery, in an analogous position to that observed in other NAD(P)H/isoalloxazine complexes [79, 194] (Figure 7.7B & 7.7C). No evidence for partial occupancy of a 6-position reduction conformer is observed, suggestive of the apparent preference for 2DHNAD(P) isomers that were observed to reduce the enzyme ~500-fold more rapidly than 6DHNAD(P) isomers (Figure 7.2, Table 7.2). One possible explanation for this apparent conformer bias is that threonine 185 (that occupies the position of a conserved arginine in animal renalases, see below) donates an apparent hydrogen bond to the nicotinamide amide oxygen, stabilizing the pose that promotes donation of the hydride from the 2-position (Figure 7.6 & 7.7). Manually flipping the nicotinamide base in the PpRen•β-NADH model followed by additional refinement did not substantially alter the electron density for the pyridyl ring (data not shown). In this alternate pose a potential interaction is observed from the dihydronicotinamide amido nitrogen to the backbone carbonyl of G307. The PpRen•β-NAD^+ structure is that of the product complex. Despite 1.78 Å resolution, the electron density map for this complex indicated very low occupancy of the base and the ribose that form the nicotinamide nucleoside. It is suggested that the proximity of the R280 (R193 in HsRen) guanidino group plays an important role in ejecting the positively charged nicotinamide

product (β-NAD(P)$^+$) from the active site. We observe that the guanidino group is displaced in the PpRen•β-NAD$^+$ structure from the position it occupies in the PpRen•β-NADH complex structure by 2.6 Å, suggesting a charge repulsion interaction.

The ADP moiety of both ligands is anchored in the same position on the surface of the protein (Figure 7.7). In this binding pose the two ribose units emerge from the pyrophosphate moiety approximately parallel to one another, a position that places the respective 3'-hydroxyl groups within 2.9 Å. This conformation does not provide an obvious explanation for the observed substrate binding preference of PpRen where β-NAD$^+$-derived substrates bind ~50-fold more tightly than those derived from β-NADP$^+$.

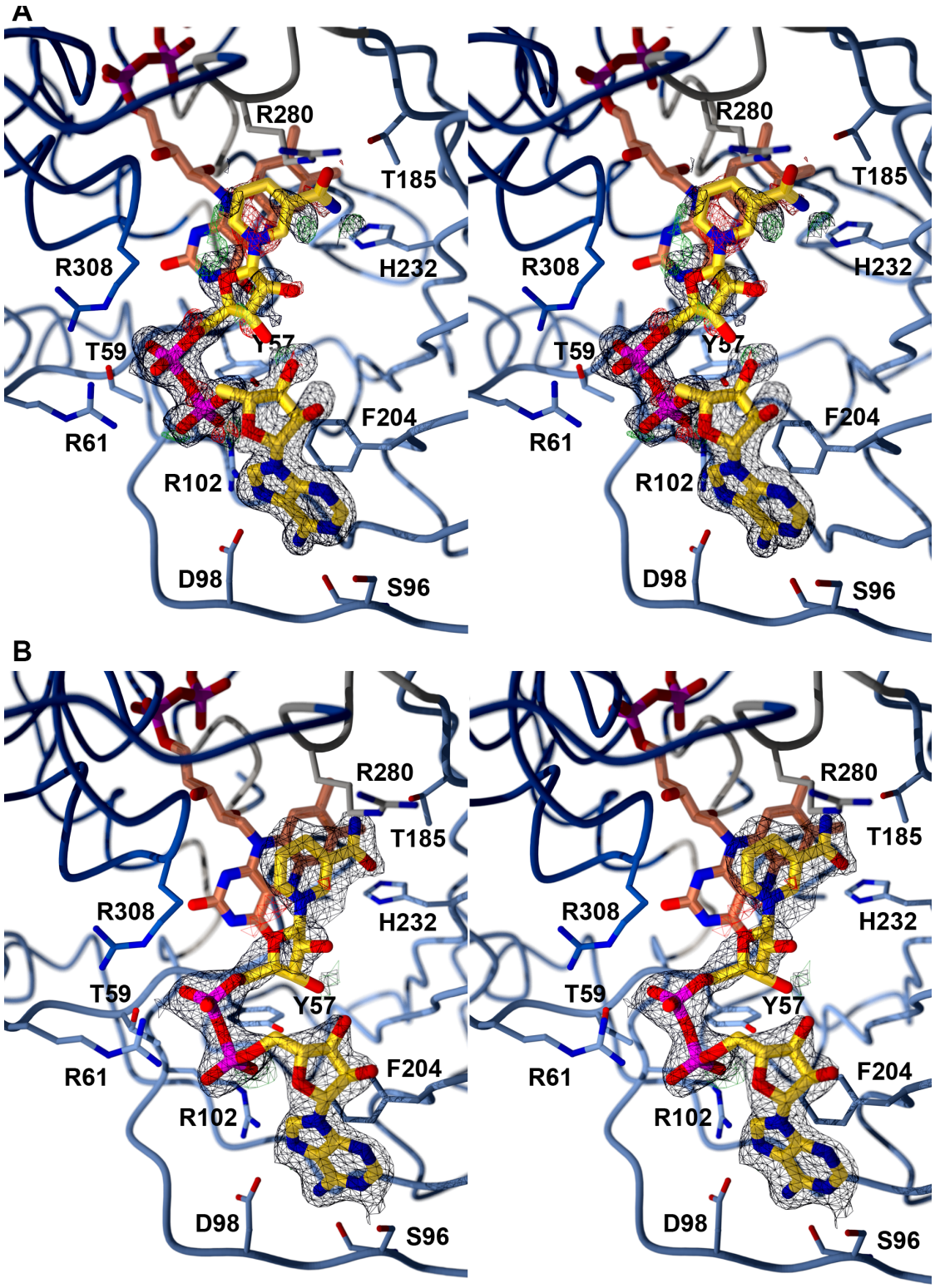

Figure 7.6. The Active Site of the PpRen β-NADH and β-NAD$^+$ complexes. **A.** Stereoview for the PpRen•β-NAD$^+$ complex showing the $2|F_o|-|F_c|$ simulated annealing composite omit electron density of the ligand (black) contoured at 1.0σ and $|F_o|-|F_c|$ electron density contoured at 3.0σ (green) and -3.0σ (red). **B.** Stereoview for the PpRen•β-NADH complex showing the $2|F_o|-|F_c|$ simulated annealing composite omit electron density of the ligand (black) contoured at 1.0σ and $|F_o|-|F_c|$ electron density contoured at 3.0σ (green) and -3.0σ (red).

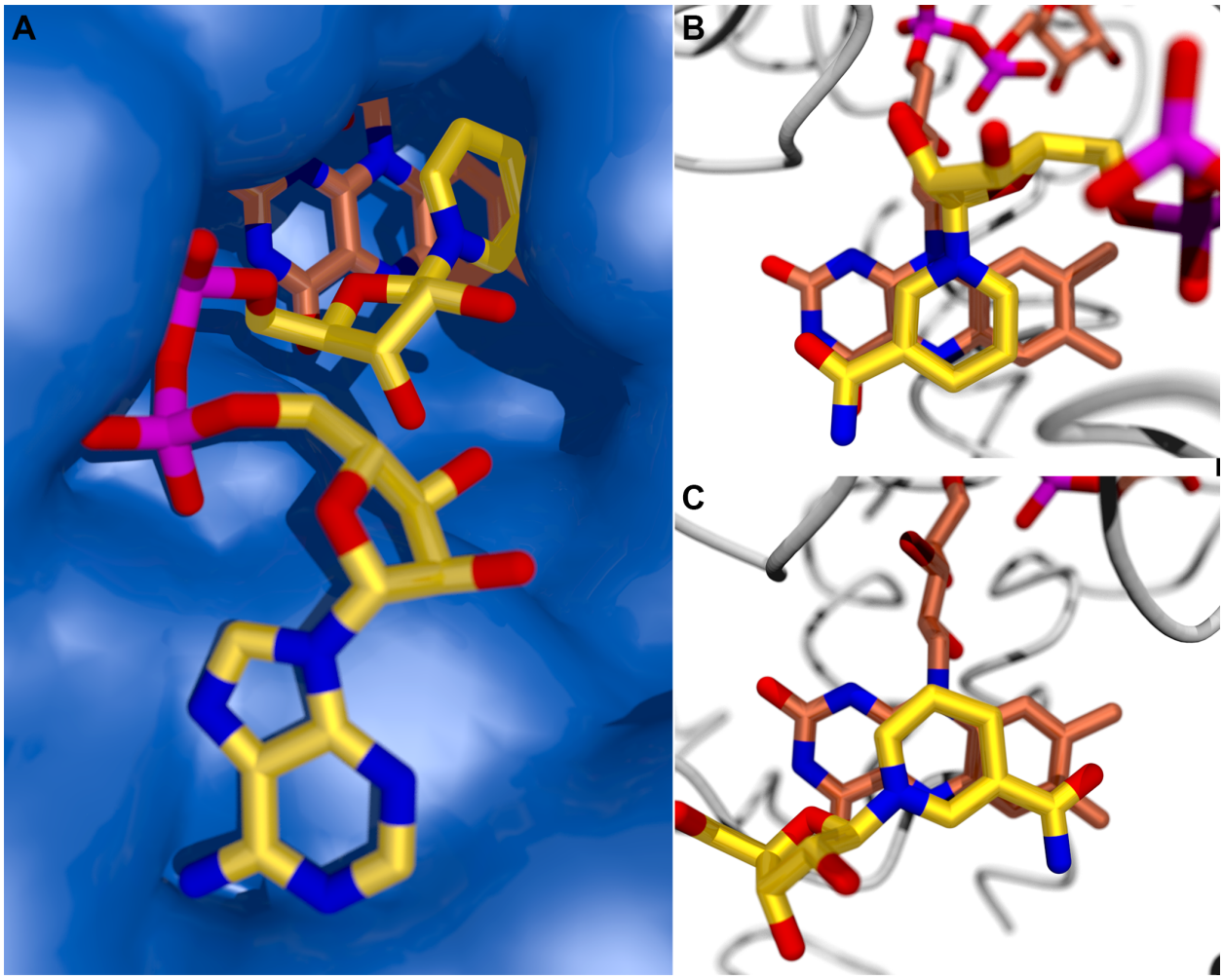

Figure 7.7. The Reductive Pose of Nicotinamide Dinucleotide Substrates. **A.** The relative positions of β-NADH and FAD on the solvent accessible surface of PpRen. **B.** The reductive complex of glutathione reductase in complex with β-NADH (PDB ID 1GRB) depicting the position of the nicotinamide 4-position 3.4 Å from the flavin isoalloxazine N5. **C.** The reductive complex of PpRen in complex with β-NADH (PDB ID 4ZCC) depicting the position of the nicotinamide 2-position 3.6 Å from the flavin isoalloxazine N5.

Discussion

The current consensus understanding for the function of renalase is that it is an animal enzyme/hormone whose catalytic activity lowers blood pressure and modulates the contraction rate of the heart by oxidative consumption of catecholamine substrates (critical evaluations of this claimed catalytic role are available [71, 125, 195]). This entrenched perception of the catalytic function of this

enzyme has persisted in the literature since the progenitor article claimed to simultaneously discover the enzyme, its catalytic activity and its physiological role[46]. We, and others, have disputed this claim and have offered evidence and counter arguments that undermine the link to catecholamines [34, 35, 72, 76, 88, 89, 94]. Moreover, the recent discovery by our group that renalase has genuine catalytic behavior with two β-NAD(P)H isomers [35] casts further doubt over the extracellular catecholamine oxidase activity claim. This new activity for renalase is more consistent with an intracellular house-keeping metabolic function. In this role β-NAD(P)H isomers that we presume to arise in non-specific reduction events and inhibit dehydrogenase enzymes are recycled back to the nicotinamide dinucleotide pool by oxidation (forming β-NAD(P)$^+$). Such an activity would be expected to be generally advantageous to living organisms and therefore likely to be detectable in Kingdoms outside the *Animalia*. In this article we present the first account of a bacterial form of renalase. In addition to the substrate profile, kinetics of catalysis and substrate/ligand preferences, we also show the structures of the enzyme in complexes with catalytically relevant NAD ligands that have poses consistent with this newly identified activity.

PpRen was first identified in 2009 by the NESGC and in the absence of known function given a generic, amine oxidase designation (PDB ID 3KKJ). In 2011, the Aliverti group solved the structure of HsRen using 3KKJ as a search model in a molecular replacement strategy (PDB ID 3Qj4) [77]. The striking similarity of the apparent active sites of HsRen and 3KKJ led us to conclude that the 3KKJ structure was from a bacterial form of renalase. The data obtained with this enzyme support that it has the same function as HsRen. In the presence of a mixture of 2DHNAD(P), 4DHNAD(P) (β-NAD(P)H) and 6DHNAD(P) PpRen oxidizes only the 2- and 6-dihydro isomers as was observed for the human enzyme (Figure 7.1). Both β-NAD$^+$- and β-NADP$^+$-derived substrates induce relative rapid reduction of

the PpRen flavin isoalloxazine ring and induce multiple turnovers indicating that they are genuine substrates for PpRen (Figure 7.2).

We have proposed that the true function of renalase is to scavenge NAD(P)H isomers to alleviate inhibition of primary metabolism. Solely in terms of dissociation constant, the substrate preference of PpRen would appear to be for β-NAD^+-derived substrates. Both 2DHNAD and 6DHNAD bind 10-50-fold more tightly than do 2DHNADP and 6DHNADP (Figure 7.2). However, substrate preference (or scavenging efficiency) is a function of both dissociation constant and the rate constant for the largely irreversible hydride transfer to the flavin and the 6-dihydro substrates reduce PpRen considerably more slowly than the 2-dihydro substrates. When the relative rate constants for reduction and dissociation constants are compared as a ratio (kred/Kd), PpRen has a 300-500–fold preference for 2-DHNAD(P) substrates. It is conceivable that this substrate preference mirrors a 2DHNAD(P) inhibitory susceptibility of one or more of the primary metabolism dehydrogenases in *P. phaseolicola*. The structures of PpRen•β-NADH and PpRen•β-NAD^+ do not reveal the basis of β-NAD^+-derived isomer binding selectivity (Figure 7.3 & 7.4A). In both the PpRen•β-NADH and PpRen•β-NAD^+ structures the oxygen atom of the 2-hydroxyl of the adenine nucleotide riboside has no interacting residue or steric constraint within an 8 Å sphere (Figure 7.7A).

It would appear that renalase's primary catalytic purpose is to accept the hydride, as reoxidation of the enzyme occurs with a rate constant only 20-fold greater than that of free $FADH_2$ autoxidation and so is only modestly catalyzed [144, 160] (Figure 7.3). This is unlike most dioxygen-reactive flavoproteins that tend to have reoxidation rate constants at least two or three orders of magnitude more rapid than that of free flavin [144, 196, 197]. There is no spectrophotometric evidence for the dissociation of the β-$NAD(P)^+$ product in the reductive half reaction, but its egress is assumed to be rapid compared to the rate constant for reoxidation at atmospheric levels of dioxygen

(~1 s^{-1}) (Figures 7.3 & 7.6). Scheme 7.3 provides a summary of the kinetic and chemical mechanism conclusions for PpRen in turnover with the preferred substrate, 2DHNAD, that were made from our observations. In this scheme the substrates bind rapidly and transfers a hydride to the flavin isoalloxazine N5. The release of products has an obligate order in which β-NAD(P)$^+$ dissociates before dioxygen reacts with the reduced flavin. This ordered release of products is based on the observation that exogenous β-NAD$^+$ can completely suppress the reoxidation of the enzyme. Once β-NAD(P)+ has dissociated the flavin reoxidizes with a rate constant that would be the *in vitro* rate-limiting process under conditions of atmospheric dioxygen.

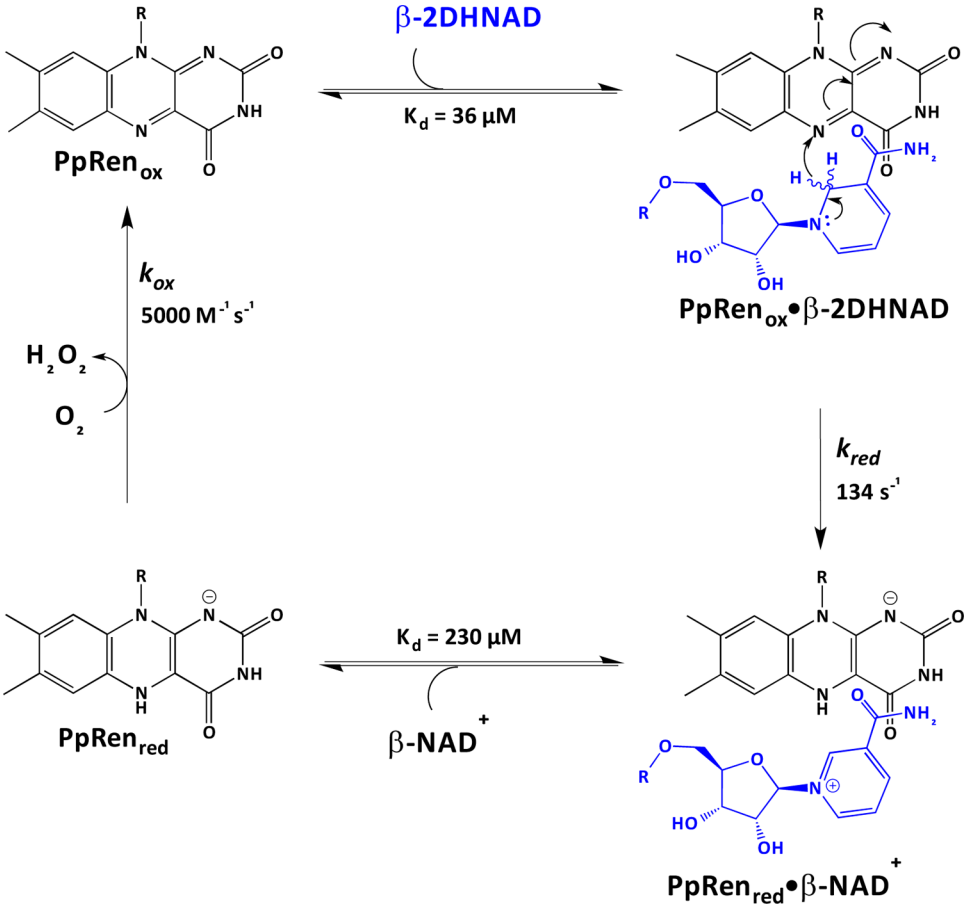

Scheme 7.3. Catalytic Cycle of PpRen with 2DHNAD as a Substrate.

The PpRen structures represent a significant advancement in our understanding of the catalysis of this enzyme. Together, the PpRen•β-NADH and PpRen•β-NAD^+ structures offer evidence of the nature of the ES and EP complexes respectively. The reduction reaction catalyzed by renalase is exceedingly simple: the transfer of a hydride equivalent to the isoalloxazine of a flavin. The primary difference between this and numerous other enzymes is that the substrate nicotinamide is bound to afford hydride transfer from alternate positions of the pyridyl base (Figure 7.7). Possibly the most interesting aspect of renalase chemistry is that it accommodates reduction from both the 2 and 6 positions and therefore must have binding modes for both substrate types. The structure of PpRen with β-NADH bound has the nicotinamide positioned such that the 2-position of the base is 3.6 Å from and directly over the N5 of the isoalloxazine ring (Figure 7.7C). No evidence of a flipped, 6-position reduction conformation, in the form of amide density in the alternate meta-position, in respect to the pyridyl nitrogen, is observed. Moreover, no density indicative of a lateral displacement of the nicotinamide to place the 6 position proximal to the flavin N5 is observed. As such it would appear that the rapid reduction rate constants observed with 2DHNAD(P) substrates are due to a more naturally optimized position whose conformer was selected in the crystalline state by the hydrogen bonding interaction with threonine 185.

Consistent with the relatively simple reaction being catalyzed, the number of conserved active site residues in renalase is small. The inner surface of the flavin re-face substrate cavity has only three fully conserved residues, H232, R280 and W276. Formally R280 is not positionally conserved, as it extends from a different secondary structural element in the bacterial enzyme (R193 in HsRen). However, the guanidino group of both residues resides in similar positions in the active site. It is posited that this charged residue is responsible for expulsion of the oxidized nicotinamide after hydride transfer and potentially facilitates the reduction chemistry by promoting the formation of the

dihydroflavin anion. H232 is conserved in all known or annotated forms of renalase (H245 in HsRen). This residue is not required for acid/base chemistry in the reductive half reaction but may serve to add to the positive potential toward the internal reaches of the active site. H232 may participate in acid/base chemistry in the oxidative half reaction by shuttling protons to aid rapid elimination of hydrogen peroxide from a transient C4a-(hydro)peroxyflavin during the oxidative half-reaction. This histidine is positioned 5.0 Å from the flavin N5 and C4a positions with both the β-NADH and β-NAD^+ ligands bound.

This study identifies the first known bacterial form of renalase. Defining true catalytic substrates for the human enzyme has both prompted re-evaluation of the true function of this enzyme and provided a means to definitively identify this activity in other organisms, including those without circulatory systems. In regard to the catalytic role of renalase, it has become very clear that claims concerning activity with catecholamines were quite incorrect, and were based on the propensity of such molecules to autoxidize in the presence of dioxygen. The elaboration of these claims throughout the last decade warrants some retrospection. While the observations included here and in prior work do not rule-out a non-catalytic moonlighting influence on vascular tone, they do argue strongly that the catalytic role of renalase serves an intracellular function that eliminates an inhibition of primary metabolism by β-NAD(P)H isomers.

Chapter VIII
Ligand Binding Phenomena that Pertain to the Metabolic Function of Renalase

Brett A. Beaupre, Joseph V. Roman, Matthew R. Hoag, Kathleen M. Meneely, Nicholas R. Silvaggi, Audrey L. Lamb and Graham R. Moran

Abstract

Renalase catalyzes the oxidation of isomers of β-NAD(P)H that carry the hydride in the 2 or 6 positions of the nicotinamide base to form β-NAD(P)$^+$. This activity is thought to alleviate inhibition of multiple β-NAD(P)-dependent enzymes of primary and secondary metabolism by these isomers. Here we present evidence for a variety of ligand binding phenomena relevant to the function of renalase. We offer evidence of the potential for primary metabolism inhibition with structures of malate dehydrogenase and lactate dehydrogenase bound to the 6-dihydroNAD isomer. The previously observed preference of renalase from *Pseudomonas* for NAD-derived substrates over those derived from NADP is accounted for by the structure of the enzyme in complex with NADPH. We also show that nicotinamide nucleosides and mononucloetides reduced in the 2- and 6-positions are renalase substrates, but bind weakly. A seven-fold enhancement of acquisition (k_{red}/K_d) for 6-dihydronicotinamide riboside was observed for human renalase in the presence of ADP. However, generally the addition of complement ligands, ADP for mononucloetide or AMP for nucleoside substrates, did not enhance the reductive half-reaction. Non-substrate nicotinamide nucleosides or nucleotides bind weakly suggesting that only β-NADH and β-NADPH compete with dinucleotide substrates for access to the active site.

Introduction

Renalase is an FAD-dependent oxidase that catalytically oxidizes two isomeric forms of β-NAD(P)H to form β-NAD(P)$^+$ and H_2O_2 (Scheme 8.1). These isomers are presumed to occur when β-NAD(P)$^+$ is reduced non-specifically forming, in addition to the native β-NAD(P)H (4-dihydroNAD(P)), 2-dihydroNAD(P) (2DHNAD(P)) and 6-dihydroNAD(P) (6DHNAD(P)) [35, 98]. Both 2DHNAD and 6DHNAD have been shown to be highly inhibitory to specific primary metabolism dehydrogenases [35]. This suggests that renalase has an intracellular metabolic house-keeping function that alleviates metabolic suppression by these isomers. This proposal differs starkly from the consensus view that renalase is a mammalian serum borne protein that is associated with an array of aberrant physiological conditions. The enzyme was originally claimed to be a kidney-derived hormone that down-modulates vascular tone in animals by the oxidation of catecholamines[46, 48, 110, 117, 198] and then later to be a cytokine that ameliorates myocardial damage resulting from an ischemic event[60]. More recently it has been said to be a suppressor of pancreatic cancer and/or an exacerbatory factor for melanoma [46, 47, 66, 68, 199]. Here we present the first structures of 6-DHNAD in complex with malate dehydrogenase and lactate dehydrogenase, confirming our assertion that β-NAD(P)H [dihydronicotinamide] isomers are detrimental to normal metabolic activity and reasserting the verified catalytic function of renalase. These structures show that 6DHNAD occupies the β-NADH-binding site occluding the association of the native nicotinamide substrate.

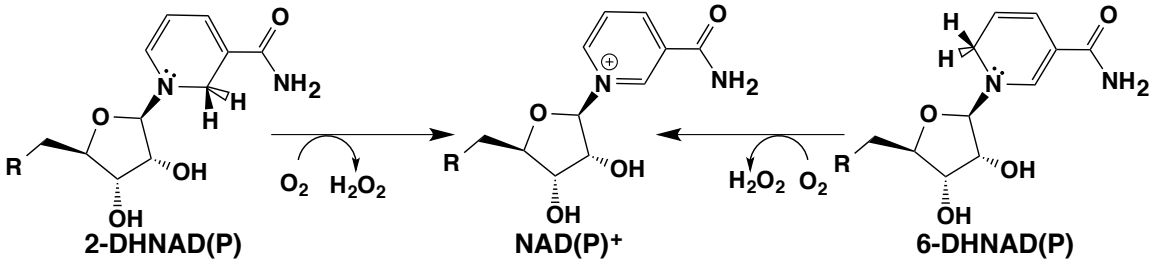

Scheme 8.1. The chemistry catalyzed by renalase.

With a modest two-electron reduction potential of -320 mV, the potential for non-specific redox reactions of β-NAD(P)$^+$ that form toxic β-NAD(P)H isomers exists in all living systems. It is therefore reasonable to expect that an intracellular detoxification activity such renalase would be found in multiple kingdoms of life. However, homology searches based on the human renalase amino acid sequence return almost exclusively homologs from *animalia*. The structure of human renalase (isoform 1; HsRen) was solved in 2011 by the Aliverti group who noted that the renalase structural topology was common to numerous redox active flavoproteins [77]. In this structure the open active site was observed to have only a small number of conserved amino acids indicating that sequence alignments based on overall alignment scores (E-values) may not detect this motif and will not necessarily identify distant forms of renalase. We have recently characterized a renalase from a Pseudomonad (19% identity to Human)[38]. As part of this study we solved the crystal structures of this form of renalase (PpRen) in complex with β-NADH (PDB ID 4ZCC, 2.1 Å; a fascimile of the ES complex) and β-NAD$^+$ (PDB ID 4ZCD, 1.7 Å; the EP complex). These structures revealed that the *si* face of the FAD isoalloxazine is closely associated with the inner surface of the active site offering the *re* face for interaction with the substrate nicotinamide base. The few conserved residues that line the dihydronicotinamide-binding cavity are: PpRen H232 (HsRen H245), W267 (HsRen W288) and R280,

which is apparently equivalent to HsRen R193, as both residues offer their guanidino group to a similar location in the active site. In both proteins, the active site cavity forms one end of an extended cleft to which β-NAD(P)-derived substrate(s) associate (Figure 8.1). Within this cleft are multiple hydrogen bonds and charge pairing interactions that in the *Pseudomonas* enzyme form a rather symmetrical set of interactions with respect to each nucleotide half of the substrate. However, the majority (8 of 11) form hydrogen bonding and/or charge pairing interactions with the pyrophosphate moiety of the substrate/product. Only one direct contact is observed for the nicotinamide amide and two for the 6 amino group of the adenine base with no hydrogen bonds from the protein engaging any of the hydroxyl groups of either ribose. This arrangement raises interesting questions about what part of the molecule contributes to the binding energy given that renalase must function in an environment in which non-substrate mono- and dinucleotides predominate. Using truncated forms of the substrate we offer evidence that, at least for human renalase, binding of the pyrophosphate moiety of the substrate has a primary contribution to stabilizing the pre-reduction E•S complex.

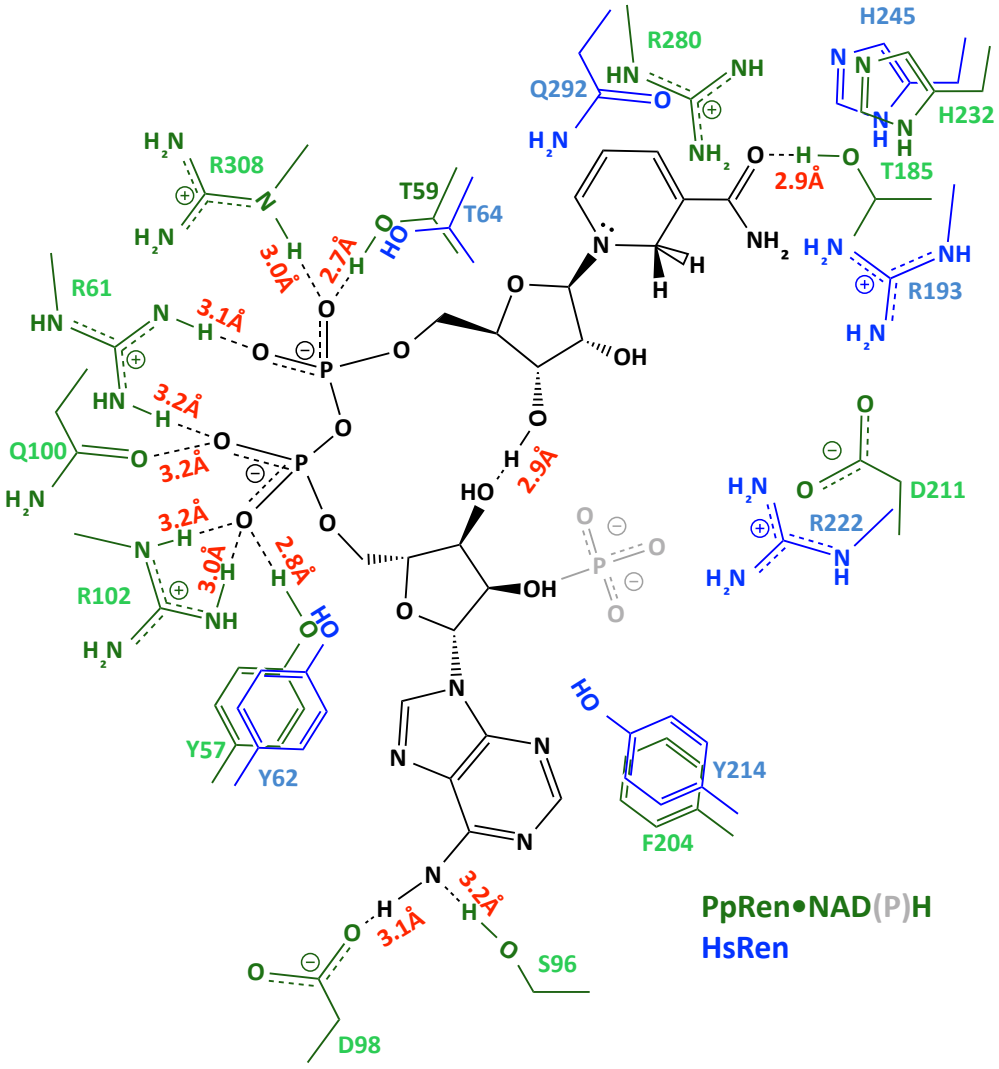

Figure 8.1: Two-Dimensional Representation of Active Site Interactions of NAD(P)H Molecules with Bacterial and Human Renalase. Structure in black is the NAD(P)H ligand; green indicates residues from *Pseudomonas phaseolicola*. Residues shown in blue are the conserved and non-conserved residues from human renalase that are proximal to the interacting residues from the *P. phaseolicola* structures. The 2'-phosphoryl of NADPH is shown in grey. Apparent hydrogen bond and charge interaction distances are shown in red.

The substrate/product binding pose exposes one face of the ligand to direct interactions with solvent (Figure 8.1). Both the human (HsRen) and bacterial (PpRen) forms of renalase exhibit a preference for substrates derived from β-NAD^+ over those derived from β-$NADP^+$ and this bias is notably more pronounced in the bacterial enzyme [38]. While this specificity bias is consistent with renalase serving to preferentially detoxify the inhibitory effect that 2DHNAD and 6DHNAD would exert

on primary metabolism enzymes, the structural basis for this selectivity was hitherto unknown. In this study we present the structure of renalase from *Pseudomonas phaseolicola* in complex with β-NADPH and evaluate the influence of the ribose 2-phospho group in regard to the observed substrate specificity.

Materials and Methods

Materials. Dibasic potassium phosphate and sodium phosphate, monobasic potassium phosphate and sodium chloride were obtained from ACROS. β-NADH (disodium salt, trihydrate) was obtained from Amresco. β-NAD^+, β-$NADP^+$, nicotinamide mononucleotide (NMN), ADP-ribose, methyl nicotinamide and nicotinic acid were purchased from Sigma. Nicotinamide riboside (NR) was purchased from High Performance Nutrition. Renalases from *H. sapiens* (HsRen) and *P. phaseolicola* (PpRen) were expressed and purified according to previously published methods[38, 94]. Old yellow enzyme was prepared as previously described[35]. 6DHNAD and 6DHNADP were prepared and purified as described[35].

Preparation and analysis of reduced forms of NR and NMN. To establish whether nucleoside and nucleotide forms of 2-dihydro- and 6-dihydronicotinamides were substrates for renalase, 0.9 mL of a 300 μM solution of oxidized nicotinamide riboside (NR^+) or nicotinamide mononucleotide (NMN^+) was combined with 100 μL of a 3 mM solution of sodium borohydride in 100 mM potassium phosphate at pH 7.5. This resulted in instantaneous generation of the three reduced forms of each parent compound (2-, 4- and 6-dihydro). Each of these mixtures was divided in two and ~12.5 μM renalase (final) was added to one sample, while the other served both as unreacted and sample stability controls. All samples were incubated for 10 min prior to ultrafiltration using a 0.5 mL Amicon 10 kDa centrifugal filter to remove renalase. 50 μL of each filtrate was loaded onto an analytical Xbridge

Peptide BEH C18 column (3.5 µM, 4.6 x 150 mm) run isocratically at 1.5 mL/min in 100 mM potassium phosphate at pH 7.5 with a Waters 600 pump coupled to a Waters 2487 dual wavelength detector, detecting simultaneously at 260 and 370 nm. The chromatographs obtained from samples to which renalase was added were corrected for the dilution.

For preparation of the 4DH forms of NR and NMN, sodium dithionite was used as a reductant in place of sodium borohydride [35]. 4DHNR and 4DHNMN were prepared by semi-preparative HPLC. The dithionite reduced mixtures were loaded onto a semi preparative Xbridge Prep C18 OBD column (5µM, 19 x 250 mm) run isocratically at 10 mL/min in 100 mM potassium phosphate buffer, pH 7.5 using a Waters 600 pump coupled to a Waters 2487 dual wavelength detector, detecting simultaneously at 260 and 340 nm. 4DHNR and 4DHNMN samples were frozen on dry ice during multiple collection cycles and then thawed and loaded onto a 35 cc Sep Pak (Waters) C18 cartridge equilibrated in 100 mM potassium phosphate pH 7.5. The bound sample and was eluted with water into 3 mL fractions. The fractions that contained the desalted 4DHNR or 4DHNMN were pooled and immediately lyophylized. Once dry, the sample was dissolved in 6 mL of cold water and stored at -80 ^{o}C.

Spectrophotometric quantification of NAD analogs. Molar extinction coefficients for 2-, 4- and 6DHNMN and 2-, 4- and 6DHNR were determined by reducing a 4 mL solution containing ~20 mM NMN^{+} or NR^{+} in 100 mM potassium phosphate buffer, pH 7.5 with 1 mL of ~66 mM sodium borohydride solution prepared in 30 mM potassium phosphate buffer, pH 11. The resulting 5 mL solution containing all three reduced isomers was separated by semi-preparative HPLC as described above. Peaks corresponding to each of the reduced isomers were collected. Both 4- and 6-dihydro forms were frozen on dry ice while the less stable 2-dihydro isomers were used immediately. The

concentration of each isomer was determined by the oxidase activities of renalase (2- and 6-dihydro forms) or old-yellow enzyme (4-dihydro form) using a Hansatech dioxygen electrode. Briefly, 1.6 mL of each sample collected was divided in two, where one half was used to obtain an absorption spectrum and the other was loaded into the oxygen electrode reaction vessel and allowed to react with either 10 μM renalase (2- and 6-dihydro NMN or NR) or 20 μM old yellow enzyme (4-dihydro NMN or NR). Based on each enzyme's reaction stoichiometry, the amount of oxygen consumed (μM) defined the concentration of the dihydronicotinamide substrate. This measurement was made three times for each isomer and the results were averaged after correction for the dilution that occurred with the addition of enzyme.

Reductive half-reactions with 2- and 6DHNMN and 2- and 6DHNR. Exclusion of dioxygen allows for observation of only the reductive half-reaction of renalase. Rate constants for reduction were determined using HsRen and PpRen as previously described [35, 38]. The post mixing concentration of HsRen was 6-11 μM and 2-5.5 μM for PpRen. Reduction of the renalase flavin cofactor was monitored at 458 nm for HsRen and 450 nm for PpRen. All half-reactions were carried out in 20 mM HEPES buffer, pH 7.5. Reactions with 2- and 6DHNR as substrates required the addition of the detergent octyl-beta-glucoside (2 mM final) in the tonometer to prevent excessive enzyme precipitation during the reaction. The reduction process was fit to equation 8.1 to obtain k_{obs} values. In this equation ΔA is the amplitude associated with the change in the enzyme's flavin absorption spectrum as it is reduced, k_{obs} is the observed rate constant for reduction of the flavin cofactor and C is the absorbance at infinite time. The k_{obs} values were then plotted against substrate concentration and fit to Equation 8.2 where the slope of the line gave k_{red}/K_d as a measure of the enzyme's substrate acquisition capacity,

where k_{red} is the limit for the rate constant for reduction and K_d is the dissociation constant for the substrate, S.

Equation 8.1 $$A_{458} = \Delta A(e^{-k_{obs}t}) + C$$

Equation 8.2 $$k_{obs} = (k_{red}/K_d)[S]$$

The available concentration of 2DHNR and 2DHNMN was limited by instability. Samples could not be pooled and further purified, but were instead collected directly from the HPLC into a glass syringe containing D-glucose (1 mM final) and sparged with argon for 3 minutes. Glucose oxidase (10 µL, 1 U/µL) was added to the glass syringe immediately before mounting onto the stopped flow spectrophotometer to consume dissolved dioxygen.

Reductive half reactions were also undertaken in the presence of counterpart ligands. 2- and 6DHNMN and 2- and 6DHNR were used as substrates for renalase in the presence of AMP for NMN and ADP for NR. These experiments used double mixing stopped-flow spectrophotometry where renalase (HsRen, 10 µM and PpRen, 5 µM) was prepared anaerobically in 20 mM HEPES buffer, pH 7.5 and mixed with AMP or ADP and allowed to age for 100 ms before being mixed/reacted with 2- or 6DHNMN and 2- or 6DHNR respectively. Data were collected and analyzed as described above. Octyl-beta-glucoside (2 mM) was added to the enzyme solution for reactions containing 2- and 6DHNR.

Inhibition of human renalase by β-NAD(P), non-substrate analogs and fragments. The 50% inhibitory concentration (IC_{50}) of NAD fragments: ADP, ADP-ribose, AMP, nicotinamide, methyl nicotinamide, NR^+, NMN^+, 4DHNR, and 4DHNMN, were estimated by observing the renalase reductive half reaction

in the absence of dioxygen and in the presence of a 6DHNAD concentration that was equal to the measured dissociation constant for that substrate (173 μM)[35]. Renalase (~4-6 μM) in 2X PBS buffer containing 1 mM D-glucose was added to the main chamber of a tonometer and glucose oxidase (25 μL, 1 U/μL) was added to the side arm prior to assembly and was kept at 4 ^{o}C. The tonometer was assembled and made anaerobic by exchanging argon for dissolved oxygen using partial vacuum followed by equilibration with high purity argon gas (5 psi) that was passed through an Alltech oxygen-reactive cartridge and sparged through anaerobic water. This process was repeated for 45 cycles where after every 3 cycles the sample was agitated during the introduction of argon gas to enhance the exchange of dissolved gases. The glucose oxidase and D-glucose/renalase solutions were combined and the tonometer was mounted on a Hitech Scientific (now TgK) DX2 stopped-flow spectrophotometer that had been scrubbed of dioxygen for >12 hrs using an anaerobic solution of 50 mM D-glucose and 15 U/mL glucose oxidase in 20 mM HEPES buffer, pH 7.0. Concentrated 6DHNAD was aliquoted to yield 173 μM after the second mixing step (four-fold dilution) and stored at -80 ^{o}C to prevent decomposition. Each aliquot was thawed and diluted to 3 mL in water containing 1 mM D-glucose. The solution containing 6DHNAD was transferred to a glass syringe and made anaerobic by sparging with high purity argon gas for 4 minutes. Glucose oxidase (10 μL, 1 U/μL) was added to the syringe immediately prior to capture and mounting onto the stopped-flow spectrophotometer. Potential inhibitory ligands were prepared in 2X PBS with 1 mM D-glucose, transferred into a glass syringe and made anaerobic as described above for 6DHNAD. The renalase solution was mixed first with the NAD analog (or fragment) solution and allowed to age for 100 ms before being mixed with the substrate (6DHNAD) solution. Reduction of the renalase flavin cofactor was observed at 458 nm. The data were fit to a single exponential decay according to equation 8.1 using Kinetic Studio software (TgK Ltd). The dependence of the observed rate constant on the concentration of the analog was fit to

Equation 8.3 to determine the IC_{50} value for each. In this equation k_{max} is the rate constant for reduction in the absence of inhibitory ligand and k_{min} is the observed rate constant with saturating inhibitory ligand (this value was manually set to zero for cases in which the inhibitory ligand had a solubility limit lower than the concentration required to saturate the enzyme).

Equation 8.3 $$v = k_{min} + \frac{k_{max} - k_{min}}{(1 + (\frac{[6DHNAD]}{K_i})}$$

Crystallization, structure determination, and model refinement of the PpRen•β-NADPH complex. Crystallization conditions for PpRen were those identified initially by the North East Structural Genomics Consortium that yielded the unliganded enzyme structure, PDB ID 3KKJ: 2 M sodium formate, 100 mM sodium acetate pH 4.6 at 20 °C. Diffraction-quality crystals were obtained by the hanging drop vapor diffusion method. The droplet was formed from 1 µL of the well solution and 1 µL of PpRen (104 µM). Crystals grew within 1-2 days to dimensions of ~200 µm x 50 µm x 10 µm. Individual crystals were lifted from the drops using nylon cryo-loops, and soaked for 1-3 minutes in 2.5 M sodium formate, 125 mM sodium acetate pH 4.7 with 10% glycerol and 40 mM β-NADPH. The loop-mounted, cryo-solution and crystal were cooled to form a glass by immersion in liquid nitrogen. X-ray diffraction data to 2.1 Å for the PpRen•β-NADPH complex were collected at beamline 21-ID-F of the Life Science Collaborative Access Team (LS-CAT) at the Advanced Photon Source (APS) at a wavelength of 0.97872 Å at 100 K. The crystal was rotated through 190°, with an oscillation angle of 0.4°. The exposure time per frame was 0.75 s with 0% attenuation. The crystal to detector distance was 220.2 mm. Data were indexed and scaled with HKL2000 [187] in space group $P2_1$ with unit cell dimensions a=63.4 Å, b=71.0 Å, c=74.8 Å, and β=107.8 °.

The structure of PpRen•β-NADPH was determined by molecular replacement in PHASER[188] with a search model derived from chain A of the *P. phaseolicola* renalase•β-NADH structure (PDB ID 4ZCC)[38] with all non-protein atoms removed and all B-factors set to 20.0 $Å^2$. After iterative cycles of manual model building in COOT[189] and maximum likelihood based refinement using the PHENIX package (phenix.refine)[190], ordered solvent molecules were added automatically in phenix.refine and culled manually in COOT. After adding solvent atoms, the FAD cofactor and β-NADPH were added to the model. During the last rounds of refinement, hydrogen atoms were added to the model using phenix.reduce[191] to improve the stereochemistry of the model. Positions of H atoms were refined using the riding model with a global B-factor. Regions of each model to be used in translation-libration-screw (TLS) refinement were identified using phenix.find_tls_groups and the TLS parameters were refined in phenix.refine. Once the refinement converged, the model was validated using the tools implemented in COOT and PHENIX[192],[193]. Side chains with poor or missing electron density were modeled in favored rotameric conformations. The B-factors were allowed to refine without additional restraints, and the occupancies were held to 1.0. Data collection and model refinement statistics are listed in Table 8.1.

Table 8.1: Structural Statistics for the MDH•6DHNAD, LDH•6DHNAD and PpRen•NADPH complexes

	MDH with 6DHNAD	LDH with 6DHNAD	PpRen with NADPH
Data collection[a]			
Beamline	9-2 (Stanford)	9-2 (Stanford)	21-ID-F (APS)
Wavelength (Å)	0.9795	0.9795	0.9787
Space group	$P2_12_12_1$	$P2_1$	$P2_1$
Cell dimensions; *a, b,*	77.5, 83.8, 89.3, 90	63.6, 126.1, 84.2, 99.9	63.4, 71.0, 74.8, 107.8
Resolution range (Å)[b]	39.40 - 1.75 (1.78 -	39.41 - 1.86 (1.89 -	46.02 – 2.09 (2.16 –
R_{merge}[c]	0.075 (0.548)	0.066 (0.574)	0.071 (0.357)
Total observations	286641 (14580)	373153 (16868)	119090 (10,650)
Total unique	58987 (3036)	108172 (5057)	37,538 (3,197)
Mean ((I) / σ(I))	14.3 (2.6)	11.8 (2.0)	11.2 (2.6)
Completeness (%)	99.2 (94.0)	98.7 (93.2)	98.0 (96.0)
Redundancy	4.9 (4.8)	3.4 (3.3)	3.2 (2.9)
Wilson B-factor (Å^2)	14.41	19.98	24.99
Refinement			
Resolution (Å)	38.76 - 1.75 (1.81 -	39.41 - 1.86 (1.93 -	46.02 – 2.09 (2.16 –
R_{cryst}[d]	0.1545 (0.1915)	0.1698 (0.2762)	0.157 (0.196)
R_{free}	0.1809 (0.2173)	0.2104 (0.3050)	0.203 (0.287)
Total unique	58918 (5659)	107967 (10506)	37198 (3037)
No. of non-H atoms			
Protein	4381	10053	4958
Ligand	88	245	172
Water	473	506	198
rms deviation bonds	0.010	0.012	0.012
rms deviation angles	1.103	1.17	1.46
Overall mean B-	17.34	26.32	35.39
Ramachandran plot			
Favored region	99.0	97.4	98.0
Allowed region	1.0	2.6	2.0
Outlier region	0.0	0.0	0.0

[a]data indexed and scaled with XDS

[b]values in paretheses are for the highest resolution shell

[c]$R_{merge} = \Sigma_h|I_h - \langle I\rangle|/\Sigma_h I_h$, where I_h is the intensity of reflection h, and $\langle I\rangle$ is the mean intensity of all symmetry-related reflections

[d]$R_{cryst} = \Sigma||F_o| - |F_c||/\Sigma|F_o|$, F_o and F_c are observed and calculated structure factor amplitudes. Five percent of the reflections were reserved for the calculation of R_{free}.

[d]Calculated with Molprobity

Structure determination, and model refinement of the MDH•6DHNAD and LDH•6DHNAD complexes. *E. coli* malate dehydrogenase (MDH) was prepared as previously described[35]. MDH crystal growth was carried out by the hanging drop method at 18 °C. Drops containing 1.5 µl of purified MDH protein at 80 µM containing 0.4 mM 6DHNAD were mixed with equal volumes of a reservoir solution

containing 0.1 M MES, pH 6.5, 21% PEG 8,000. Large crystals (400 x 200 x 50 µm) formed in 1-2 weeks[200]. For data collection, crystals were retreived with a nylon cryo-loop and washed with 0.1 M MES, pH 6.5, 21% PEG 8,000, 0.5 mg/ml MDH supplemented with 20% (v/v) glycerol as a cryoprotectant. The cryo-solution and crystal were cooled to form a glass by immersion in liquid nitrogen.

L-lactate dehydrogenase (LDH) from rabbit muscle was purchased from Sigma-Aldrich as an ammonium sulfate suspension. The suspension was diluted five-fold with 50 mM HEPES, pH 7.5, 50 mM NaCl, 1 mM DTT, desalted using a PD-10 column (GE Healthcare) into the same buffer, and concentrated to 410 µM. LDH crystal growth was carried out by the hanging drop method at 18 ^{o}C. A volume of 1.5 µL of LDH protein containing 1.2 mM 6DHNAD was mixed with an equal volume of a reservoir solution containing 0.1 M Tris buffer, pH 7.5, 0.1 M sodium acetate, 15% PEG 8,000. Large crystals (400 x 300 x 100 µm) formed in 3-4 days. For data collection, crystals were soaked with 0.3 µL of 9.3 mM 6DHNAD for 40 minutes and washed with 0.1 M Tris buffer, pH 7.5, 0.05 M sodium acetate, 14% PEG 8,000 supplemented with 25% (v/v) PEG 400 as a cryoprotectant and flash cooled in liquid nitrogen. Data collection and model refinement statistics are listed in Table 8.1.

All MDH and LDH diffraction data were collected at the Stanford Synchrotron Radiation Laboratory (SSRL; Stanford, CA), beamline 9-2. MDH•6DHNAD diffraction data were collected (0.2° oscillation images for a total of 131°) at a wavelength of 0.9795 Å at 100 K. The exposure time per frame was 2.83 s with 0 % attenuation and a crystal to detector distance of 280.2 mm. The data were indexed and scaled with XDS to 1.75 Å. The crystals were assigned to the space group $P2_12_12_1$ with unit cell dimensions a = 77.5 Å, b = 83.8 Å, c = 89.3 Å. Molecular replacement calculations for MDH were performed using PHASER in the PHENIX program suite[201, 202], using molecule A of 3HHP[203] as the search model with waters removed, yielding a clear solution with a log-likelihood gain of 9,078

and a TFZ score of 89.0. Model building and refinement were performed in iterative cycles using COOT[204] and phenix.refine. The MDH structure model includes residues 1-78, 90-311 in molecule A and 1-79, 90-311 in molecule B of 312 total residues. The model includes two 6DHNAD molecules, one in each NADH binding site, and 473 water molecules.

LDH•6DHNAD diffraction data (0.2° oscillation images for a total of 180°) were collected with a wavelength of 0.9795 Å at 100 K. The exposure time per frame was 0.860 s with 0% attenuation and a crystal to detector distance of 285.3 mm. The data were indexed and scaled with XDS to 1.86 Å. The crystals were assigned to the space group $P2_1$ with unit cell dimensions a = 63.6 Å, b = 126.1 Å, c = 84.2 Å, and β = 99.9°. Data collection and model refinement statistics are listed in Table 8.1. Molecular replacement calculations for LDH were performed using PHASER in the PHENIX program suite, using molecule A from 4I9H[205] as the search model with ligand and waters removed yielding a clear solution with a log-likelihood gain of 15,192 with a TFZ score of 86.9. Model building and refinement were performed using COOT and phenix.refine. The LDH structure model includes residues 1-13, 17-331 in molecule A; 2-98, 109-331 in molecule B; 2-13, 17-329 in molecule C; and 1-329 in molecule D of 331 total residues. The model also includes 4 6DHNAD molecules, one in each β-NADH-binding site. The 6DHNAD in molecule D was best modeled with two orientations of the adenine ring. There are 506 water molecules and 5 sulfates modelled. The sulfate ions were derived from the ammonium sulfate suspension in which the protein was purchased.

Structural analysis. Protein structure figures were generated using PyMOL [206]. The atomic coordinates and structure factors have been deposited in the Protein Data Bank (Research Collaboratory for Structural Bioinformatics, Rutgers University, New Brunswick, NJ) as entries 5KKA for

the MDH•6DHNAD structure, 5KKC for the MDH•6DHNAD structure and 5KRQ for the PpRen•β-NADPH structure.

Single crystal spectrophotometry. In order to verify that the MDH•6DHNAD and LDH•6DHNAD structures contained 6DHNAD and not a decomposition product of this relatively unstable molecule, absorption spectra where recorded from the same crystals of these complexes that were used for structural elucidation. Absorbance spectra (220-500 nm) were recorded on SSRL beamline 9-2 by measuring counts for dark (D) and reference (R) scans adjacent to the crystal and then focusing the beam on the crystal or sample (S) to measure transmittance. Absorption spectra were then obtained according to equation 8.4.

Equation 8.4 $$A = log_{10}[(R - D)/(S - D)]$$

A five-axis pico-motor stage was used to align the microspec objective lenses with each other and three larger stages were used to align the pair of objectives to the sample position. An approximately 50 µm diameter circular beam was used. The system used a Hamamatsu light source with both deuterium and halogen lamps, UV solarization-resistant optical fibers, reflective Newport Schwardchild objectives, and an Ocean Optics QE65000 Spectrum Analyzer.

Results

HPLC substrate analysis of 2-, 4- and 6DHNMN and 2-, 4- and 6DHNR. All three reduced isomers of NR and NMN were reacted with renalase to determine which were substrates. Control reactions were run in the absence of enzyme to define initial reference concentrations and account for losses due to

decomposition. Analysis of the chromatographs obtained indicated that, much like the β-NAD(P)-derived substrates, only 2- and 6DHNR and 2- and 6DHNMN are consumed by renalase (Figure 8.2 A and C). The extinction coefficient spectrum for the dihydronicotinamide chromophore was determined for each reduced form using spectrophotometry in conjunction with a dioxygen electrode. This procedure yielded extinction coefficients of ε_{338nm} = 7100 ± 300 M^{-1} cm^{-1} for 4DHNMN, ε_{338nm} = 7300 ± 200 $M^{-1}cm^{-1}$ for 6DHNMN, ε_{391nm} = 7000 ± 100 $M^{-1}cm^{-1}$ for 2DHNMN, ε_{340nm} = 7200 ± 100 $M^{-1}cm^{-1}$ for 4DHNR, ε_{345nm} = 10400 ± 600 $M^{-1}cm^{-1}$ for 6DHNR and ε_{389nm} = 8700 ± 500 $M^{-1}cm^{-1}$ for 2DHNR (Figure 8.2 B and D).

Reductive half-reactions and the effect of complimentary ligands with 2- and 6DHNR and 2- and 6DHNMN. We have previously reported that 2- and 6DHNAD(P) molecules are substrates for renalase. Here we report data for reductive half reactions of renalase from both *H. sapiens* and *P. phaseolicola* with 2- and 6DHNR and 2- and 6DHNMN as substrates (Figure 8.2) with and without the complimentary co-ligand of each: ADP or AMP, respectively (Figure 8.3). Similar to the β-NAD- and β-NADP-derived substrates, the 6DH isomers of NR and NMN proved sufficiently stable to be purified, desalted and stored as described above and the 2DH isomers were considerably less stable, dictating that they be used immediately after elution from preparative HPLC. As such the concentration of the 2DH substrates was limited by the ability of the semi preparative C18 column to resolve the 2DH isomer from other species present (~100 μM for 2DHNR and 2DHNMN). Observation of the reduction of the flavin cofactor (458 nm for HsRen and 450 nm for PpRen) by 2- and 6DHNR and 2 and 6NMN in the presence or absence of the respective compliment ligand (ADP for nicotinamide riboside species or AMP for nicotinamide mononucleotide) was carried out under anaerobic conditions at 25 ^{o}C. The complimentary ligand at high concentration (generally limited by solubility) was mixed with renalase

in the first mixing step and allowed to age for 100 ms. Reduction experiments used largely pseudo-first order concentration ranges: 6DHNR (57 to 949 µM), 6DHNMN (78 to 675 µM), 2DHNR (32 µM to 105 µM) and 2DHNMN (47 µM to 83 µM). These data were fit to a single exponential decay to obtain a measure of observed rate constant values (Equation 8.1).

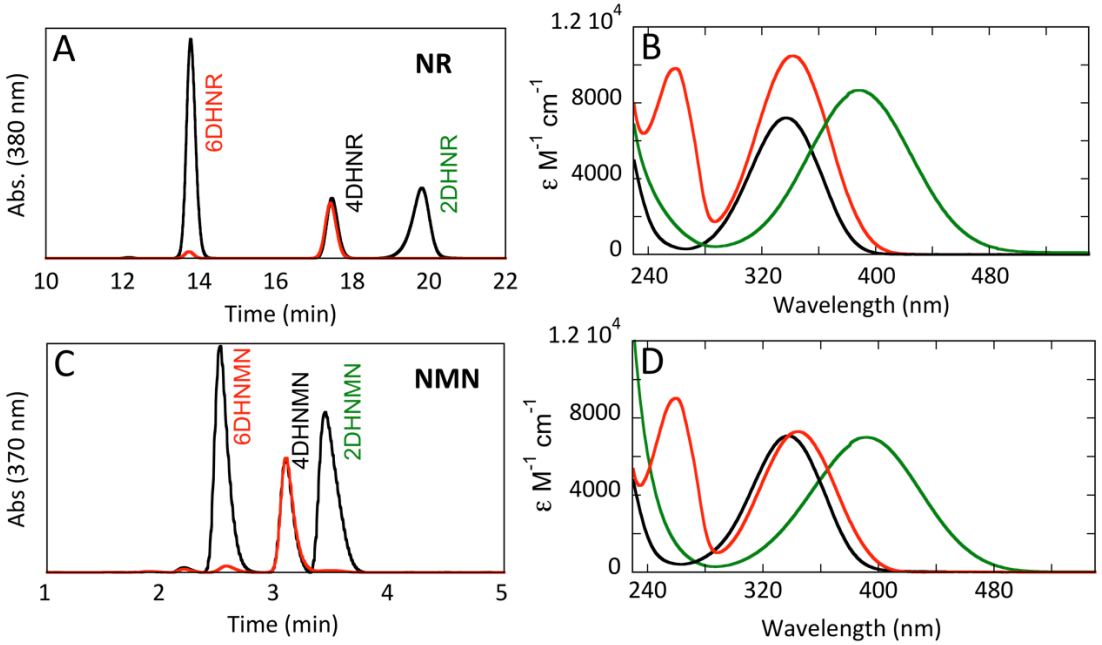

Figure 8.2. Oxidation of Dihydronicotinamide Nucleosides (NR) and Mononucleotide (NMN) Substrates by Renalase. NR^+ and NMN^+ were reduced by the addition of sodium borohydride forming three reduced isomers of each. These mixtures were then reacted with renalase (12.5 µM) for 10 minutes. A and C are HPLC chromatograms that showed the three species formed by reduction without (black trace) and with (red trace) the incubation with renalase. B and D are the extinction coefficient spectra for each of the reduced forms obtained, each corresponding to the chromatograms shown to the left.

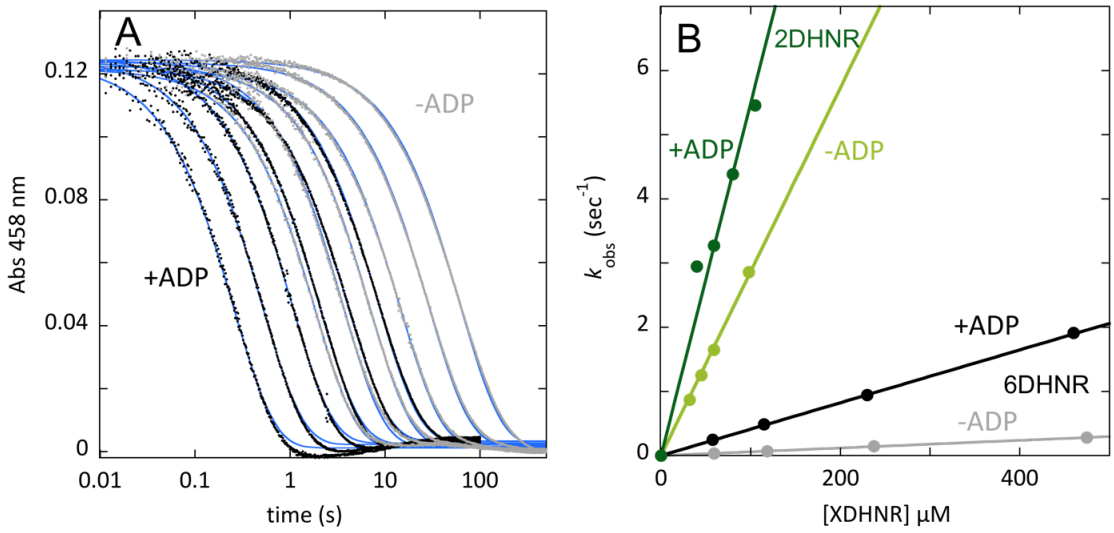

Substrate	Complimentary Ligand	k_{red}/K_d nM^{-1}/s^{-1} HsRen	Factor	k_{red}/K_d nM^{-1}/s^{-1} PpRen	Factor
6DHNMN	+AMP (1.12 mM)	30.0 ± 0.3		0.032 ± 0	
	-AMP	30 ± 1	1.0	0.063 ± 0.002	2.0
2DHNMN	AMP (1.12 mM)	160 ± 2		22 ± 1	
	-AMP	170 ± 4	1.1	26 ± 2	1.2
6DHNR	ADP (3.95 mM)	59 ± 0		0.039 ± 0.005	
	-ADP	4.1 ± 0	7.0	0.028 ± 0.004	0.7
2DHNR	ADP (4.83 mM)	29.0 ± 0.3		1.0 ± 0.1	
	-ADP	55 ± 3	1.9	0.55 ± 0.04	0.6

Figure 8.3. Reductive Half Reactions with 2- and 6Dihydro- NMN and NR with and without complementary ligands. **A.** Representative reduction traces for HsRen (10 µM) reacting with 6DHNR in the presence (black) and absence (grey) of 4 mM ADP. Data were fit to a single exponential according to equation 8.1. Lines of best fit over the data (blue). **B.** Secondary plot showing the effect of added ADP on the observed rate constant for reduction of HsRen by both 2- and 6DHNAD. Data were fit to equation 8.2 to determine values for K_{red}/K_d from the slope term.

Plotting k_{obs} data versus the concentration of substrate (2- and 6DHNR +/- ADP, 2- and 6DHNMN +/- AMP) gave a linear dependence for all data sets, where the slope is k_{red}/K_d. A linear dependence suggests that the reduction reaction is reliant on relatively weak binding interactions for these substrates, and the concentrations attained were insufficient to show curvature in the dependence plot that would be indicative of pre-equilibrium binding. For PpRen the addition of complementary or counterpart ligands (AMP for NMN, ADP for NR) had no significant effect. For

HsRen, addition of ADP (4-5 mM) in together with 6DHNR resulted in a 7-fold increase in k_{red}/K_d (Figure 8.3), but the equivalent analysis for 2- and 6DHNMN with HsRen with the AMP counterpart ligand showed no measurable difference for k_{red}/K_d. These data suggest that the β−phosphate of bound ADP induces a conformation change that aids in hydride transfer from 6DHNMN to the Flavin. More generally, however, the data show that untethered occupancy of the distal portions of the dinucleotide binding site do not dramatically enhance the rate of hydride transfer. For all substrates, maximal rates for hydride transfer are observed with intact dinucleotides.

Inhibition of renalase by β-NAD(P) analogs. Dissociation constants for non-substrate fragments and isomers were measured by determination of the 50% suppression (IC_{50}) of the observed rate constant for reduction in the presence of a substrate (6DHNAD) concentration equal to the K_d for that substrate (a concentration that was also pseudo-first order with respect to the enzyme concentration). For those molecules that were inhibitory, IC_{50} values were calculated by fitting a plot of k_{obs} for reduction versus the concentration of the substrate fragments, AMP, ADP, ADP-ribose, nicotinamide, methyl nicotinamide, NR or NMN to equation 8.3 (Figure 8.4). This analysis was hampered to some extent by apparent IC_{50} values greater than or similar to the solubility limit for these molecules. However, the data show that it is generally the case that the phospho-group proximal to the nicotinamide has a greater contribution to ligand binding than does the distal. With the exception of 4DHNR, molecules that did not contain this proximal phospho group, such as AMP, nicotinamide and methyl nicotinamide, did not show measureable inhibition of 6DHNAD oxidation. However, derivatives that did contain the proximal phosphate, ADP, ADP-ribose and 4DHNMN, displayed observable inhibition yielding estimated K_d values of 15, 12.4 and 1 mM, respectively. Titration of oxidized forms of NR and NMN did not yield any substrate inhibition even though the 4-dihydro form of both molecules was

observed to be inhibitory. Moreover, the products (β-NAD^+ and β-$NADP^+$) have been shown to bind with low millimolar binding constants. This likely reflects competing cumulative interactions at the active site and along the ligand binding cleft. The positive charge of the oxidized nicotinamide is likely repelled from the active site by the local positive electrostatic environment adjacent to the nicotinamide binding site resulting from conserved histidine and arginines (Figure 8.1), and we have proposed in prior work that this potential aids product dissociation[38]. Truncated and reduced non-substrate isomers (4DHNR, 4DHNMN) avoid this repulsive influence but cannot form other interactions with the AMP/ADP moiety that would aid binding. We therefore conclude that, in the oxidized state (NR^+ and NMN^+), the active site charge-repulsion is dominant over other binding interactions.

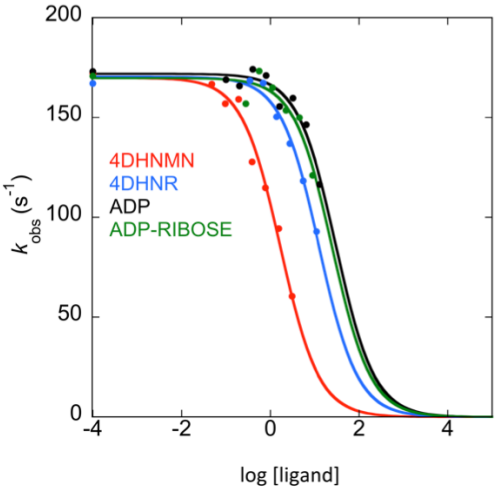

Ligand	K_d (mM)
ADP	15.0±0.6 [a]
ADP-ribose	12.4±0.5 [a]
NAD^+	2.8±0.3
4DHNR	6.1±0.5 [a]
4DHNMN	1.0±0.5 [a]
4DHNADP (NADPH)	1.5±0.4 [b]
4DHNAD (NADH)	0.6±0.1 [b]
6DHNAD	0.17±0.01 [b]
2DHNAD	0.17±0.01 [b]

a- Values estimated from suppression of the reduction rate constant obtained in the presence of 6DHNAD at a concentration equivalent to the K_d for that substrate (170 µM).

b- Values reproduced for reference from Beaupre et al., 2015[35].

Figure 8.4. Estimates of Binding constants for substrate fragments and substrate analogs with HsRen. The plot shows the partial IC_{50} curves used to estimate the binding constants of non-substrate ligands that exhibited inhibition. The fit of the curve to equation 8.3 gave IC_{50} values that by the methods used is twice the K_d (or K_i) for the inhibitory ligand [171]. No evidence of inhibition of the reductive half reaction was observed for AMP (7.6 mM), nicotinamide (68 mM), N-methyl-nicotinamide (7.8 mM), NR^+ (7.3) mM), NMN^+(2.6 mM) with values in parentheses indicating maximal concentration tested for evidence of inhibition.

The PpRen•NADPH complex. Our prior investigation of renalase from *P. phaseolicola* indicated that this form of renalase exhibited a pronounced substrate preference profile. The bacterial enzyme reacted with 2DH-substrates 160 to 350-fold more rapidly than 6DH-substrates. This bias seemed to be accounted for by a hydrogen bond from the nicotinamide amide to threonine 185 that stabilized a substrate binding pose in which the 2-dihydro hydride was proximal (3.6 Å) and the nicotinamide ring parallel to the flavin N-5 (Figure 8.1)[38]. As mentioned above, this form of renalase also bound β-NAD-derived substrates (6DH and 2DH) and non-substrates (4DH) 15 to 50-fold more tightly than those derived from β-NADP, indicating that the added 2'-phosphoryl group impedes binding by 6-10 kJ/mole. Such a substrate binding preference would be expected if the function of renalase is to

ameliorate the inhibitory threat to primary metabolism where β-NAD is the predominant nicotinamide dinucleotide co-substrate. The structural basis for this substrate preference is described here with the structure of the PpRen•β-NADPH complex, which was solved to 2.1 Å-resolution (Figure 8.5). This structure is very similar to the PpRen•β-NADH structure (4ZCC) we previously published, however, the nicotinamide nucleoside moiety is disordered and not visible in the electron density maps. The most striking aspect of this structure is that the NADPH 2'-phosphoryl group does not appear to interact favorably or unfavorably, with regard to binding, with any residue from the protein. While it is near the terminal amide of glutamine 206 (3.4 Å), the β-carbon of phenylalanine 204 (3.9 Å) and aspartate 211(~6.0 Å), none of these residues are oriented to form energetically significant binding interactions. It therefore seems likely that for the bacterial enzyme β-NADP-derived ligands are to a greater extent partitioned into the aqueous medium than those derived from β-NAD and that this is the basis for the NAD vs NADP ligand selectivity.

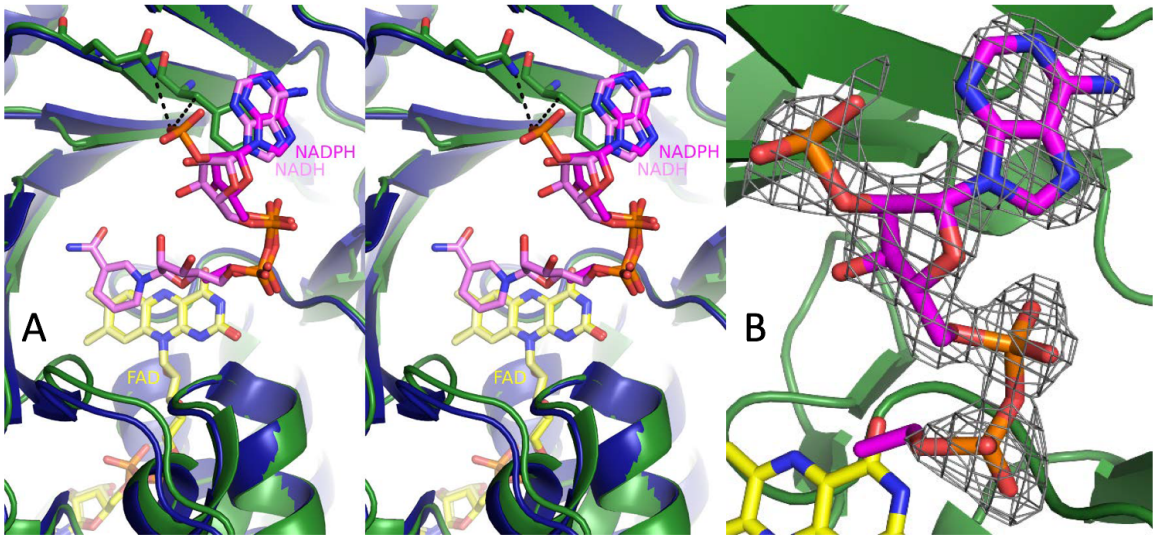

Figure 8.5. β-NADH vs β-NADPH Binding to PpRen. **A.** Stereo view of the β-NADH-renalase (PDB: 4ZCC, blue cartoon) overlaid on the NADPH-renalase (structure determined here, green cartoon). FAD is colored with carbon atoms yellow for both molecules. The β-NADH is shown with pink carbon atoms and the NADPH is magenta. The two most proximal residues are shown with carbon atoms green. The phe204 ring stacks with the adenine ring of β-NAD(P)H. The β-carbon of phe204 is 3.9 Å from one oxygen of the 2-phosphoryl group. The amide-nitrogen of gln206 is 3.4 Å from the same oxygen; however, the density is poor for this sidechain. Note that the FAD is buried, and that the β-NAD(P)H is bound to a cleft on the exterior of the protein. B. A simulated annealing omit map contoured at 3σ surrounds the β-NADPH (omitted in calculation) shows that the nicotinamide and nicotinamide-ribose of NADPH are not resolved in the map.

The MDH•6DHNAD and LDH•6DHNAD complexes. The final composite omit maps for the MDH•6DHNAD or LDH•6DHNAD structures showed that two 6DHNAD inhibitor complex structures were obtained. The MDH•6DHNAD structure was refined to 1.75 Å-resolution and the LDH•6DHNAD structure was refined to 1.86 Å-resolution (Figure 8.6). These structures indicate, as might be predicted, that 6DHNAD occupies the NAD(H)-binding site of both enzymes and does not appear to promote the binding of the respective co-substrate. As a consequence of the high affinity of 6DHNAD for MDH and LDH, these structures serve as two examples of the inhibitory threat posed by non-specific reduction of NAD^+ molecules.

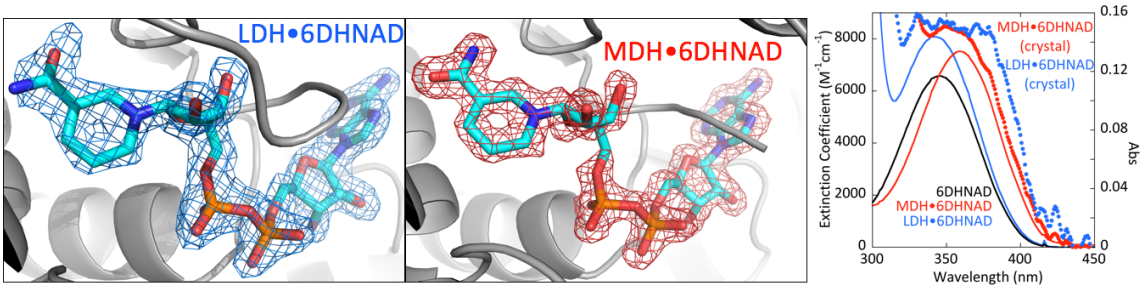

Figure 8.6. 6DHNAD inhibitory complex structures with MDH and LDH with 6DHNAD bound. Structural figures show that simulated annealing omit maps contoured at 3σ surround the 6DHNAD. **C. Absorption** Spectra recorded in solution (solid lines) and from the crystals used to solve the structures shown at left (dotted lines). These spectra show the presence of the 6DHNAD dihydronicotinamide chromophore in the crystals used to solve the structures.

There are four structures of MDH available on the PDB database; MDH•NAD^+ (1IB6), MDH•NAD^+•pyruvate (1IE3), MDH•NAD^+•citrate (1EMD), and a high resolution structure of the unliganded enzyme (3HHP)[200, 207, 208]. The binding of the 6DHNAD to MDH is positionally identical to the other published MDH•NAD structures with the exception of MDH•NAD^+•citrate (1EMD) where the nicotinamide ring is pivoted to accommodate the citrate. While the omit map suggests a small pucker of the nicotinamide ring at position 6, cyclohexadiene or piperidine-diene rings do not normally have appreciable out of plane distortions. The overall structure of the MDH molecules from all of the structures (those published and those presented here) are very similar, with the only difference being in the loop (residues 81 – 90) that closes over the active site when citrate (or sulfate) is present (1EMD, 1IB6). This loop is open in the MDH•6DHNAD structure presented here (5KKA), in the prior unliganded structure (3HHP), and in the structure with pyruvate (1IE3). This loop is disordered in several of the MDH molecules in the asymmetric units of these structures, whether there is substrate bound or not.

There are also several structures of LDH in the PDB. There is a prior structure of the rabbit muscle LDH•NAD•oxamate ternary complex (3H3F) and 4 other structures with a variety of inhibitors

bound[209]. There is also a structure of the human muscle LDH•NAD•oxalate complex (4OKN)[210]. The structure of rabbit muscle LDH•6DHNAD presented here aligns well with both the rabbit and human structures and the NAD aligns well in all of the structures. The 6DHNAD in the LDH structure presented here (5KKC) also appears to have a small pucker in the nicotinamide ring. Similar to the MDH structures, there is a loop that closes over the active site (residues 97-107) that is disordered in all of the molecules of our structure's asymmetric unit, but is seen in the open and closed positions in the other two structures, irrespective of whether there is a substrate analog or inhibitor bound.

6DHNAD Crystal Occupancy from Single Crystal Spectrophotometry. 6DHNAD is a relatively unstable molecule that degrades with a half-life of around 24 hours under the conditions used for crystallization (data not shown). For both the MDH•6DHNAD and LDH•6DHNAD structures, the crystals were formed by co-crystallization with the inhibitory ligand. LDH was exposed to the ligand again prior to mounting in the loop during cryo-protection. To verify occupancy of 6DHNAD in both the MDH and LDH structures, single crystal spectrophotometry was performed on both complexes (Figure 8.6). For both MDH and LDH, the the extinction coefficient of the 6DHNAD nicotinamide increases when bound. For the MDH•6DHNAD complex the 6DHNAD λmax shifts from 345 nm to ~360 nm, while for the LDH•6DHNAD complex the 6DHNAD dihydronicotinamide λmax wavelength is largely unaltered when bound to the enzyme. For the MDH•6DHNAD complex the extinction coefficient of the dihydronicotinamide absorption transition increases by a factor of 1.14, while for the LDH•6DHNAD complex it increases by a factor of 1.23. Both crystals exhibited far UV absorption features indicative of a bound dihydronicotinamide establishing that 6DHNAD occupies the active site of the crystals used to solve the MDH and LDH structures presented.

Discussion

The data presented here and in prior work are consistent with an intracellular housekeeping function for renalase. Non-specific reduction of N-substituted nicotinamides (chiefly $NAD(P)^+$) yields three forms of the dihydronicotinamide base. We have shown that two such isomers derived from reduction of NAD^+ are inhibitors of enzymes that require NADH molecules as substrates. Renalase serves to oxidize these inhibitory isomers and recycle them by forming $NAD(P)^+$ (Scheme 8.1). Prior work has shown that renalases isolated from different kingdoms have the same activity but unique structural features and substrate specificity profiles [38, 77]. In this study we present data that accounts for some aspects of the specificity profile of human and bacterial renalase, explore binding to the active site using analog and truncated substrate and non-substrate molecules, and also offer structures of one inhibitory NADH isomer (6DHNAD) bound to two primary metabolism dehydrogenases.

To date, only Human (HsRen) and *Pseudomonas* (PpRen) forms of renalase have been identified. The structures of these enzymes indicate that the portion of the active site of renalase that interacts with the FAD isoalloxazine and substrate/product nicotinamide has few conserved residues. For both forms of the enzyme, the remainder of the active site is an extended cleft on the surface of the protein. Ligand-bound structures of PpRen indicate that this cleft accommodates the remainder of the substrate and forms apparent hydrogen bonds and charge pairing interactions with the phospho groups and the adenine base; moieties that are common to all mono- and dinucleotide substrates and/or cofactors (Figure 8.1). Renalase functions in an intracellular environment in which potentially competing inhibitory ligands predominate (AMP, ADP, ATP, NADH, NADPH, 4DHNR & 4DHNMN) relative to the concentration of available substrates (6DHNAD, 2DHNAD, 6DHNAP, 2DHNADP, 6DHNR, 2DHNR, 6DHNMN and 2DHNMN), that are assumed to be maintained at low concentration by the

irreversible oxidase activity of renalase. Our data indicate that non-substrate ligands tend to either bind weakly (or possibly do not bind) to renalase (Figure 8.4). Nicotinamide ribosides and nucleotides are predominantly found in four forms in the cell: NAD, NADP, NR and NMN. We have shown that the 2- and 6-dihydronicotinamides of each of these molecules are substrates for renalase [35] (Figure 8.2) and that renalase has the capacity to kinetically select against oxidizing 4-dihydronicotinamide substrates by positioning the nicotinamide such that the FAD N5, the presumed site for hydride transfer [79], is distant from the 4-position of the nicotinamide [38]. The NR and NMN substrates bind to renalase weakly (Figure 8.3), to the extent that no curvature was observed in the plot of the observed rate constant for reduction versus substrate concentration, suggesting quasi-collision based chemistry within the limited range of substrate concentration available to assess these dependencies (Figure 8.3). However, these molecules behave as substrates as they reduce the renalase cofactor approximately 5-orders of magnitude more rapidly than does β-NADH (4DHNAD). If the substrate forms of NR and NMN bound in the same conformation as that portion of β-NAD(P)(H) observed in the PpRen•β-NADH and PpRen•β-NAD^+ structures[38], NR could make only one hydrogen bond and NMN would form a maximum of two hydrogen bonds and two complementary charge-pair interactions accounting for the six-fold difference in the K_d for 4DHNMN compared to 4DHNR (Figure 8.1). One curiosity that was observed for HsRen is that the simultaneous addition of a high concentration of the complement co-ligand (ADP for NR) stimulated the rate of reduction by a factor of seven for 6DHNR. This emphasizes that the substrate-binding sites in HsRen and PpRen are fundamentally different and suggests that, for HsRen, catalysis can be enhanced by occupancy of the distant portions of the substrate binding cleft relative to the site of hydride transfer. Moreover, it suggests that for HsRen an intact pyrophosphate moiety increases the rate of reduction.

The structure of the PpRen•β-NADPH complex was solved to account for the unique specificity profile of the bacterial enzyme. PpRen exhibits a 6-10 kJ/mol preference to bind NAD-derived molecules compared to NADP-derived ligands [38]. The structure of the PpRen•β-NADPH complex indicates that the 2'-phospho-group of β-NADPH does not interact in a manner conducive to binding with any residue on the surface of the enzyme. As such, there is no partner residue to satisfy the negative charge of the phospho group, dictating that this charged moiety would retain its hydration shell when bound to PpRen. Such a binding pose would mean that β-NADPH would be fractionally more partitioned into bulk solvent when bound, undermining its capacity to remain associated. Comparing HsRen and PpRen, β-NAD and NADP-derived ligands bind with similar affinity to HsRen [35], whereas PpRen binds NAD-derived ligands with dissociation constants that indicate 13 to 50-fold higher affinity than for ligands derived from NADP [38]. This difference in dinucleotide specificity is potentially accounted for by the presence of an arginine (Arg222) in HsRen whose guanidino group is adjacent the position occupied by the 2'-phospho group (as observed in the PpRen•β-NADPH structure; Figure 8.1). In the equivalent position of the PpRen•β-NADPH structure is an aspartate residue (Asp211) whose carboxylate resides 6.0 Å from the β-NADPH 2'-phospho group.

In prior studies, we demonstrated that 2- and 6DHNAD molecules were competitively inhibitory to specific enzymes that have β-NADH as substrate [35]. The assumption was that the isomeric forms are sufficiently similar in shape and charge distribution to mimic β-NADH molecules. These isomers bound with K_i values in the sub-micromolar range with *E.coli* malate dehydrogenase exhibiting a K_i of 34 nM for 6DHNAD. Here we present the structures of *E.coli* malate dehydrogenase and rabbit muscle lactate dehydrogenase bound to 6DHNAD. Instability of the 2- and 6DHNAD molecules dictates that we verify that these molecules are present in the structures as solved. To do this we used the dihydro-nicotinamide chromophore to observe the absorption of the ligand by single

crystal spectrophotomtery (Figure 8.6). The spectra obtained indicate that both the MDH and LDH structures were solved with 6DHNAD bound (given that this was the only reduced form of NAD added). As may be readily predicted, 6DHNAD occupies the binding site for β-NADH/β-NAD^+ in these enzymes [208, 209], convincingly demonstrating two examples of the mode of competitive inhibition of primary metabolism enzymes by 6DHNAD and by extension 2DHNAD molecules.

Chapter IX
Comparative Metabolomics in the Search for Endogenous Oxidative Substrates of OYE

Matthew R. Hoag, Aishwarya Shevade, Sergei Kuchin, and Graham R. Moran

Abstract

"Old yellow enzyme" (OYE) was discovered in 1932 by Warburg and Christian and represents the first discovered flavoenzyme. It has been shown to oxidize NADPH and to deliver the hydride to a wide variety of synthetic small-molecule acceptors. Since its discovery it has been the subject of much study and speculation with regard to its cellular role; a number of papers have established a broad array of artificial hydride acceptors, most being α,β-unsaturated aldehydes and ketones, but an endogenous substrate for the oxidative half-reaction has remained elusive. It has been hypothesized that OYE serves to "detoxify" exogenous electrophilic toxins by reducing them, though this is a difficult premise to prove or disprove barring the identification of an endogenous substrate. We hypothesize that OYE might serve to replenish the pool of NAD+ available for glycolysis during periods of anaerobiosis by transferring the hydride from the reduced nicotinamide substrates to a variety of endogenous hydride acceptors; this would explain the marked promiscuity observed in the oxidative half-reactions of these enzymes. In this paper we investigate the reductive and oxidative half-reactions of OYE2 and OYE3, the two homologs of the enzyme that exist in *Saccharomyces cerevisiae*, with the goal of first measuring the specificities of the enzymes for nicotinamide dinucleotide substrates and for artificial hydride acceptors, and then to perform a metabolomics study using LCMS on extracts from double-knockout yeast cultures in order to identify endogenous substrates of the OYE oxidative half-reaction in yeast. While no such molecule was successfully identified, we report our methods and results in order to facilitate future study in this vein, and we also report new results from our biochemical characterization of these *cerevisiae* enzymes.

Introduction

In 1932, Warburg and Christian [211, 212] studied yeast extracts containing G6P, an enzyme now known to be glucose-6-phosphate dehydrogenase, and a "coferment" or small molecule now known as NADPH. They found that this mixture consumed a small and limited amount of oxygen; only upon addition of another yellow fraction of the extract, termed "gelbeferment", the respiratory cycle was complete and continuous consumption of oxygen was observed. This yellow fraction was subsequently dubbed "Old Yellow Enzyme" and represents the first discovered flavoenzyme. After denaturation it was shown to consist of a colorless apoprotein and a heat-stable yellow dye, later determined to be FMN.

Nine decades later and after considerable study, a cellular role for this enzyme remains elusive. A major confounding factor in the elucidation of a cellular role has proven to be the promiscuity of the enzyme with respect to its oxidative half-reaction; while it has been shown to be reduced by NADPH with high specificity, a wide variety of small synthetic molecules have been shown to accept a hydride from the reduced enzyme [213-217], with many such molecules also binding tightly to the enzyme. This has puzzled researchers, and because many α,β-unsaturated aldehydes and ketones have been found to be OYE hydride acceptors, one role frequently ascribed to the enzyme is that of detoxification of exogenous reactive electrophiles, a role analogous to that of p450 enzymes. Convincing evidence for or against such a role would be difficult to obtain, and it does seem dubious; the main reasons for its suggestion seem to be the promiscuity of the enzyme and that no endogenous molecules have so far been identified as hydride acceptors.

Many structures of OYE and its family members have been solved [218-224]. In general, OYE exists in the cytosol as a globular dimeric [218] or monomeric [222] enzyme (though higher oligomeric states have been observed in some family members [225] with a tightly but non-covalently bound FMN cofactor. The N5 of the flavin is positioned at the opening of a TIM barrel, which represents the overall fold of the enzyme, with the *si*-face of the cofactor exposed to solvent.

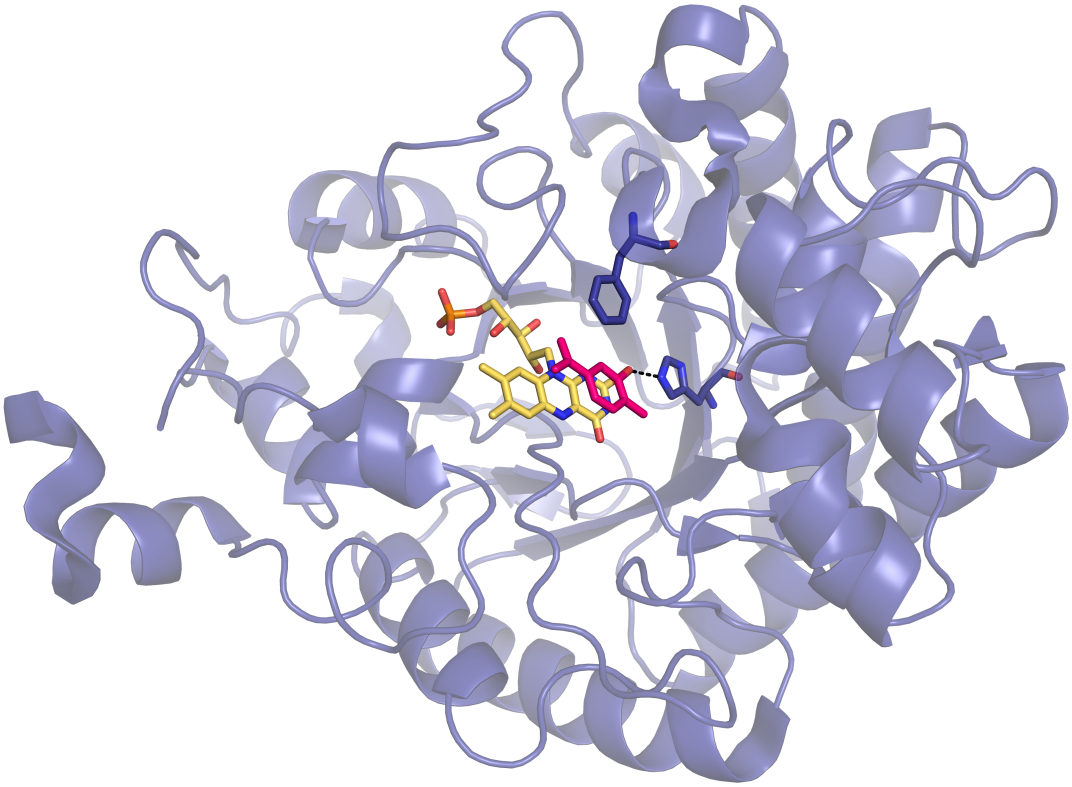

Figure 9.1. Overall fold of OYE1 and active site in complex with a ligand derived from R-carvone [224] (pdb accession code: 4gxm).

The mechanism of the enzyme proceeds similarly to that of other flavin-dependent dehydrogenases. As the reductive half-reaction of the mechanism, NADPH or NADH binds at the active site and the hydride is then transferred from NAD(P)H to the N5 position of the FMN cofactor, facilitated by quantum tunneling [226]. The first product NAD(P)+ is then released from the enzyme,

and the substrate for the oxidative half reaction then binds at the active site. In the case of α,β-unsaturated alkenes, the hydride is transferred from the N5 of the flavin to the β-carbon of the alkene substrate with the concerted transfer of a solvent-derived proton transferred to Cα, resulting in the reduction of the C=C bond [215]. The reduced substrate is finally released from the active site. Interestingly, molecular oxygen reacts slowly with the reduced flavin, so reoxidation of the enzyme in the cell by molecular oxygen is thought to be negligible.

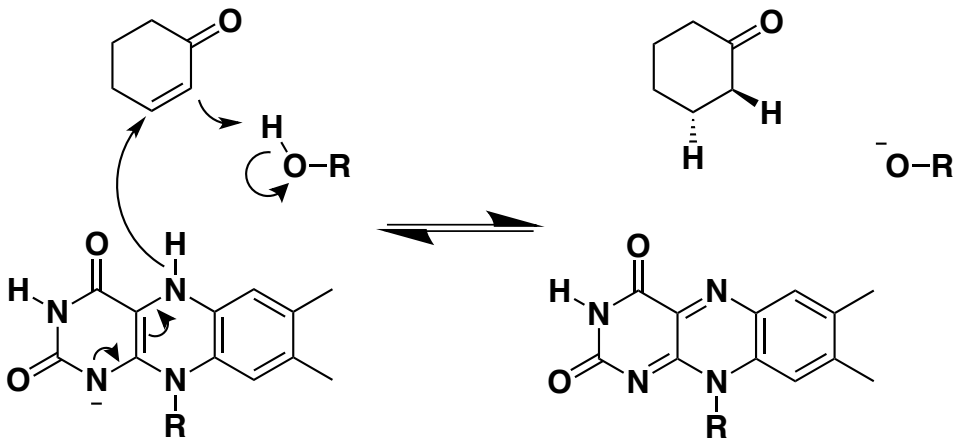

Figure 9.2. Proposed concerted mechanism for the reduction of activated alkenes by OYE.

We hypothesize that the cellular role of OYE enzymes is not to detoxify exogenous electrophiles but instead to replenish the pool of NAD(P)+ molecules available to glycolysis and the pentose phosphate pathway during periods of anaerobiosis. The enzyme would achieve this by accepting the hydride from NAD(P)H and transferring it to an endogenous acceptor, making more NAD(P)+ available for glycolysis and the pentose phosphate pathway thus promoting the survival of the organism during periods of low oxygen. The promiscuity of the enzyme would lend itself to the

transfer of the hydride to a wide variety of endogenous acceptor molecules. In this study, we hoped to identify one or more such endogenous hydride acceptors of the OYE reaction using an approach based in metabolomics and using comparative LCMS for analysis. Briefly, we went about this by culturing a mutant *Saccharomyces cerevisiae* strain with the genes for both OYE homologs (OYE2 and OYE3) deleted, producing small-molecule metabolite extracts of these cultures, reacting this extract with both *cerevisiae* enzymes, filtering the enzyme out of the mixture, and then comparing this sample with the unreacted extract using LCMS in order to identify MS peaks corresponding to metabolites that have been consumed or produced in the reaction. The resulting masses were then cross-referenced with online metabolome databases (YMDB and HMDB) in order to identify candidate molecules, these were then studied with the enzymes using transient-state kinetic methods. Intrinsic binding constants and oxidative rate constants were measured in order to verify whether the candidate molecules behave as substrates of the reaction.

Materials and Methods

Materials: β-NADH and β-NADPH were sourced from Amresco. Potassium phosphate (mono and dibasic), and glycerol were from Acros. Plasmids derived from pET-28a and containing the OYE gene (either OYE2 or OYE3, optimized for expression in *E. coli*) were ordered from Enzymax. Competent NEB5 and BL21 DE3 *Escherichia coli* cells were obtained from New England Biolabs. Talon© metal affinity resin was from Thermo-Fisher Scientific. Peptone, yeast extract, and sodium chloride for YEP broth were obtained from Fisher Scientific. Known OYE hydride acceptors cyclohexenone, 4-MeO-CNA, nitrocyclohexene, methylene blue, and 4-HO-3-MeO-CAN were sourced from Acros. Candidate

molecules maltol, p-coumarate, o-coumarate, uracil, and shikimate were obtained from Acros. Zymolyase was ordered from Zymo Research. Ammonium formate (LCMS grade) was obtained from Sigma Aldrich.

Protein Expression and Purification: The genes for ScOYE2 and ScOYE3 were optimized for expression in *E. coli* and pET-28a derived plasmids containing each gene were ordered from Enzymax. BL21(DE3) competent *E. coli* cells were transformed with each plasmid, and cells were plated on LB agar (50 mg/mL kanamycin). Cultures were incubated at 37 °C overnight, and individual colonies were selected for use in inoculating LB broth. Broth was incubated at 37 °C with shaking at 250 rpm until growth reached early log phase, about 3 hours. Cell stocks were produced by dividing into aliquots, adding glycerol to a final concentration of 20%, and storing at -80 °C.

For expression, cell stocks were thawed and 5 L LB broth (50 mg/mL kanamycin) was inoculated with 500 µL thawed cell stock. Cultures were incubated at 37 °C with shaking at 220 rpm, until mid-log phase (OD_{600} = 0.9). Cultures were then induced with 100 µM IPTG, and incubated for 3 hours at 37 °C with shaking at 220 rpm. Cells were then centrifuged at 3500 rpm and the supernatants decanted. Cell pellets were resuspended in 100 mL ice-cold HEPES (50 mM, ph 7.5) and lysed by sonication (output: 8, cycle: constant) using a Branson sonifier for 12 minutes. Sonicate was then centrifuged at 10,000 rpm for 45 minutes and the supernatant decanted and retained. The supernatant was loaded at 1 mL/min onto a BD Talon column pre-equilibrated with 50 mM HEPES, pH 7.5. A wash step of 200 mL at 1 mL/min was performed, the wash buffer consisting of 50 mM HEPES, 10 mM imidazole, pH 7.5. Finally, a gradient from 10 – 300 mM imidazole in 50 mM HEPES (pH 7.5) was run to elute the protein, collecting fractions of 6 mL. A single symmetric peak was observed on the protein chromatogram, indicative of highly purified protein (verified by gel electrophoresis).

Yellow fractions were pooled and enzyme concentration was measured spectrophotometrically based on the previously measured extinction coefficient of the flavin at 464 nm (11,300 $M^{-1}cm^{-1}$). Total yields were routinely ~60 mg (12 mg/L) enzyme for OYE2, and ~30 mg (6 mg/L) for OYE3 (Reducing the expression temperature of OYE3 to 22 °C over 30 hours slightly improved yield). Imidazole was removed by buffer 100,000-fold exchange into 20 mM HEPES, pH 7.5 by centrifugation at 10000 rpm at 4 °C using Amicon 10 KDa cutoff spin-filters. Finally, enzyme was concentrated to ~500 µM using Amicon spin-filters and divided into aliquots for storage at -80 °C.

Reductive Half-Reactions of OYE2 & OYE3 with Nicotinamide Dinucleotides: Reductive half-reactions of OYE2 and OYE3 were studied by mixing enzyme with a range of concentrations of either NADH or NADPH on a Hi-Tech DX2 stopped-flow spectrophotometer. Enzyme (~15 µM) in 20 mM potassium phosphate, pH 7.5 was added to a tonometer and was made anaerobic by applying 45 alternating cycles of vacuum and argon using a Schlenk line, with gentle agitation every three cycles to promote exchange of gasses. 1 mM glucose was included in the body of the tonometer with enzyme, and once anaerobic 20 U of glucose oxidase was added from a sidearm to scrub the tonometer of oxygen. The tonometer was then mounted on the stopped-flow instrument that had been scrubbed of oxygen using 20 mM glucose and 15.5 U/mL glucose oxidase for at least 16 hours. Nicotinamide dinucleotide substrate samples were prepared in 20 mM potassium phosphate, 1 mM glucose, pH 7.5, placed in a gastight syringe and sparged with argon for at least 5 minutes. 7 U glucose oxidase was then added under argon through the Luer Lock tip to scrub the syringe of oxygen. The syringe was then mounted onto to the stopped-flow instrument and mixed with the enzyme, monitoring reduction of the FMN cofactor as a decrease in absorbance at 464 nm. NADPH concentrations mixed with OYE2 ranged from 1.25 – 160 µM, and NADH concentrations ranged from 0.64 – 215 µM. For OYE3 the NADPH

concentrations ranged from 0.3 – 5 μM, and 5 – 2700 μM for NADH. Kinetic traces were then fit globally using Kintek Explorer software to a model consisting of a reversible bimolecular substrate-binding step forming the E•S complex followed by an irreversible reduction step. Quality of the fits and constraints on each rate constant were evaluated using the FitSpace Explorer algorithm.

Oxidative Half-Reactions: Oxidative half-reactions were observed using a Hi-Tech DX2 stopped-flow spectrophotometer in double-mixing mode. Enzyme and substrate solutions were preapared as in the reductive half-reactions, taking care to exclude molecular oxygen. For the first mix, enzyme (~7 μM) was mixed with an equal concentration of NADPH to reduce the FMN cofactor. An age time of 300 s was then used to allow the reaction to complete, before the second mix of varying concentrations of the oxidizing agent; either a hydride acceptor or molecular oxygen. In the case of molecular oxygen, a Maxtec maxblend gas blender was used to mix oxygen with a varying proportion of nitrogen gas. Oxygen concentrations were quantified by sparging buffer in a Hansatech Clark-type oxygen electrode before sparging each substrate solution in a gastight syringe. Reoxidation of the OYE flavin cofactor was monitored as an increase in absorbance at 464 nm. Kinetic traces were then fit globally using Kintek Explorer software to a model consisting of a reversible bimolecular substrate-binding step forming the E•S complex followed by a reversible oxidation step and then by a reversible product release step.

Dissociation Constants for Hydride Acceptors to Oxidized OYE: Dissociation constants of various hydride acceptors and ligands to the oxidized enzymes were measured by titrating each ligand to the enzyme and monitoring spectrophotometric perturbations the oxidized OYE flavin spectrum in the range of 400 – 500 nm and charge-transfer bands (near 600 nm) when present. 20 μM enzyme was

used, and spectra were measured after each addition of ligand. Spectra were corrected for dilution, and the maximum change in absorbance was plotted against ligand concentration. This produced a hyperbola that was then fit to the quadratic form of the single-site binding equation (eq 9.1) to yield the dissociation constant, where [E] is enzyme concentration and [EL] is the concentration of the enzyme•ligand complex. Raw data were fit, using change in absorbance at a defined wavelength as a measure of [EL] and the maximum change in absorbance at that wavelength as [E].

$$[\mathrm{EL}] = \frac{([\mathrm{L}]+[\mathrm{E}]+\mathrm{K}_L)-\sqrt{([\mathrm{L}]+[\mathrm{E}]+\mathrm{K}_\mathrm{L})^2-4([\mathrm{L}]+[\mathrm{E}])}}{2} \qquad (9.1)$$

Single- and Double-Deletion Yeast Mutants: All strains were isogenic to W303 [227] and are listed in table 9.1. To construct the heterozygous *OYE2*/*oye2*Δ::*KanMX6* diploid strain AMS253, the wild-type diploid strain MMY25 was transformed with an *oye2*Δ::*KanMX6* knock-out cassette amplified by PCR as described previously [228] using primers AS58 and AS59; all primers used are listed in table 9.2. Haploid *oye2*Δ::*KanMX6* strain AMS264 (*MAT***a**) was recovered from AMS253 by tetrad analysis. The knock out genotypes were confirmed by PCR analysis of genomic DNA using primers AS54* and AS55* (not to be confused with AS54 and AS55). The *OYE3*/*oye3*Δ::*KanMX6* heterozygous diploid AMS255 was constructed similarly; the knock-out cassette was generated using primers AS60 and AS61. The confirmation primers used were AS56* and AS57* (not to be confused with AS56 and AS57). Haploid *oye3*Δ::*KanMX6* strain AMS272 (*MAT*α) was generated from AMS255 by tetrad analysis. Then haploid strains AMS264 (*MAT***a** *oye2*Δ *OYE3*) and AMS272 (*MAT*α *OYE2 oye3*Δ) were crossed under the microscope to produce a doubly heterozygous diploid strain AMS257. Haploid *oye2*Δ *oye3*Δ double mutant strain AMS287 (*MAT***a**) was generated by tetrad analysis of AMS257. The double mutant genotype of AMS287 was confirmed by PCR analysis of its genomic DNA using primers AS54*, AS55*,

AS56*, AS57*. General methods for yeast transformation and classical genetics were as described previously [229].

Table 9.1. *S. cerevisiae* strains

Strain	**Genotype**
W303-1A	*MAT***a** *ade2-1 can1–100 his3–11,15 leu2–3,112 trp1–1 ura3–1*
W303-1B	*MAT*α *ade2-1 can1–100 his3–11,15 leu2–3,112 trp1–1 ura3–1*
MMY25	Isogenic to diploid W303-1A x W303-1B
AMS253	MMY25 *OYE2*/*oye2*Δ::*KanMX6*
AMS255	MMY25 *OYE3*/*oye3*Δ::*KanMX6*
AMS264	*MAT***a** *ade2-1 can1–100 his3–11,15 leu2–3,112 trp1–1 ura3–1* *oye2*Δ::*KanMX6*
AMS272	*MAT*α *ade2-1 can1–100 his3–11,15 leu2–3,112 trp1–1 ura3–1* *oye3*Δ::*KanMX6* AMS264 x AMS272
AMS257	
AMS287	*MAT***a** *ade2-1 can1–100 his3–11,15 leu2–3,112 trp1–1 ura3–1* *oye2*Δ::*KanMX6 oye3*Δ::*KanMX6*

Table 9.2. Oligonucleotide primers

Primer	Sequence
AS54*	5'- CTT GAT GAG GTA GCA GAT TCC TGG -3'
AS55*	5'- TTA ATA TTC ATG ATG TAG AAT GAC CGA TTC C -3'
AS56*	5’- GCT CCT TAG TAA GCA GTT TGC GTT C -3'
AS57*	5'- GCG GTG GAT TTA CGT CAA TGG GC -3'
AS58	5'- CCT TAT GTT AAA CGG TCC AGA TAT AGA ATA AAT CAT CAT ATT AAG CCC TGT TTA GCT TGC CTC GTC CC -3'
AS59	5'- GAA AGC CCA GTT TAC TCC TTT CCA CAA AGA TAT AAA TCT GTT GCT GCC CAA GCA AGA ATT CGA GCT CGT TTA AAC -3'
AS60	5'- AAG TAC GTA CTT GAT ATA TAC AAC AAC TGT AGT TCA GTA TAG CGA AGT TCC TGT TTA GCT TGC CTC GTC CC -3'
AS61	5'- AAT ACA TAA CAT CAA TGT CTT TAT TCA TGA TTT CAG TTC TTG TTC CAA CCG AAT TCG AGC TCG TTT AAA C -3'

Small Molecule Metabolite Extracts: Cultures of a *Saccharomyces cerevisiae* mutant with genes for both OYE homologs deleted were prepared both aerobically and under anaerobiosis, and were then harvested to extract polar small-molecule metabolites. In the case of anaerobic cultures, cells were grown in 200 mL YEP medium in Erlenmeyer flasks sealed with rubber septa, and 10 alternating cycles of vacuum and argon were applied using a Schlenk line while swirling the flasks in order to remove oxygen from the headspace. Cultures were grown at 30 °C with shaking at 180 rpm, and were harvested once they reached and OD_{600} of 0.4. Small-molecule extracts were then prepared by

centrifuging cultures at 3000 × *g* for 7 minutes at 4 °C. The cell pellet was then decanted and washed with ice-cold 20 mM HEPES, pH 7.5. The resuspension was centrifuged again and the pellet were resuspended in 1 mL HEPES (2 mM, pH 7.5) (is this correct??). This was reacted with zymolyase (how much??) for 30 minutes to remove the cell wall while sonicating (cycle: 25%, output: 3, sonication time: 10 min) on ice, monitoring released protein by BCA assay to ensure complete lysis. The lysate was then centrifiuged at 10,000 rpm for 10 minutes at 4 °C and filtered using an Amicon 10 KDa MW-cutoff spin filter. Small molecule extracts were then stored at -80 °C for later use.

To produce OYE reacted metabolite extracts, small-molecule *cerevisiae* metabolite extracts were thawed on ice and pooled. The pooled extract was then spiked with 200 µM NADPH and divided into two equal volumes. OYE2 and OYE3 were added to a final concentration of 20 µM to one metabolite sample, and an equal volume of enzyme buffer (20 mM HEPES, pH 7.5) was added to the other for use as a control. Both samples were incubated for 30 minutes on ice to allow the enzyme to react, and then both were filtered using Amicon 10,000 Da MW-cutoff spin filters at 4 °C to remove enzyme from the reacted sample, divided into aliquots and stored at -80 °C.

LCMS: Enzyme-reacted and control samples were analyzed using a Shimadzu LCMS-IT-TOF. Samples were diluted 10-fold with LCMS grade water (Sigma-Aldrich), and 10 uL of each dilution was analyzed by LCMS over 110 minutes on an LCMS-IT-TOF (Shimadzu Scientific Instruments) with a Shim-pack XR-ODS column. The mobile phase consisted of aqueous 5 mM ammonium formate solution with a total flow rate of 0.8 mL/min. An ESI source was used, and acquisition was performed in scan mode from 200-8000 m/z for both positive- and negative ion modes. A 10 msec ion accumulation time was used, and event time was set to 100 msec. A gradient was run, holding mobile phase conditions at 0%

acetonitrile for 35 minutes after injection, a linear gradient from 0% to 40% acetonitrile (Sigma Aldrich) over 75 minutes, and finally holding at 40% acetonitrile for another 30 minutes.

Three runs each of the reacted sample and of the control were performed, and the data were analyzed using XCMS software. Settings used for feature detection were: 30 ppm, 10s minimum peak width, 250s maximum peak width, signal/noise threshold of 6, 0.05 mzdiff, integration method 1, 3 prefilter peaks, prefilter intensity of 100, 0 noise filter. Settings used for retention time correction were: peakgroups method, loess non-linear alignment, ignore sample class, bandwidth of 30, mzwidth of 0.25, gaussian fitting, span of 0.2. Alignment settings used were: bandwidth of 90s, minfrac of 0.25, mzwidth of 0.3. For statistical anysis, the following settings were used: Unpaired parametric t-test (Welch t-test), perform post-hoc analysis, 0.01 p-value threshold of highly significant features, 1.5-fold change threshold, 0.09 p-value threshold of significant features, normalization by loess regression.

Results

Specificities of the Reductive Half-Reaction for Nicotinamide Dinucleotides: The *Saccharomyces cerevisiae* genome contains two OYE homologs, OYE2 and OYE3, unlike that of *Saccharomyces pastorianus* which only has one (OYE1). While the pastorianus enzyme has been studied in detail and shown selectivity for NADPH over NADH, little work has been done on the *cerevisiae* enzymes, and their specificities were hitherto unknown. The reductive half-reactions of *cerevisiae* OYE2 and OYE3 were studied by mixing each enzyme with various concentrations of NADH and NADPH under anaerobiosis. Hydride transfer to the OYE flavin cofactor was observed as a decrease in the extinction coefficient of the mixture at 464nm which corresponds to the two-electron reduction of the flavin. Data were fitted using Kintek Explorer software, yielding the rate constants and dissociation constants shown in figures 9.3 and 9.4. The dissociation constant of NADPH to OYE2 was measured to be less

than 1 μM and the reductive rate constant to be 2.5 s^{-1}. For NADH to OYE2, the dissociation constant was measured to be 3.4 μM with a reductive rate constant of 0.3 s^{-1}. These results show similar specificities for both NADH and NADPH to the enzyme, a relationship contrary to the one observed previously in the pastorianus enzyme, for which NADPH has been shown to be the preferred substrate by a factor of 55-fold [230, 231]. NADPH is the preferred substrate in the previously accepted model of the OYE mechanism, and this is the first known result showing similar specificities of an OYE homolog for both dinucleotides, and suggests that at least in *cerevisiae*, the transfer of hydride equivalents to the unknown acceptor molecules is linked to the oxidation of both dinucleotides in the cell. The fact that NADH is also a highly specific substrate for OYE2 supports our hypothesis that OYE is involved in replenishing the pool of NAD+ for glycolysis during periods of anaerobiosis. In each experiment for OYE2, an early kinetic phase that fit the kinetic model incorporating slow substrate release (k_{off} for NADH) was observed, allowing the k_{off} of NADH to be measured at 2.92 s^{-1}. Such a phase was not observed in the data from OYE3. The reductive half-reaction of OYE3 revealed this enzyme to have a specificity preference for NADPH over NADH similar to that of the *pastorianus* enzyme. The K_d for NADPH was measured to be 2 μM <show error> and the reductive rate constant to be 11 s^{-1}, while the K_d for NADH was measured to be 650 μM with a reductive rate constant of 4 s^{-1}.

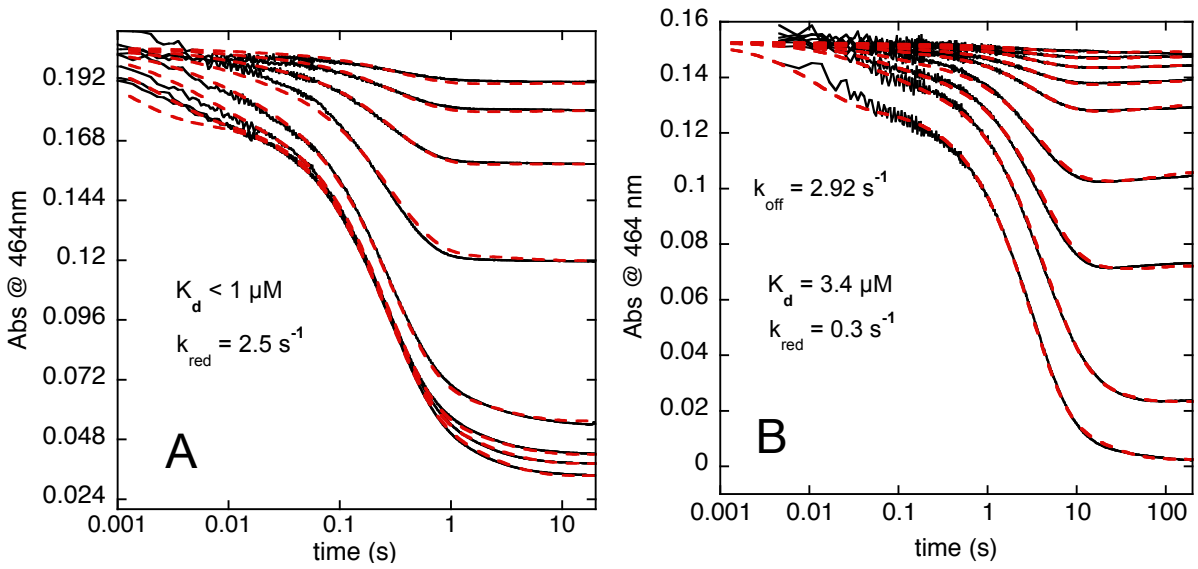

Figure 9.3. Reductive half-reaction of OYE2 studied by anaerobic stopped-flow spectrophotometry. 15 µM enzyme was shot against various concentrations of NADPH (panel A) or NADH (panel B). NADPH concentrations ranged from 1.25 – 160 µM, and NADH concentrations ranged from 0.64 – 215 µM. Reduction of the flavin cofactor was monitored at 464 nm, and kinetic traces were fitted globally using Kintek Explorer software to a model consisting of a reversible bimolecular substrate-binding step followed by a reversible reaction step, and finally a reversible bimolecular product release step. Terms were included for NAD(P)H binding to the reduced enzyme and for product NAD(P)+ binding to the oxidized enzyme.

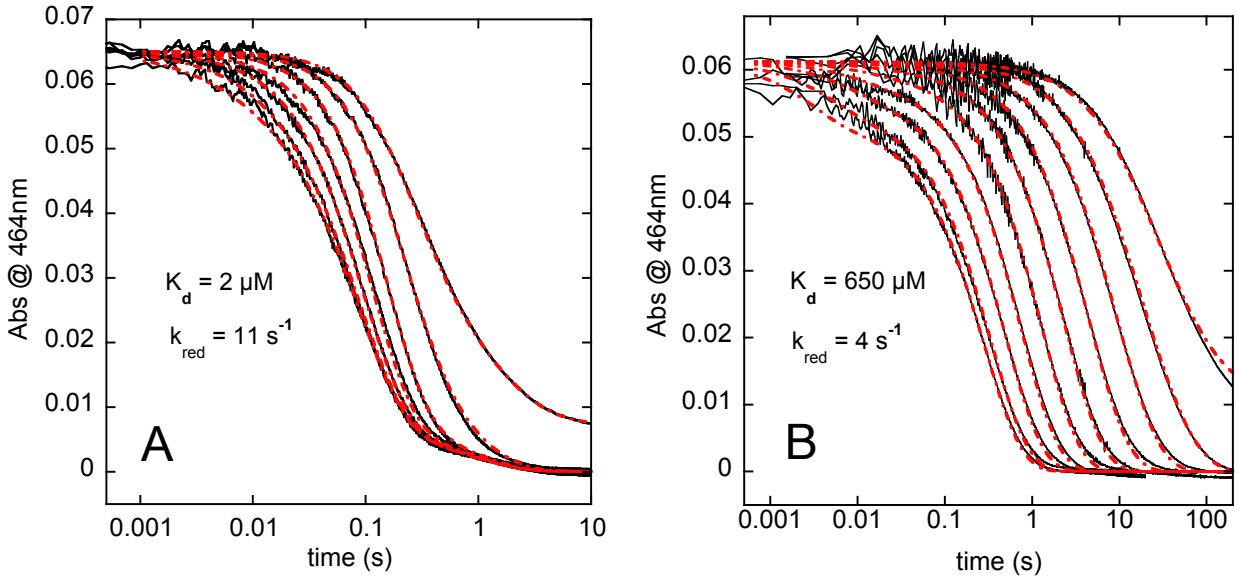

Figure 9.4. Reductive half-reaction of OYE3 studied by anaerobic stopped-flow spectrophotometry. 15 µM enzyme was shot against various concentrations of NADPH (panel A) or NADH (panel B). NADPH concentrations ranged from 0.3 – 5 µM, and NADH concentrations ranged from 5 – 2700 µM. Reduction of the flavin cofactor was monitored at 464 nm, and kinetic traces were fitted globally using Kintek Explorer software to a model consisting of a reversible bimolecular substrate-binding step followed by an irreversible reaction step, and in the case of NADPH a reversible bimolecular product release step.

Oxidative Half-Reaction with Known Hydride Acceptors: The oxidative half-reaction of each enzyme was studied by double-mixing stopped-flow spectrophotometry under anaerobic conditions. Equimolar NADPH was mixed with the enzyme for the first mix and aged for 300 seconds. For the second mix, various concentrations of the hydride acceptor were shot against the reduced enzyme, and the two-electron oxidation of the OYE flavin cofactor was observed as an increase in the extinction coefficient at 464 nm. Data were fit using Kinetic Explorer software to yield oxidative rate constants and dissociation constants for each acceptor. The hydride acceptors tested were 2-cyclohexenone, 4-methoxycinnamaldehyde, 1-nitrocyclohexene, methylene blue, and 4-hydroxy-3-methoxycinnamaldehyde, all synthetic molecules that had previously been reported as hydride acceptors for the *pastorianus* enzyme. The aim of these experiments was to obtain more explicit data from molecules known to accept the OYE hydride and establish whether evidence of pre-equilibrium

binding is observed. Results from any subsequently identified endogenous substrates could then be compared to these two categories; endogenous molecules that do show tight binding were regarded as more likely native substrates while those that react in a collision-based manner without binding are less likely to be native OYE substrates owing to the lack of specificity.

Measured oxidative rate constants and binding constants are summarized in table 9.3. Charge-transfer bands were observed in the absorption spectra of the *cerevisiae* enzymes during binding titrations for unreactive ligands to the oxidized enzymes, and for substrates evidence for charge-transfer was afforded by close fits of the oxidative half-reaction data to kinetic models that include a concentration-dependent elevation of the extinction coefficient at 464 nm within the dead time of the instrument. All known hydride acceptors tested with the *cerevisiae* enzymes showed evidence of binding. It was reported in the literature that nitrocyclohexene accepted the hydride from the *pastorianus* enzyme but in a collision-based manner without evidence of binding; that this substrate bound to both *cerevisiae* enzymes suggests that significant stabilization of the E_R•S complex is afforded for the *cerevisiae* enzymes but that the *pastorianus* enzyme lacks such stabilization [232].

Also, it should be noted that oxygen reacts quite slowly with the reduced flavin (1375 $M^{-1}s^{-1}$ for OYE2 and 233 $M^{-1}s^{-1}$ for OYE3), lending credence to earlier assertions in the literature that molecular oxygen effects minimal reoxidation of the reduced flavin *in vitro*.

Candidate Molecule	Structure	OYE2 k_{ox} (s^{-1})	$OYE2_{ox}$•L K_d (μM)	$OYE2_{red}$•L K_d (μM)	OYE3 k_{ox} (s^{-1})	$OYE3_{ox}$•L K_d (μM)	$OYE3_{red}$•L K_d (μM)
Cyclohexenone	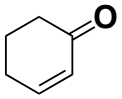	--	16	--	17	--	352
4-MeO-CNA	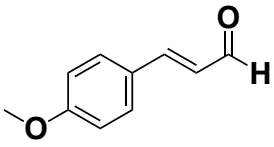	2.7	--	31	*	*	*
Nitrocyclohexene	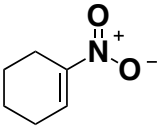	--	120	--	26	--	103
Methylene Blue	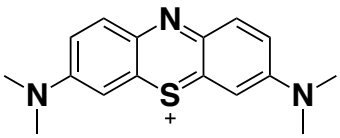	--	34	--	*	*	*
4-HO-3-MeO-CNA	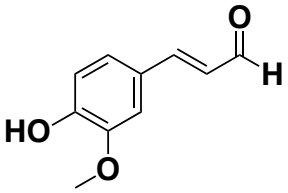	1.5	--	115	*	*	*

Table 9.3. Artificial hydride acceptors for OYE1 tested with OYE2 and OYE3; * Not measured.

Metabolomics of the OYE Reaction in Saccharomyces cerevisiae: The primary aim of these studies is to identify endogenous molecules that accept a hydride from the reduced enzymes. To this end, comparative LCMS studies were performed on small-molecule metabolite extracts of double knockout *cerevisiae* (ΔOYE2,ΔOYE3) cultures that had been reacted with both enzymes and on unreacted samples with added buffer as a control. Three replicates of each run were performed, and the LCMS datasets from both samples were compared using XCMS software. Features in the data that the software identified to be significantly changed between the two samples were singled out and the

corresponding masses were cross-referenced with MS data found in online metabolome databases (YMDB, HMDB). Candidate endogenous substrate molecules were identified in this way, and were ordered and tested with OYE2 and OYE3 in the oxidative half-reaction.

Saccharomyces cerevisiae cultures were grown under both aerobic and anaerobic conditions, in case any endogenous hydride acceptor might only accumulate significantly under anaerobiosis. Cultures were grown at 30 °C with shaking at 180 rpm and were harvested when they reached and OD_{600} of 0.4. Small-molecule extracts were then prepared and frozen, and reacted with either 20 µM OYE2 and OYE3 or an equivalent volume of buffer in the case of the control samples. These were then analyzed by LCMS using an IT-TOF and XCMS software. Possible substrate peaks (those that were depleted in the reacted samples with respect to the controls) and product peaks (those that were enriched in the reacted samples) were identified and included m/z values summarized in table 9.4.

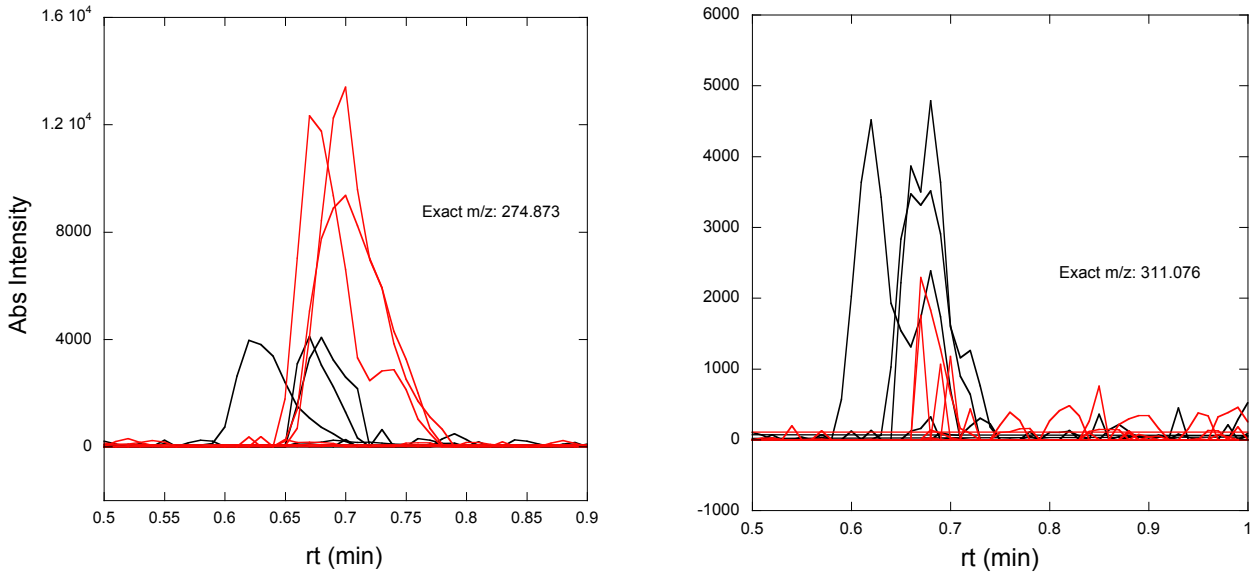

Figure 9.5. Example EICs identified by XCMS as changing significantly between the two samples. The EIC in the left pane resembles a "product" peak; the metabolite is enriched in the reacted sample (red chromatogram) with respect to the control (black chromatogram). The EIC in the right pane suggest a "substrate" peak; the molecule is consumed in the reaction (red) with respect to the control (black)

rt (min)	m/z	Candidate Molecule	Structure	Ion	Enriched or Depleted?	Commercially Available?	OYE2 K_d (μM)
0.71	144.062	p-coumarate	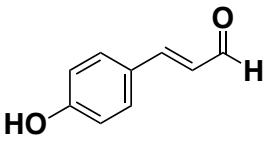	M +3ACN + 2H	-	Yes	47
0.71	144.062	o-coumarate	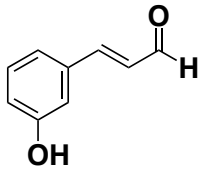	M +3ACN + 2H	-	Yes	*
0.71	144.062	maltol	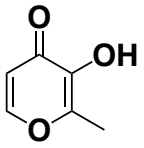	M + NH_4	-	Yes	90
0.72	274.873	???	???	???	+	--	*
79.60	228.191	3-oxo-7,8-dihydro-α-ionol	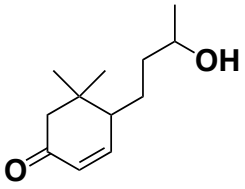	M + NH_4	-	No	*
45.42	349.179	3-dehydroshikimate	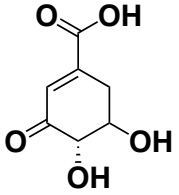	2M + H	-	No	*
0.68	311.076	2,3-dihydro-2,5-dihydroxy-6-methyl-4-H-pyranone	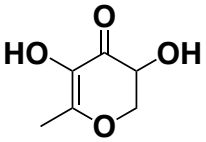	2M + Na	-	No	*

Table 9.4. Candidate molecules identified by cross-referencing XCMS-detected peaks with the Yeast Metabolome Database (YMDB). Commercially available molecules were tested against OYE2 and OYE3 using double-mixing stopped-flow spectrophotometry and monitoring reoxidation of the flavin cofactor at 464 nm. None of the molecules tested were able to accept a hydride from either reduced enzyme. The dissociation constants of maltol and p-coumarate to OYE2 were measured by titration of the ligand to the enzyme while monitoring spectrophotometric perturbation of the flavin.

Commercially available candidate molecules with masses (from YMDB) in agreement with candidate peaks were ordered and studied with OYE2 and OYE3 using double-mixing stopped-flow spectrophotometry, monitoring reoxidation of the OYE flavin (as used in the study of oxidative half-reactions with known hydride acceptors). Molecules tested include p-coumarate, o-coumarate, maltol, shikimate, and uracil (though it was not identified as a feature in the LCMS studies). None of the candidate molecules tested were able to accept a hydride from the reduced enzyme, though maltol and p-coumarate were shown to bind to the enzyme (with dissociation constants of 90 μM and 47 μM, respectively) using binding titrations that measured perturbation of the oxidized OYE flavin spectrum (see table 9.4). It is possible that during preparation of the enzyme-reacted metabolome samples, these molecules bound to the enzyme and were filtered out of the sample with the enzyme at the filtration step, showing up in the comparative LCMS data as depleted metabolite peaks and misidentified as condidate substrates. It's also possible that these metabolite peaks were misidentified, and that the enzymes happened to bind these molecules owing to their promiscuities; both maltol and p-coumarate produced intense charge-transfer bands upon titration to the enzyme.

Discussion

The aim of this study was to identify endogenous substrates of OYE capable of accepting a hydride from the reduced enzyme. While several candidate molecules were identified, none were found to react with the enzymes. Limitations in the method include the degree of chromatographic separation of metabolites during LCMS, the ability to produce metabolite samples at sufficient concentration to be able to quantify many different metabolites which may be at low individual concentrations within the cell while at the same time avoiding detector saturation from more concentrated metabolites, efficient extraction of small-molecule metabolites from yeast cells, control

of oxygen during anaerobic sample culture and during harvesting, control of contaminants in the sample that might compromise sensitivity of the mass spectrometer, and accuracy and completeness of online metabolome and mass spectrometry databases. Extractions were performed in aqueous buffer; less polar solvents such as methanol could be used in order to extract a wider variety of molecules at substantial concentrations. Additionally, a cryostat could be used in order to more effectively control the temperature of the metabolite samples during harvesting and reaction. A bioreactor could be used for culture, and harvesting and experimental procedures could be performed in a glove box for more control over anaerobiosis.

This study did yield new biochemical characterization of these *cerevisiae* enzymes, however. Their nicotinamide dinucleotide substrate specificities were previously unknown; here we report intrinsic rate constants and binding constants measured for the reductive half-reactions of these enzymes. The K_d of NADH to OYE3 was measured to be 325-fold higher than that of NADPH, a specificity profile similar to that of the *pastorianus* enzyme, the specificities of OYE2 for both substrates were quite similar, suggesting that this enzyme is able to efficiently accept a hydride from either substrate. This would allow the enzyme to replenish both pools of oxidized molecules (NAD+ and NADP+) during anaerobiosis, consistent with our hypothesis for the cellular role of these enzymes.

The single-deletion *cerevisiae* mutants were also produced. These mutants could be studied by culturing both strains, producing small-molecule metabolite extracts as before, and then analyzing the metabolite profile of each mutant using LCMS. These profiles could be compared with each other and with that of extracts from wild-type cultures. This could inform on any differences in substrate

specificities between the two enzymes as well as any possible "downstream" effects of each knockout on the small-molecule metabolome.

References

1. Linster, C.L., E. Van Schaftingen, and A.D. Hanson, *Metabolite damage and its repair or pre-emption.* Nat Chem Biol, 2013. **9**(2): p. 72-80.
2. Moran, G.R., *The catalytic function of renalase: A decade of phantoms.* Biochim Biophys Acta, 2016. **1864**(1): p. 177-86.
3. Kunkel, T.A., *DNA replication fidelity.* J Biol Chem, 2004. **279**(17): p. 16895-8.
4. Kunkel, T.A. and D.A. Erie, *DNA mismatch repair.* Annu Rev Biochem, 2005. **74**: p. 681-710.
5. Kunkel, T.A., *Evolving views of DNA replication (in)fidelity.* Cold Spring Harb Symp Quant Biol, 2009. **74**: p. 91-101.
6. Cramer, P., D.A. Bushnell, and R.D. Kornberg, *Structural basis of transcription: RNA polymerase II at 2.8 angstrom resolution.* Science, 2001. **292**(5523): p. 1863-76.
7. Kellinger, M.W., et al., *Dissecting chemical interactions governing RNA polymerase II transcriptional fidelity.* J Am Chem Soc, 2012. **134**(19): p. 8231-40.
8. Xu, L., et al., *Molecular basis of transcriptional fidelity and DNA lesion-induced transcriptional mutagenesis.* DNA Repair (Amst), 2014. **19**: p. 71-83.
9. Browne, B.A., A.I. Ramos, and D.M. Downs, *PurF-independent phosphoribosyl amine formation in yjgF mutants of Salmonella enterica utilizes the tryptophan biosynthetic enzyme complex anthranilate synthase-phosphoribosyltransferase.* J Bacteriol, 2006. **188**(19): p. 6786-92.
10. Sinha, S., et al., *Crystal structure of Bacillus subtilis YabJ, a purine regulatory protein and member of the highly conserved YjgF family.* Proc Natl Acad Sci U S A, 1999. **96**(23): p. 13074-9.
11. Volz, K., *A test case for structure-based functional assignment: the 1.2 A crystal structure of the yjgF gene product from Escherichia coli.* Protein Sci, 1999. **8**(11): p. 2428-37.
12. Miyakawa, T., et al., *Crystal structure of the YjgF/YER057c/UK114 family protein from the hyperthermophilic archaeon Sulfolobus tokodaii strain 7.* Proteins, 2006. **62**(2): p. 557-61.
13. Liu, X., et al., *Crystal structures of RidA, an important enzyme for the prevention of toxic side products.* Sci Rep, 2016. **6**: p. 30494.
14. Burman, J.D., et al., *The crystal structure of Escherichia coli TdcF, a member of the highly conserved YjgF/YER057c/UK114 family.* BMC Struct Biol, 2007. **7**: p. 30.
15. Lambrecht, J.A., B.A. Browne, and D.M. Downs, *Members of the YjgF/YER057c/UK114 family of proteins inhibit phosphoribosylamine synthesis in vitro.* J Biol Chem, 2010. **285**(45): p. 34401-7.
16. Lambrecht, J.A., J.M. Flynn, and D.M. Downs, *Conserved YjgF protein family deaminates reactive enamine/imine intermediates of pyridoxal 5'-phosphate (PLP)-dependent enzyme reactions.* J Biol Chem, 2012. **287**(5): p. 3454-61.
17. Lambrecht, J.A., G.E. Schmitz, and D.M. Downs, *RidA proteins prevent metabolic damage inflicted by PLP-dependent dehydratases in all domains of life.* MBio, 2013. **4**(1): p. e00033-13.

18. Flynn, J.M. and D.M. Downs, *In the absence of RidA, endogenous 2-aminoacrylate inactivates alanine racemases by modifying the pyridoxal 5'-phosphate cofactor.* J Bacteriol, 2013. **195**(16): p. 3603-9.
19. Howden, A.J. and G.M. Preston, *Nitrilase enzymes and their role in plant-microbe interactions.* Microb Biotechnol, 2009. **2**(4): p. 441-51.
20. Thimann, K.V. and S. Mahadevan, *Nitrilase. I. Occurrence, Preparation, and General Properties of the Enzyme.* Arch Biochem Biophys, 1964. **105**: p. 133-41.
21. Pace, H.C. and C. Brenner, *The nitrilase superfamily: classification, structure and function.* Genome Biol, 2001. **2**(1): p. REVIEWS0001.
22. Kobayashi, M., M. Goda, and S. Shimizu, *Nitrilase catalyzes amide hydrolysis as well as nitrile hydrolysis.* Biochem Biophys Res Commun, 1998. **253**(3): p. 662-6.
23. Ramteke, P.W., et al., *Nitrile-converting enzymes: an eco-friendly tool for industrial biocatalysis.* Biotechnol Appl Biochem, 2013. **60**(5): p. 459-81.
24. Barglow, K.T., et al., *Functional proteomic and structural insights into molecular recognition in the nitrilase family enzymes.* Biochemistry, 2008. **47**(51): p. 13514-23.
25. Pace, H.C., et al., *Crystal structure of the worm NitFhit Rosetta Stone protein reveals a Nit tetramer binding two Fhit dimers.* Curr Biol, 2000. **10**(15): p. 907-17.
26. Peracchi, A., et al., *Nit1 is a metabolite repair enzyme that hydrolyzes deaminated glutathione.* Proc Natl Acad Sci U S A, 2017. **114**(16): p. E3233-E3242.
27. Xu, J., et al., *Renalase is a novel, soluble monoamine oxidase that regulates cardiac function and blood pressure.* J Clin Invest, 2005. **115**(5): p. 1275-80.
28. Desir, G.V., et al., *Renalase lowers ambulatory blood pressure by metabolizing circulating adrenaline.* J Am Heart Assoc, 2012. **1**(4): p. e002634.
29. Boomsma, F. and K.F. Tipton, *Renalase, a catecholamine-metabolising enzyme?* J Neural Transm (Vienna), 2007. **114**(6): p. 775-6.
30. Baroni, S., et al., *Is renalase a novel player in catecholaminergic signaling? The mystery of the catalytic activity of an intriguing new flavoenzyme.* Curr Pharm Des, 2013. **19**(14): p. 2540-51.
31. Milani, M., et al., *FAD-binding site and NADP reactivity in human renalase: a new enzyme involved in blood pressure regulation.* J Mol Biol, 2011. **411**(2): p. 463-73.
32. Beaupre, B.A., M.R. Hoag, and G.R. Moran, *Renalase does not catalyze the oxidation of catecholamines.* Arch Biochem Biophys, 2015. **579**: p. 62-6.
33. Beaupre, B.A., et al., *Renalase is an alpha-NAD(P)H oxidase/anomerase.* J Am Chem Soc, 2013. **135**(37): p. 13980-7.
34. Beaupre, B.A., et al., *Kinetics and equilibria of the reductive and oxidative half-reactions of human renalase with alpha-NADPH.* Biochemistry, 2013. **52**(49): p. 8929-37.
35. Beaupre, B.A., et al., *Metabolic function for human renalase: oxidation of isomeric forms of beta-NAD(P)H that are inhibitory to primary metabolism.* Biochemistry, 2015. **54**(3): p. 795-806.
36. Loshon, C.A., et al., *Formation and properties of lactate dehydrogenase inhibitors in NADH.* Clin Chem, 1977. **23**(9): p. 1576-80.
37. Margolis, S.A., B.F. Howell, and R. Schaffer, *Lactate dehydrogenase inhibitors in NADH preparations.* Clin Chem, 1977. **23**(9): p. 1581-4.
38. Hoag, M.R., et al., *Bacterial Renalase: Structure and Kinetics of an Enzyme with 2- and 6-Dihydro-beta-NAD(P) Oxidase Activity from Pseudomonas phaseolicola.* Biochemistry, 2015. **54**(24): p. 3791-802.
39. Stover, P. and V. Schirch, *The metabolic role of leucovorin.* Trends Biochem Sci, 1993. **18**(3): p. 102-6.

40. Roje, S., et al., *Cloning and characterization of mitochondrial 5-formyltetrahydrofolate cycloligase from higher plants.* J Biol Chem, 2002. **277**(45): p. 42748-54.
41. Field, M.S., D.M. Szebenyi, and P.J. Stover, *Regulation of de novo purine biosynthesis by methenyltetrahydrofolate synthetase in neuroblastoma.* J Biol Chem, 2006. **281**(7): p. 4215-21.
42. Girgis, S., et al., *5-Formyltetrahydrofolate regulates homocysteine remethylation in human neuroblastoma.* J Biol Chem, 1997. **272**(8): p. 4729-34.
43. Stover, P. and V. Schirch, *Serine hydroxymethyltransferase catalyzes the hydrolysis of 5,10-methenyltetrahydrofolate to 5-formyltetrahydrofolate.* J Biol Chem, 1990. **265**(24): p. 14227-33.
44. Baggott, J.E., *Hydrolysis of 5,10-methenyltetrahydrofolate to 5-formyltetrahydrofolate at pH 2.5 to 4.5.* Biochemistry, 2000. **39**(47): p. 14647-53.
45. Jeanguenin, L., et al., *Moonlighting glutamate formiminotransferases can functionally replace 5-formyltetrahydrofolate cycloligase.* J Biol Chem, 2010. **285**(53): p. 41557-66.
46. Xu, J., et al., *Renalase is a novel, soluble monoamine oxidase that regulates cardiac function and blood pressure.* The Journal of clinical investigation, 2005. **115**(5): p. 1275-80.
47. Desir, G.V., *Renalase is a novel renal hormone that regulates cardiovascular function.* Journal of the American Society of Hypertension : JASH, 2007. **1**(2): p. 99-103.
48. Desir, G.V., *Renalase deficiency in chronic kidney disease, and its contribution to hypertension and cardiovascular disease.* Current opinion in nephrology and hypertension, 2008. **17**(2): p. 181-5.
49. Desir, G.V., *Regulation of blood pressure and cardiovascular function by renalase.* Kidney international, 2009. **76**(4): p. 366-70.
50. Medvedev, A.E., A.V. Veselovsky, and V.I. Fedchenko, *Renalase, a new secretory enzyme responsible for selective degradation of catecholamines: achievements and unsolved problems.* Biochemistry. Biokhimiia, 2010. **75**(8): p. 951-8.
51. Desir, G.V., *Role of renalase in the regulation of blood pressure and the renal dopamine system.* Current opinion in nephrology and hypertension, 2011. **20**(1): p. 31-6.
52. Gu, R., et al., *Renalase deficiency in heart failure model of rats--a potential mechanism underlying circulating norepinephrine accumulation.* PloS one, 2011. **6**(1): p. e14633.
53. Wu, Y., et al., *Renalase deficiency aggravates ischemic myocardial damage.* Kidney international, 2011. **79**(8): p. 853-60.
54. Baraka, A. and S. El Ghotny, *Cardioprotective effect of renalase in 5/6 nephrectomized rats.* Journal of cardiovascular pharmacology and therapeutics, 2012. **17**(4): p. 412-6.
55. Desir, G.V., et al., *Renalase lowers ambulatory blood pressure by metabolizing circulating adrenaline.* Journal of the American Heart Association, 2012. **1**(4): p. e002634.
56. Koc-Zorawska, E., et al., *Vascular adhesion protein-1 and renalase in regard to diabetes in hemodialysis patients.* Archives of medical science : AMS, 2012. **8**(6): p. 1048-52.
57. Lee, H.T., et al., *Renalase protects against ischemic AKI.* Journal of the American Society of Nephrology : JASN, 2013. **24**(3): p. 445-55.
58. Sizova, D., et al., *Renalase regulates renal dopamine and phosphate metabolism.* American journal of physiology. Renal physiology, 2013. **305**(6): p. F839-44.
59. Desir, G.V. and A.J. Peixoto, *Renalase in hypertension and kidney disease.* Nephrology, dialysis, transplantation : official publication of the European Dialysis and Transplant Association - European Renal Association, 2014. **29**(1): p. 22-8.
60. Guo, X., et al., *Renalase: its role as a cytokine, and an update on its association with type 1 diabetes and ischemic stroke.* Current opinion in nephrology and hypertension, 2014. **23**(5): p. 513-8.

61. He, B., et al., *Correlation between plasma renalase level and coronary artery disease.* Pakistan journal of medical sciences, 2014. **30**(5): p. 863-967.
62. Li, X., et al., *Renalase, a new secretory enzyme: Its role in hypertensive-ischemic cardiovascular diseases.* Medical science monitor : international medical journal of experimental and clinical research, 2014. **20**: p. 688-92.
63. Elcioglu, O.C., et al., *Renalase: Another puzzle piece between hypertension and simple renal cysts?* Int Urol Nephrol, 2015. **47**(7): p. 1181-6.
64. Li, X., et al., *Renalase protects the cardiomyocytes of Sprague-Dawley rats against ischemia and reperfusion injury by reducing myocardial cell necrosis and apoptosis.* Kidney Blood Press Res, 2015. **40**(3): p. 215-22.
65. Quelhas-Santos, J., et al., *Renalase regulates peripheral and central dopaminergic activities.* Am J Physiol Renal Physiol, 2015. **308**(2): p. F84-91.
66. Wang, L., et al., *Identification of a receptor for extracellular renalase.* PLoS One, 2015. **10**(4): p. e0122932.
67. Giordano, F.J., Y. Wang, and G.V. Desir, *A Remote Role for Renalase.* EBioMedicine, 2016. **9**: p. 27-8.
68. Guo, X., et al., *Inhibition of renalase expression and signaling has antitumor activity in pancreatic cancer.* Sci Rep, 2016. **6**: p. 22996.
69. Hollander, L., et al., *Renalase Expression by Melanoma and Tumor-Associated Macrophages Promotes Tumor Growth through a STAT3-Mediated Mechanism.* Cancer Res, 2016. **76**(13): p. 3884-94.
70. Wang, Y., et al., *Extracellular renalase protects cells and organs by outside-in signalling.* J Cell Mol Med, 2017.
71. Malyszko, J., et al., *Renalase, hypertension, and kidney - the discussion continues.* Angiology, 2013. **64**(3): p. 181-7.
72. Baroni, S., et al., *Is renalase a novel player in catecholaminergic signaling? The mystery of the catalytic activity of an intriguing new flavoenzyme.* Current pharmaceutical design, 2013. **19**(14): p. 2540-51.
73. Hennebry, S.C., et al., *Renalase, a novel soluble FAD-dependent protein, is synthesized in the brain and peripheral nerves.* Molecular psychiatry, 2010. **15**(3): p. 234-6.
74. Coordinators, N.R., *Database Resources of the National Center for Biotechnology Information.* Nucleic Acids Res, 2017. **45**(D1): p. D12-D17.
75. Pearson, W.R., *An introduction to sequence similarity ("homology") searching.* Curr Protoc Bioinformatics, 2013. **Chapter 3**: p. Unit3 1.
76. Pandini, V., et al., *Synthesis of human renalase1 in Escherichia coli and its purification as a FAD-containing holoprotein.* Protein expression and purification, 2010. **72**(2): p. 244-53.
77. Milani, M., et al., *FAD-binding site and NADP reactivity in human renalase: a new enzyme involved in blood pressure regulation.* Journal of molecular biology, 2011. **411**(2): p. 463-73.
78. Beaupre, B.A., et al., *Ligand binding phenomena that pertain to the metabolic function of renalase.* Arch Biochem Biophys, 2016. **612**: p. 46-56.
79. Pai, E.F. and G.E. Schulz, *The catalytic mechanism of glutathione reductase as derived from x-ray diffraction analyses of reaction intermediates.* J Biol Chem, 1983. **258**(3): p. 1752-7.
80. Romero, E. and G. Gadda, *Alcohol oxidation by flavoenzymes.* Biomolecular concepts, 2014. **5**(4): p. 299-318.
81. Olucha, J., et al., *Two structures of an N-hydroxylating flavoprotein monooxygenase: ornithine hydroxylase from Pseudomonas aeruginosa.* J Biol Chem, 2011. **286**(36): p. 31789-98.

82. He, P. and G.R. Moran, *Structural and mechanistic comparisons of the metal-binding members of the vicinal oxygen chelate (VOC) superfamily.* Journal of inorganic biochemistry, 2011. **105**(10): p. 1259-1272.
83. Han, L., et al., *Streptomyces wadayamensis MppP Is a Pyridoxal 5'-Phosphate-Dependent l-Arginine alpha-Deaminase, gamma-Hydroxylase in the Enduracididine Biosynthetic Pathway.* Biochemistry, 2015. **54**(47): p. 7029-40.
84. Stepanov, V.M., et al., *Subtilisin and alpha-chymotrypsin catalyzed synthesis of peptides containing arginine and lysine p-nitroanilides as C-terminal moieties.* Bioorg Med Chem, 1995. **3**(5): p. 479-85.
85. Malyszko, J., et al., *Hypertension and kidney disease: is renalase a new player or an innocent bystander?* Journal of hypertension, 2012. **30**(3): p. 457-62.
86. Kalyanaraman, B., P.I. Premovic, and R.C. Sealy, *Semiquinone Anion Radicals from Addition of Amino-Acids, Peptides, and Proteins to Quinones Derived from Oxidation of Catechols and Catecholamines - an Electron-Spin-Resonance Spin Stabilization Study.* Journal of Biological Chemistry, 1987. **262**(23): p. 11080-11087.
87. Napolitano, A., P. Manini, and M. d'Ischia, *Oxidation chemistry of catecholamines and neuronal degeneration: an update.* Curr Med Chem, 2011. **18**(12): p. 1832-45.
88. Boomsma, F. and K.F. Tipton, *Renalase, a catecholamine-metabolising enzyme?* Journal of neural transmission, 2007. **114**(6): p. 775-6.
89. Eikelis, N., et al., *Does renalase degrade catecholamines?* Kidney international, 2011. **79**(12): p. 1380; author reply 1380-1.
90. Zbroch, E., et al., *Kidney and hypertension: is there a place for renalase?* Polskie Archiwum Medycyny Wewnetrznej, 2012. **122**(4): p. 174-9.
91. Desir, G.V., L. Wang, and A.J. Peixoto, *Human renalase: a review of its biology, function, and implications for hypertension.* Journal of the American Society of Hypertension : JASH, 2012. **6**(6): p. 417-26.
92. Beaupre, B.A., et al., *Renalase is an alpha-NAD(P)H oxidase/anomerase.* Journal of the American Chemical Society, 2013. **135**(37): p. 13980-7.
93. Beaupre, B.A., M.R. Hoag, and G.R. Moran, *Renalase does not catalyze the oxidation of catecholamines.* Archives of biochemistry and biophysics, 2015. **579**: p. 62-6.
94. Beaupre, B.A., et al., *Renalase Is an alpha-NAD(P)H Oxidase/Anomerase (JACS Spotlight Article).* Journal of the American Chemical Society, 2013. **135**(37): p. 13980-7.
95. Klemm, A., et al., *Determination, purification, and characterization of alpha-NADH and alpha-NADPH.* Methods in enzymology, 1997. **280**: p. 171-86.
96. Oppenheimer, N.J. and N.O. Kaplan, *The alpha beta epimerization of reduced nicotinamide adenine dinucleotide.* Archives of biochemistry and biophysics, 1975. **166**(2): p. 526-35.
97. Oppenheimer, N.J., *Chemistry and Solution Conformation of Pyridine Nucleotides*, in *The Pyridine Nucletide coenzymes*, J. Everse, B. Anderson, and K.-S. You, Editors. 1982, Academic Press Inc.: New York. p. 51-90.
98. Godtfredsen, S.E. and M. Ottesen, *1,6-Dihydro-NAD as an Humidity-Induced Lactate Dehydrogenase Inhibitor in NADH Preparations.* Carlesberg Research Communications, 1978. **43**: p. 171-175.
99. Chakraverty, K. and S. Chaykin, *1,6 DPNH, an enzymatically active form of reduced DPN.* Biochemical and biophysical research communications, 1964. **15**(3): p. 262-8.
100. Chakraverty, K., et al., *Reduced 1,6-dihydrodiphosphopyridine nucleotide. Chemical properties and enzymatic modification.* The Journal of biological chemistry, 1969. **244**(15): p. 4208-17.

101. Godtfredsen, S.E., M. Ottesen, and N.R. Andersen, *On the Mode of Formation of 1,6-Dihydro-NAD in NADH Preparations.* Carlesberg Research Communications, 1979. **44**: p. 65-75.
102. Chaykin, S. and L. Meissner, *The borohydride reduction products of DPN.* Biochemical and biophysical research communications, 1964. **14**: p. 233-40.
103. Chaykin, S., et al., *Tritium-labeled DPN+ and TPN+.* Biochimica et biophysica acta, 1966. **124**(1): p. 1-12.
104. Chaykin, S., L. King, and J.G. Watson, *The reduction of DPN+ and TPN+ with sodium borohydride.* Biochimica et biophysica acta, 1966. **124**(1): p. 13-25.
105. Ballou, D.P., *Flavoprotein Monooxygenases*, in *Flavins and Flavoproteins*. 1984. p. 605-618.
106. Bagci, B., et al., *Renalase gene polymorphism is associated with increased blood pressure in preeclampsia.* Pregnancy Hypertens, 2016. **6**(2): p. 115-20.
107. Sonawane, P.J., et al., *Transcriptional Regulation of the Novel Monoamine Oxidase Renalase: Crucial Roles of Transcription Factors Sp1, STAT3, and ZBP89.* Biochemistry, 2014. **53**(44): p. 6878-92.
108. Zbroch, E., et al., *Circulating levels of renalase, norepinephrine, and dopamine in dialysis patients.* Renal failure, 2013. **35**(5): p. 673-9.
109. Desir, G., *Novel insights into the physiology of renalase and its role in hypertension and heart disease.* Pediatric nephrology, 2012. **27**(5): p. 719-25.
110. Li, G., et al., *Catecholamines regulate the activity, secretion, and synthesis of renalase.* Circulation, 2008. **117**(10): p. 1277-82.
111. Farzaneh-Far, R., et al., *A functional polymorphism in renalase (Glu37Asp) is associated with cardiac hypertrophy, dysfunction, and ischemia: data from the heart and soul study.* PloS one, 2010. **5**(10): p. e13496.
112. Buraczynska, M., et al., *Renalase gene polymorphisms in patients with type 2 diabetes, hypertension and stroke.* Neuromolecular medicine, 2011. **13**(4): p. 321-7.
113. Wybraniec, M.T. and K. Mizia-Stec, *Renalase and Biomarkers of Contrast-Induced Acute Kidney Injury.* Cardiorenal Med, 2015. **6**(1): p. 25-36.
114. Qi, C., et al., *Serum Renalase Levels Correlate with Disease Activity in Lupus Nephritis.* PLoS One, 2015. **10**(10): p. e0139627.
115. Shi, W.B. and H.Y. Wang, *The association study on renalase polymorphism and hypertension: a meta-analysis.* Int J Clin Exp Med, 2015. **8**(6): p. 9505-11.
116. Jones, S., et al., *Core signaling pathways in human pancreatic cancers revealed by global genomic analyses.* Science, 2008. **321**(5897): p. 1801-6.
117. Luft, F.C., *Renalase, a catecholamine-metabolizing hormone from the kidney.* Cell metabolism, 2005. **1**(6): p. 358-60.
118. Przybylowski, P., et al., *Serum renalase depends on kidney function but not on blood pressure in heart transplant recipients.* Transplantation proceedings, 2011. **43**(10): p. 3888-91.
119. Malyszko, J., et al., *Renalase, a novel regulator of blood pressure, is predicted by kidney function in renal transplant recipients.* Transplantation proceedings, 2011. **43**(8): p. 3004-7.
120. Zbroch, E., et al., *Renalase in peritoneal dialysis patients is not related to blood pressure, but to dialysis vintage.* Peritoneal dialysis international : journal of the International Society for Peritoneal Dialysis, 2012. **32**(3): p. 348-51.
121. Zbroch, E., et al., *Renalase, kidney function, and markers of endothelial dysfunction in renal transplant recipients.* Polskie Archiwum Medycyny Wewnetrznej, 2012. **122**(1-2): p. 40-4.

122. Zbroch, E., et al., *Renalase, a novel enzyme involved in blood pressure regulation, is related to kidney function but not to blood pressure in hemodialysis patients.* Kidney & blood pressure research, 2012. **35**(6): p. 395-9.
123. Quelhas-Santos, J. and M. Pestana, *Letter on 'Sodium-dependent modulation of systemic and urinary renalase expression and activity in the rat remnant kidney'.* Journal of hypertension, 2013. **31**(6): p. 1274-5.
124. Zhang, R., et al., *An association study on renalase polymorphisms and ischemic stroke in a chinese population.* Neuromolecular medicine, 2013. **15**(2): p. 396-404.
125. Malyszko, J., H. Bachorzewska-Gajewska, and S. Dobrzycki, *Renalase, kidney and cardiovascular disease: Are they related or just coincidentally associated?* Adv Med Sci, 2014. **60**(1): p. 41-49.
126. Quelhas-Santos, J. and M. Pestana, *Plasma renalase in chronic kidney disease: differences and similarities between humans and rats.* Current hypertension reviews, 2014. **10**(3): p. 166-70.
127. Quelhas-Santos, J., et al., *Plasma and urine renalase levels and activity during the recovery of renal function in kidney transplant recipients.* Experimental biology and medicine, 2014. **239**(4): p. 502-8.
128. Wang, F., et al., *Renalase might be associated with hypertension and insulin resistance in Type 2 diabetes.* Renal failure, 2014. **36**(4): p. 552-6.
129. Wang, F., et al., *Serum renalase is related to catecholamine levels and renal function.* Clinical and experimental nephrology, 2014.
130. Wybraniec, M.T., et al., *Low plasma renalase concentration in hypertensive patients after surgical repair of coarctation of aorta.* Journal of the American Society of Hypertension : JASH, 2014. **8**(7): p. 464-74.
131. Li, H., et al., *Renalase as a Novel Biomarker for Evaluating the Severity of Hepatic Ischemia-Reperfusion Injury.* Oxid Med Cell Longev, 2016. **2016**: p. 3178562.
132. Wybraniec, M.T., et al., *Plasma renalase concentration before and after radiofrequency renal denervation in patients with resistant hypertension.* J Hum Hypertens, 2016. **30**(6): p. 410-1.
133. Humes, H.D., *Acute renal failure: prevailing challenges and prospects for the future.* Kidney international. Supplement, 1995. **50**: p. S26-32.
134. Stec, A., et al., *Polymorphism of the renalase gene in end-stage renal disease patients affected by hypertension.* Nephrology, dialysis, transplantation : official publication of the European Dialysis and Transplant Association - European Renal Association, 2012. **27**(11): p. 4162-6.
135. Alhasan, R. and D. Njus, *The epinephrine assay for superoxide: why dopamine does not work.* Analytical biochemistry, 2008. **381**(1): p. 142-7.
136. Misra, H.P. and I. Fridovich, *The role of superoxide anion in the autoxidation of epinephrine and a simple assay for superoxide dismutase.* The Journal of biological chemistry, 1972. **247**(10): p. 3170-5.
137. Oppenheimer, N.J., *Chemistry and Solution Confromation of Pyridine Nucleotides*, in *The Pyridine Nucletide coenzymes*, J. Everse, B. Anderson, and K.-S. You, Editors. 1982, Academic Press Inc.: New York. p. 51-90.
138. Anand, R. and R. Marmorstein, *Structure and mechanism of lysine-specific demethylase enzymes.* The Journal of biological chemistry, 2007. **282**(49): p. 35425-9.
139. Chen, Y., et al., *Crystal structure of human histone lysine-specific demethylase 1 (LSD1).* Proceedings of the National Academy of Sciences of the United States of America, 2006. **103**(38): p. 13956-61.

140. Schreuder, H.A., et al., *Crystal structure of the p-hydroxybenzoate hydroxylase-substrate complex refined at 1.9 A resolution. Analysis of the enzyme-substrate and enzyme-product complexes.* J Mol Biol, 1989. **208**(4): p. 679-96.
141. Faust, A., et al., *The structure of a bacterial L-amino acid oxidase from Rhodococcus opacus gives new evidence for the hydride mechanism for dehydrogenation.* Journal of molecular biology, 2007. **367**(1): p. 234-48.
142. Pawelek, P.D., et al., *The structure of L-amino acid oxidase reveals the substrate trajectory into an enantiomerically conserved active site.* The EMBO journal, 2000. **19**(16): p. 4204-15.
143. Tan, T.C., et al., *H-bonding and positive charge at the N5/O4 locus are critical for covalent flavin attachment in trametes pyranose 2-oxidase.* Journal of molecular biology, 2010. **402**(3): p. 578-94.
144. Gadda, G., *Oxygen activation in flavoprotein oxidases: the importance of being positive.* Biochemistry, 2012. **51**(13): p. 2662-9.
145. Freire, E., O.L. Mayorga, and M. Straume, *Isothermal Titration Calorimetry.* Analytical Chemistry, 1990. **62**(18): p. A950-A959.
146. Pfleiderer, v.-G. and C. Woenckhaus, *alpha-Nicotinamid-adenin-dinucletid.* Ann Chem, 1965. **690**: p. 170-175.
147. Suzuki, K., H. Nakano, and S. Suzuki, *Natural occurrence and enzymatic synthesis of alpha-nicotinamide adenine dinucleotide phosphate.* The Journal of biological chemistry, 1967. **242**(14): p. 3319-25.
148. Neumann, J.M., et al., *PMR-relaxation and steric computations give unequivocal nucleoside conformations.* Biochimica et biophysica acta, 1977. **479**(4): p. 427-40.
149. Fujimoto, S., et al., *Mechanisms of hydrogen peroxide-induced relaxation in rabbit mesenteric small artery.* European journal of pharmacology, 2001. **412**(3): p. 291-300.
150. Miura, H., et al., *Role for hydrogen peroxide in flow-induced dilation of human coronary arterioles.* Circulation research, 2003. **92**(2): p. e31-40.
151. Kokusho, Y., et al., *Hydrogen peroxide derived from beating heart mediates coronary microvascular dilation during tachycardia.* Arteriosclerosis, thrombosis, and vascular biology, 2007. **27**(5): p. 1057-63.
152. Weir, M.R. and V.J. Dzau, *The renin-angiotensin-aldosterone system: a specific target for hypertension management.* American journal of hypertension, 1999. **12**(12 Pt 3): p. 205S-213S.
153. Boyer, R.F., *A spectrophotometric assay of polyphenoloxidase activity. A special project in enzyme characterization.* Journal of chemical education, 1977. **54**(9): p. 585-6.
154. Beaupre, B.A., et al., *Renalase is an α-NAD(P)H Oxidase/Anomerase.* J. Am. Chem. Soc., 2013. **In press**.
155. Massey, V., *A Simple Method for the Determination of Redox Potentials*, in *Flavins and flavoproteins*, B. Curti, R. S., and Z. G., Editors. 1990, Walter de Gruyter & Co: New York. p. 59-66.
156. Prince, R.C., S.J. Linkletter, and P.L. Dutton, *The thermodynamic properties of some commonly used oxidation-reduction mediators, inhibitors and dyes, as determined by polarography.* Biochimica et biophysica acta, 1981. **635**(1): p. 132-48.
157. Strickland, S., G. Palmer, and V. Massey, *Determination of dissociation constants and specific rate constants of enzyme-substrate (or protein-ligand) interactions from rapid reaction kinetic data.* J.Biol.Chem., 1975. **250**: p. 4048-4052.
158. Crozier-Reabe, K.R., R.S. Phillips, and G.R. Moran, *Kynurenine 3-monooxygenase from Pseudomonas fluorescens: substrate-like inhibitors both stimulate flavin reduction and*

stabilize the flavin-peroxo intermediate yet result in the production of hydrogen peroxide. Biochemistry, 2008. **47**(47): p. 12420-33.
159. Moran, G.R., et al., *Electrostatic effects on substrate activation in para-hydroxybenzoate hydroxylase: studies of the mutant lysine 297 methionine.* Biochemistry, 1997. **36**(24): p. 7548-56.
160. Valton, J., et al., *Mechanism and regulation of the Two-component FMN-dependent monooxygenase ActVA-ActVB from Streptomyces coelicolor.* The Journal of biological chemistry, 2008. **283**(16): p. 10287-96.
161. Creeke, P.I., et al., *Whole blood NAD and NADP concentrations are not depressed in subjects with clinical pellagra.* The Journal of nutrition, 2007. **137**(9): p. 2013-7.
162. Fava, C., et al., *The Renalase Asp37Glu polymorphism is not associated with hypertension and cardiovascular events in an urban-based prospective cohort: the Malmo Diet and cancer study.* BMC medical genetics, 2012. **13**: p. 57.
163. Fedchenko, V., et al., *Renalase mRNA levels in the brain, heart, and kidneys of spontaneously hypertensive rats with moderate and high hypertension.* Medical science monitor basic research, 2013. **19**: p. 267-70.
164. Fedchenko, V.I., et al., *Construction of the coding sequence of the transcription variant 2 of the human renalase gene and its expression in the prokaryotic system.* International journal of molecular sciences, 2013. **14**(6): p. 12764-79.
165. Malyszko, J., et al., *Renalase, stroke, and hypertension in hemodialyzed patients.* Renal failure, 2012. **34**(6): p. 727-31.
166. Przybylowski, P., et al., *Renalase and endothelial dysfunction in heart transplant recipients.* Transplantation proceedings, 2013. **45**(1): p. 394-6.
167. Dziedzic, M., et al., *Relationship between renalase and N-terminal pro-B-type natriuretic peptide (NT pro-BNP) in haemodialysis patients.* Annals of agricultural and environmental medicine : AAEM, 2014. **21**(1): p. 132-5.
168. Wang, S., et al., *Regulation of renalase expression by D5 dopamine receptors in rat renal proximal tubule cells.* American journal of physiology. Renal physiology, 2014. **306**(6): p. F588-96.
169. Pace, N.C., et al., *How to measure and predict the molar absorption coefficient of a protein.* Prot.Sci., 1995. **4**: p. 2411-2423.
170. Cheng, Y. and W.H. Prusoff, *Relationship between the inhibition constant (K1) and the concentration of inhibitor which causes 50 per cent inhibition (I50) of an enzymatic reaction.* Biochemical pharmacology, 1973. **22**(23): p. 3099-108.
171. Cortes, A., et al., *Relationships between inhibition constants, inhibitor concentrations for 50% inhibition and types of inhibition: new ways of analysing data.* The Biochemical journal, 2001. **357**(Pt 1): p. 263-8.
172. Lowry, O.H., J.V. Passonneau, and M.K. Rock, *The stability of pyridine nucleotides.* The Journal of biological chemistry, 1961. **236**: p. 2756-9.
173. Dalziel, K., *The purification of nicotinamide adenine dinucleotide and kinetic effects of nucleotide impurities.* The Journal of biological chemistry, 1963. **238**: p. 1538-43.
174. Biellmann, J.F., et al., *Structure of lactate dehydrogenase inhibitor generated from coenzyme.* Biochemistry, 1979. **18**(7): p. 1212-7.
175. Wenz, I., et al., *Purification and characterization of commercial NADH and accompanying dehydrogenase inhibitors.* Journal of chromatography, 1976. **120**(1): p. 187-96.
176. Mathews, M.B. and E.E. Conn, *The Reaction of Diphosphopyridine Nucleotide with Sodium Borohydride.* Journal of the American Chemical Society, 1953. **75**: p. 5428-5430.

177. Xu, J. and G.V. Desir, *Renalase, a new renal hormone: its role in health and disease.* Current opinion in nephrology and hypertension, 2007. **16**(4): p. 373-8.
178. Zhao, Q., et al., *Renalase gene is a novel susceptibility gene for essential hypertension: a two-stage association study in northern Han Chinese population.* Journal of molecular medicine, 2007. **85**(8): p. 877-85.
179. Guo, Y. and W. Jiang, *[Research progress with renalase and cardiovascular disease].* Zhong nan da xue xue bao. Yi xue ban = Journal of Central South University. Medical sciences, 2012. **37**(5): p. 537-40.
180. Czarkowska-Paczek, B., et al., *Exercise differentially regulates renalase expression in skeletal muscle and kidney.* The Tohoku journal of experimental medicine, 2013. **231**(4): p. 321-9.
181. Wang, F., et al., *Epinephrine Evokes Renalase Secretion via alpha-Adrenoceptor/NF-kappaB Pathways in Renal Proximal Tubular Epithelial Cells.* Kidney & blood pressure research, 2014. **39**(4): p. 252-9.
182. Wang, Y., et al., *Effect of salt intake and potassium supplementation on serum renalase levels in Chinese adults: a randomized trial.* Medicine, 2014. **93**(6): p. e44.
183. Quelhas-Santos, J. and M. Pestana, *Plasma Renalase Expression in Chronic Kidney Disease: Differences and Similarities between Humans and Rats.* Curr Hypertens Rev, 2015.
184. Wang, J., et al., *Identification, expression and tissue distribution of a renalase homologue from mouse.* Molecular biology reports, 2008. **35**(4): p. 613-20.
185. Birchfield, N.B., B. Latli, and J.E. Casida, *Human protoporphyrinogen oxidase: Relation between the herbicide binding site and the flavin cofactor.* Biochemistry, 1998. **37**: p. 6905-6910.
186. Mizutani, H., et al., *Three-dimensional structure of porcine kidney D-amino acid oxidase at 3.0 Å resolution.* J.Biochem., 1996. **120**: p. 14-17.
187. Otwinowski, Z. and W. Minor, *Processing of X-ray diffraction data collection in oscillation mode.* Methods Enzymol, 1997. **276**: p. 307-325.
188. McCoy, A.J., et al., *Phaser crystallographic software.* J Appl Crystallogr, 2007. **40**(Pt 4): p. 658-674.
189. Emsley, P., et al., *Features and development of Coot.* Acta Crystallogr D Biol Crystallogr, 2010. **66**(Pt 4): p. 486-501.
190. Afonine, P.V., et al., *Joint X-ray and neutron refinement with phenix.refine.* Acta Crystallogr D Biol Crystallogr, 2010. **66**(Pt 11): p. 1153-63.
191. Word, J.M., et al., *Asparagine and glutamine: using hydrogen atom contacts in the choice of side-chain amide orientation.* J Mol Biol, 1999. **285**(4): p. 1735-47.
192. Urzhumtseva, L., et al., *Crystallographic model quality at a glance.* Acta Crystallographica Section D-Biological Crystallography, 2009. **65**: p. 297-300.
193. Chen, V.B., et al., *MolProbity: all-atom structure validation for macromolecular crystallography.* Acta Crystallogr D Biol Crystallogr, 2010. **66**(Pt 1): p. 12-21.
194. Karplus, P.A. and G.E. Schulz, *Refined structure of glutathione reductase at 1.54 A resolution.* Journal of molecular biology, 1987. **195**(3): p. 701-29.
195. Moran, G.R., *The Catalytic Function of Renalase: A Decade of Phantoms.* Biochim Biophys Acta, 2015. **in press**.
196. Entsch, B., V. Massey, and D.P. Ballou, *Intermediates in flavoprotein catalyzed hydroxylations.* Biochem Biophys Res Commun, 1974. **57**(4): p. 1018-25.
197. Crozier-Reabe, K. and G.R. Moran, *Form follows function: structural and catalytic variation in the class a flavoprotein monooxygenases.* International journal of molecular sciences, 2012. **13**(12): p. 15601-39.

198. Gosh, R.R., et al., *Effect of renalase inhibition on blood pressure. .* J Am Soc Nephrol, 2006. **17**: p. 208A (abstract).
199. Hollander, L., et al., *Renalase expression by melanoma and tumor associated-macrophages promotes tumor growth through a STAT3-mediated mechanism.* Cancer Res, 2016.
200. Zaitseva, J., K.M. Meneely, and A.L. Lamb, *Structure of Escherichia coli malate dehydrogenase at 1.45 A resolution.* Acta Crystallogr Sect F Struct Biol Cryst Commun, 2009. **65**(Pt 9): p. 866-9.
201. Adams, P.D., et al., *PHENIX: a comprehensive Python-based system for macromolecular structure solution.* Acta Crystallogr. D 2010. **D66**(Pt 2): p. 213-21.
202. Afonine, P.V., et al., *Towards automated crystallographic structure refinement with phenix.refine.* Acta Crystallogr D Biol Crystallogr, 2012. **68**(Pt 4): p. 352-67.
203. Zaitseva, J., K.M. Meneely, and A.L. Lamb, *Structure of Escherichia coli malate dehydrogenase at 1.45 A resolution.* Acta Crystallogr Sect F, 2009. **65**(Pt 9): p. 866-9.
204. Emsley, P. and K. Cowtan, *Coot: model-building tools for molecular graphics.* Acta Cryst. , 2004. **D60**(Pt 12 Pt 1): p. 2126-32.
205. Kohlmann, A., et al., *Fragment growing and linking lead to novel nanomolar lactate dehydrogenase inhibitors.* J Med Chem, 2013. **56**(3): p. 1023-40.
206. DeLano, W., *The PyMOL Molecular Graphics System*, in http://www.pymol.org. 2002, DeLano Scientific: San Carlos, CA.
207. Bell, J.K., et al., *Structural analyses of a malate dehydrogenase with a variable active site.* J Biol Chem, 2001. **276**(33): p. 31156-62.
208. Hall, M.D. and L.J. Banaszak, *Crystal structure of a ternary complex of Escherichia coli malate dehydrogenase citrate and NAD at 1.9 A resolution.* J Mol Biol, 1993. **232**(1): p. 213-22.
209. Swiderek, K., et al., *Modeling of isotope effects on binding oxamate to lactic dehydrogenase.* J Phys Chem B, 2009. **113**(38): p. 12782-9.
210. Kolappan, S., et al., *Structures of lactate dehydrogenase A (LDHA) in apo, ternary and inhibitor-bound forms.* Acta Crystallogr D Biol Crystallogr, 2015. **71**(Pt 2): p. 185-95.
211. Warburg, O., Christian, W. , *Ein zweites sauerstoffübertragendes Ferment und sein Absorptionsspektrum.* Die Naturwissenschaften, 1932. **20**(37): p. 688-689.
212. Warburg, O., Christian, W., *Uber des Gelbeferment und seine Wirkungen.* 1933. **266**: p. 377-411.
213. Toogood, H.S., J.M. Gardiner, and N.S. Scrutton, *Biocatalytic Reductions and Chemical Versatility of the Old Yellow Enzyme Family of Flavoprotein Oxidoreductases.* Chemcatchem, 2010. **2**(8): p. 892-914.
214. Mansell, D.J., et al., *Biocatalytic Asymmetric Alkene Reduction: Crystal Structure and Characterization of a Double Bond Reductase from Nicotiana tabacum.* ACS Catal, 2013. **3**(3): p. 370-379.
215. Kohli, R.M. and V. Massey, *The oxidative half-reaction of Old Yellow Enzyme. The role of tyrosine 196.* J Biol Chem, 1998. **273**(49): p. 32763-70.
216. Stott, K., et al., *Old Yellow Enzyme. The discovery of multiple isozymes and a family of related proteins.* J Biol Chem, 1993. **268**(9): p. 6097-106.
217. Fitzpatrick, T.B., N. Amrhein, and P. Macheroux, *Characterization of YqjM, an Old Yellow Enzyme homolog from Bacillus subtilis involved in the oxidative stress response.* J Biol Chem, 2003. **278**(22): p. 19891-7.
218. Fox, K.M. and P.A. Karplus, *Old yellow enzyme at 2 A resolution: overall structure, ligand binding, and comparison with related flavoproteins.* Structure, 1994. **2**(11): p. 1089-105.

219. Kitzing, K., et al., *The 1.3 A crystal structure of the flavoprotein YqjM reveals a novel class of Old Yellow Enzymes.* J Biol Chem, 2005. **280**(30): p. 27904-13.
220. Barna, T., et al., *Crystal structure of bacterial morphinone reductase and properties of the C191A mutant enzyme.* Journal of Biological Chemistry, 2002. **277**(34): p. 30976-30983.
221. Breithaupt, C., et al., *X-ray structure of 12-oxophytodienoate reductase 1 provides structural insight into substrate binding and specificity within the family of OYE.* Structure, 2001. **9**(5): p. 419-29.
222. Barna, T.M., et al., *Crystal structure of pentaerythritol tetranitrate reductase: "flipped" binding geometries for steroid substrates in different redox states of the enzyme.* J Mol Biol, 2001. **310**(2): p. 433-47.
223. Opperman, D.J., *Structural investigation into the C-terminal extension of the ene-reductase from Ralstonia (Cupriavidus) metallidurans.* Proteins-Structure Function and Bioinformatics, 2017. **85**(12): p. 2252-2257.
224. Pompeu, Y.A., B. Sullivan, and J.D. Stewart, *X-ray Crystallography Reveals How Subtle Changes Control the Orientation of Substrate Binding in an Alkene Reductase.* Acs Catalysis, 2013. **3**(10): p. 2376-2390.
225. Opperman, D.J., et al., *Crystal structure of a thermostable old yellow enzyme from Thermus scotoductus SA-01.* Biochem Biophys Res Commun, 2010. **393**(3): p. 426-31.
226. Basran, J., et al., *H-tunneling in the multiple H-transfers of the catalytic cycle of morphinone reductase and in the reductive half-reaction of the homologous pentaerythritol tetranitrate reductase.* J Biol Chem, 2003. **278**(45): p. 43973-82.
227. Thomas, B.J. and R. Rothstein, *Elevated Recombination Rates in Transcriptionally Active DNA.* Cell, 1989. **56**(4): p. 619-630.
228. Strogolova, V., et al., *Mitochondrial Porin Por1 and Its Homolog Por2 Contribute to the Positive Control of Snf1 Protein Kinase in Saccharomyces cerevisiae.* Eukaryotic Cell, 2012. **11**(12): p. 1568-1572.
229. Rose MD, W.F., Hieter P, *Methods in yeast genetics: A laboratory course manual*. 1990: Cold Spring Harbor Laboratory Press, Cold Spring Harbor, New York.
230. Brown, B.J., et al., *On the active site of Old Yellow Enzyme. Role of histidine 191 and asparagine 194.* J Biol Chem, 1998. **273**(49): p. 32753-62.
231. Massey, V. and L.M. Schopfer, *Reactivity of old yellow enzyme with alpha-NADPH and other pyridine nucleotide derivatives.* J Biol Chem, 1986. **261**(3): p. 1215-22.
232. Meah, Y. and V. Massey, *Old yellow enzyme: stepwise reduction of nitro-olefins and catalysis of aci-nitro tautomerization.* Proc Natl Acad Sci U S A, 2000. **97**(20): p. 10733-8.

Curriculum Vitae

Matt Hoag

Education

Ph.D program, University of Wisconsin - Milwaukee, 2014 - present
Major, Focus: Biochemistry, Enzymology
Principal Investigator: Prof. Graham R Moran, Ph.D

B.S., Chemistry and Biology, University of Wisconsin - Milwaukee, 2013
Undergraduate Research Advisor: Prof. Graham R Moran, Ph.D

Dissertation Title: Renalase as an Intracellular Metabolite Repair Enzyme

Graduate Achievements and Positions Held

- Distinguished Graduate Student Fellowship, University of Wisconsin - Milwaukee (Fall 2016, Spring 2017)
- Presented "Pterin-Dependent Hydroxylases: Nature's Unique strategy for Aromatic Amino Acid Hydroxylation" for Chemistry Department Graduate Seminar (Sept. 2015)
- Research experience in Moran lab (Jan 21, 2014 - present)
- Teaching Assistantship (01/21/2014 - 05/08/2014)
- Research Assistantship (9/2/2014 - present)

Undergraduate Achievements

- Research experience in Moran lab (Jan 22, 2013 - Jan 21, 2014)
- 1st Place, Surf Undergraduate Poster Session (Aug. 2013)
- SURF funding award (Summer 2013, Fall 2013)

Research Skills

- Extensive knowledge of and experience with mechanistic enzymology, molecular cloning, heterologous protein expression and purification, site-directed mutagenesis, cell culture, electrophoresis, circular dichroism, fluorimetry, stopped-flow spectrophotometry, rapid-quench, isothermal titration calorimetry, spectrophotometric binding titrations, steady state and pre-steady state kinetic analyses, equilibrium and kinetic isotope effects

- Experience with flow cytometry and fluorescence-activated cell sorting

- Experience with various methods and utilities for protein structural analysis including Pymol and Coot

- Experience writing and editing scientific papers and fellowship proposals

Programming Skills

- Proficient in C/C++, Python, x86 and x64 assembly
- Experience with Ruby, Java, and PHP

Publications

1. Kenjic N, Hoag MR, Moraski G, Caperelli C, Moran G, Lamb AL. (2018) PvdF of pyoverdin biosynthesis is a structurally unique N10- formyltetrahydrofolate-dependent formyltransferase. Manuscript submitted for publication.

2. Moran GR, Hoag MR. (2017) The enzyme: Renalase. Archives of Biochemistry and Biophysics. 632, 66-76.

3. Beaupre BA, Roman JV, MR Hoag MR, Silvaggi NS, Lamb AL, Moran GR. (2016) Ligand binding phenomena that pertain to the metabolic function of renalase. Archives of Biochemistry and Biophysics. 612, 46-56.

4. Hoag MR, Roman J, Beaupre BA, Silvaggi NS, Moran GR. (2015) Bacterial renalase : Structure and Kinetics of an Enzyme with 2- and 6-Dihydro-β-NAD(P) Oxidase Activity from Pseudomonas phaseolicola. Biochemistry. 54, 3791-3802.

5. Beaupre BA, Hoag, MR, Moran GR. (2015) Renalase Does Not Catalyze the Oxidation of Catecholamines Archives of Biochemistry and Biophysics. 579, 62-66.

6. Beaupre BA, Hoag MR, Roman J, Försterling FH, Moran GR. (2015) Metabolic Function for Human Renalase: Oxidation of Isomeric Forms of β-NAD(P)H that Are Inhibitory to Primary Metabolism. Biochemistry. 54, 795-806.

7. Beaupre BA, Hoag MR, Carmichael BR, Moran GR (2013) Kinetics and Equilibria of the Reductive and Oxidative Half-Reactions of Human Renalase with α-NADPH. Biochemistry. 52, 8929-8937.

8. Beaupre BA, Carmichael BR, Hoag MR, Shah DD, Moran GR. (2013) Renalase is an α-NAD(P)H Oxidase/Anomerase. Journal of the American Chemical Society. 135, 13980-13987.

Posters

1. Uncovering the Metabolic Roles of Atypical Diaphorase Enzymes. Matthew R. Hoag, Joseph V. Roman, Brett A. Beaupre, Nicholas R. Silvaggi. Kathleen M. Meneely, Audrey L. Lamb, Aishwarya Shevade, Sergei Kuchin, Graham R. Moran. Presented at the 37th Midwest Enzyme Conference, Loyola University, Chicago, IL. Oct. 2017.

2. Biochemical Characterization of Atypical Diaphorase Enzymes. Matthew R. Hoag, Joseph V. Roman, Brett A. Beaupre, Graham R. Moran. Presented at the Enzymes, Coenzymes, and Metabolic Pathways Gordon Conference, Waterville Valley, NH. July 2017.

3. Emerging Details of an Expanding Family of Enzymes. Matthew R. Hoag, Joseph V. Roman, Brett A. Beaupre, Graham R. Moran. Presented at the 25th Enzyme Mechanisms Conference, St. Pete Beach, FL. Jan. 2017.

4. Insights into Binding and Selectivity of Renalase Afforded by Pseudomonas pv. phaseolicola. Matthew R. Hoag, Joseph V. Roman, Brett A. Beaupre, Graham R. Moran. Presented at the 35th Midwest Enzyme Conference, Chicago, IL. Oct. 2016.

5. The Biochemistry of Renalase. Brett A. Beaupre, Matthew R. Hoag, Joseph V. Roman and Graham R. Moran. Presented at the 34th Midwest Enzyme Conference, Illinois Institute of Technology, Chicago, IL. Sept. 2015.

6. The Biochemistry of Renalase. Brett A. Beaupre, Matthew R. Hoag, Joseph V. Roman and Graham R. Moran. Presented at the Enzymes, Coenzymes, and Metabolic Pathways Gordon Conference, Waterville Valley, NH. July 2015.

7. Renalase, a new Metabolic Housekeeping Enzyme. Matthew R. Hoag, Brett A. Beaupre, and Graham R. Moran. Presented at the 24th Enzyme Mechanisms Conference, Galveston, TX. Jan. 2015.

8. The Importance of Metals in MST Enzymes. Kathleen M. Meneely, Graham R. Moran, Audrey L. Lamb. Presented at the 24th Enzyme Mechanisms Conference, Galveston, TX. Jan. 2015.

9. NAD(P)H Aqueous Speciation Reveals a Metabolic Function for Human Renalase Brett A. Beaupre, Matthew R. Hoag, and Graham R. Moran. Presented at the 24th Enzyme Mechanisms Conference, Galveston, TX. Jan. 2015.

10. NAD(P)H Aqueous Speciation Reveals a Metabolic Function for Human Renalase. Brett A. Beaupre, Matthew R. Hoag, Joseph V. Roman, Brenton R. Carmichael, Dhara D. Shah and Graham R. Moran. Presented at the 33th Midwest Enzyme Conference, Northwestern University, Evanston, IL. Sept. 2014.

11. The True Role of Human Renalase Elucidated. Matthew R. Hoag, Brett A. Beaupre, Joseph R. Roman, Brenton R. Carmichael, Dhara D. Shah and Graham R. Moran. Presented at the 33rd Midwest Enzyme Conference, Northwestern University, Evanston, IL. Sept. 2014.

12. The Importance of Magnesium in MST Enzymes. Kathleen M. Meneely, Qianyi Luo, Graham R. Moran and Audrey L. Lamb. Presented at the Enzymes, Coenzymes, and Metabolic Pathways Gordon Conference, Waterville Valley, NH. July 2014.

13. NAD(P)H Aqueous Speciation Reveals A Metabolic Function for Human Renalase. Brett A. Beaupre, Brenton R. Carmichael, Matthew R. Hoag, Dhara D. Shah and Graham R. Moran. Presented at the Enzymes, Coenzymes, and Metabolic Pathways Gordon Conference, Waterville Valley, NH. July 2014.

14. Identification of the Native Substrate of Human Renalase & Proposed Chemical Mechanism. Matthew R. Hoag, Brett A. Beaupre, Brenton R. Carmichael, Dhara D. Shah, Graham R. Moran. Presented at UW System Symposium for Undergraduate Research, University of Wisconsin - Milwaukee, Milwaukee, WI. April 2014.

15. Renalase, A Novel α-NAD(P)H Anomerase/Oxidase. Brett A. Beaupre, Brenton R. Carmichael, Matthew R. Hoag, Dhara D. Shah and Graham R. Moran. Presented at the 33rd Midwest Enzyme Conference, Loyola University, Chicago, IL. Oct. 2013.

16. Discovery of the Native Substrate of Human Renalase Isoform 1 & Proposed Chemical Mechanism. Matthew R. Hoag, Brett A. Beaupre, Brenton R. Carmichael, Dhara D. Shah, Graham R. Moran. Presented at SURF Undergraduate Poster Session, University of Wisconsin - Milwaukee, Milwaukee, WI. Aug. 2013.